A STUDY OF WATER MASS TRANSPORTS IN THE GULF OF THAILAND USING AN OCEAN CIRCULATION MODEL

MR. KRIANGSAK PIAMPHOLPHAN

A DISSERTATION SUBMITTED IN PARTIAL FULFILLMENT OF THE REQUIREMENTS FOR THE DEGREE OF DOCTOR OF PHILOSOPHY
(APPLIED MATHEMATICS)
DEPARTMENT OF MATHEMATICS
FACULTY OF SCIENCE
KING MONGKUT'S UNIVERSITY OF TECHNOLOGY THONBURI
2014

A Study of Water Mass Transports in the Gulf of Thailand using an Ocean Circulation Model

Mr. Kriangsak Piampholphan M.Sc. (Applied Mathematics)

A Dissertation Submitted in Partial Fulfillment of the Requirements
for the Degree of Doctor of Philosophy (Applied Mathematics)
Department of Mathematics
Faculty of Science
King Mongkut's University of Technology Thonburi
2014

Dissertation Committee

..... Chairman
(Lect. Pisuttawan Sripirom Sirininlakul, Ph.D.)

..... Member and Dissertation Advisor
(Asst. Prof. Anirut Luadsong, Ph.D.)

..... Member
(Lect. Teerapol Saleewong, Ph.D.)

..... Member
(Lect. Angkool Wangwongchai, Ph.D.)

Thesis Title	A Study of Water Mass Transports in the Gulf of Thailand using an Ocean Circulation Model
Thesis Credits	36
Candidate	Mr. Kriangsak Piampholphan
Thesis Advisor	Asst. Prof. Dr. Anirut Luadsong
Program	Doctor of Science
Field of Study	Applied Mathematics
Department	Mathematics
Faculty	Science
B.E.	2557

Abstract

This research aims to investigate heat content of volume in the Gulf of Thailand and heat, freshwater, and water mass transports across the connection section between the Gulf of Thailand and the South China Sea. The Model grid used in this research is the orthogonal curvilinear grid which is constructed via cubic splines and solving Laplace's equation. For the vertical grid, the sigma coordinate is introduced to deal with significant topographical variability. The data used for calculating the heat content of volume and heat, freshwater, and water mass transports consist of bottom topography, current velocities, potential temperature, salinity, and density and are calculated from the primitive equations. A numerical method used to solve the primitive equations is the finite difference method. The results show that the heat content of volume in the third and fourth layers are the highest values because in these layers there are large volumes and high temperatures. The lowest heat content of volume is in the last layer. The total heat contents of volume in the Gulf of Thailand are high during May to October and low during November to April. For transportations of heat, freshwater, and water mass in the Gulf of Thailand, the results show that the highest and lowest values of heat, freshwater, and water mass transports in each month occur at the same region, and the direction of heat and water mass transports are all same in the Gulf of Thailand, but the freshwater transport is the opposite direction of heat and water mass transports. The highest values of heat, freshwater, and water mass transports occur between latitudes 8°N to 9°N and at the connection section between the Gulf of Thailand and the South China Sea in the winter, summer, and the end of the rainy season. Their lowest values occur at latitude 9°N in the winter and summer, and between latitudes 10°N to 11°N in the rainy season and the end of the rainy season. For the direction of heat and water mass transports, the heat and water mass at the upper Gulf of Thailand which is upper than 9°N in the end of the winter and summer move northward, and they move southward in the end of the rainy season, and nothward and southward alternately in the onset of the winter. At the lower Gulf of Thailand which is lower than 9°N, they move out of the Gulf of Thailand in the winter, and they move in and out of the Gulf of Thailand alternately in the summer and the end of the rainy season. For the rainy season, they move northward at the upper Gulf of Thailand

which is upper than 10°N, and they move in and out of the Gulf of Thailand alternately at lower Gulf of Thailand which is lower than 10°N. In order to validate the results, a comparison was made with the results of Wyrtki's research which investigated the water mass transports of the Southeast Asian Waters. In a comparison of the results, it can be summarized that the results of our research are on track.

Keywords : Heat Content of Volume/ Heat Transport/ Freshwater Transport/ Water Mass Transport/ Gulf of Thailand/ South China Sea/ Primitive Equations/

Dissertation Title	A Study of Water Mass Transports in the Gulf of Thailand using an Ocean Circulation Model
Dissertation Credits	36
Candidate	Mr. Kriangsak Piampholphan
Dissertation Advisor	Asst. Prof. Dr. Anirut Luadsong
Program	Doctor of Philosophy
Field of Study	Applied Mathematics
Department	Mathematics
Faculty	Science
Academic Year	2014

Abstract

This research aims to investigate heat content of volume and transports of heat, freshwater, and water mass in the Gulf of Thailand. The model grid used in this research is the orthogonal curvilinear grid which is constructed from cubic splines and solving Laplace's equation. For the vertical grid, the sigma coordinate is introduced to deal with significant topographical variability. The data used for calculating the heat content of volume and heat, freshwater, and water mass transports consist of bottom topography, current velocities, potential temperature, salinity, and density and are calculated from the primitive equations. A numerical method used to solve the primitive equations is the finite difference method. The results show that the heat content of volume in the third and fourth layers are the highest values because in these layers there are large volumes and high temperatures. The lowest heat content of volume is in the last layer. The total heat contents of volume in the Gulf of Thailand are high during May to October and low during November to April. For the transports of heat, freshwater, and water mass in the Gulf of Thailand, their highest and lowest values in each month occur at the same region, and the direction of heat and water mass transports are all same in the Gulf of Thailand, but the freshwater transport is the opposite direction of heat and water mass transports. The highest values of heat, freshwater, and water mass transports occur between latitudes 8°N to 9°N in the rainy season, and occur at the connection section between the Gulf of Thailand and the South China Sea in the winter, summer, and the end of the rainy season. Their lowest values occur at latitude 9°N in the winter and summer, and occur between latitudes 10°N to 11°N in the rainy season and the end of the rainy season. For the direction of heat and water mass transports, the heat and water mass at the upper Gulf of Thailand which is upper than 9°N in the end of the winter and summer move northward, and they move southward in the end of the rainy season, and nothward and southward alternately in the onset of the winter. At the lower Gulf of Thailand which is lower than 9°N, they move out of the Gulf of Thailand in the winter, and they move in and out of the Gulf of Thailand alternately in the summer and the end of the rainy season. For the rainy season, they move northward at the upper Gulf of Thailand which is upper than 10°N, and they move in and out of the Gulf of Thailand alternately at lower Gulf of Thailand which is lower than 10°N. In order to validate the results, a comparison was made

with the results of Wyrtki's research which investigated the water mass transports of the Southeast Asian Waters. It can be summarized from the comparison that the results of our research are on track.

Keywords : Freshwater Transport / Gulf of Thailand / Heat Content of Volume / Heat Transport / South China Sea / Water Mass Transport

ACKNOWLEDGEMENTS

I would like to thank Asst. Prof. Dr. Anirut Luadsong, my dissertation advisor, who gives good advices during work. I would like to thank Dr. Pisuttawan Sripirom Sirininlakul from the Department of Mathematics, Srinakharinwirot University, Dr. Teerapol Saleewong and Dr. Angkool Wangwongchai from the Department of Mathematics, King Mongkut's University of Technology Thonburi, who sacrifice to be the member of the examination committee in this time.

Also, I would like to thank Asst. Prof. Dr. Nitima Aschariyaphotha from the Ratchaburi Learning Park, King Mongkut's University of Technology Thonburi, who teaches me about oceanography and how to use an Ocean Circulation Model. Furthermore, she also gives good advices during study in Ph.D. program.

CONTENTS

PAGE

LIST OF TABLES

TABLE **PAGE**

LIST OF FIGURES

FIGURE **PAGE**

FIGURE **PAGE**

FIGURE **PAGE**

FIGURE **PAGE**

FIGURE **PAGE**

FIGURE **PAGE**

FIGURE **PAGE**

LIST OF SYMBOLS

SYMBOL	
H	bottom topography
K_M	vertical kinematic viscosity
K_H	vertical diffusivity
A_M	horizontal kinematic viscosity
A_H	horizontal heat diffusivity
U, V	horizontal velocities
W	vertical velocity
T	potential temperature
S	salinity
ρ	water density
ρ_0	reference density
F_x, F_y	horizontal viscosity term
F_T, F_S	hrizontal diffusion term
H_v	mean horizontal transport of volume
p	pressure
g	gravitational acceleration
Q	the heat content of volume
c_p	specific heat capacity
F_Q	zonally integrated meridional heat transport
F_W	zonally integrated meridional freshwater transport

SYMBOL

EK	total kinetic energy
EA	total potential energy
EAS	total surface potential energy

LISTS OF TECHNICAL TERMS AND ABBREVIATIONS

GoT	Gulf of Thailand
SCS	South China Sea
POM	Princeton Ocean Model
DBDB5	Digital Bathymetric Data Base 5-minute
ECMWF	The European Centre for Medium-Range Weather Forecasts

CHAPTER 1 INTRODUCTION

1.1 Rational

The Gulf of Thailand (GoT) connected to the South China Sea (SCS) situates between longitudes 98°E to 107°E and latitudes 4°N to 14°N approximately. It is surrounded by the Kingdom of Thailand, the Kingdom of Cambodia, the Socialist Republic of Vietnam and Malaysia, as shown in Fig. 1.1. The Gulf of Thailand is

Figure 1.1 The Gulf of Thailand.

shallow with mean depth of 45 metres and maximum depth about 85 metres. Since the GoT is shallow, it has phenomena such as tide, elevation of water mass, wind wave, storm, current, and water mass transport. These phenomena are extremely important knowledge to manage the natural resource, marine environment, shipping, and tourism, which are advantage for countries adjoined the GoT, especially with Thailand.

The popular tools used to investigate the information about oceanography or marine science are buoys, satellites, and ocean circulation models. It has to be noted that the use of buoys or satellites lead to very high costs and spend a lot of time for investigation, especially for the wide domain. A popular tool for investigation is the ocean circulation model which spends low costs and a little time for computation. The ocean circulation model can be used to simulate the current velocities, temperature, and salinity. Examples of ocean circulation models used for investigating information about oceanography are Modelo Hidrodinâmico (MOHID), Geophysical

Fluid Dynamics Laboratory Modular Ocean Model (MOM), Princeton Ocean Model (POM), and Parallel Ocean Program (POP), etc.

The ocean circulation model which is often found to simulate oceanic currents, temperature, salinity, and other water properties in the Gulf of Thailand is Princeton Ocean Model (POM). POM is a sigma coordinate model with an imbedded second moment turbulence closure sub-model. The sigma coordinate is the vertical coordinate which is scaled on the water depth. The horizontal grid uses curvilinear orthogonal coordinates and an "Arakawa C" differencing scheme. The horizontal time differencing is explicit whereas the vertical differencing is implicit. The model has a free surface and a split time step in the external and internal modes.

An important role of the ocean is water mass transports, which are the net movement of water mass from one location to another. The importance of this study is basic knowledge and useful for managing resources in the sea. It can lead to analyzing effects that may occur in the sea after water mass is transported in or out of the sea. The water mass transport is very useful to the sailors, fishermen, marine scientists, tourists, sea travelers, and other occupations concerning with shipment and seafaring. In the present, there has been little research done on water mass transports. Most research has found that water mass transports have been studied at the surface or bottom only, but in this research, we would like to investigate the water mass transports at all vertical plane sections in the Gulf of Thailand. This can tell us that how the property and direction of the movement of water mass are. Thus the water mass transports in the GoT should be investigated.

1.2 Literature Reviews

Hernández-Guerra et al. [8] studied the water masses, circulation and transport in the eastern boundary current of the North Atlantic Subtropical Gyre. Conductivity-temperature-depth (CTD) sections carried out in September 1998 are used to describe them. The surface water mass (<600 m) consists of North Atlantic Central Water (NACW) flowing south with a net mass transport of 2.3×10^9 kg s^{-1}. A tongue of relatively fresh water, consisting of Antarctic Intermediate Water (AAIW), was found approximately in the 600-1100 m depth layer. This tongue was 200-km wide, stretching from the African coast almost to Gran Canaria Island, and transported a net mass of 1.1×10^9 kg s^{-1} northward. This system of currents is what constitutes the real eastern boundary current of the North Atlantic Subtropical Gyre.

Chu et al. [7] reported the evaluation of the POM using SCS Monsoon Experiment (SCSMEX) data. A two-step technique is used to initialize POM with temperature, salinity, and velocity for 1 April 1998 and integrate it from 1 April 1998 with synoptic surface forcing for 3 months with and without data assimilation. Hydrographic and current data acquired from the SCSMEX from April through June 1998 are used to verify, and to assimilate into, POM. The mean SCSMEX data (Apr-Jun 1998) are about 0.58°C warmer than the mean climatological data above the 50-m depth, and slightly cooler than the mean climatological data below the 50-m depth, and are fresher than the climatological data at all depths and with the maximum bias

(0.2-0.25 ppt) at 75-m depth. POM without data assimilation has the capability to predict the circulation pattern and the temperature field reasonably well, but has no capability to predict the salinity field. The model errors have Gaussian-type distribution for temperature hindcast, and non-Gaussian distribution for salinity hindcast with six to eight times more frequencies of occurrence on the negative side than on the positive side. Data assimilation enhances the model capability for ocean hindcast, if even only CTD data are assimilated. When the model is reinitialized using the assimilated data at the end of a month (30 Apr; 31 May 1998) and the model is run for a month without data assimilation (hindcast capability test), the model errors for both temperature and salinity hindcast are greatly reduced, and they have Gaussian-type distributions for both temperature and salinity hindcast. Hence, POM gains capability in salinity hindcast when CTD data are assimilated.

Yaiprasert et al. [30] studied the floating circle of objects simulation with the POM for the GoT. The motion of a group of particles floating on the sea surface were set up so that they formed a circle. The radius reflected uncertainties of longitude and latitude directions while the centre was set at the point of interest. POM was incorporated with tidal forcing on the boundary, which included used current forcing on the inflow by wind velocities, high resolution and realistic ocean bottom topography, temperature and salinity. The model domain for the Gulf of Thailand extended from latitude 3°N-14°N and longitude 99°E-109°E. A horizontal grid resolution of 0.1 degree (approximately 11.1 km) was used in the model. Therefore, the grids consisted of 101×111 cells. Twenty one levels in sigma coordinate were used in vertical resolution. The model results were verified using TOPEX/Poseidon and JASON satellite data. The results of the simulation were used to gain a better understanding of the sea current and object movement patterns in the GoT.

Phaksopa and Sojisuporn [21] studied the storm surge in the GoT generated by Typhoon Linda in 1997 using the POM. The model was forced by eight tidal components (M_2, K_1, O_1, S_2, Q_1, P_1, K_2, and N_2) at the open boundary. The model results were verified using tidal data from 23 tide gauges in the Gulf of Thailand. The results showed that the calculated values from POM corresponded well with the observed ones. Then, the model was used to simulate sea level fluctuation in response to typhoon Linda which entered the Gulf in November 1997. In addition to tidal forcing at the open boundary, 12-hours predicted atmospheric pressure and wind field from Navy Operational Global Atmosphere Prediction System (NOGAPS) were forced above the model surface. The model results showed that POM can simulate Linda's storm-surge even though the model underestimated the peak rise and sea level fluctuation was out of phase by approximately 1 hour sometimes. The reason for this might be that coarse grid, average atmospheric and wind fields were used in this study. In addition, the unreal of land-sea boundary and depth value from ETOPO5 might give rise to abnormal high sea level at some area in the model.

Aschariyaphotha et al. [2] studied the simulation of current circulations in the GoT using the POM. The model run is executed using wind stress calculated from climatological monthly mean wind, restoring-type surface heat and salt, and climatological monthly mean freshwater flux data. It is initialized by the temperature

and salinity data from Levitus94 data set, with zero velocity. Force at the lateral boundary is prescribed from IAP-model and the radiation conditions. The model domain has two open boundaries, i.e. eastern boundary and southern boundary. The northern boundary and western boundary are closed by land. The simulations showed that the strong circulations are clockwise during summer and rainy seasons of Thailand, which are in the northeast and southwest monsoon periods respectively. They occur near Pattani and Narathiwat provinces during summer and in the central GoT during the rainy seasons.

Aschariyaphotha et al. [3] studied about simulation of seasonal circulations and thermohaline variabilities in the Gulf of Thailand based on the POM. The results showed that the temperature in the GoT is warmer than the temperature of the other parts connected to the SCS. At any depth of inflow from SCS into the GoT, the salinity is high, but in the outflow from the GoT at the surface, the salinity is low. The strong circulations are clockwise during summer and the rainy seasons of Thailand, which are the East Asian monsoon periods, northeasterly and southwesterly during summer. They occur near Pattani and Narathiwat provinces during summer and in the central GoT during the rainy seasons. Sensitivity experiments were designed to investigate the effects of wind forcing and open boundary conditions. Wind forcing is shown to be the important factor for generating the circulation in the GoT. The lateral velocity at the open boundaries is of considerable importance to current circulation for the rainy and end of the rainy seasons, with insignificant effect for the winter and summer seasons of Thailand.

Alves et al. [1] studied the hydrological structure, circulation and water mass transport in the Gulf of Cadiz. Hydrological and LADCP data from four experiments at sea (Semane, 1999; 2000/1; 2000/3; 2001) are used to describe them. These data were gathered on meridional sections along $8°20'$ W and $6°15'$ W and between these longitudes on a zonal section along $35°50'$ N. The mesoscale and the submesoscale structures (Mediterranean Water Undercurrents, meddies, cyclones) observed along these sections are characterized in terms of thermohaline properties and of velocity. The transports of mass and salt in each class of density (North Atlantic Central Water, Mediterranean Water, North Atlantic Deep Water) are computed with an inverse model. The model indicates a general eastward flux in the Central Water layer, and a westward flux in the Mediterranean Water layer, but there is also a horizontal recirculation and entrainment in these two layers, as well as strong transports associated with the meddy and cyclone found during Semane (1999).

Jónsson and Valdimarsson [11] studied the water mass transport variability to the North Icelandic shelf, 1994-2010. In the Denmark Strait between Greenland and Iceland, the north-flowing warm, saline Atlantic Water (AW) of the Irminger Current meets the south-flowing cold, relatively fresh Polar Water (PW) of the East Greenland Current. A mixture of these two surface water masses then flows along the shelf north of Iceland. The mixture can vary from being almost pure AW to consisting, to a large extent, of PW. The relative quantities of each water mass to some extent determine the productivity and the living conditions on the shelf north of Iceland. The flow has been monitored with current meters on a section north of Iceland since 1994, and these measurements, together with hydrographic data, are

used to study its structure and variability. The amount of AW carried by the flow is calculated along with the associated heat transport. In the period 1994-2010, the flow consisted on average of 68% of AW with a transport of 0.88 Sv and an associated heat transport of 24 TW. There is notable seasonal variation in the flow and strong interannual variability.

Aschariyaphotha and Wongwises [4] presented simulations of seasonal current circulations and its variabilities forced by runoff from freshwater in the Gulf of Thailand. A numerical three-dimensional ocean model, based on the POM, with rectangular coordinates in horizontal and vertical sigma coordinates was implemented for the GoT. The results showed the clockwise circulations during summer and rainy seasons of Thailand. They occur in the central GoT. Two experiments were designed to investigate the effects of freshwater runoff. The freshwater runoff is shown to be the important factor for generating current circulation in the upper GoT at the end of the rainy seasons. The current speed is weakened when the runoff is removed. The sea surface elevations also decrease when the freshwater runoff is removed, especially in October, where it is reduced by about 50%.

1.3 Objective of the Dissertation

To study water mass transports in the Gulf of Thailand using an ocean circulation model.

1.4 Scopes of the Dissertation

1. To study literatures concerning with simulation of oceanic currents, temperature, salinity, and other water properties in the Gulf of Thailand using an ocean circulation model.
2. To study three-dimensional primitive equations and numerical ocean model.
3. To study transport equations.
4. To calculate current velocities, potential temperature, salinity, and density in the Gulf of Thailand using an ocean circulation model..
5. To calculate the water mass transports.
6. To validate the results.

CHAPTER 2 THEORIES

2.1 Heat Content

Heat Content is a value of heat energy, which is obtained from the sun, burning a fuel, electrical energy, geothermal, and nuclear energy, in an object. When the object gains heat energy, as a result it has high temperature. On the other hand, if the object emits heat energy, it has low temperature. Thus heat energy is direct variation with temperature change.

The heat content of the object is also dependent on type of objects. There are different properties for gaining and emitting heat energy in each type of the object. This property is called heat capacity. If we consider the heat capacity per unit mass, this property is called specific heat capacity. The specific heat capacity is the amount of heat required to change a unit mass of a substance by one degree in temperature. The specific heat capacity of seawater is 3898 J/(kg ° C) [18].
The heat content of unit mass can be expressed as

$$Q = mc_pT \tag{2.1}$$

where

Q is the heat content (Joules, J);
m is the mass (kg);
c_p is the specific heat capacity (J/(kg ° C)), and
T is the potential temperature (° C).

2.2 Governing Equations

2.2.1 Primitive Equations

The primitive equations are a system of equations used for calculating the current velocities, temperature, salinity, and density. It consists of 5 main parts, which are the continuity equation, the momentum equations, the hydrostatic equation, the conservation equations for temperature and salinity, and the equation of state. A three-dimensional primitive equations in Cartesian coordinate can be expressed as follows.

$$\frac{\partial U}{\partial x} + \frac{\partial V}{\partial y} + \frac{\partial W}{\partial z} = 0 \tag{2.2}$$

$$\frac{\partial U}{\partial t} + U\frac{\partial U}{\partial x} + V\frac{\partial U}{\partial y} + W\frac{\partial U}{\partial z} - fV = -\frac{1}{\rho_0}\frac{\partial p}{\partial x} + \frac{\partial}{\partial z}\left(K_M\frac{\partial U}{\partial z}\right) + F'_x \tag{2.3}$$

$$\frac{\partial V}{\partial t} + U\frac{\partial V}{\partial x} + V\frac{\partial V}{\partial y} + W\frac{\partial V}{\partial z} + fU = -\frac{1}{\rho_0}\frac{\partial p}{\partial y} + \frac{\partial}{\partial z}\left(K_M\frac{\partial V}{\partial z}\right) + F'_y \tag{2.4}$$

$$\rho g = -\frac{\partial p}{\partial z} \tag{2.5}$$

$$\frac{\partial T}{\partial t} + U\frac{\partial T}{\partial x} + V\frac{\partial T}{\partial y} + W\frac{\partial T}{\partial z} = \frac{\partial}{\partial z}\left(K_H \frac{\partial T}{\partial z}\right) + F'_T \tag{2.6}$$

$$\frac{\partial S}{\partial t} + U\frac{\partial S}{\partial x} + V\frac{\partial S}{\partial y} + W\frac{\partial S}{\partial z} = \frac{\partial}{\partial z}\left(K_H \frac{\partial S}{\partial z}\right) + F'_S \tag{2.7}$$

$$\rho = \rho(T, S, p) \tag{2.8}$$

where

U and V are the horizontal velocities in the x- and y-directions, respectively;
W is the vertical velocity in the z-direction;
x, y, and z are the eastward, northward, and upward directions, respectively;
t is the time;
f is the curvature and Coriolis terms, which the Coriolis term is equal to $2\Omega \sin \varphi$;
Ω is the angular rotation rate of the Earth; φ is the latitude;
ρ_0 is the reference seawater density:
p is the pressure;
K_M is the vertical kinematic viscosity;
ρ is the seawater density:
g is the gravitational acceleration;
T is the potential temperature;
K_H is the vertical diffusivity, and
S is the salinity.

The variables F'_x, F'_y, F'_T, and F'_S are the horizontal viscosity and diffusion terms defined as

$$F'_x = \frac{\partial}{\partial x}\left(2A_M \frac{\partial U}{\partial x}\right) + \frac{\partial}{\partial y}\left[A_M\left(\frac{\partial U}{\partial y} + \frac{\partial V}{\partial x}\right)\right], \tag{2.9}$$

$$F'_y = \frac{\partial}{\partial y}\left(2A_M \frac{\partial V}{\partial y}\right) + \frac{\partial}{\partial x}\left[A_M\left(\frac{\partial U}{\partial y} + \frac{\partial V}{\partial x}\right)\right], \tag{2.10}$$

$$F'_T = \frac{\partial}{\partial x}\left(A_H \frac{\partial T}{\partial x}\right) + \frac{\partial}{\partial y}\left(A_H \frac{\partial T}{\partial y}\right), \tag{2.11}$$

and

$$F'_S = \frac{\partial}{\partial x}\left(A_H \frac{\partial S}{\partial x}\right) + \frac{\partial}{\partial y}\left(A_H \frac{\partial S}{\partial y}\right) \tag{2.12}$$

where A_M is the horizontal kinematic viscosity, and A_H is the horizontal heat diffusivity.

2.2.2 Transport Equations

The transport equations for the ocean are used to describe transport of some quantities in the ocean which consist of water mass, heat, and freshwater transports. The mean horizontal transport of volume across an ocean basin of width L and depth $H(x)$ is defined as

$$H_v = \int_0^L \int_{-H(x)}^0 v dz dx \tag{2.13}$$

where v is the velocity component normal to the section.

The zonally integrated meridional heat transport is

$$F_Q = c_p \int_0^L \int_{-H(x)}^0 \rho v T dz dx \tag{2.14}$$

where ρ is the seawater density; c_p is the specific heat capacity, and T is the potential temperature.

The zonally integrated meridional freshwater transport is

$$F_W = \int_0^L \int_{-H(x)}^0 \rho v (1 - S) dz dx \tag{2.15}$$

where S is the salinity.

2.2.3 Heat Equation

The heat content of volume V is

$$Q = c_p \iiint_V \rho T dz dx dy \tag{2.16}$$

where ρ is the seawater density; c_p is the specific heat capacity, and T is the potential temperature.

2.3 Cubic Spline Interpolation

Cubic spline interpolation is a popular method for an interpolation. It is a piecewise function that its properties consist of the curves passed through all specified data points, continuous function, and continuous first and second order derivatives within an interval and its boundaries. The cubic spline interpolation yields an interpolation formula on each interval between x_i to x_{i+1} for $i = 0, 1, 2, ..., n-1$. It is begun with a cubic polynomial on each interval between x_i to x_{i+1} for $i = 0, 1, 2, ..., n-1$ which is expressed as

$$y_i(x) = a_i + b_i(x - x_i) + c_i(x - x_i)^2 + d_i(x - x_i)^3 \tag{2.17}$$

where a_i, b_i, c_i, and d_i are unknown coefficients.

For the first and second derivatives of $y_i(x)$ it is expressed as follows.

$$y_i^{'}(x) = b_i + 2c_i(x - x_i) + 3d_i(x - x_i)^2 \tag{2.18}$$

$$y_i^{''}(x) = 2c_i + 6d_i(x - x_i) \tag{2.19}$$

The unknown coefficients is determined by applying the above-mentioned spline properties. The properties of curves passed through all specified data points are expressed as $y_i(x_i) = y_i$ and $y_i(x_{i+1}) = y_{i+1}$ for $i = 0, 1, 2, ..., n-1$ and the properties of continuous derivatives are expressed as $y_i^{''}(x_i) = y_i^{''}$ and $y_i^{''}(x_{i+1}) = y_{i+1}^{''}(x_{i+1})$ for

$i = 0, 1, 2, ..., n-2$.

It is a convenient work to substitute $x_{i+1} - x_i$ with h_i for $i = 0, 1, 2, ..., n-1$.

The condition of $y_i(x_i) = y_i$ results in

$$a_i = y_i. \tag{2.20}$$

The condition of $y_i^{''}(x_i) = y_i^{''}$ yields

$$2c_i = y_i^{''}$$

or

$$c_i = \frac{y_i^{''}}{2}. \tag{2.21}$$

The condition of $y_i^{''}(x_{i+1}) = y_{i+1}^{''}(x_{i+1})$ results in

$$2c_i + 6d_i h_i = 2c_{i+1}. \tag{2.22}$$

Applying Eq. (2.21) into Eq. (2.22) and rearranging its equation, it yields

$$d_i = \frac{y_{i+1}^{''} - y_i^{''}}{6h_i}. \tag{2.23}$$

The condition of $y(x_{i+1}) = y_{i+1}$ yields

$$a_i + b_i h_i + c_i h_i^2 + d_i h_i^3 = y_{i+1}. \tag{2.24}$$

Applying Eqs. (2.20), (2.21), and (2.23) into Eq. (2.24) and rearranging its equation, it yields

$$b_i = \frac{y_{i+1} - y_i}{h_i} - \frac{h_i}{2} y_i^{''} - \frac{h_i}{6}(y_{i+1}^{''} - y_i^{''}). \tag{2.25}$$

Substituting a_i, b_i, c_i, and d_i from above into Eq. (2.17) and rearranging its equation, this yields

$$y(x) = y_i(x) = Ay_i + By_{i+1} + Cy_i^{''} + Dy_{i+1}^{''} \tag{2.26}$$

where

$$A = \frac{x_{i+1} - x}{h_i}, \tag{2.27}$$

$$B = 1 - A = \frac{x - x_i}{h_i}, \tag{2.28}$$

$$C = \frac{h_i^2}{6}(A^3 - A), \tag{2.29}$$

and

$$D = \frac{h_i^2}{6}(B^3 - B). \tag{2.30}$$

The equation (2.26) is the cubic spline interpolation formula on an interval between x_i and x_{i+1} for $i = 0, 1, 2, ..., n-1$.

It is a complete cubic spline interpolation formula if the second derivatives of the function $y(x)$ at the points x_i, those are $y_i^{''}$, are known at all points i, $i =$

$0, 1, 2, ..., n-1$. These points can be determined by applying the first derivative continuity at the points x_i, $i = 1, 2, ..., n-2$. Consider the general two intervals at (x_{i-1}, x_i) and (x_i, x_{i+1}), the first derivatives of the function $y(x)$, Eq. (2.26), with respect to x at the point x_i on the intervals (x_{i-1}, x_i) and (x_i, x_{i+1}) are

$$y^{'}(x_i) = \frac{y_i - y_{i-1}}{x_i - x_{i-1}} + \frac{x_i - x_{i-1}}{6} y_{i-1}^{''} + \frac{x_i - x_{i-1}}{3} y_i^{''} \tag{2.31}$$

and

$$y^{'}(x_i) = \frac{y_{i+1} - y_i}{x_{i+1} - x_i} - \frac{x_{i+1} - x_i}{3} y_i^{''} + \frac{x_{i+1} - x_i}{6} y_{i+1}^{''}, \tag{2.32}$$

respectively.

From the first derivative continuity at the point x_i, $i = 1, 2, ..., n-2$, the first derivative of the function $y(x)$ with respect to x on the interval (x_{i-1}, x_i) at the point x_i is equal to the first derivative of the function $y(x)$ with respect to x on the interval (x_i, x_{i+1}) at the point x_i, that is

$$\frac{y_i - y_{i-1}}{x_i - x_{i-1}} + \frac{x_i - x_{i-1}}{6} y_{i-1}^{''} + \frac{x_i - x_{i-1}}{3} y_i^{''} = \frac{y_{i+1} - y_i}{x_{i+1} - x_i} - \frac{x_{i+1} - x_i}{3} y_i^{''} + \frac{x_{i+1} - x_i}{6} y_{i+1}^{''}. \tag{2.33}$$

Rearranging this equation, it yields

$$\frac{x_i - x_{i-1}}{6} y_{i-1}^{''} + \frac{x_{i+1} - x_{i-1}}{3} y_i^{''} + \frac{x_{i+1} - x_i}{6} y_{i+1}^{''} = \frac{y_{i+1} - y_i}{x_{i+1} - x_i} - \frac{y_i - y_{i-1}}{x_i - x_{i-1}}, \tag{2.34}$$

which has $n-2$ equations with n unknown variables $y_i^{''}$, for $i = 0, 1, 2, ..., n-1$. Hence the second derivatives $y_i^{''}$, $i = 0, 1, 2, ..., n-1$, have many results. For a unique result, the boundary conditions have to be applied.

There are several boundary conditions of splines which are invented for determining $y_i^{''}$, $i = 0, 1, 2, ..., n-1$. The popular boundary conditions of splines consist of natural spline, spline 2^{nd} derivative, and parabolic runout spline. Natural spline is to specify the second derivative of the function $y(x)$ at the boundary point to be zero, that is $y_0^{''} = 0$ and/or $y_{n-1}^{''} = 0$. Spline 2^{nd} derivative is to specify a value, not zero, of the second derivative of the function $y(x)$ at the boundary point. Parabolic runout spline is to set the second derivatives of the function $y(x)$ at the boundary points equal to the nearest point of the second derivatives of the function $y(x)$, those are $y_0^{''} = y_1^{''}$ and $y_{n-1}^{''} = y_{n-2}^{''}$.

2.4 Bilinear Interpolation

Bilinear interpolation is an interpolation method using linear interpolation with x and y coordinates on a two dimensional rectangular grid. A value of the unknown function at any random points can be approximated by using the 4 nearest surrounding points of the known function.

Consider the Fig. 2.1 where the points (x_1, y_1), (x_1, y_2), (x_2, y_1), and (x_2, y_2) are the known functions, and the point (x, y) is the unknown function. To interpolate the function at the point (x, y), it can be divided into 2 steps. The first step is

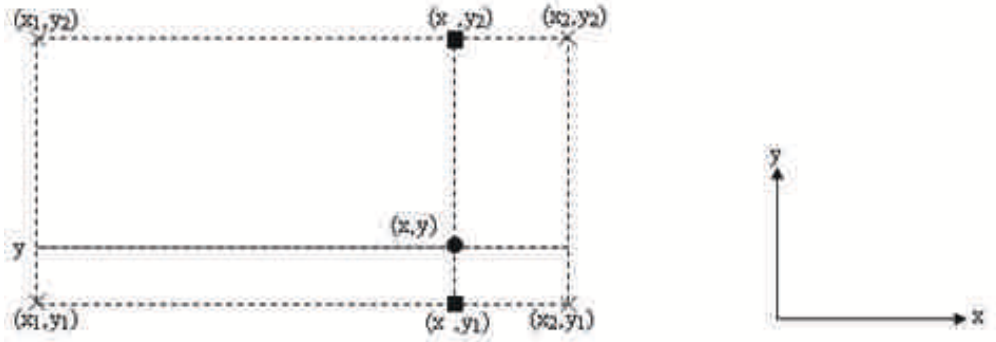

Figure 2.1 The points of the known and unknown functions with x and y coordinates on the two dimensional rectangular grid.

to interpolate functions in x-direction using the linear interpolation on the interval between x_1 and x_2.

$$f(x, y_1) \approx \frac{x_2 - x}{x_2 - x_1} f(x_1, y_1) + \frac{x - x_1}{x_2 - x_1} f(x_2, y_1) \tag{2.35}$$

and

$$f(x, y_2) \approx \frac{x_2 - x}{x_2 - x_1} f(x_1, y_2) + \frac{x - x_1}{x_2 - x_1} f(x_2, y_2). \tag{2.36}$$

The final step is similar to the first step. It is to interpolate the functions in y-direction using the linear interpolation on the interval between y_1 and y_2. That is

$$f(x, y) \approx \frac{y_2 - y}{y_2 - y_1} f(x, y_1) + \frac{y - y_1}{y_2 - y_1} f(x, y_2). \tag{2.37}$$

2.5 Laplace's Equation

Laplace's equation is a type of elliptic equation, which is a linear partial differential equation of second order. Laplace's equation in Cartesian coordinate is expressed as

$$\Delta u = 0 \tag{2.38}$$

where Δ is the Laplacian operator defined as

$$\Delta = \frac{\partial^2}{\partial x_1^2} + \frac{\partial^2}{\partial x_2^2} + ... + \frac{\partial^2}{\partial x_n^2}. \tag{2.39}$$

Laplace's equation describes steady-state phenomena of temperature distributions, potential of an electrostatic fields, flows, and stress distributions. A solution u of Laplace's equation is called a Harmonic function.

2.6 Types of Boundary Conditions

There are three most common types of boundary conditions such as Dirichlet, Neumann, and Robin conditions. Dirichlet condition is specifying the value of the function u at each point on the boundary. Neumann condition is specifying the normal

derivative, $\frac{\partial u}{\partial \vec{n}} = \vec{n} \cdot \nabla u$ where $\vec{n}$ and ∇ are the unit outward normal vector and gradient operator, respectively, at each point on the boundary. Robin condition is a combination of Dirichlet and Neumann conditions specified at each point on the boundary.

2.7 Sigma Coordinate

The sigma coordinate is the vertical coordinate which is scaled on the seawater column depth. The value σ on the sigma coordinate ranges from 0 and -1 where $\sigma = 0$ and $\sigma = -1$ are the seawater levels at the surface elevation and bottom topography, respectively, as shown in Fig. 2.2.

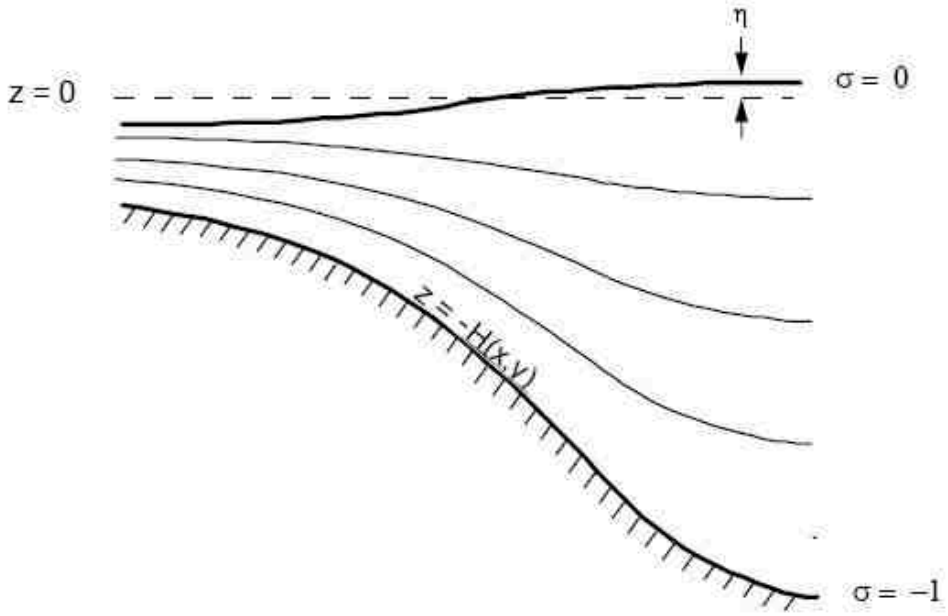

Figure 2.2 The sigma coordinate system. [16]

The sigma coordinate system deals with significant topographical variability that encountered in estuaries and slopes. The governing equations for transformation from Cartesian to sigma coordinates are

$$x^* = x, \tag{2.40}$$

$$y^* = y, \tag{2.41}$$

$$\sigma = \frac{z - \eta(x, y, t)}{D(x, y, t)}, \tag{2.42}$$

and

$$t^* = t \tag{2.43}$$

where

x, y, and z are the conventional Cartesian coordinates;
t is the time;
$D(x, y, t) = H(x, y) + \eta(x, y, t)$ is the seawater column depth;
$H(x, y)$ is the bottom topography, and
$\eta(x, y, t)$ is the surface elevation.

2.8 Finite Difference Method

Finite difference method is a numerical method for solving problems of engineering and mathematical physics. The principle of finite difference method is derivatives in a partial differential equation approximated by linear combinations of function values at the grid points. First, we recall the Taylor series expansion of a function $u(x)$

$$u(x) = u(x_i) + \frac{(x-x_i)}{1!}\left(\frac{\partial u(x_i)}{\partial x}\right) + \frac{(x-x_i)^2}{2!}\left(\frac{\partial^2 u(x_i)}{\partial x^2}\right) + \frac{(x-x_i)^3}{3!}\left(\frac{\partial^3 u(x_i)}{\partial x^3}\right) + \frac{(x-x_i)^4}{4!}\left(\frac{\partial^4 u(x_i)}{\partial x^4}\right) + ... \tag{2.44}$$

It is a convenient work to specify $u_i \approx u(x_i)$ where $i = 0, 1, 2, ..., N$ and $\Delta x = x_{i+1} - x_i = x_i - x_{i-1}$ which is mesh size. Thus it follows that

$$u_{i+1} = u_i + \Delta x \left(\frac{\partial u}{\partial x}\right)_i + \frac{(\Delta x)^2}{2}\left(\frac{\partial^2 u}{\partial x^2}\right)_i + \frac{(\Delta x)^3}{6}\left(\frac{\partial^3 u}{\partial x^3}\right)_i + ... \tag{2.45}$$

and

$$u_{i-1} = u_i - \Delta x \left(\frac{\partial u}{\partial x}\right)_i + \frac{(\Delta x)^2}{2}\left(\frac{\partial^2 u}{\partial x^2}\right)_i - \frac{(\Delta x)^3}{6}\left(\frac{\partial^3 u}{\partial x^3}\right)_i + ... \tag{2.46}$$

From Eq. (2.45) we can recast in first order derivative with respect to x at the point i, that is

$$\left(\frac{\partial u}{\partial x}\right)_i = \frac{u_{i+1} - u_i}{\Delta x} - \frac{\Delta x}{2}\left(\frac{\partial^2 u}{\partial x^2}\right)_i - \frac{(\Delta x)^2}{6}\left(\frac{\partial^3 u}{\partial x^3}\right)_i + ...$$

or

$$\left(\frac{\partial u}{\partial x}\right)_i = \frac{u_{i+1} - u_i}{\Delta x} + O(\Delta x)$$

where $O(\Delta x)$ is truncation error. If we truncate this equation before $O(\Delta x)$ term, we have the approximation

$$\left(\frac{\partial u}{\partial x}\right)_i \approx \frac{u_{i+1} - u_i}{\Delta x} \tag{2.47}$$

which is called the forward difference approximation to first order derivative $\left(\frac{\partial u}{\partial x}\right)_i$. Similarly, Eq. (2.46) can recast in first order derivative with respect to x at the point i, which is

$$\left(\frac{\partial u}{\partial x}\right)_i = \frac{u_i - u_{i-1}}{\Delta x} + O(\Delta x).$$

We have also the approximation, that is

$$\left(\frac{\partial u}{\partial x}\right)_i \approx \frac{u_i - u_{i-1}}{\Delta x} \tag{2.48}$$

which is called the backward difference approximation.

We can obtain the central difference approximation by subtracting Eq. (2.46) from Eq. (2.45), that is

$$\left(\frac{\partial u}{\partial x}\right)_i \approx \frac{u_{i+1} - u_{i-1}}{2\Delta x} \tag{2.49}$$

in which truncation error is $O(\Delta x^2)$.

This type of analysis can be extended to arrive at the central difference approximation of the second order derivative $\left(\frac{\partial^2 u}{\partial x^2}\right)_i$. Let us consider the sum of Eqs. (2.45) and (2.46), that is

$$\left(\frac{\partial^2 u}{\partial x^2}\right)_i = \frac{u_{i+1} - 2u_i + u_{i-1}}{(\Delta x)^2} + O(\Delta x^2).$$

It follows that

$$\left(\frac{\partial^2 u}{\partial x^2}\right)_i \approx \frac{u_{i+1} - 2u_i + u_{i-1}}{(\Delta x)^2} \tag{2.50}$$

This is the central difference approximation of the second order derivative $\left(\frac{\partial^2 u}{\partial x^2}\right)_i$. We now extend the finite difference approximations to partial derivatives. Let us firstly consider $\frac{\partial u}{\partial y}$ and $\frac{\partial u}{\partial x}$, it follows that

$$\left(\frac{\partial u}{\partial y}\right)_{i,j} \approx \frac{u_{i,j+1} - u_{i,j-1}}{2\Delta y} \tag{2.51}$$

which is the central difference approximation of the first order derivative in two variables.

Similarly

$$\left(\frac{\partial u}{\partial x}\right)_{i,j} \approx \frac{u_{i+1,j} - u_{i-1,j}}{2\Delta x}. \tag{2.52}$$

We can extend to the approximation of second order derivative in two variables. It is started from considering $\frac{\partial^2 u}{\partial x \partial y}$, that is

$$\frac{\partial^2 u}{\partial x \partial y} = \frac{\partial}{\partial x}\left(\frac{\partial u}{\partial y}\right) = \frac{\partial}{\partial y}\left(\frac{\partial u}{\partial x}\right). \tag{2.53}$$

The approximation of Eq. (2.53) is

$$\left(\frac{\partial^2 u}{\partial x \partial y}\right)_{i,j} \approx \frac{\left(\frac{\partial u}{\partial y}\right)_{i+1,j} - \left(\frac{\partial u}{\partial y}\right)_{i-1,j}}{2\Delta x}. \tag{2.54}$$

From Eq. (2.51) we can apply to approximate $\left(\frac{\partial u}{\partial y}\right)_{i+1,j}$ and $\left(\frac{\partial u}{\partial y}\right)_{i-1,j}$ terms, those are

$$\left(\frac{\partial u}{\partial y}\right)_{i+1,j} \approx \frac{u_{i+1,j+1} - u_{i+1,j-1}}{2\Delta y} \tag{2.55}$$

and

$$\left(\frac{\partial u}{\partial y}\right)_{i-1,j} \approx \frac{u_{i-1,j+1} - u_{i-1,j-1}}{2\Delta y}. \tag{2.56}$$

Substituting Eqs. (2.55) and (2.56) into Eq. (2.54), we obtain

$$\left(\frac{\partial^2 u}{\partial x \partial y}\right)_{i,j} \approx \frac{u_{i+1,j+1} - u_{i+1,j-1} - u_{i-1,j+1} + u_{i-1,j-1}}{4\Delta x \Delta y} \tag{2.57}$$

which is the central difference approximation of the second order derivative for two variables.

CHAPTER 3 METHODOLOGY

There are two main steps used to investigate the water mass transports. The first step is to simulate the current velocities, temperature salinity, and density from the primitive equations using an Ocean Circulation Model (OCM) and, the final step is to calculate the water mass transports from the simulated data using the transport equations. The procedure of this study is as follows.

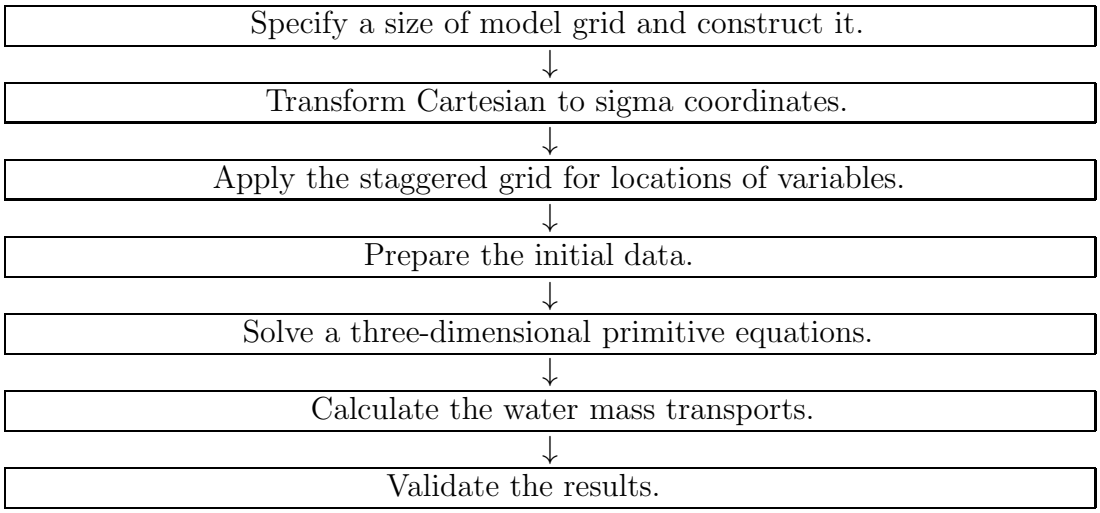

The details of each procedure are in the following topics.

3.1 Model Grid

A grid type which is generally used for computing at points in a problem domain is the rectangular grid. It is easy to compute, especially with simple domains such as rectangles. For more complex domains, the rectangular grid may not be as effective due to the nature of either the landscape or the coastal area. However, this difficulty can be overcome by increasing the number of mesh which in turn increases the number of generated points on boundaries of the domain. This result requires very high costs and a lot of time to compute. For this reason we would like to use the orthogonal curvilinear grid designed to match the problem domain, keeping the number of mesh identical to the rectangular grid. It is low cost and uses less time to compute. In this research, the study domain is the Gulf of Thailand. There are algorithms and details of constructing the orthogonal curvilinear grid as follows.

3.1.1 To Specify a Size of Model grid

In this research, we specify the number of horizontal grid points as 43×97.

3.1.2 To Specify Border Points

The border points on north boundary are specified as (100°E, 13.3°N) and (101°E, 13.3°N).

The border points on south boundary are specified as (101°E, 5.5°N) and (105.2°E, 5.5°N).

The border points on east boundary are specified as (105.2°E, 5.5°N), (104.5°E, 10.5°N), and (101°E, 13.3°N).

The border points on west boundary are specified as (101°E, 5.5°N), (98.9°E, 9.5°N), and (100°E, 13.3°N).

These data are depicted in Fig. 3.1.

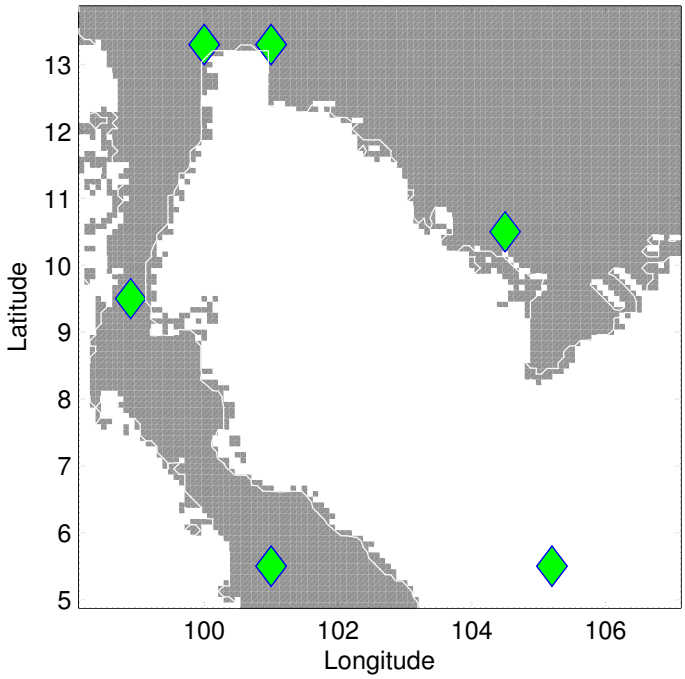

Figure 3.1 Border points of the model grid.

3.1.3 To Construct Grid Points of the Model Grid

Each point on boundaries of the model grid is constructed via the cubic spline with boundary conditions of natural spline and spline 2^{nd} derivative. These points are used to be the boundary condition for the grid points inside the model grid. For each point inside the model grid, it is constructed by solving Laplace's equation using the second-order finite difference approximation.

The model grid is shown in Fig. 3.2. The figures 3.3 and 3.4 show the grid spacing (km) in x direction, Δx, and y direction, Δy, respectively. The grid spacing in x

direction is between 2 to 40 kilometres and the grid spacing in y direction is between 5 to 35 kilometres.

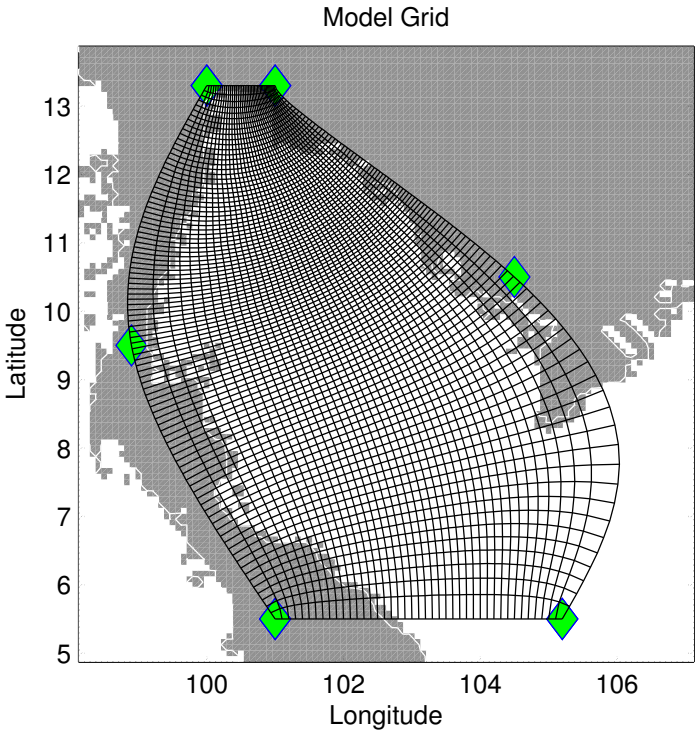

Figure 3.2 The model grid.

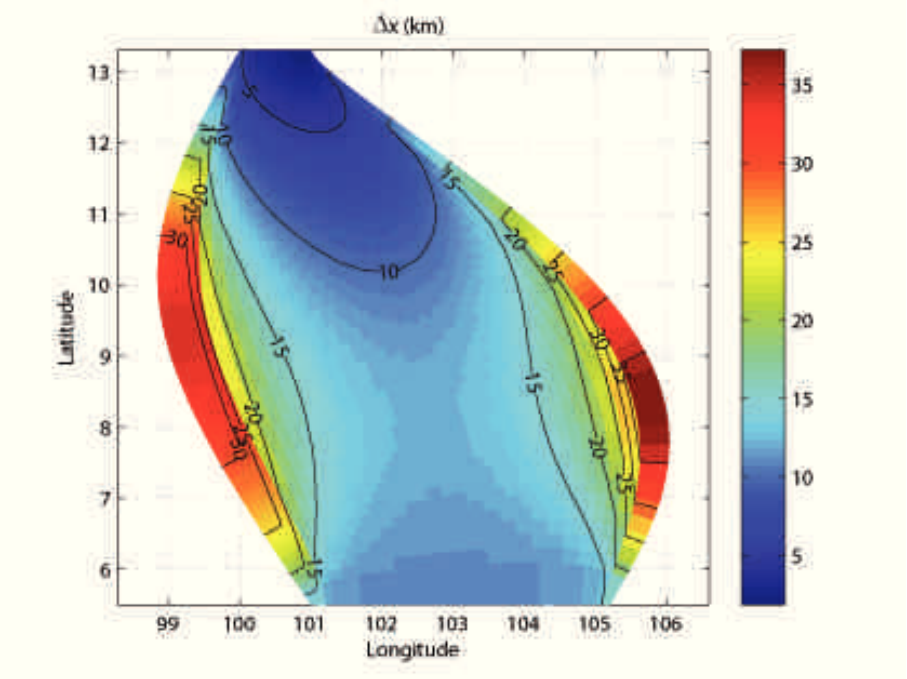

Figure 3.3 The grid spacing (km) in x direction.

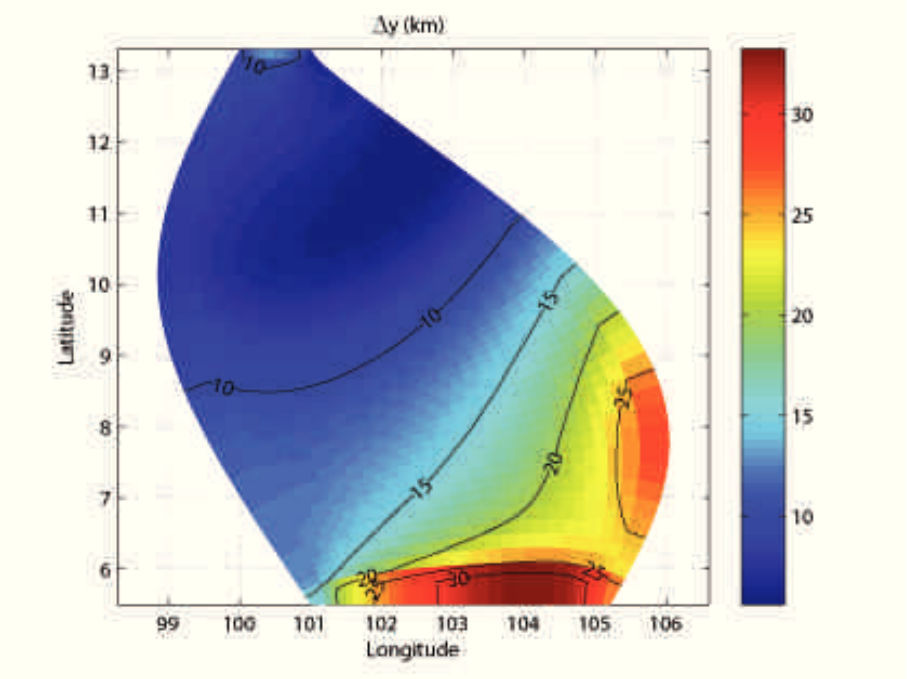

Figure 3.4 The grid spacing (km) in y direction.

3.2 Sigma Levels

Since the values of current velocities, temperature, salinity, and density depend on layer levels of depth of seawater, the vertical coordinate influences their values. In this research, we use the sigma coordinate in specifying levels of vertical coordinate. The number of vertical column of current velocities, temperature, salinity, and density in the sigma coordinate for this research are specified as 9 levels. At the first level of the sigma coordinate, σ_1, which is the seawater level at the surface elevation, the sigma value is equal to 0 and at the last level of the sigma coordinate, σ_{kb}, which is the seawater level at the bottom topography, the sigma value is equal to -1, where kb is the vertical grid index at the bottom, as shown in Fig. 3.5. The level $\sigma_{k+\frac{1}{2}}$ for $k = 1, 2, ..., kb-1$ in the figure is between levels σ_k and $\sigma_k + \frac{1}{2}$. For this research, kb is equal to 9. In determining the value σ at each level in seawater column depth, the formula for calculating the sigma value at each level is different. The interval of calculating the sigma value is divided to be 3 intervals. The first and second intervals of the seawater column depth are at the levels 2 to $kl1$ and $kl1+1$ to $kl2$, respectively, where $kl1$ and $kl2$ are the last level of the first and second intervals, respectively. While the third interval of the seawater column depth, there are different numbers of levels for the values σ_k and $\sigma_{k+\frac{1}{2}}$. The third interval of the values σ_k and $\sigma_{k+\frac{1}{2}}$ are at the levels $kl2+1$ to $kb-1$ and $kl2+\frac{3}{2}$ to $kb-\frac{3}{2}$, respectively. The sigma values at first and third intervals are determined via log distributions and at the second interval they are determined via linear distribution. The equations for calculating the values σ_k and $\sigma_{k+\frac{1}{2}}$ on the sigma coordinate are expressed as [5]

$$\sigma_k = -\frac{2e^{(k-2)ln(2)}}{(kl2-kl1+4)e^{(kl1-2)ln(2)}} \tag{3.1}$$

and

$$\sigma_{k+\frac{1}{2}} = -\frac{2e^{(k-1.50)ln(2)}}{(kl2-kl1+4)e^{(kl1-2)ln(2)}} \tag{3.2}$$

for the first interval,

$$\sigma_k = -\frac{k-kl1+2}{kl2-kl1+4} \tag{3.3}$$

and

$$\sigma_{k+\frac{1}{2}} = -\frac{k-kl1+2+0.50}{kl2-kl1+4} \tag{3.4}$$

for the second interval,

$$\sigma_k = \frac{2e^{(kb-k-1)ln(2)}}{(kl2-kl1+4)e^{(kb-kl2-1)ln(2)}} - 1 \tag{3.5}$$

and

$$\sigma_{k+\frac{1}{2}} = \frac{2e^{(kb-k-1.50)ln(2)}}{(kl2-kl1+4)e^{(kb-kl2-1)ln(2)}} - 1 \tag{3.6}$$

for the third interval, and

$$\sigma_{1+\frac{1}{2}} = -\frac{1}{(kl2-kl1+4)(e^{(kl1-2)ln(2)})}, \tag{3.7}$$

and

$$\sigma_{kb-\frac{1}{2}} = -1 + \frac{1}{(kl2 - kl1 + 4)(e^{(kb-kl2-1)ln(2)})} \tag{3.8}$$

for the first and last levels of the value $\sigma_{k+\frac{1}{2}}$.

In this research, $kl1$ and $kl2$ are specified as 4 and 7, respectively (Blumberg suggested $kl1 = 4$ and $kl2 = kb - 2$).

The total sigma levels for this research are expressed in Table 3.1.

Table 3.1 The sigma levels for the research.

k	σ_k	$\sigma_{k+\frac{1}{2}}$	$\Delta\sigma_k$	$\Delta\sigma_{k+\frac{1}{2}}$
1	0.0000	-0.0357	0.0714	0.0653
2	-0.0714	-0.1010	0.0714	0.1010
3	-0.1429	-0.2020	0.1429	0.1551
4	-0.2857	-0.3571	0.1429	0.1429
5	-0.4286	-0.5000	0.1429	0.1429
6	-0.5714	-0.6429	0.1429	0.1551
7	-0.7143	-0.7980	0.1429	0.1306
8	-0.8571	-0.9286	0.1429	
9	-1.0000			

The values $\Delta\sigma_k$, which is the difference between the values σ_k and σ_{k+1}, and $\Delta\sigma_{k+\frac{1}{2}}$, which is the difference between the values $\sigma_{k+\frac{1}{2}}$ and $\sigma_{k+\frac{3}{2}}$, are obtained from

$$\Delta\sigma_k = \sigma_k - \sigma_{k+1} \tag{3.9}$$

for $k = 1, 2, ..., 8$ and

$$\Delta\sigma_{k+\frac{1}{2}} = \sigma_{k+\frac{1}{2}} - \sigma_{k+\frac{3}{2}} \tag{3.10}$$

for $k = 1, 2, ..., 7$.

3.3 Transformation of Coordinates

A main goal for this research is to solve the primitive equations in order to determine the current velocities, temperature, salinity, and density. Since in this research, we use the sigma coordinate in dealing with the significant topographical variability that encountered in estuaries and slopes, the primitive equations are transformed from Cartesian to sigma coordinates, which are based on the transformation

$$x^* = x, \tag{3.11}$$

$$y^* = y, \tag{3.12}$$

$$\sigma = \frac{z - \eta(x, y, t)}{D(x, y, t)}, \tag{3.13}$$

and

$$t^* = t \tag{3.14}$$

where

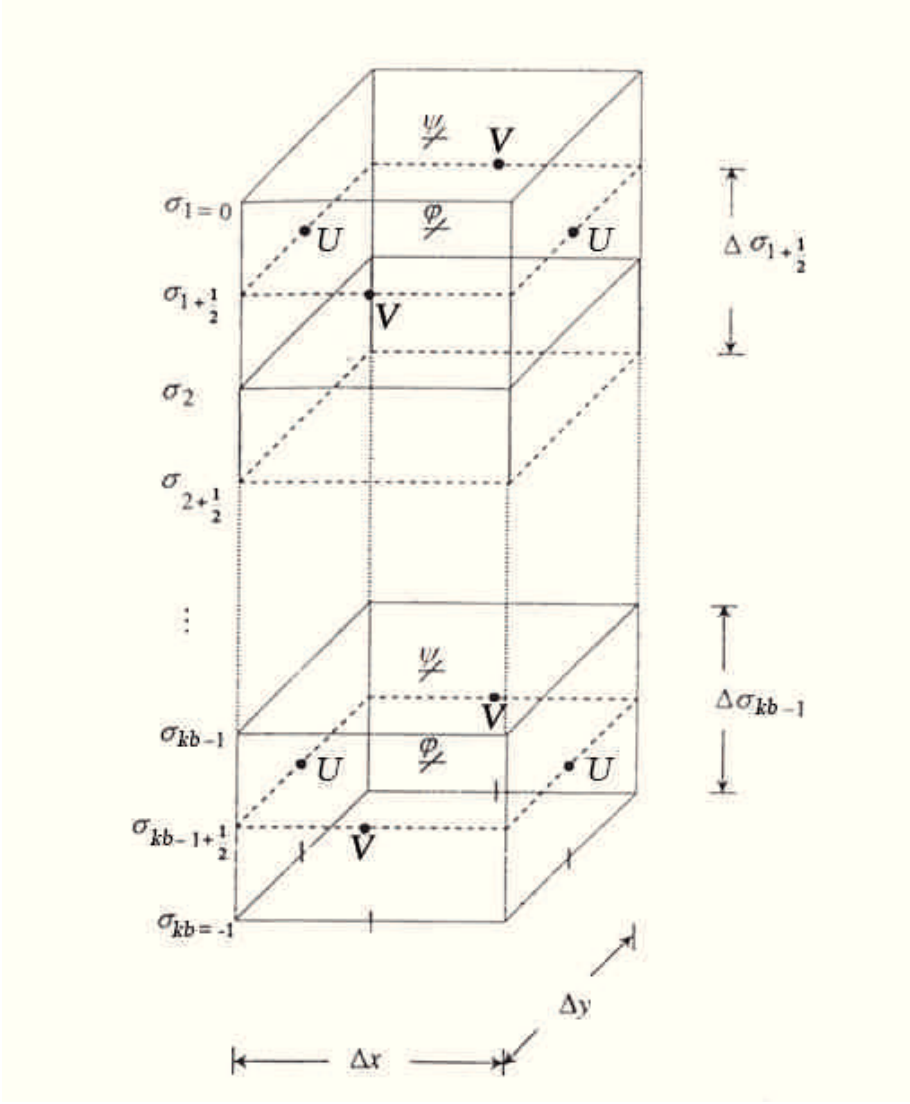

Figure 3.5 The sigma levels and the locations of variables on the finite difference grid. The variable φ represents T, S, and ρ and the variable ψ represents ω, K_M, and K_H. [16]

x, y, and z are the conventional Cartesian coordinates;
t is the time;
$D(x, y, t) = H(x, y) + \eta(x, y, t)$ is the seawater column depth;
$H(x, y)$ is the bottom topography, and
$\eta(x, y, t)$ is the surface elevation.

Let us consider an arbitrary variable, $\phi(x, y, z, t)$, in Cartesian coordinate system. The relationship linking in Cartesian coordinate system to a new variable in sigma coordinate system can be written as

$$\phi(x, y, z, t) = \phi^*(x^*, y^*, \sigma, t^*). \tag{3.15}$$

The chain rule for ϕ is

$$\frac{\partial \phi}{\partial x} = \frac{\partial \phi^*}{\partial x^*} + \frac{\partial \phi^*}{\partial \sigma}\frac{\partial \sigma}{\partial x} = \frac{\partial \phi^*}{\partial x^*} - \frac{\partial \phi^*}{\partial \sigma}\frac{1}{D}\left(\frac{\partial \eta}{\partial x} + \sigma\frac{\partial D}{\partial x}\right), \tag{3.16}$$

$$\frac{\partial \phi}{\partial y} = \frac{\partial \phi^*}{\partial y^*} + \frac{\partial \phi^*}{\partial \sigma}\frac{\partial \sigma}{\partial y} = \frac{\partial \phi^*}{\partial y^*} - \frac{\partial \phi^*}{\partial \sigma}\frac{1}{D}\left(\frac{\partial \eta}{\partial y} + \sigma\frac{\partial D}{\partial y}\right), \tag{3.17}$$

$$\frac{\partial \phi}{\partial t} = \frac{\partial \phi^*}{\partial t^*} + \frac{\partial \phi^*}{\partial \sigma}\frac{\partial \sigma}{\partial t} = \frac{\partial \phi^*}{\partial t^*} - \frac{\partial \phi^*}{\partial \sigma}\frac{1}{D}\left(\frac{\partial \eta}{\partial t} + \sigma\frac{\partial D}{\partial t}\right), \tag{3.18}$$

and

$$\frac{\partial \phi}{\partial z} = \frac{\partial \phi^*}{\partial \sigma}\frac{1}{D}. \tag{3.19}$$

For the transformation from Cartesian vertical velocity, W, to sigma vertical velocity, ω, it is defined as

$$W = \omega + U\left(\sigma\frac{\partial D}{\partial x} + \frac{\partial \eta}{\partial x}\right) + V\left(\sigma\frac{\partial D}{\partial y} + \frac{\partial \eta}{\partial y}\right) + \sigma\frac{\partial D}{\partial t} + \frac{\partial \eta}{\partial t}. \tag{3.20}$$

We apply relationships in Eqs. (3.11) to (3.20) to transform the primitive equations in Cartesian to sigma coordinates. The derivation of the primitive equations in sigma coordinate can be seen in Appendix. After conversion to sigma coordinate, all asterisks will be dropped for notation convenience. The primitive equations in sigma coordinate can be written as

$$\frac{\partial DU}{\partial x} + \frac{\partial DV}{\partial y} + \frac{\partial \omega}{\partial \sigma} + \frac{\partial \eta}{\partial t} = 0, \tag{3.21}$$

$$\begin{aligned}&\frac{\partial UD}{\partial t} + \frac{\partial U^2 D}{\partial x} + \frac{\partial UVD}{\partial y} + \frac{\partial U\omega}{\partial \sigma} - fVD + gD\frac{\partial \eta}{\partial x}\\ &+\frac{gD^2}{\rho_0}\int_\sigma^0 \left[\frac{\partial \rho'}{\partial x} - \frac{\sigma'}{D}\frac{\partial D}{\partial x}\frac{\partial \rho'}{\partial \sigma'}\right] d\sigma' = \frac{\partial}{\partial \sigma}\left[\frac{K_M}{D}\frac{\partial U}{\partial \sigma}\right] + F_x,\end{aligned} \tag{3.22}$$

$$\begin{aligned}&\frac{\partial VD}{\partial t} + \frac{\partial UVD}{\partial x} + \frac{\partial V^2 D}{\partial y} + \frac{\partial V\omega}{\partial \sigma} + fUD + gD\frac{\partial \eta}{\partial y}\\ &+\frac{gD^2}{\rho_0}\int_\sigma^0 \left[\frac{\partial \rho'}{\partial y} - \frac{\sigma'}{D}\frac{\partial D}{\partial y}\frac{\partial \rho'}{\partial \sigma'}\right] d\sigma' = \frac{\partial}{\partial \sigma}\left[\frac{K_M}{D}\frac{\partial V}{\partial \sigma}\right] + F_y,\end{aligned} \tag{3.23}$$

$$\frac{\partial TD}{\partial t} + \frac{\partial TUD}{\partial x} + \frac{\partial TVD}{\partial y} + \frac{\partial T\omega}{\partial \sigma} = \frac{\partial}{\partial \sigma}\left[\frac{K_H}{D}\frac{\partial T}{\partial \sigma}\right] + F_T, \tag{3.24}$$

and

$$\frac{\partial SD}{\partial t} + \frac{\partial SUD}{\partial x} + \frac{\partial SVD}{\partial y} + \frac{\partial S\omega}{\partial \sigma} = \frac{\partial}{\partial \sigma}\left[\frac{K_H}{D}\frac{\partial S}{\partial \sigma}\right] + F_S, \tag{3.25}$$

where

U and V are the horizontal velocities in x- and y-directions, respectively;
D is the seawater column depth;
ω is the velocity component normal to sigma surfaces;
η is the surface elevation;
x and y are the eastward and northward directions, respectively;
σ is the upward direction in sigma coordinate;
t is the time;
f is the curvature and Coriolis terms, which the Coriolis term is equal to $2\Omega \sin\varphi$;
Ω is the angular rotation rate of the Earth; φ is the latitude;
g is the gravitational acceleration;

ρ_0 is the reference seawater density:
ρ' is the seawater density:
K_M is the vertical kinematic viscosity;
F_x and F_y are the horizontal viscosity terms;
T is the potential temperature;
S is the salinity;
K_H is the vertical diffusivity, and
F_T and F_S are the horizontal diffusion terms.

The horizontal viscosity and diffusion terms are defined according to

$$F_x = \frac{\partial}{\partial x}\left(2DA_M\frac{\partial U}{\partial x}\right) + \frac{\partial}{\partial y}\left[DA_M\left(\frac{\partial U}{\partial y} + \frac{\partial V}{\partial x}\right)\right], \tag{3.26}$$

$$F_y = \frac{\partial}{\partial y}\left(2DA_M\frac{\partial V}{\partial y}\right) + \frac{\partial}{\partial x}\left[DA_M\left(\frac{\partial U}{\partial y} + \frac{\partial V}{\partial x}\right)\right], \tag{3.27}$$

$$F_T = \frac{\partial}{\partial x}\left(HA_H\frac{\partial T}{\partial x}\right) + \frac{\partial}{\partial y}\left(HA_H\frac{\partial T}{\partial y}\right), \tag{3.28}$$

and

$$F_S = \frac{\partial}{\partial x}\left(HA_H\frac{\partial S}{\partial x}\right) + \frac{\partial}{\partial y}\left(HA_H\frac{\partial S}{\partial y}\right) \tag{3.29}$$

where A_M is the horizontal kinematic viscosity and A_H is the horizontal heat diffusivity.

The horizontal kinematic viscosity is calculated from the Smagorinsky formula, which is

$$A_M = C\Delta x\Delta y\frac{1}{2}\left[\left(\frac{\partial U}{\partial x}\right)^2 + \left(\frac{\partial V}{\partial y}\right)^2 + \left(\frac{\partial V}{\partial x} + \frac{\partial U}{\partial y}\right)^2/2\right]^{1/2} \tag{3.30}$$

where C is the coefficient of the Smagorinsky diffusivity. For the horizontal heat diffusivity, it is calculated from

$$A_H = TPRNI \times A_M \tag{3.31}$$

where $TPRNI$ is the inverse horizontal turbulent Prandtl number.

3.4 Vertical Boundary Conditions

The vertical boundary conditions for Eq. (3.21) are

$$\omega(0) = 0 \tag{3.32}$$

and

$$\omega(-1) = 0. \tag{3.33}$$

The surface boundary conditions for Eqs. (3.22) and (3.23) are

$$\frac{K_M}{D}\frac{\partial U}{\partial \sigma} = - < wu(0) > \tag{3.34}$$

and

$$\frac{K_M}{D}\frac{\partial V}{\partial \sigma} = - < wv(0) >, \tag{3.35}$$

respectively, where $< wu(0) >$ and $< wv(0) >$ are the input values of the surface turbulence momentum fluxes.

The bottom boundary conditions for Eqs. (3.22) and (3.23) are

$$\frac{K_M}{D}\frac{\partial U}{\partial \sigma} = C_z[U^2 + V^2]^{1/2}U \tag{3.36}$$

and

$$\frac{K_M}{D}\frac{\partial V}{\partial \sigma} = C_z[U^2 + V^2]^{1/2}V, \tag{3.37}$$

respectively, where

$$C_z = MAX\left[\frac{\kappa^2}{[ln(1+\sigma_{kb-1})H/z_0]^2}, 0.0025\right] \tag{3.38}$$

is the drag coefficient. κ is the von Karman constant and z_0 is the roughness parameter.

The surface boundary conditions for Eqs. (3.24) and (3.25) are

$$\frac{K_H}{D}\frac{\partial T}{\partial \sigma} = - < wt(0) > \tag{3.39}$$

and

$$\frac{K_H}{D}\frac{\partial S}{\partial \sigma} = - < ws(0) >, \tag{3.40}$$

respectively, where $< wt(0) >$ and $< ws(0) >$ are the temperature and salinity fluxes at the surface, respectively.

The bottom boundary conditions for Eqs. (3.24) and (3.25) are

$$\frac{K_H}{D}\frac{\partial T}{\partial \sigma} = 0 \tag{3.41}$$

and

$$\frac{K_H}{D}\frac{\partial S}{\partial \sigma} = 0, \tag{3.42}$$

respectively.

3.5 The Vertically Integrated Equations

The equations, governing the dynamics of coastal circulation, contain fast moving external gravity waves and slow moving internal gravity waves. The vertically integrated equations (external mode) are separated from the vertical structure equations (internal mode). This technique, known as mode splitting [14;22], permits the calculation of the free surface elevation with little sacrifice in computational time by solving the velocity transport separately from the three-dimensional calculation of the velocity and the thermodynamic properties.

The velocity external mode equations are obtained by integrating the internal mode equations over the depth, thereby eliminating all vertical structure. The equations (3.21), (3.22), and (3.23) are integrated from $\sigma = -1$ to $\sigma = 0$ and use the specified vertical boundary conditions.

The velocity external mode equations are expressed as

$$\frac{\partial D\overline{U}}{\partial x} + \frac{\partial D\overline{V}}{\partial y} + \frac{\partial \eta}{\partial t} = 0, \tag{3.43}$$

$$\frac{\partial \overline{U}D}{\partial t} + \frac{\partial \overline{U^2}D}{\partial x} + \frac{\partial \overline{UV}D}{\partial y} - f\overline{V}D + gD\frac{\partial \eta}{\partial x} + \frac{gD}{\rho_0}\int_{-1}^{0}\int_{\sigma}^{0}\left[D\frac{\partial \rho'}{\partial x} - \sigma'\frac{\partial D}{\partial x}\frac{\partial \rho'}{\partial \sigma'}\right]d\sigma' d\sigma$$
$$= - < wu(0) > + < wu(-1) > + \overline{F}_x, \tag{3.44}$$

and

$$\frac{\partial \overline{V}D}{\partial t} + \frac{\partial \overline{UV}D}{\partial x} + \frac{\partial \overline{V^2}D}{\partial y} + f\overline{U}D + gD\frac{\partial \eta}{\partial y} + \frac{gD}{\rho_0}\int_{-1}^{0}\int_{\sigma}^{0}\left[D\frac{\partial \rho'}{\partial y} - \sigma'\frac{\partial D}{\partial y}\frac{\partial \rho'}{\partial \sigma'}\right]d\sigma' d\sigma$$
$$= - < wv(0) > + < wv(-1) > + \overline{F}_y \tag{3.45}$$

where $\overline{U}$ and $\overline{V}$ are the vertically integrated velocities in the x and y directions, respectively, which are expressed as

$$\overline{U} = \int_{-1}^{0} U d\sigma \tag{3.46}$$

and

$$\overline{V} = \int_{-1}^{0} V d\sigma. \tag{3.47}$$

3.6 Staggered Grid

A mathematical technique used to solve the primitive equations is the finite difference method. The study domain is discretized using a staggered grid. The different unknown variables are not located at the same grid points. The staggered grid arrangement for this research is depicted in Fig. 3.5 and 3.6, which is called C-grid. In plan view, the grid locations of temperature and salinity are as same as the model grid, but the grid locations of horizontal current velocities are not as same as the model grid. The locations of $U_{i,j,k}$, $U_{i+1,j,k}$, $V_{i,j,k}$, and $V_{i,j+1,k}$ are on grid points at the position $(i - \frac{1}{2}, j, k)$, $(i + \frac{1}{2}, j, k)$, $(i, j - \frac{1}{2}, k)$, and $(i, j + \frac{1}{2}, k)$ of the model grid, respectively. For elevation view, the grid locations of the vertical current velocity are at levels σ_k directly, but the grid locations of the other are at levels $\sigma_{k+\frac{1}{2}}$.

3.7 Initial Data

Initial data are prepared for solving the primitive equations. They consist of bottom topography, climatological monthly mean wind, and climatological monthly mean temperature and salinity. These data need to be on all grid points of the model grid

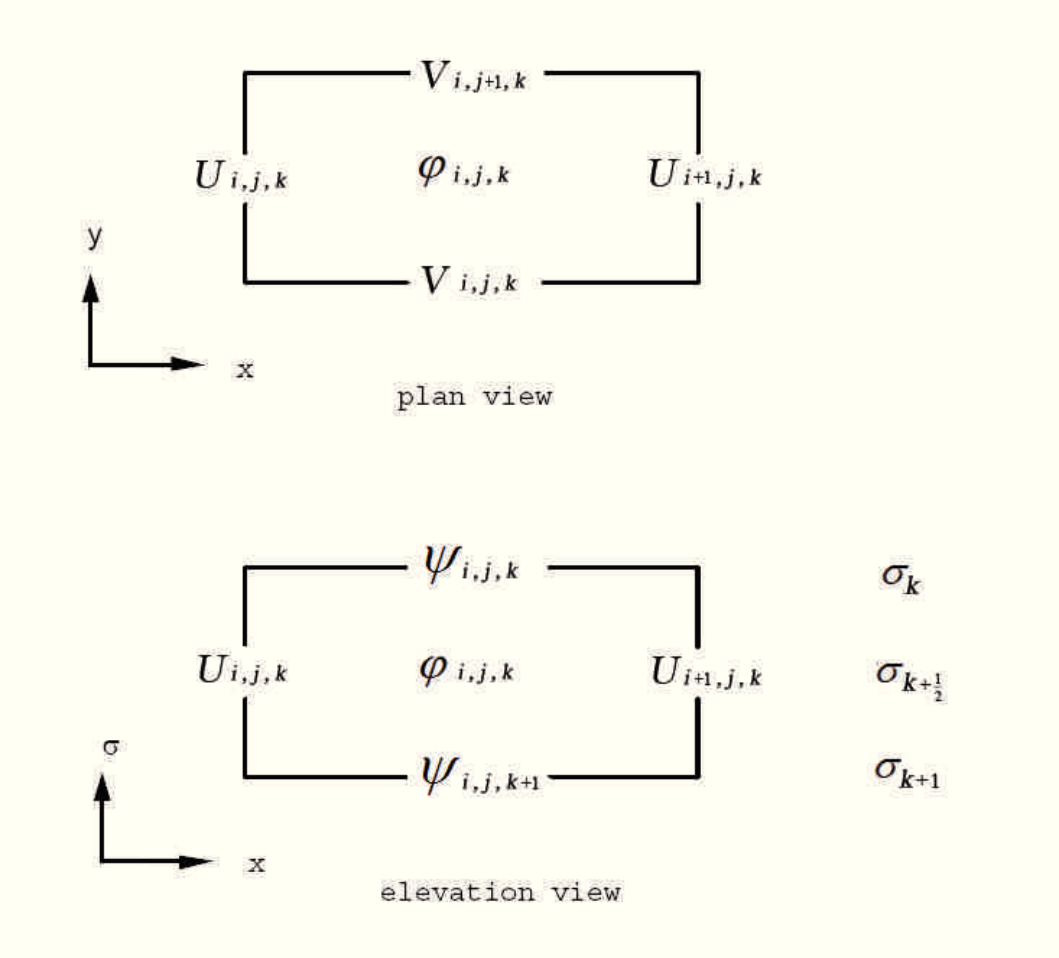

Figure 3.6 The staggered grid. The variable φ represents T, S, and ρ and the variable ψ represents ω, K_M, and K_H. [16]

in order to be able to calculate current velocities, temperature, salinity, and density at all grid points on the model grid, but these data cannot be on all grid points of the model grid because most data from observation do not cover at all points of domains. The available data consist of bottom topography, which is derived from Digital Bathymetric Data Base 5-minute (DBDB5) with 1/12 degree resolution for longitudes 98.125°E to 107.125°E and latitudes 4.875°N to 14.875°N, as shown in Fig. 3.7, climatological monthly mean wind, which is derived from the European Centre for Medium-Range Weather Forecasts (ECMWF) with 2.5 degree resolution for longitudes 95°E to 107.5°E and latitudes 2.5°N to 15°N, and climatological monthly mean temperature and salinity in 6 levels, which derived from Levitus94 with 1 degree resolution for longitudes 97.5°E to 106.5°E and latitudes 4.5°N to 15.5°N. The locations of wind and temperature and salinity are shown in Fig. 3.8 and 3.9, respectively, which the blue points are the locations of data.

Since these data are not on all grid points of the model grid, they have to be interpolated these data into the model grid in order to be the initial data using bilinear interpolations. For interpolating temperature and salinity in vertical levels of the sigma coordinate, they are interpolated via the cubic splines with boundary conditions of natural spline. The example results of interpolated data in each month are

shown in Fig. 3.10 to Fig. 3.58.

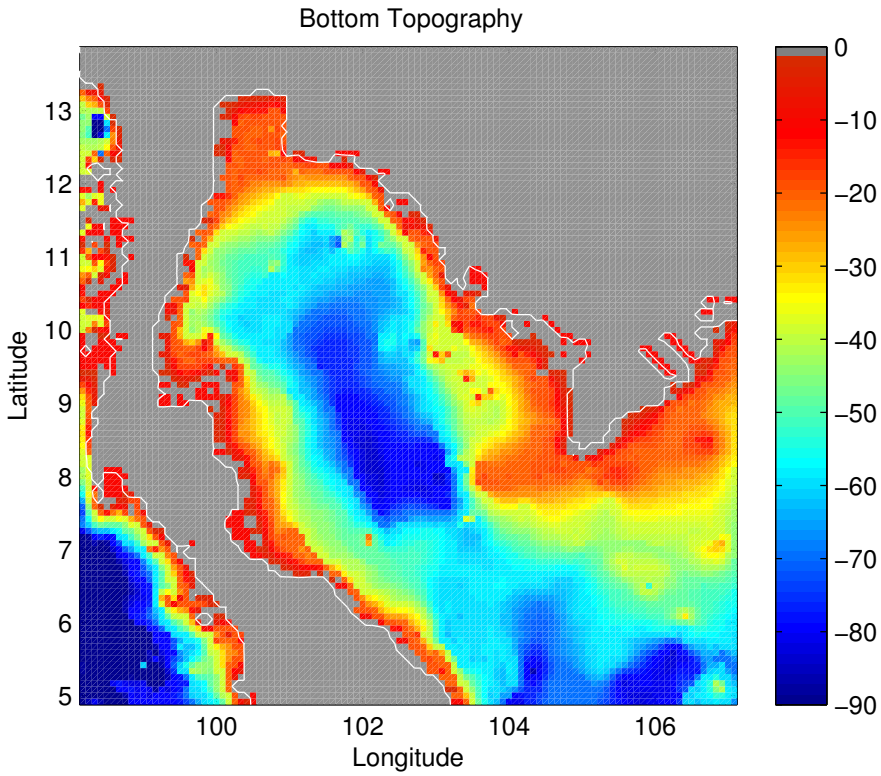

Figure 3.7 The bottom topography (m).

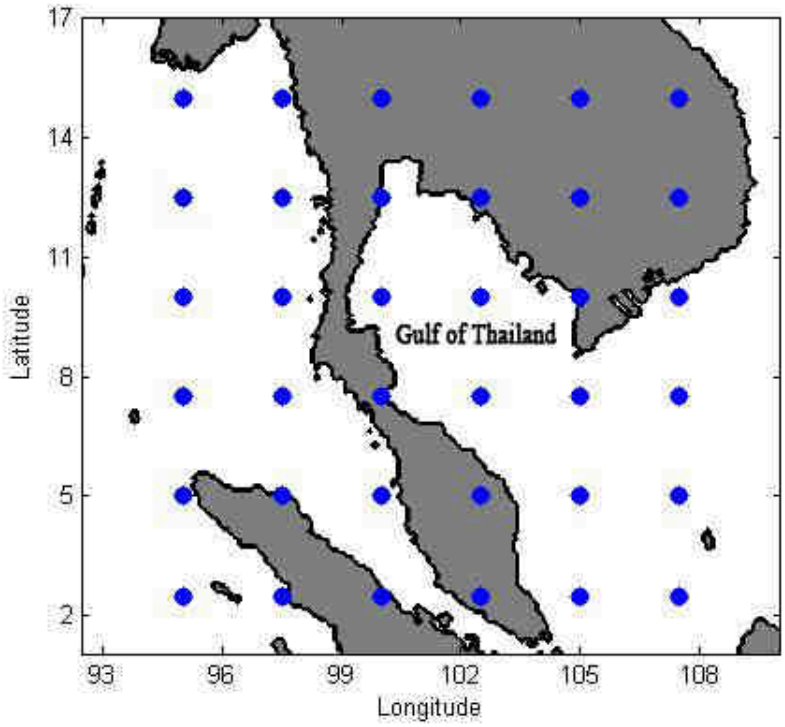

Figure 3.8 The locations of wind data.

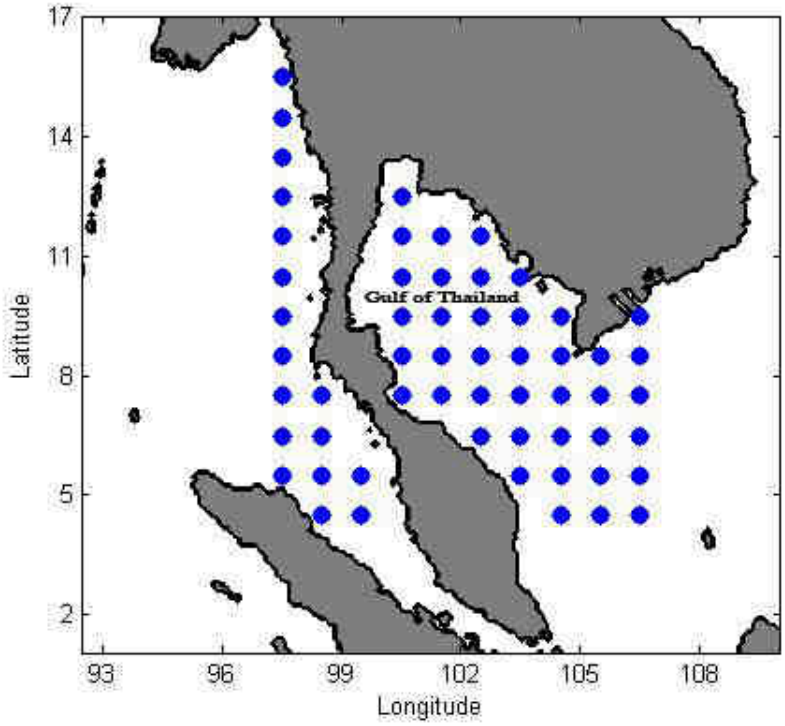

Figure 3.9 The locations of temperature and salinity data.

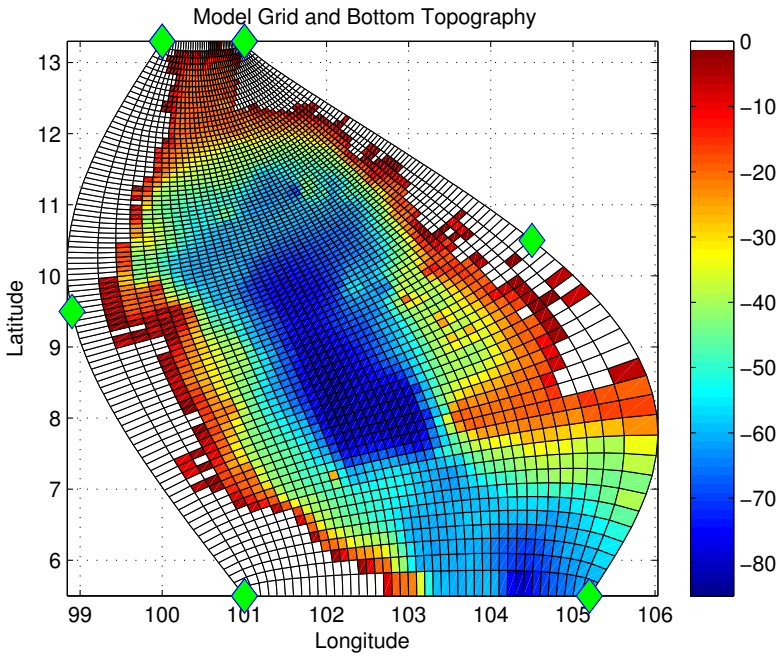

Figure 3.10 The Model grid and bottom topography (m).

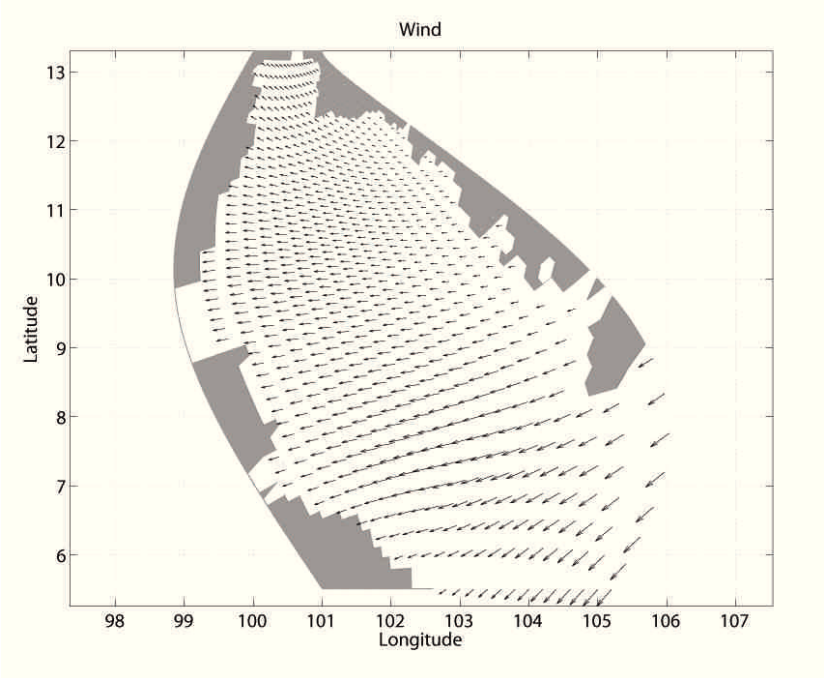

Figure 3.11 Wind in January. (Maximum speed is 7.4904 m/s.)

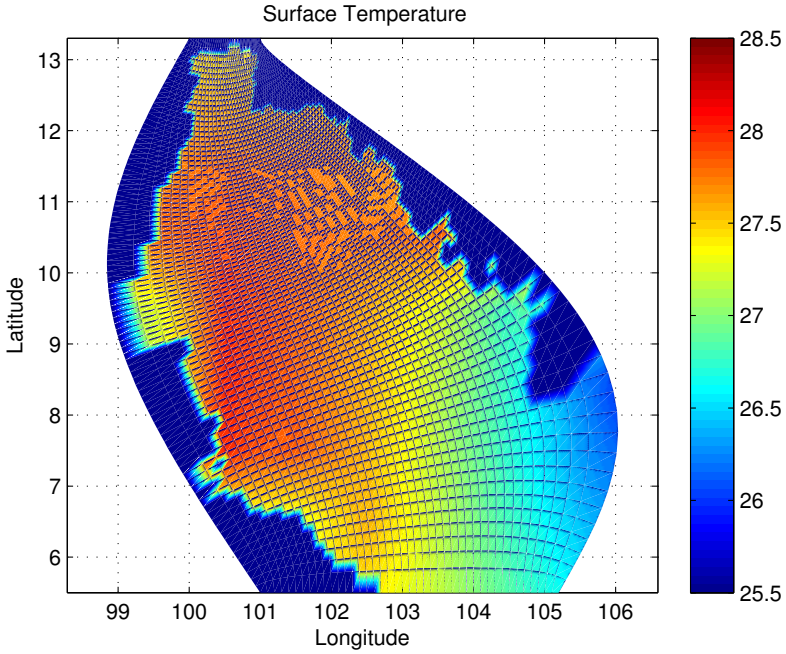

Figure 3.12 The surface temperature (°C) in January.

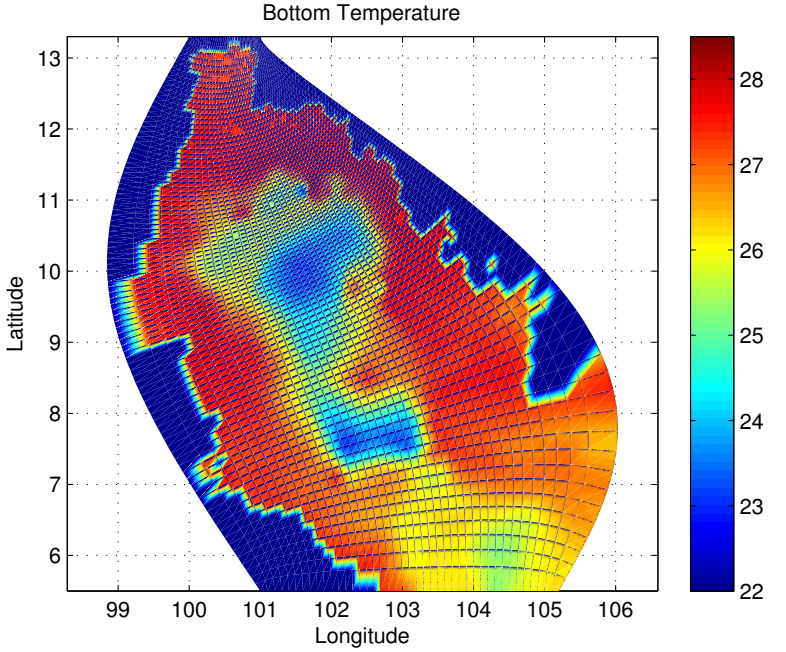

Figure 3.13 The bottom temperature (°C) in January.

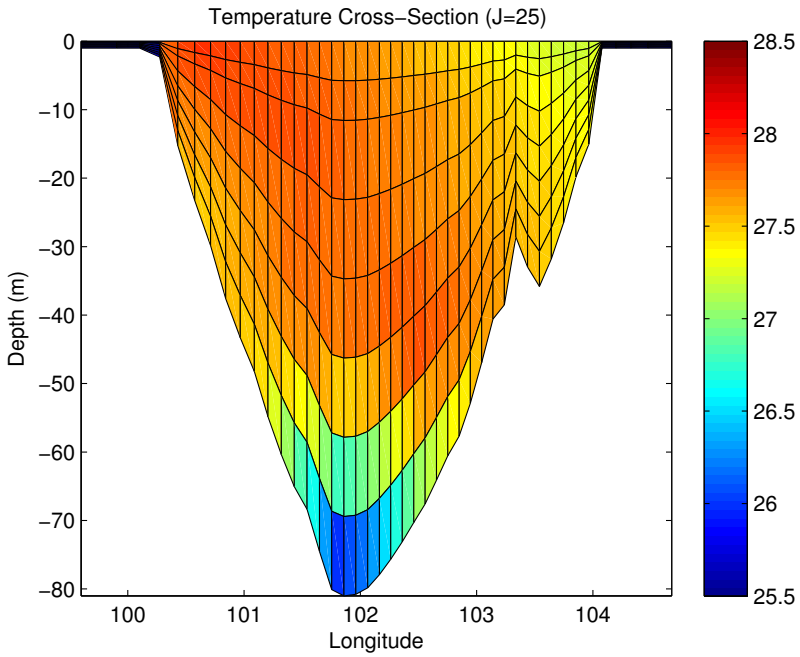

Figure 3.14 The temperature cross-section (°C) at J=25 in January.

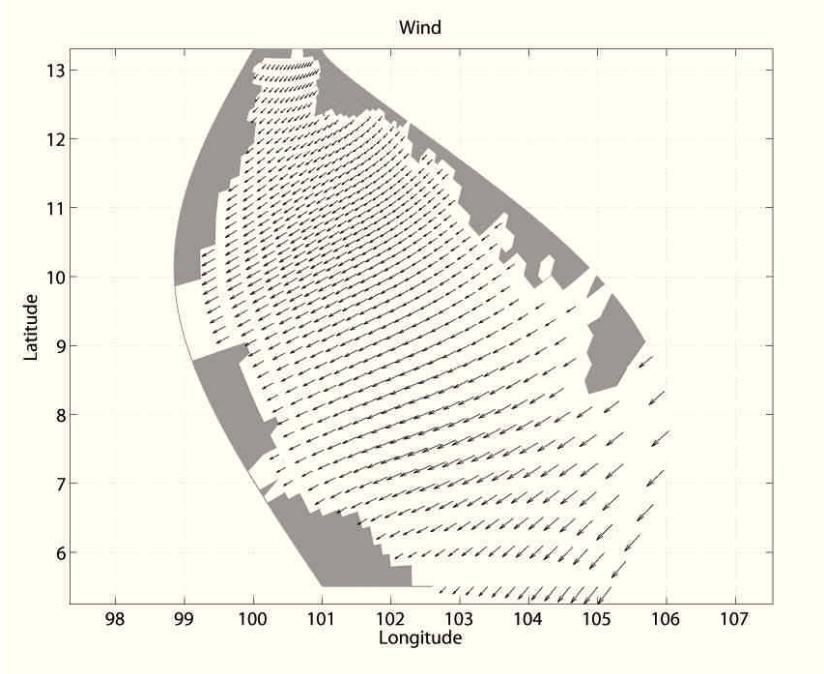

Figure 3.15 Wind in February. (Maximum speed is 5.9183 m/s.)

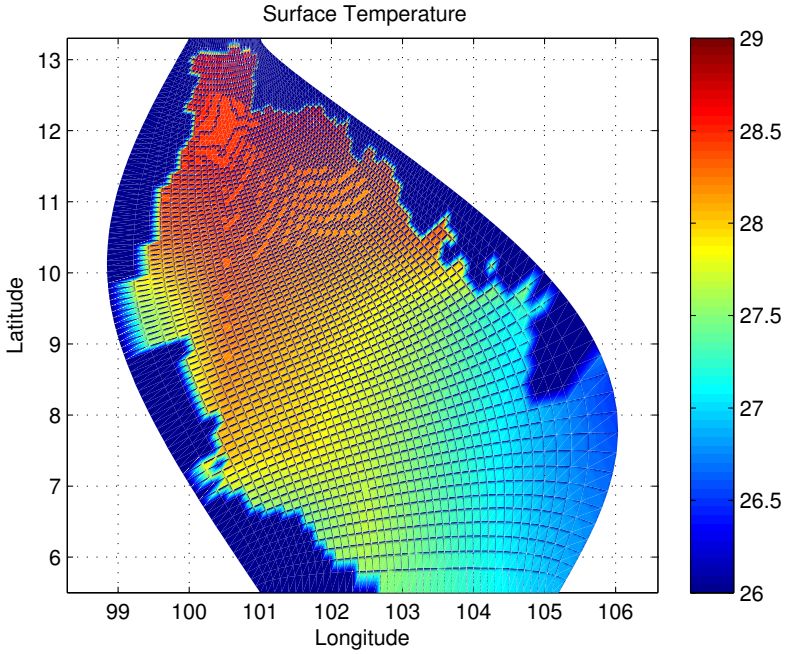

Figure 3.16 The surface temperature (°C) in February.

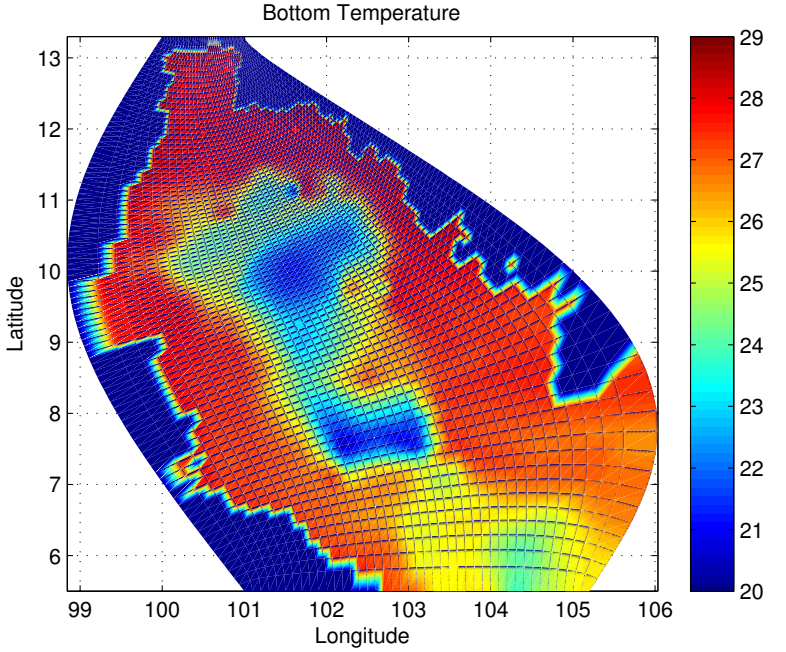

Figure 3.17 The bottom temperature (°C) in February.

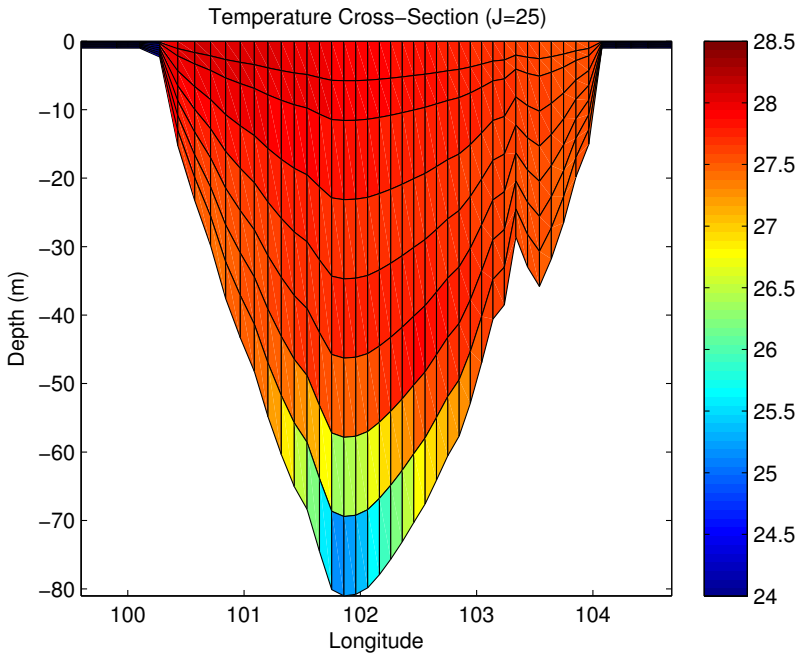

Figure 3.18 The temperature cross-section (°C) at J=25 in February.

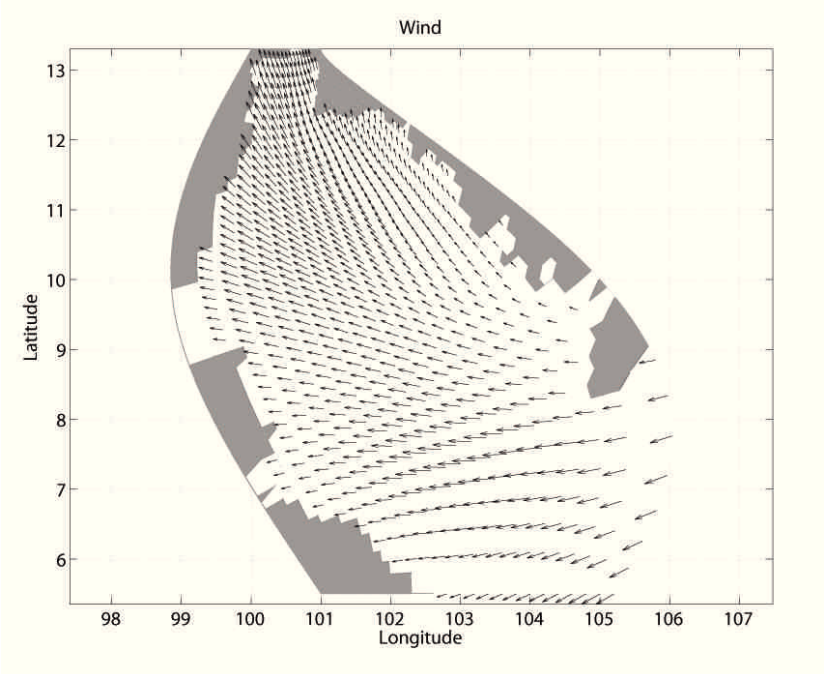

Figure 3.19 Wind in March. (Maximum speed is 5.2736 m/s.)

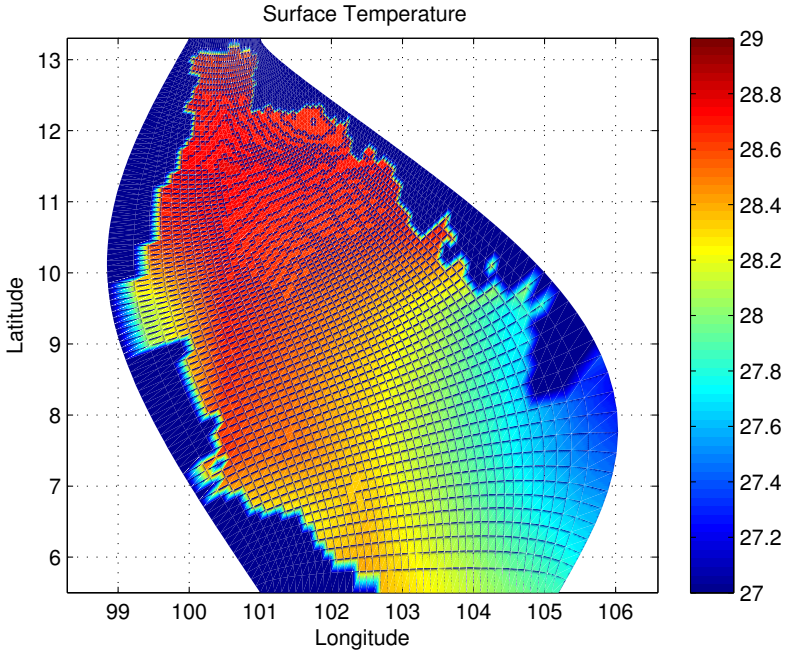

Figure 3.20 The surface temperature (°C) in March.

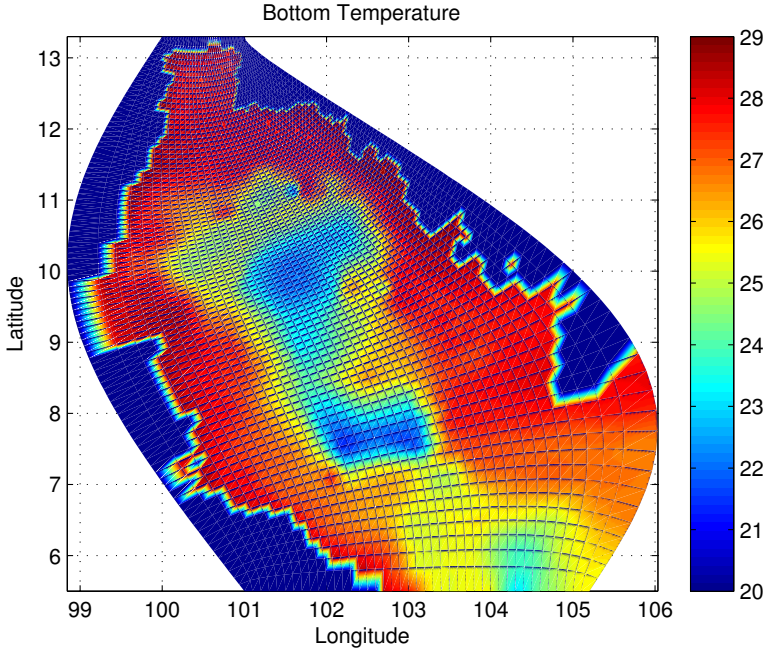

Figure 3.21 The bottom temperature (°C) in March.

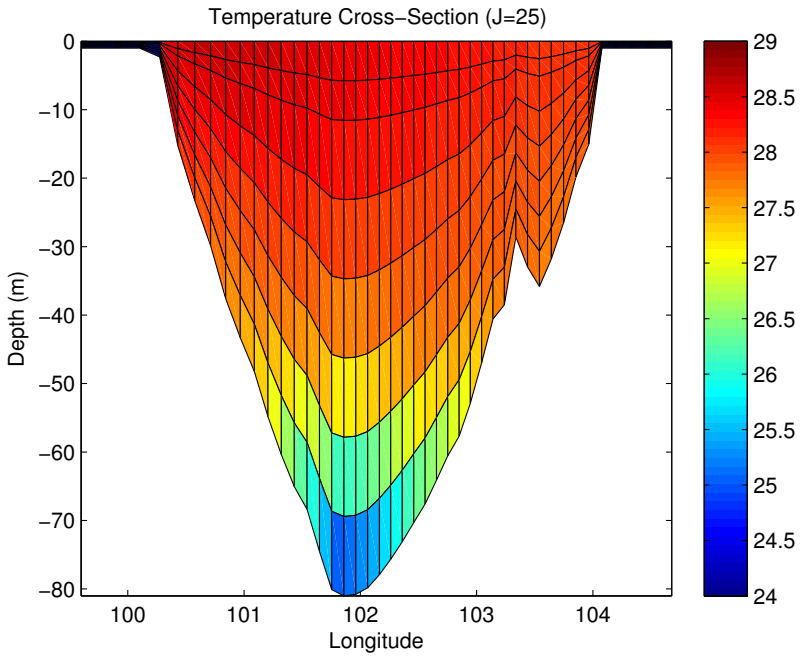

Figure 3.22 The temperature cross-section (°C) at J=25 in March.

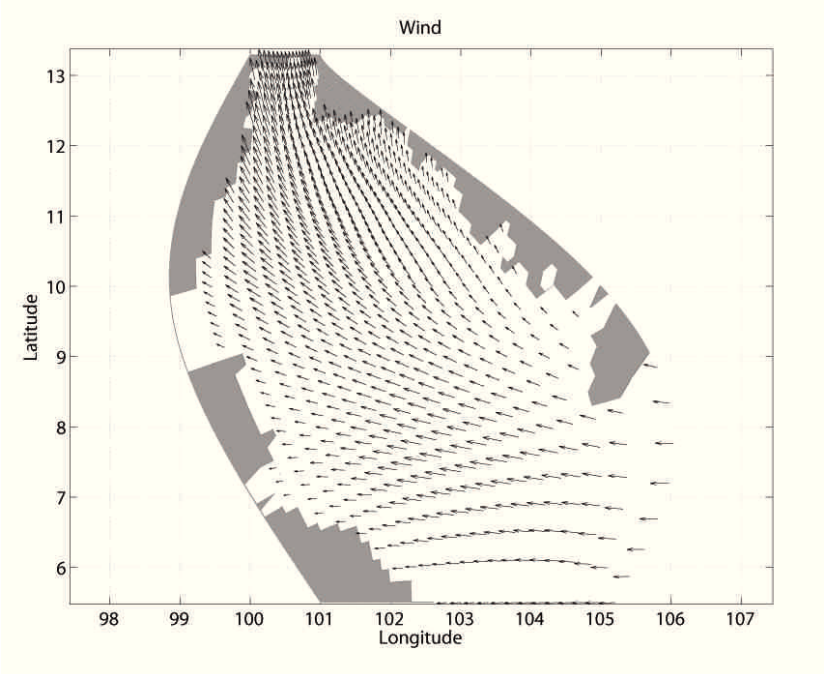

Figure 3.23 Wind in April. (Maximum speed is 3.5464 m/s.)

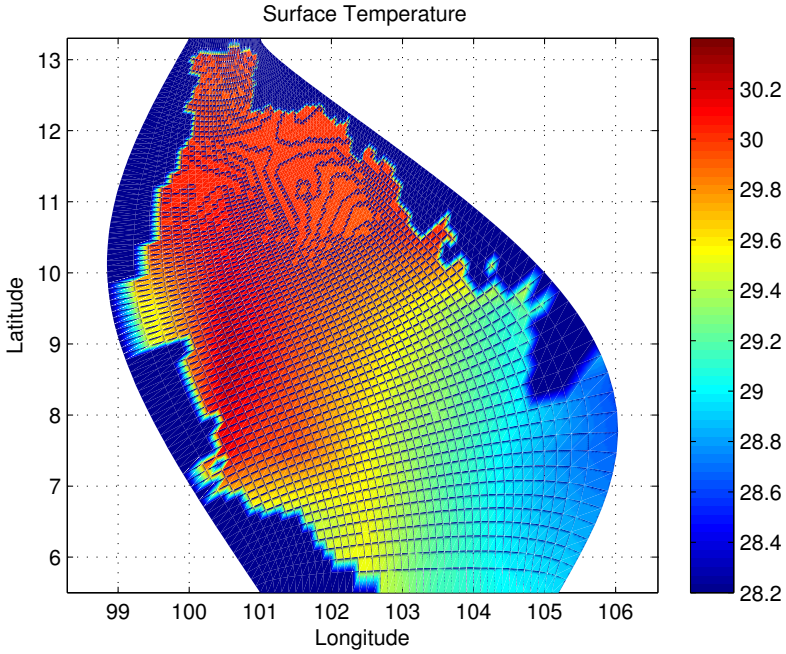

Figure 3.24 The surface temperature (°C) in April.

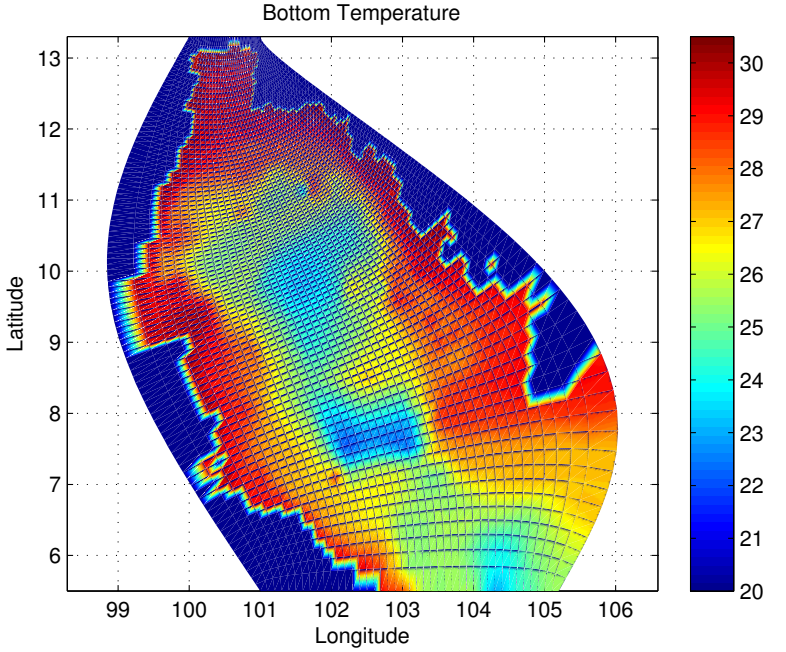

Figure 3.25 The bottom temperature (°C) in April.

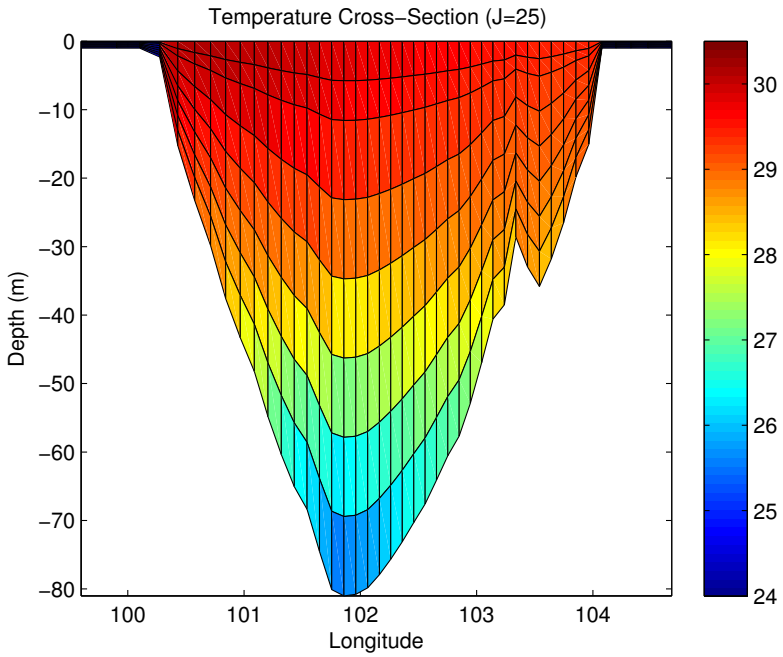

Figure 3.26 The temperature cross-section (°C) at J=25 in April.

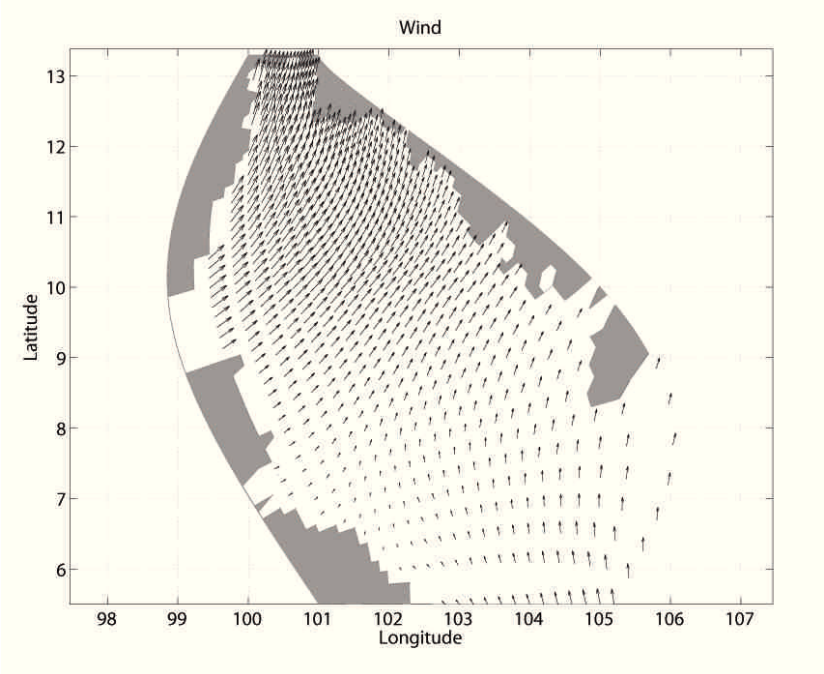

Figure 3.27 Wind in May. (Maximum speed is 3.0414 m/s.)

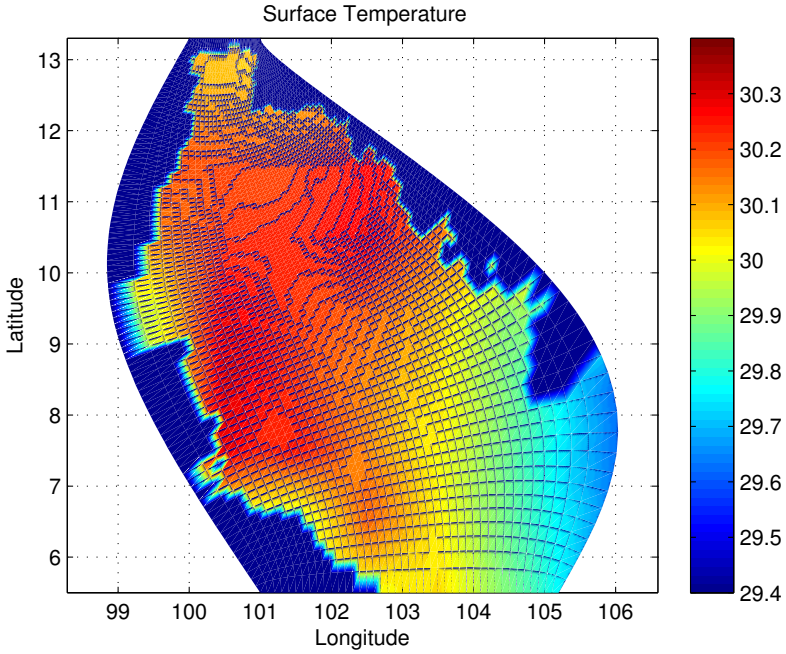

Figure 3.28 The surface temperature (°C) in May.

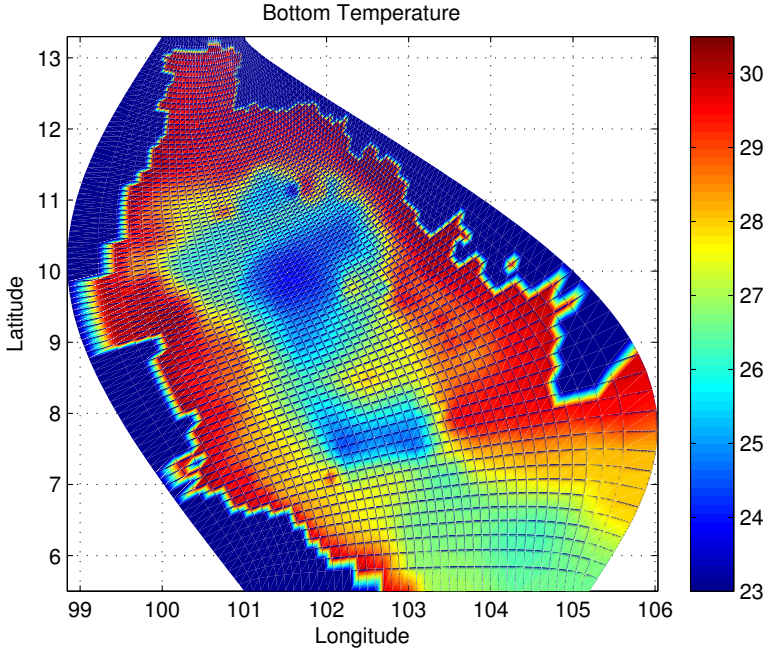

Figure 3.29 The bottom temperature (°C) in May.

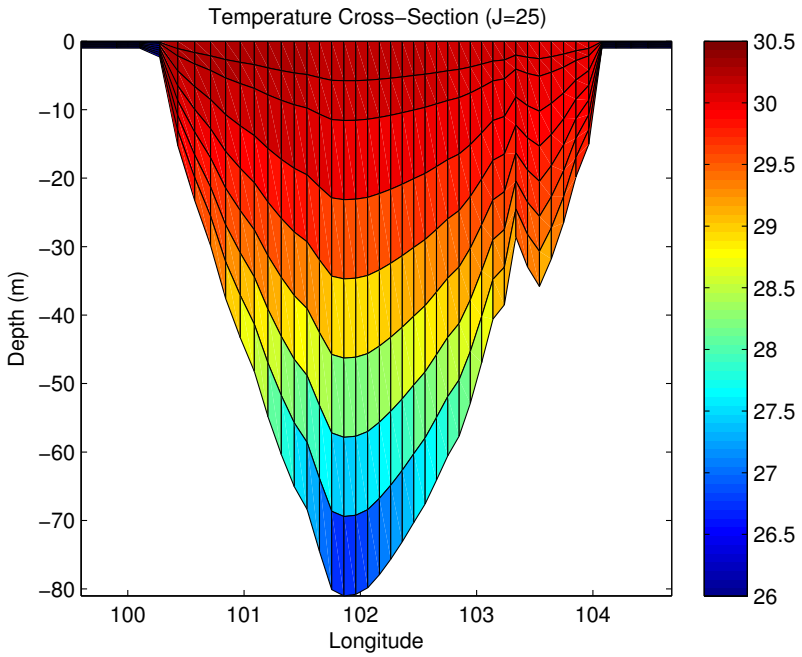

Figure 3.30 The temperature cross-section (°C) at J=25 in May.

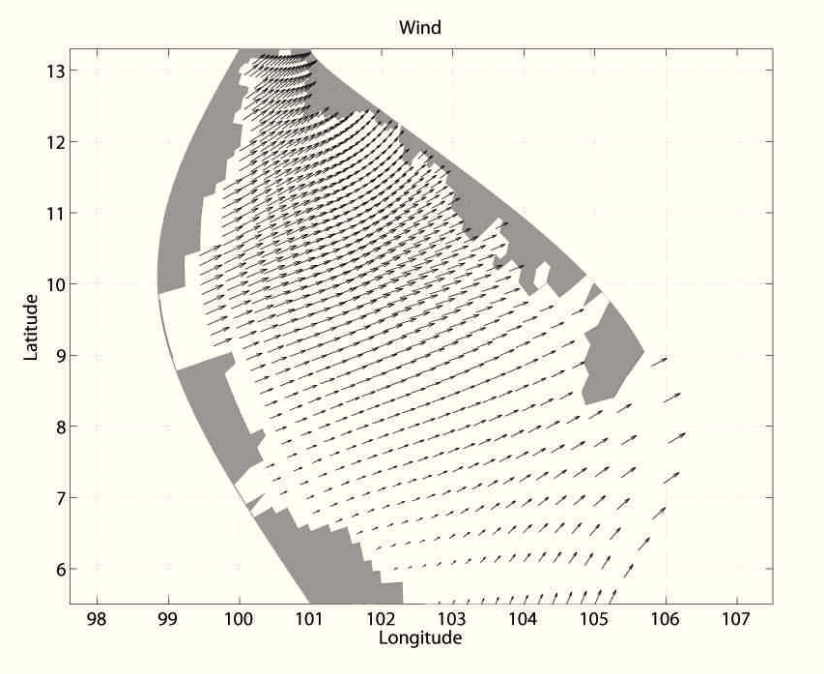

Figure 3.31 Wind in June. (Maximum speed is 5.0501 m/s.)

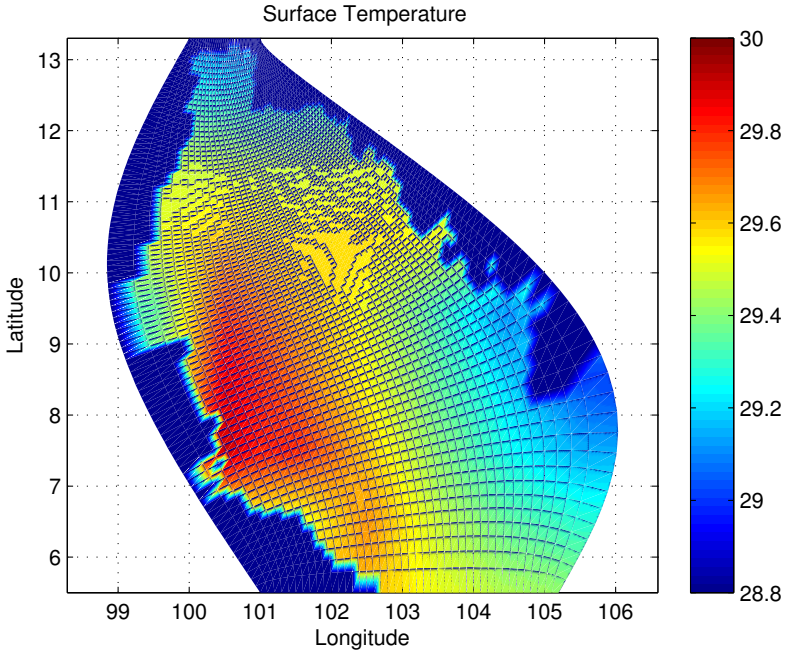

Figure 3.32 The surface temperature (°C) in June.

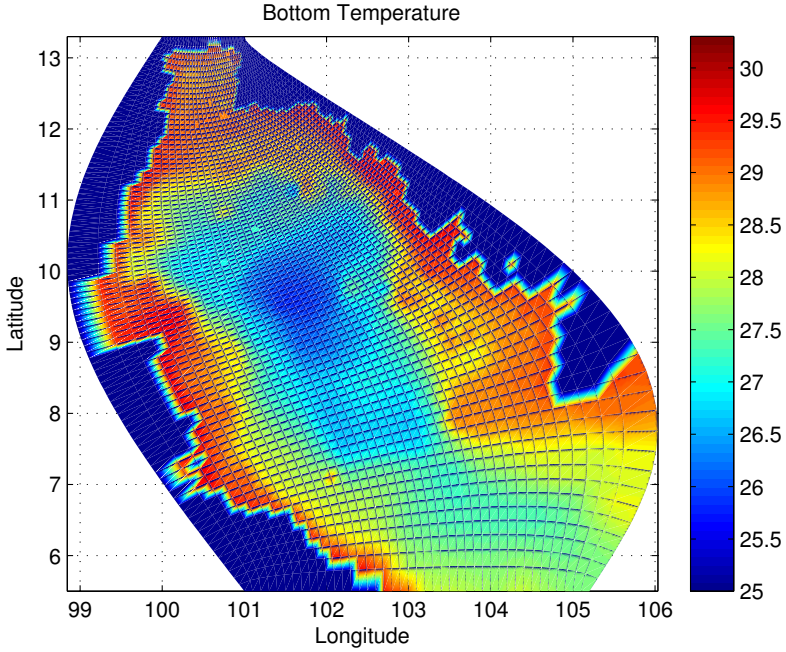

Figure 3.33 The bottom temperature (°C) in June.

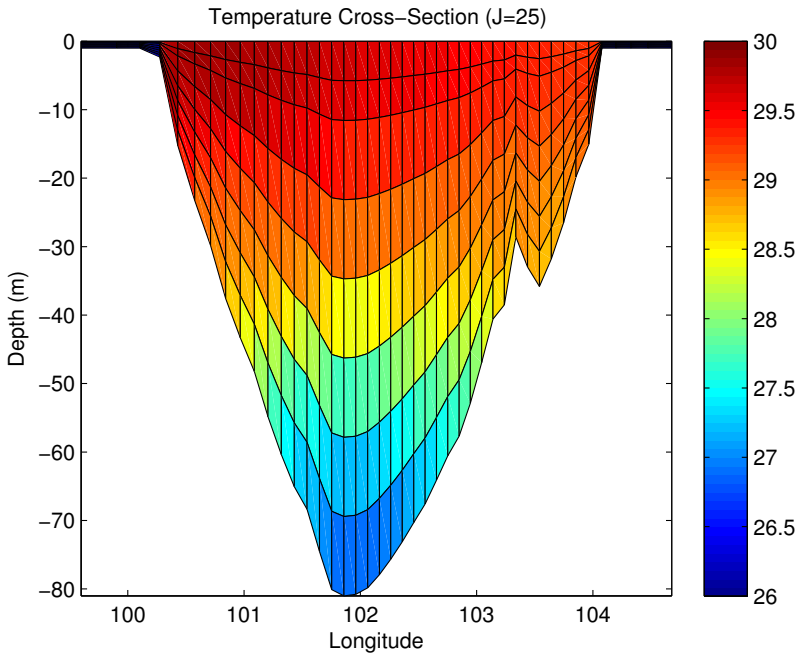

Figure 3.34 The temperature cross-section (°C) at J=25 in June.

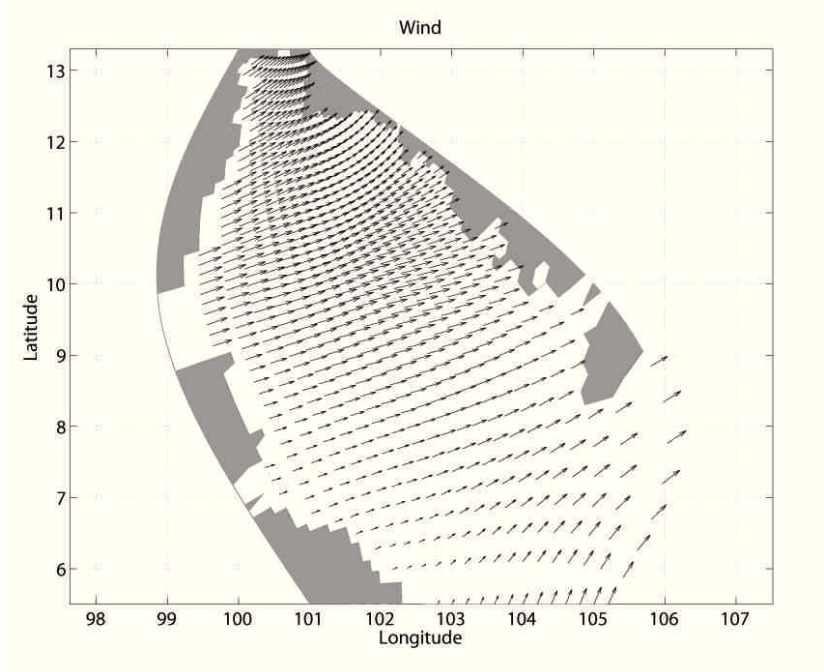

Figure 3.35 Wind in July. (Maximum speed is 4.9370 m/s.)

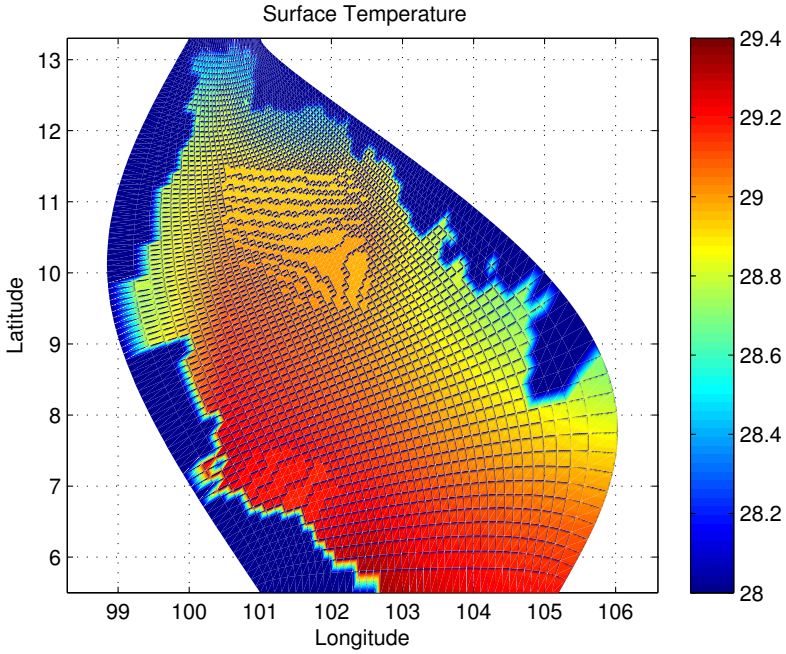

Figure 3.36 The surface temperature (°C) in July.

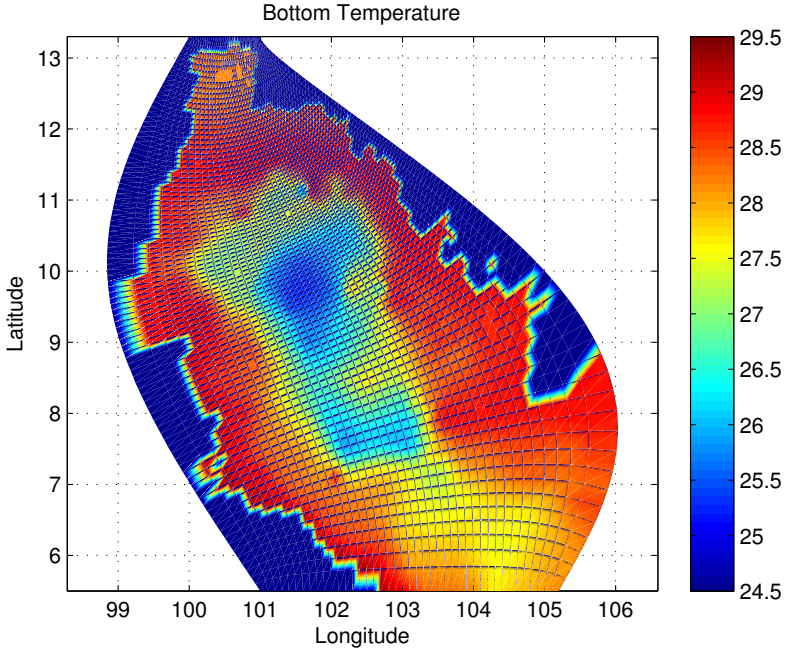

Figure 3.37 The bottom temperature (°C) in July.

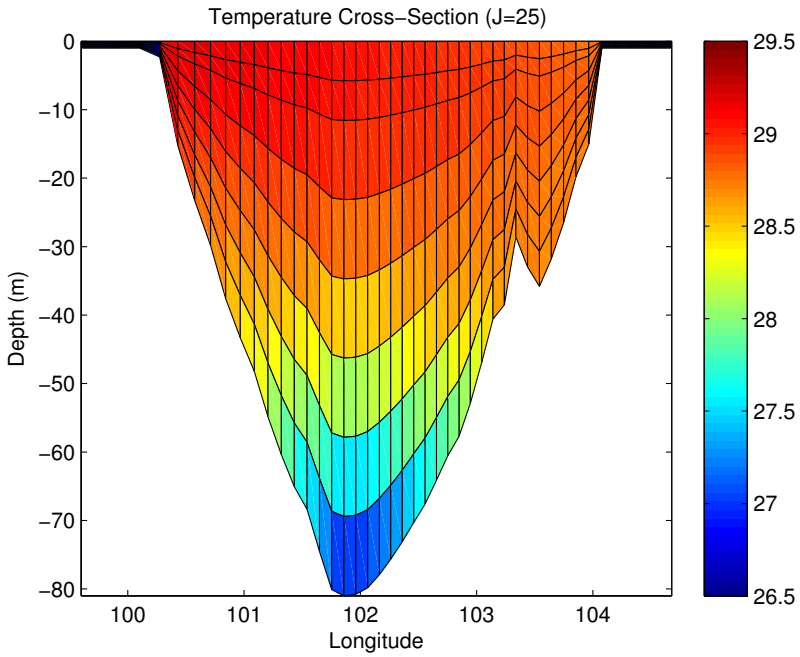

Figure 3.38 The temperature cross-section (°C) at J=25 in July.

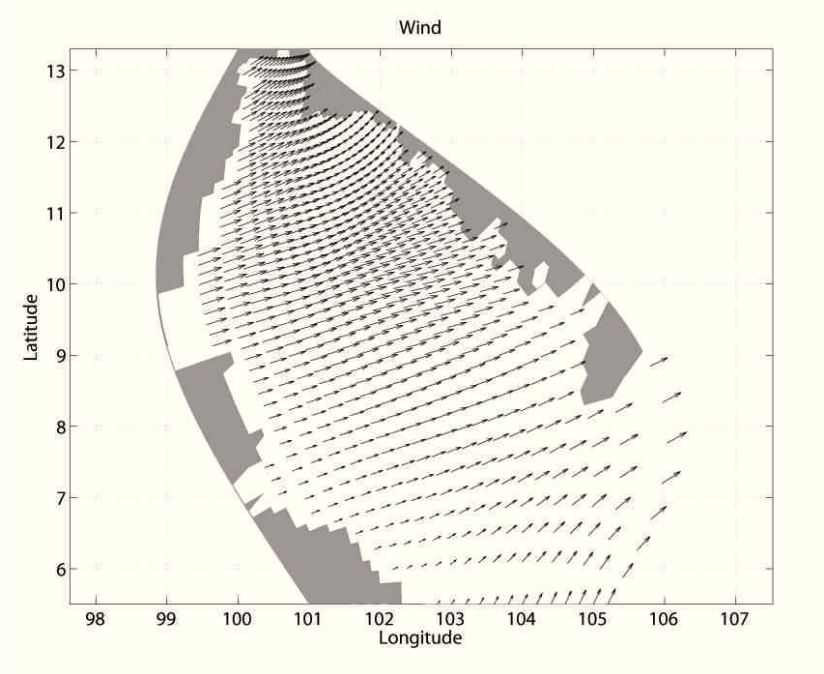

Figure 3.39 Wind in August. (Maximum speed is 5.4451 m/s.)

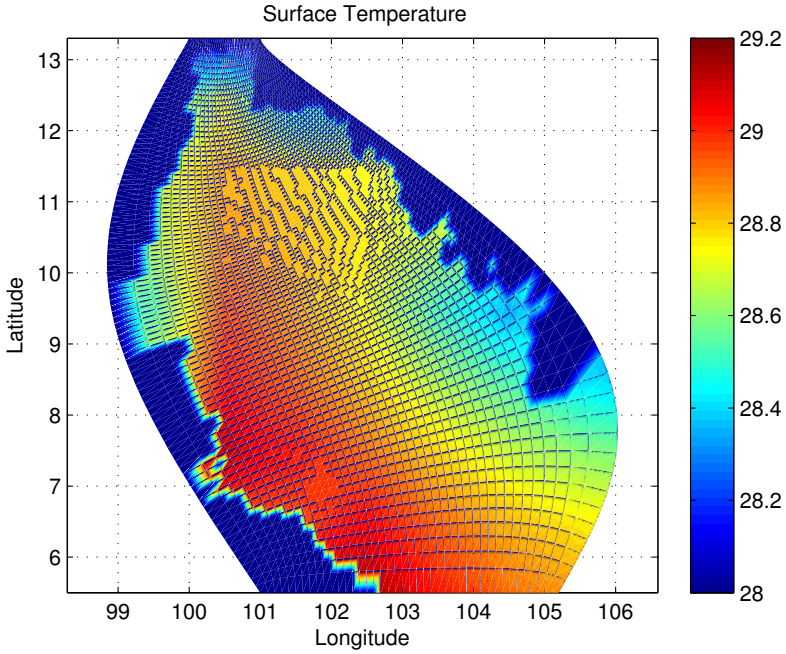

Figure 3.40 The surface temperature (°C) in August.

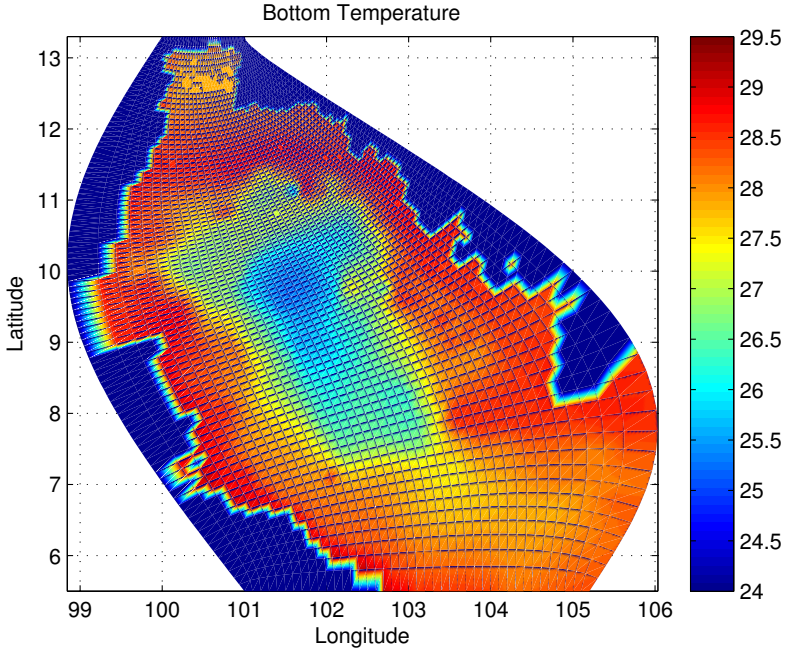

Figure 3.41 The bottom temperature (°C) in August.

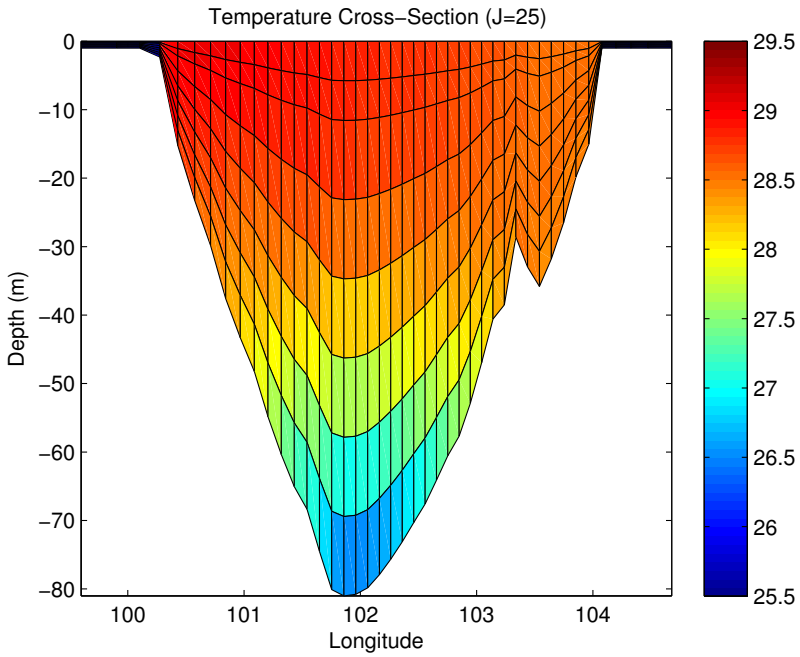

Figure 3.42 The temperature cross-section (°C) at J=25 in August.

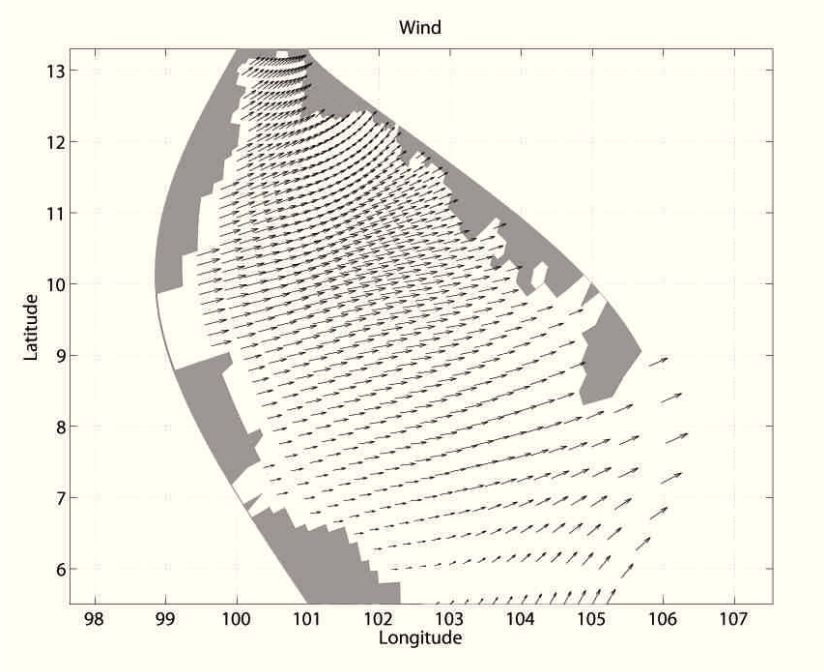

Figure 3.43 Wind in September. (Maximum speed is 4.0134 m/s.)

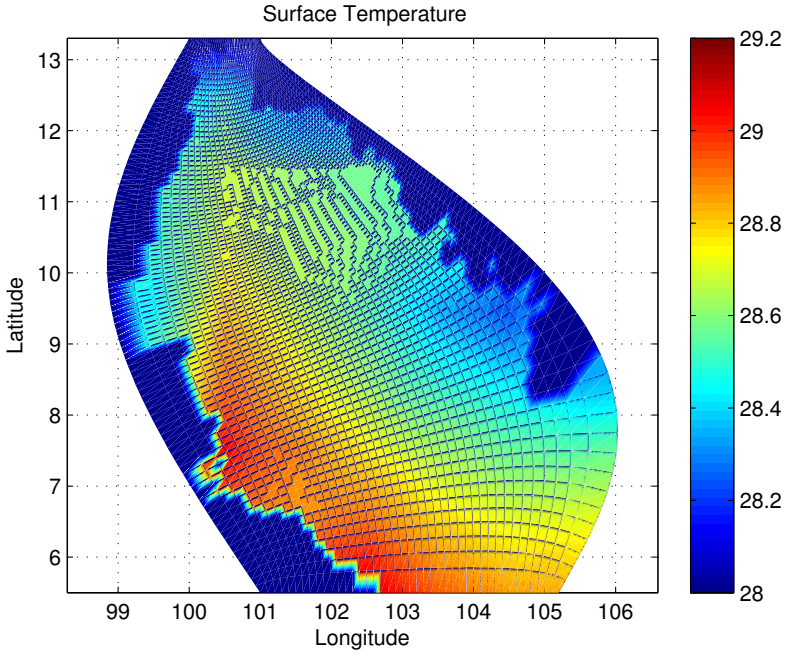

Figure 3.44 The surface temperature (°C) in September.

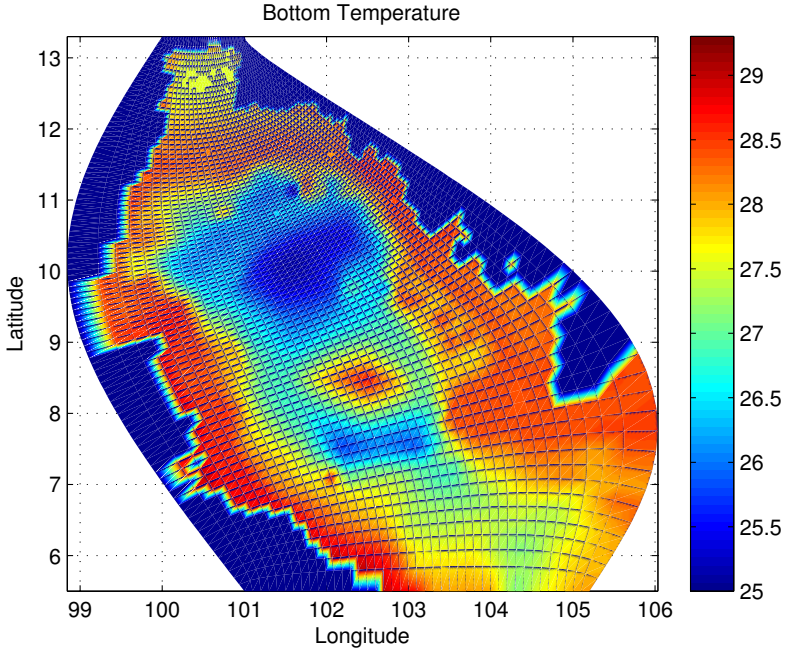

Figure 3.45 The bottom temperature (°C) in September.

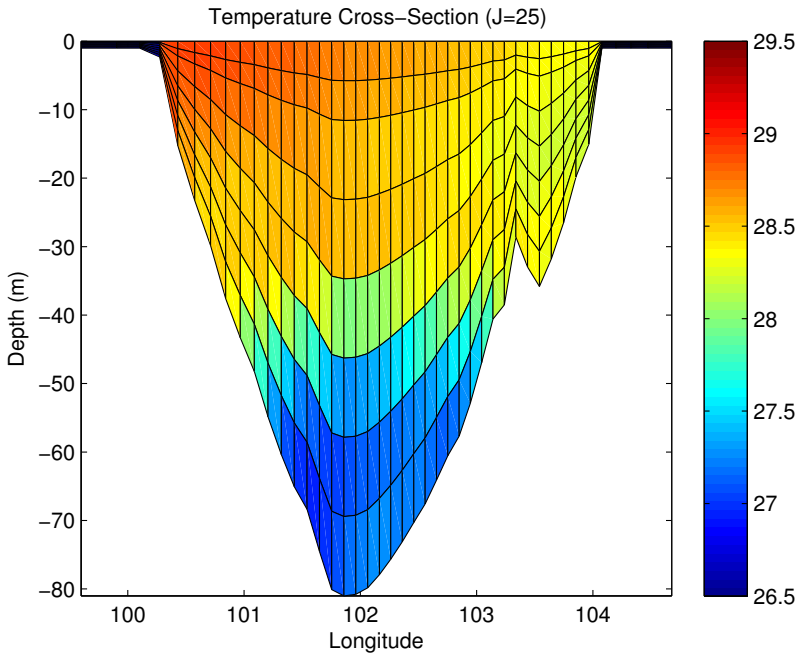

Figure 3.46 The temperature cross-section (°C) at J=25 in September.

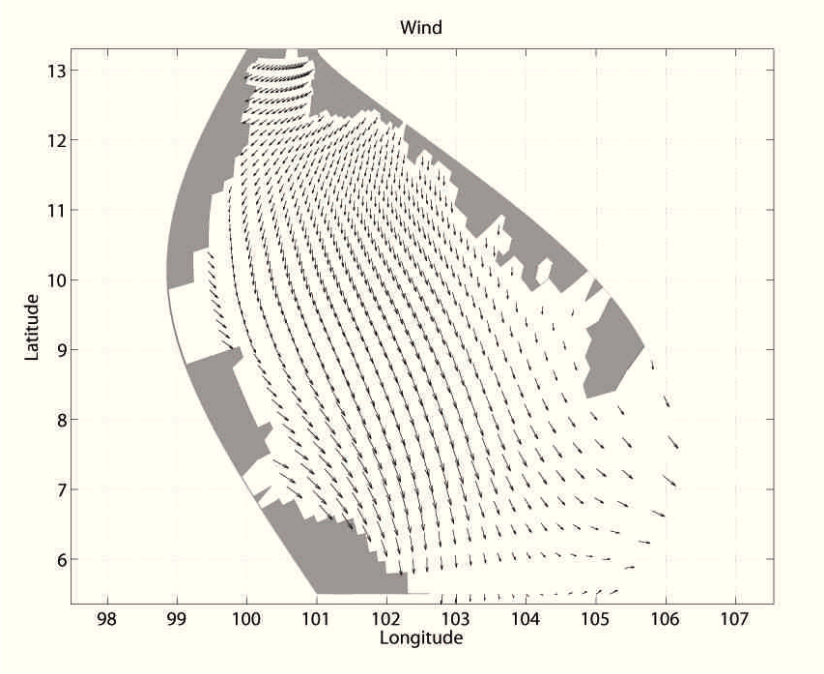

Figure 3.47 Wind in October. (Maximum speed is 0.8890 m/s.)

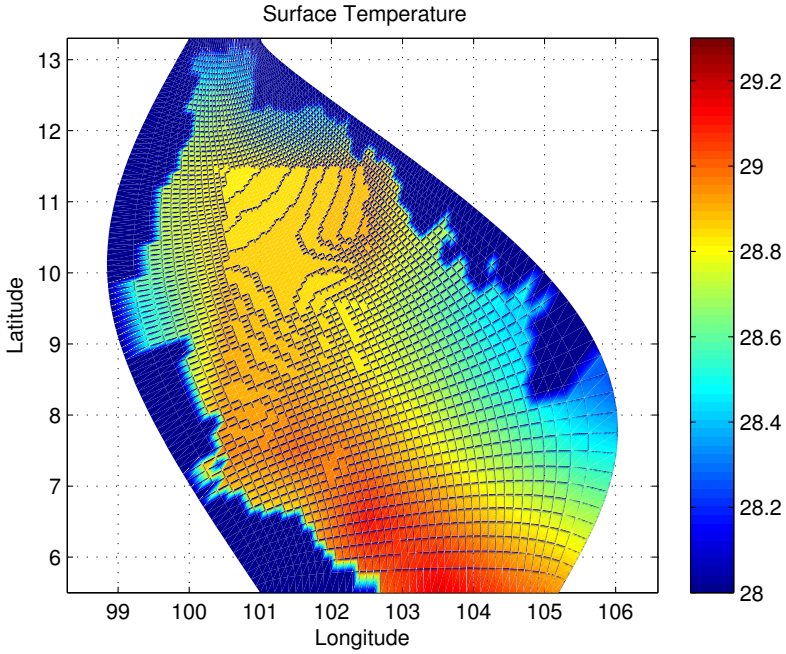

Figure 3.48 The surface temperature (°C) in October.

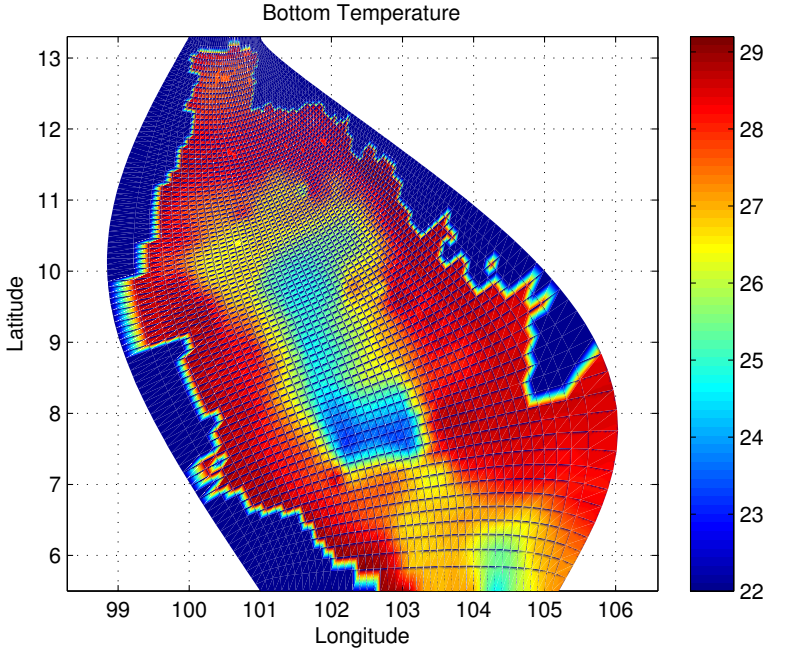

Figure 3.49 The bottom temperature (°C) in October.

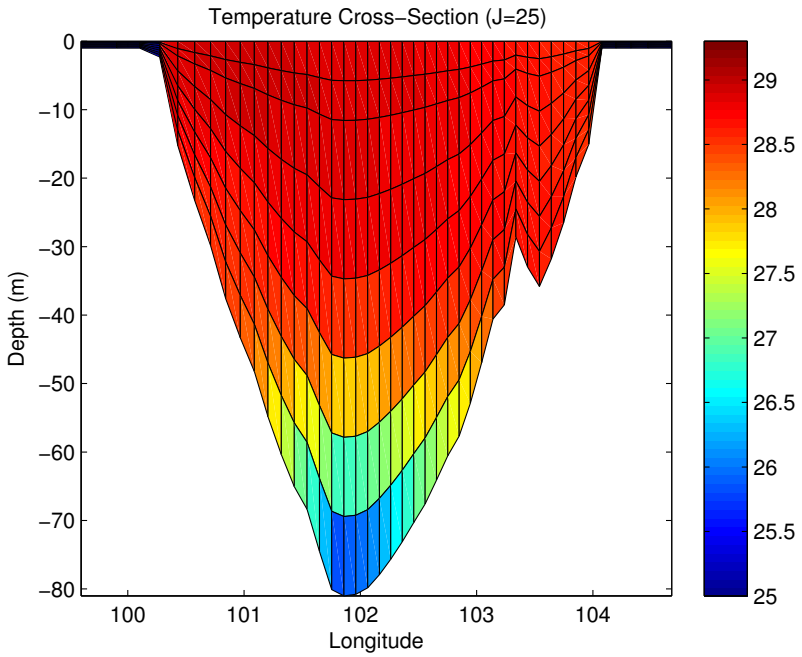

Figure 3.50 The temperature cross-section (°C) at J=25 in October.

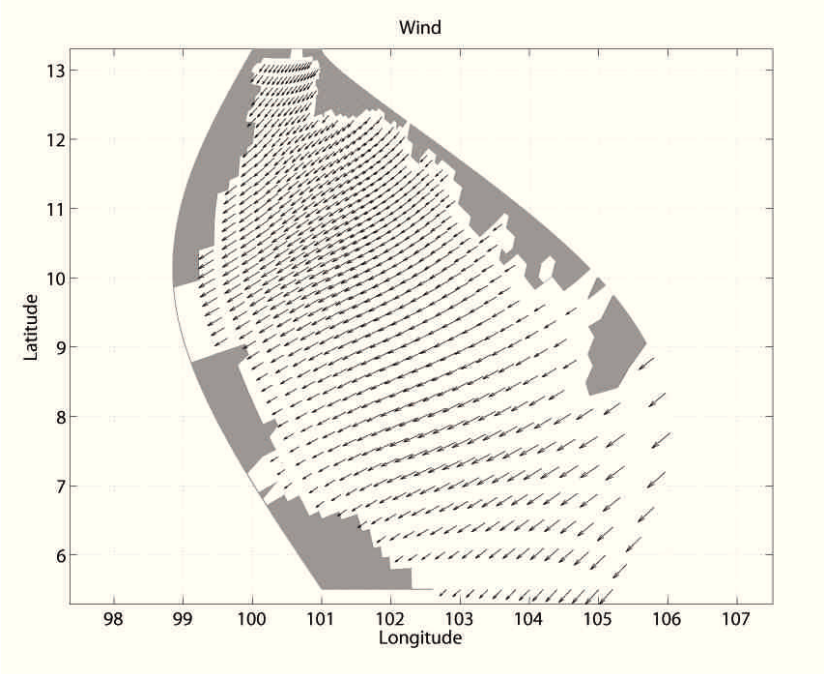

Figure 3.51 Wind in November. (Maximum speed is 4.9630 m/s.)

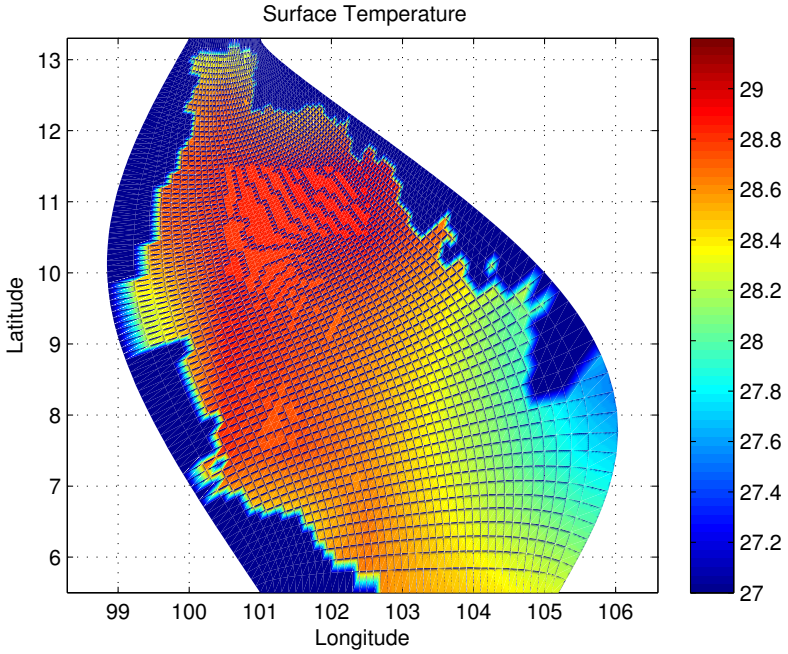

Figure 3.52 The surface temperature (°C) in November.

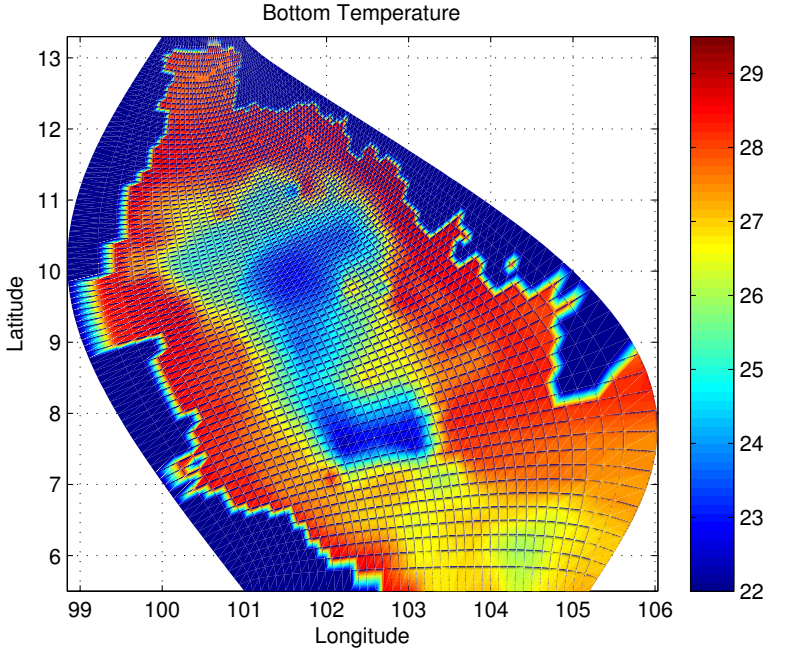

Figure 3.53 The bottom temperature (°C) in November.

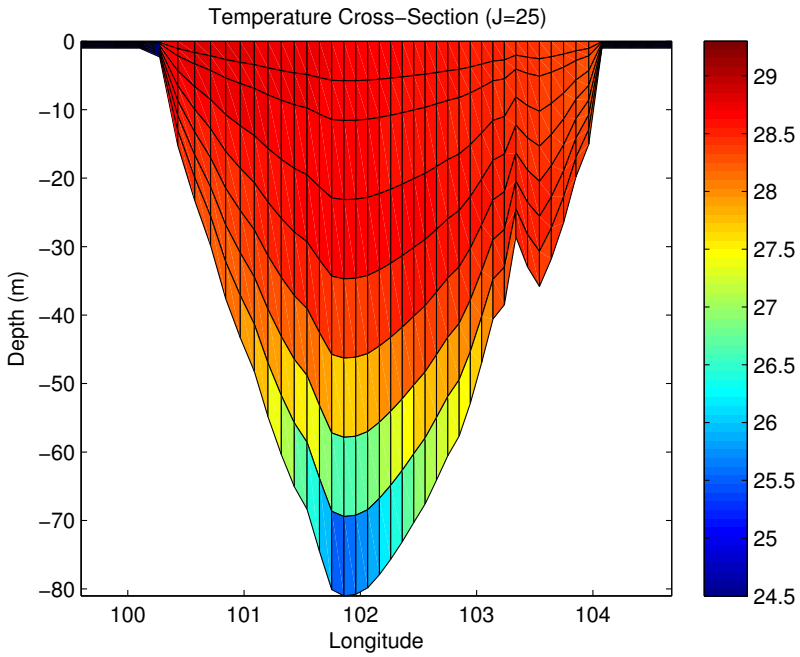

Figure 3.54 The temperature cross-section (°C) at J=25 in November.

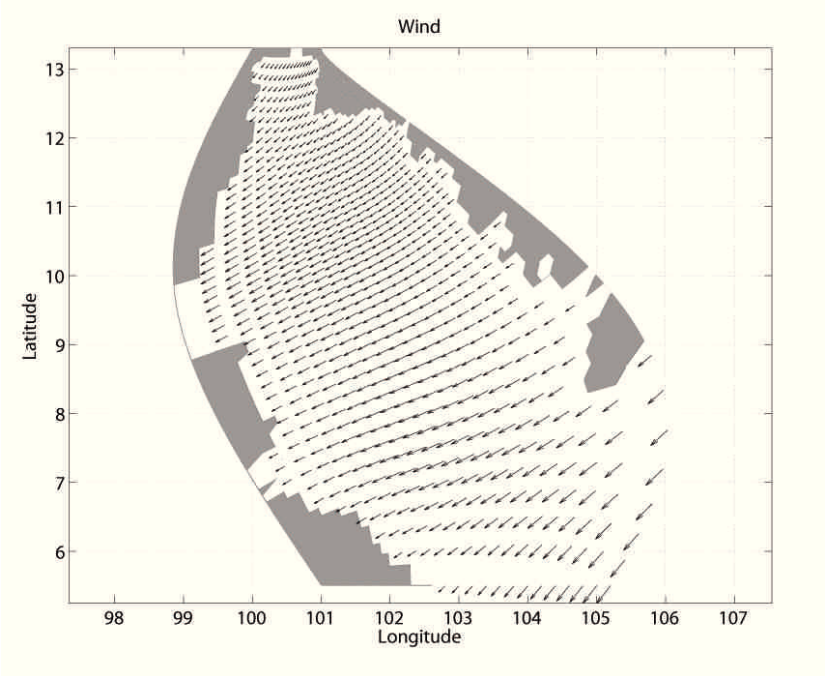

Figure 3.55 Wind in December. (Maximum speed is 7.3848 m/s.)

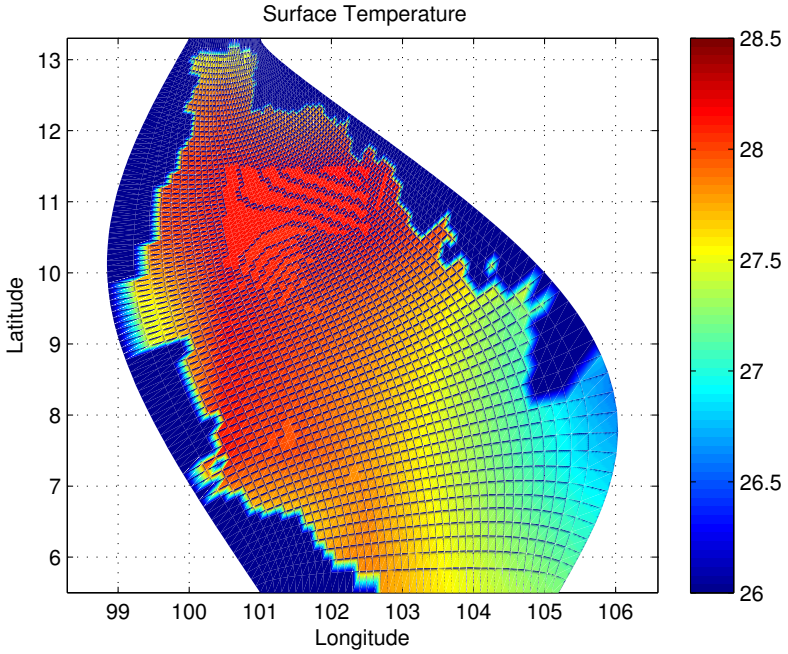

Figure 3.56 The surface temperature (°C) in December.

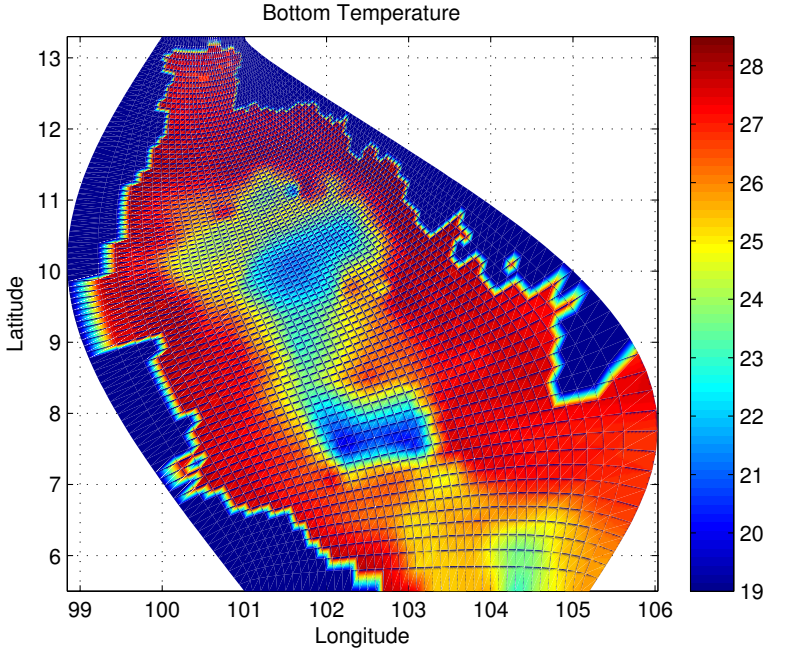

Figure 3.57 The bottom temperature (°C) in December.

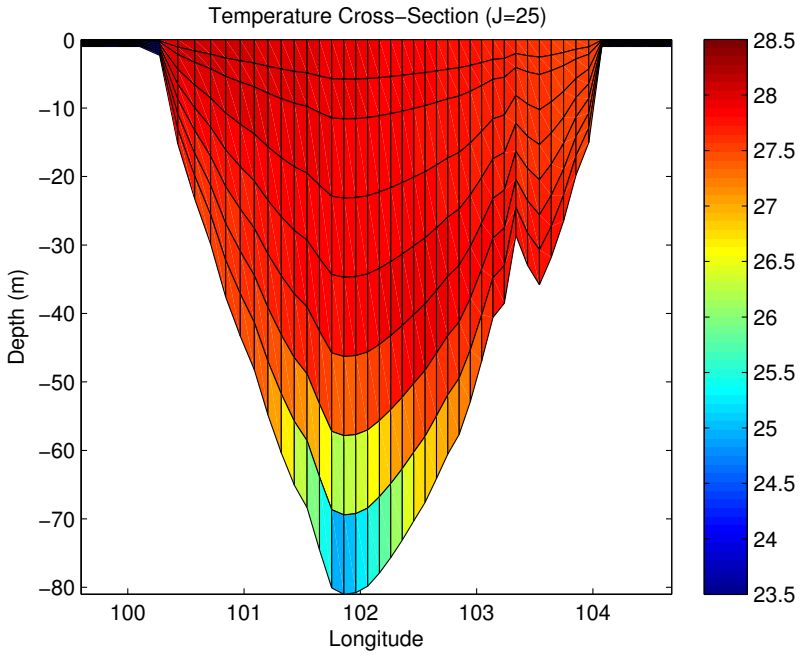

Figure 3.58 The temperature cross-section (°C) at J=25 in December.

3.8 Lateral Boundary Conditions

Lateral boundary conditions are divided into two types, which are close and open lateral boundary conditions. The close and open lateral boundaries are contiguous to coastlines and seawater, respectively. The current velocities normal to land, the tangential velocities in the horizontal friction, and the potential temperature, salinity, and surface elevation at the close lateral boundary are set to zero. For the open lateral boundary conditions, the surface elevation is a free-slip condition, the current velocities are governed by radiation conditions, and the potential temperature and salinity are governed by upstream advection conditions. The radiation conditions concerning with the current velocities for the external mode are expressed as

$$H\overline{U} \pm c_e\eta = BC \tag{3.48}$$

and

$$H\overline{V} \pm c_e\eta = BC, \tag{3.49}$$

where c_e is equal to $\sqrt{gH}$ and BC is a constant value, which is set to a known value approximately balancing the left side of the equation.

The radiation conditions concerning with the current velocities for the internal mode are expressed as

$$\frac{\partial U}{\partial t} \pm c_i\frac{\partial U}{\partial x} = 0 \tag{3.50}$$

and

$$\frac{\partial V}{\partial t} \pm c_i\frac{\partial V}{\partial y} = 0, \tag{3.51}$$

where $c_i = \sqrt{H/H_{max}}$ is the baroclinic phase speed.

The upstream advection conditions on the potential temperature and salinity are expressed as

$$\frac{\partial(T,S)}{\partial t} + U\frac{\partial(T,S)}{\partial x} = 0 \tag{3.52}$$

and

$$\frac{\partial(T,S)}{\partial t} + V\frac{\partial(T,S)}{\partial y} = 0. \tag{3.53}$$

3.9 Initial Conditions

The initial conditions for the horizontal and vertical current velocities are all set to zero. For the initial conditions of the potential temperature and salinity, they are obtain from interpolating climatological monthly mean temperature and salinity from Levitus94 to the model grid.

3.10 Numerical Methods

The primitive equations form a set of simultaneous partial differential equations which may be difficult to solve using analytical methods. A mathematical technique used for solving the primitive equations is a numerical method using discretized equations on a grid which is easy and efficient method. A numerical method used in this research is the finite difference method. An arbitrary variable $\phi(x, y, \sigma, t)$ is written in the form of $\phi^n_{i,j,k}$ where the superscript n is a time level and the subscript i, j, k is a position of the variable on the staggered grid.

3.10.1 Finite Difference Equations

The primitive equations are differenced as in both internal and external modes. The continuity equation for the internal mode, Eq. (3.21), is differenced as

$$\begin{aligned}
&\frac{(D^n_{i+1,j} + D^n_{i,j})U^n_{i+1,j,k} - (D^n_{i,j} + D^n_{i-1,j})U^n_{i,j,k}}{2\Delta x_{i,j}} \\
&+\frac{(D^n_{i,j+1} + D^n_{i,j})V^n_{i,j+1,k} - (D^n_{i,j} + D^n_{i,j-1})V^n_{i,j,k}}{2\Delta y_{i,j}} \\
&+\frac{\omega^n_{i,j,k} - \omega^n_{i,j,k+1}}{\Delta\sigma_k} + \frac{\eta^{n+1}_{i,j} - \eta^{n-1}_{i,j}}{2\Delta t_I} = 0
\end{aligned} \tag{3.54}$$

where Δt_I is the internal mode time step.

The momentum equations in x and y directions for internal mode, Eqs. (3.22) and (3.23), are differenced as

$$\begin{aligned}
&\frac{U^{n+1}_{i,j,k}(D^{n+1}_{i,j} + D^{n+1}_{i-1,j}) - U^{n-1}_{i,j,k}(D^{n-1}_{i,j} + D^{n-1}_{i-1,j})}{4\Delta t_I} \\
&+\frac{1}{4(\Delta x_{i,j} + \Delta x_{i-1,j})}\Big[\big(U^n_{i+1,j,k}(D^n_{i+1,j} + D^n_{i,j}) + U^n_{i,j,k}(D^n_{i,j} + D^n_{i-1,j})\big)\,(U^n_{i+1,j,k} + U^n_{i,j,k}) \\
&\quad - \big(U^n_{i,j,k}(D^n_{i,j} + D^n_{i-1,j}) + U^n_{i-1,j,k}(D^n_{i-1,j} + D^n_{i-2,j})\big)\,(U^n_{i,j,k} + U^n_{i-1,j,k})\Big]
\end{aligned}$$

$$+\frac{1}{4(\Delta y_{i,j}+\Delta y_{i-1,j})}\left[\left(V^n_{i,j+1,k}(D^n_{i,j+1}+D^n_{i,j})+V^n_{i-1,j+1,k}(D^n_{i-1,j+1}+D^n_{i-1,j})\right)\right.$$
$$\left.\times(U^n_{i,j+1,k}+U^n_{i,j,k})-\left(V^n_{i,j,k}(D^n_{i,j}+D^n_{i,j-1})+V^n_{i-1,j,k}(D^n_{i-1,j}+D^n_{i-1,j-1})\right)(U^n_{i,j,k}+U^n_{i,j-1,k})\right]$$
$$+\frac{(U^n_{i,j,k-1}+U^n_{i,j,k})(\omega^n_{i,j,k}+\omega^n_{i-1,j,k})-(U^n_{i,j,k}+U^n_{i,j,k+1})(\omega^n_{i,j,k+1}+\omega^n_{i-1,j,k+1})}{2\Delta\sigma_k}$$
$$-\frac{\tilde{f}^n_{i,j,k}(V^n_{i,j+1,k}+V^n_{i,j,k})D^n_{i,j}+\tilde{f}^n_{i-1,j,k}(V^n_{i-1,j+1,k}+V^n_{i-1,j,k})D^n_{i-1,j}}{4}$$
$$-\frac{\hat{f}_{i,j}(V^n_{i,j+1,k}+V^n_{i,j,k})D^n_{i,j}+\hat{f}_{i-1,j}(V^n_{i-1,j+1,k}+V^n_{i-1,j,k})D^n_{i-1,j}}{4}$$
$$+g(D^n_{i,j}+D^n_{i-1,j})\left(\frac{\eta^n_{i,j}-\eta^n_{i-1,j}}{\Delta x_{i,j}+\Delta x_{i-1,j}}\right)+\frac{g(D^n_{i,j}+D^n_{i-1,j})}{4\rho_0}$$
$$\times\sum_{m=1}^{k}\left[(D^n_{i,j}+D^n_{i-1,j})\left(\frac{\rho^n_{i,j,k-1}-\rho^n_{i-1,j,k-1}+\rho^n_{i,j,k}-\rho^n_{i-1,j,k}}{\Delta x_{i,j}+\Delta x_{i-1,j}}\right)-(\sigma_{k-1/2}+\sigma_{k+1/2})\right.$$
$$\left.\times\left(\frac{D^n_{i,j}-D^n_{i-1,j}}{\Delta x_{i,j}+\Delta x_{i-1,j}}\right)\left(\frac{\rho^n_{i,j,k-1}+\rho^n_{i-1,j,k-1}-\rho^n_{i,j,k}-\rho^n_{i-1,j,k}}{\Delta\sigma_{k-1/2}}\right)\right]\Delta\sigma_{k-1/2}$$
$$=\frac{1}{(D^{n+1}_{i,j}+D^{n+1}_{i-1,j})\Delta\sigma_k}\left[\left((K_M)^n_{i,j,k}+(K_M)^n_{i-1,j,k}\right)\frac{(U^{n+1}_{i,j,k-1}-U^{n+1}_{i,j,k})}{\Delta\sigma_{k-1/2}}\right.$$
$$\left.-\left((K_M)^n_{i,j,k+1}+(K_M)^n_{i-1,j,k+1}\right)\frac{(U^{n+1}_{i,j,k}-U^{n+1}_{i,j,k+1})}{\Delta\sigma_{k+1/2}}\right]+(F_x)^{n-1}_{i,j,k} \tag{3.55}$$

and

$$\frac{V^{n+1}_{i,j,k}(D^{n+1}_{i,j}+D^{n+1}_{i,j-1})-V^{n-1}_{i,j,k}(D^{n-1}_{i,j}+D^{n-1}_{i,j-1})}{4\Delta t_I}$$
$$+\frac{1}{4(\Delta x_{i,j}+\Delta x_{i,j-1})}\left[\left(U^n_{i+1,j,k}(D^n_{i+1,j}+D^n_{i,j})+U^n_{i+1,j-1,k}(D^n_{i+1,j-1}+D^n_{i,j-1})\right)\right.$$
$$\left.\times(V^n_{i+1,j,k}+V^n_{i,j,k})-\left(U^n_{i,j,k}(D^n_{i,j}+D^n_{i-1,j})+U^n_{i,j-1,k}(D^n_{i,j-1}+D^n_{i-1,j-1})\right)(V^n_{i,j,k}+V^n_{i-1,j,k})\right]$$
$$+\frac{1}{4(\Delta y_{i,j}+\Delta y_{i,j-1})}\left[\left(V^n_{i,j+1,k}(D^n_{i,j+1}+D^n_{i,j})+V^n_{i,j+1,k}(D^n_{i,j}+D^n_{i,j-1})\right)\right.$$
$$\left.\times(V^n_{i,j+1,k}+V^n_{i,j,k})-\left(V^n_{i,j,k}(D^n_{i,j}+D^n_{i,j-1})+V^n_{i,j-1,k}(D^n_{i,j-1}+D^n_{i,j-2})\right)(V^n_{i,j,k}+V^n_{i,j-1,k})\right]$$
$$+\frac{(V^n_{i,j,k-1}+V^n_{i,j,k})(\omega^n_{i,j,k}+\omega^n_{i,j-1,k})-(V^n_{i,j,k}+V^n_{i,j,k+1})(\omega^n_{i,j,k+1}+\omega^n_{i,j-1,k+1})}{2\Delta\sigma_k}$$
$$+\frac{\tilde{f}^n_{i,j,k}(U^n_{i+1,j,k}+U^n_{i,j,k})D^n_{i,j}+\tilde{f}^n_{i,j-1,k}(U^n_{i,j-1,k}+U^n_{i+1,j-1,k})D^n_{i,j-1}}{4}$$
$$+\frac{\hat{f}_{i,j}(U^n_{i+1,j,k}+U^n_{i,j,k})D^n_{i,j}+\hat{f}_{i,j-1}(U^n_{i,j-1,k}+U^n_{i+1,j-1,k})D^n_{i,j-1}}{4}$$
$$+g(D^n_{i,j}+D^n_{i,j-1})\left(\frac{\eta^n_{i,j}-\eta^n_{i,j-1}}{\Delta y_{i,j}+\Delta y_{i,j-1}}\right)+\frac{g(D^n_{i,j}+D^n_{i,j-1})}{4\rho_0}$$
$$\times\sum_{m=1}^{k}\left[(D^n_{i,j}+D^n_{i,j-1})\left(\frac{\rho^n_{i,j,k-1}-\rho^n_{i,j-1,k-1}+\rho^n_{i,j,k}-\rho^n_{i,j-1,k}}{\Delta y_{i,j}+\Delta y_{i,j-1}}\right)-(\sigma_{k-1/2}+\sigma_{k+1/2})\right.$$

$$\times \left(\frac{D^n_{i,j} - D^n_{i,j-1}}{\Delta y_{i,j} + \Delta y_{i,j-1}} \right) \left(\frac{\rho^n_{i,j,k-1} + \rho^n_{i,j-1,k-1} - \rho^n_{i,j,k} - \rho^n_{i,j-1,k}}{\Delta \sigma_{k-1/2}} \right) \Bigg] \Delta \sigma_{k-1/2}$$

$$= \frac{1}{(D^{n+1}_{i,j} + D^{n+1}_{i,j-1}) \Delta \sigma_k} \Bigg[\left((K_M)^n_{i,j,k} + (K_M)^n_{i,j-1,k} \right) \frac{(V^{n+1}_{i,j,k-1} - V^{n+1}_{i,j,k})}{\Delta \sigma_{k-1/2}}$$

$$- \left((K_M)^n_{i,j,k+1} + (K_M)^n_{i,j-1,k+1} \right) \frac{(V^{n+1}_{i,j,k} - V^{n+1}_{i,j,k+1})}{\Delta \sigma_{k+1/2}} \Bigg] + (F_y)^{n-1}_{i,j,k}, \tag{3.56}$$

respectively, where

$$\tilde{f}^n_{i,j,k} = \frac{(V^n_{i,j+1,k} - V^n_{i,j,k})(\Delta y_{i+1,j} - \Delta y_{i-1,j}) - (V^n_{i,j+1,k} - V^n_{i,j,k})(\Delta y_{i+1,j} - \Delta y_{i-1,j})}{4 \Delta x_{i,j} \Delta y_{i,j}} \tag{3.57}$$

is the curvature term and

$$\hat{f}_{i,j} = (1.458 \times 10^{-4}) \sin \left(\frac{\varphi_{i,j} \pi}{180} \right) \tag{3.58}$$

is the Coriolis term. The conservation equations for temperature and salinity, Eqs. (3.24) and (3.25), are differenced as

$$\frac{T^{n+1}_{i,j,k} D^{n+1}_{i,j} - T^{n-1}_{i,j,k} D^{n-1}_{i,j}}{2 \Delta t_I}$$

$$+ \frac{(T^n_{i+1,j,k} + T^n_{i,j,k}) U^n_{i+1,j,k} (D^n_{i+1,j} + D^n_{i,j}) + (T^n_{i,j,k} + T^n_{i-1,j,k}) U^n_{i,j,k} (D^n_{i,j} + D^n_{i-1,j})}{4 \Delta x_{i,j}}$$

$$+ \frac{(T^n_{i,j+1,k} + T^n_{i,j,k}) V^n_{i,j+1,k} (D^n_{i,j+1} + D^n_{i,j}) + (T^n_{i,j,k} + T^n_{i,j-1,k}) V^n_{i,j,k} (D^n_{i,j} + D^n_{i,j-1})}{4 \Delta y_{i,j}}$$

$$+ \frac{(T^n_{i,j,k-1} + T^n_{i,j,k}) \omega^n_{i,j,k} - (T^n_{i,j,k} + T^n_{i,j,k+1}) \omega^n_{i,j,k+1}}{2 \Delta \sigma_k}$$

$$= \frac{1}{D^{n+1}_{i,j} \Delta \sigma_k} \left[(K_H)^n_{i,j,k} \frac{(T^{n+1}_{i,j,k-1} - T^{n+1}_{i,j,k})}{\Delta \sigma_{k-1/2}} - (K_H)^n_{i,j,k+1} \frac{(T^{n+1}_{i,j,k} - T^{n+1}_{i,j,k+1})}{\Delta \sigma_{k+1/2}} \right] + (F_T)^{n-1}_{i,j,k} \tag{3.59}$$

and

$$\frac{S^{n+1}_{i,j,k} D^{n+1}_{i,j} - S^{n-1}_{i,j,k} D^{n-1}_{i,j}}{2 \Delta t_I}$$

$$+ \frac{(S^n_{i+1,j,k} + S^n_{i,j,k}) U^n_{i+1,j,k} (D^n_{i+1,j} + D^n_{i,j}) + (S^n_{i,j,k} + S^n_{i-1,j,k}) U^n_{i,j,k} (D^n_{i,j} + D^n_{i-1,j})}{4 \Delta x_{i,j}}$$

$$+ \frac{(S^n_{i,j+1,k} + S^n_{i,j,k}) V^n_{i,j+1,k} (D^n_{i,j+1} + D^n_{i,j}) + (S^n_{i,j,k} + S^n_{i,j-1,k}) V^n_{i,j,k} (D^n_{i,j} + D^n_{i,j-1})}{4 \Delta y_{i,j}}$$

$$+ \frac{(S^n_{i,j,k-1} + S^n_{i,j,k}) \omega^n_{i,j,k} - (S^n_{i,j,k} + S^n_{i,j,k+1}) \omega^n_{i,j,k+1}}{2 \Delta \sigma_k}$$

$$= \frac{1}{D^{n+1}_{i,j} \Delta \sigma_k} \left[(K_H)^n_{i,j,k} \frac{(S^{n+1}_{i,j,k-1} - S^{n+1}_{i,j,k})}{\Delta \sigma_{k-1/2}} - (K_H)^n_{i,j,k+1} \frac{(S^{n+1}_{i,j,k} - S^{n+1}_{i,j,k+1})}{\Delta \sigma_{k+1/2}} \right] + (F_S)^{n-1}_{i,j,k}, \tag{3.60}$$

respectively.

The horizontal viscosity and diffusion terms in Eqs. (3.26) to (3.29) are differenced as

$$
\begin{aligned}
(F_x)^{n-1}_{i,j,k} = \frac{4}{\Delta x_{i,j}+\Delta x_{i-1,j}} \Bigg[& D^n_{i,j}(A_M)^{n-1}_{i,j,k}\left(\frac{U^{n-1}_{i+1,j,k}-U^{n-1}_{i,j,k}}{\Delta x_{i,j}}\right) \\
& -D^n_{i-1,j}(A_M)^{n-1}_{i-1,j,k}\left(\frac{U^{n-1}_{i,j,k}-U^{n-1}_{i-1,j,k}}{\Delta x_{i-1,j}}\right)\Bigg] + \frac{1}{2(\Delta y_{i,j}+\Delta y_{i-1,j})} \\
& \times \left[(D^n_{i,j+1}+D^n_{i-1,j+1}+D^n_{i,j}+D^n_{i-1,j})\right. \\
& \times \left((A_M)^{n-1}_{i,j+1,k}+(A_M)^{n-1}_{i-1,j+1,k}+(A_M)^{n-1}_{i,j,k}+(A_M)^{n-1}_{i-1,j,k}\right) \\
& \times \left(\frac{U^{n-1}_{i,j+1,k}-U^{n-1}_{i,j,k}}{\Delta y_{i,j+1}+\Delta y_{i-1,j+1}+\Delta y_{i,j}+\Delta y_{i-1,j}} + \frac{V^{n-1}_{i,j+1,k}-V^{n-1}_{i-1,j+1,k}}{\Delta x_{i,j+1}+\Delta x_{i-1,j+1}+\Delta x_{i,j}+\Delta x_{i-1,j}}\right) \\
& -(D^n_{i,j}+D^n_{i-1,j}+D^n_{i,j-1}+D^n_{i-1,j-1}) \\
& \times \left((A_M)^{n-1}_{i,j,k}+(A_M)^{n-1}_{i-1,j,k}+(A_M)^{n-1}_{i,j-1,k}+(A_M)^{n-1}_{i-1,j-1,k}\right) \\
& \left.\times \left(\frac{U^{n-1}_{i,j,k}-U^{n-1}_{i,j-1,k}}{\Delta y_{i,j}+\Delta y_{i-1,j}+\Delta y_{i,j-1}+\Delta y_{i-1,j-1}} + \frac{V^{n-1}_{i,j,k}-V^{n-1}_{i-1,j,k}}{\Delta x_{i,j}+\Delta x_{i-1,j}+\Delta x_{i,j-1}+\Delta x_{i-1,j-1}}\right)\right],
\end{aligned}
\tag{3.61}
$$

$$
\begin{aligned}
(F_y)^{n-1}_{i,j,k} = \frac{4}{\Delta y_{i,j}+\Delta y_{i,j-1}} \Bigg[& D^n_{i,j}(A_M)^{n-1}_{i,j,k}\left(\frac{V^{n-1}_{i,j+1,k}-V^{n-1}_{i,j,k}}{\Delta y_{i,j}}\right) \\
& -D^n_{i,j-1}(A_M)^{n-1}_{i,j-1,k}\left(\frac{V^{n-1}_{i,j,k}-V^{n-1}_{i,j-1,k}}{\Delta y_{i,j-1}}\right)\Bigg] + \frac{1}{2(\Delta x_{i,j}+\Delta x_{i,j-1})} \\
& \times \left[(D^n_{i+1,j}+D^n_{i,j}+D^n_{i+1,j-1}+D^n_{i,j-1})\right. \\
& \times \left((A_M)^{n-1}_{i+1,j,k}+(A_M)^{n-1}_{i,j,k}+(A_M)^{n-1}_{i+1,j-1,k}+(A_M)^{n-1}_{i,j-1,k}\right) \\
& \times \left(\frac{U^{n-1}_{i+1,j,k}-U^{n-1}_{i+1,j-1,k}}{\Delta y_{i+1,j}+\Delta y_{i,j}+\Delta y_{i+1,j-1}+\Delta y_{i,j-1}} + \frac{V^{n-1}_{i+1,j,k}-V^{n-1}_{i,j,k}}{\Delta x_{i+1,j}+\Delta x_{i,j}+\Delta x_{i+1,j-1}+\Delta x_{i,j-1}}\right) \\
& -(D^n_{i,j}+D^n_{i-1,j}+D^n_{i,j-1}+D^n_{i-1,j-1}) \\
& \times \left((A_M)^{n-1}_{i,j,k}+(A_M)^{n-1}_{i-1,j,k}+(A_M)^{n-1}_{i,j-1,k}+(A_M)^{n-1}_{i-1,j-1,k}\right) \\
& \left.\times \left(\frac{U^{n-1}_{i,j,k}-U^{n-1}_{i,j-1,k}}{\Delta y_{i,j}+\Delta y_{i-1,j}+\Delta y_{i,j-1}+\Delta y_{i-1,j-1}} + \frac{V^{n-1}_{i,j,k}-V^{n-1}_{i-1,j,k}}{\Delta x_{i,j}+\Delta x_{i-1,j}+\Delta x_{i,j-1}+\Delta x_{i-1,j-1}}\right)\right],
\end{aligned}
\tag{3.62}
$$

and

$$
\begin{aligned}
(F_\phi)^{n-1}_{i,j,k} = \frac{1}{2\Delta x_{i,j}} \Bigg[& (H_{i+1,j}+H_{i,j})\left((A_H)^{n-1}_{i+1,j,k}+(A_H)^{n-1}_{i,j,k}\right)\left(\frac{\phi^{n-1}_{i+1,j,k}-\phi^{n-1}_{i,j,k}}{\Delta x_{i+1,j}+\Delta x_{i,j}}\right) \\
& -(H_{i,j}+H_{i-1,j})\left((A_H)^{n-1}_{i,j,k}+(A_H)^{n-1}_{i-1,j,k}\right)\left(\frac{\phi^{n-1}_{i,j,k}-\phi^{n-1}_{i-1,j,k}}{\Delta x_{i,j}+\Delta x_{i-1,j}}\right)\Bigg]
\end{aligned}
$$

$$+\frac{1}{2\Delta y_{i,j}}\left[(H_{i,j+1}+H_{i,j})\left((A_H)^{n-1}_{i,j+1,k}+(A_H)^{n-1}_{i,j,k}\right)\left(\frac{\phi^{n-1}_{i,j+1,k}-\phi^{n-1}_{i,j,k}}{\Delta y_{i,j+1}+\Delta y_{i,j}}\right)\right.$$
$$\left.-(H_{i,j}+H_{i,j-1})\left((A_H)^{n-1}_{i,j,k}+(A_H)^{n-1}_{i,j-1,k}\right)\left(\frac{\phi^{n-1}_{i,j,k}-\phi^{n-1}_{i,j-1,k}}{\Delta y_{i,j}+\Delta y_{i,j-1}}\right)\right] \tag{3.63}$$

where ϕ represents T and S.

The horizontal kinematic viscosity, A_M, is differenced as

$$(A_M)^{n-1}_{i,j,k}=C\Delta x_{i,j}\Delta y_{i,j}\frac{1}{2}\left[\left(\frac{U^{n-1}_{i+1,j,k}-U^{n-1}_{i,j,k}}{\Delta x_{i,j}}\right)^2+\left(\frac{V^{n-1}_{i,j+1,k}-V^{n-1}_{i,j,k}}{\Delta y_{i,j}}\right)^2\right.$$
$$+\left(\frac{V^{n-1}_{i+1,j+1,k}+V^{n-1}_{i+1,j,k}-V^{n-1}_{i-1,j+1,k}-V^{n-1}_{i-1,j,k}}{4\Delta x_{i,j}}\right.$$
$$\left.\left.+\frac{U^{n-1}_{i+1,j+1,k}+U^{n-1}_{i,j+1,k}-U^{n-1}_{i+1,j-1,k}-U^{n-1}_{i,j-1,k}}{4\Delta y_{i,j}}\right)^2\right]^{\frac{1}{2}}. \tag{3.64}$$

For the external mode equations, the continuity equation and momentum equations in x and y directions, Eqs. (3.43), (3.44), and (3.45), are differenced as

$$\frac{(D^n_{i+1,j}+D^n_{i,j})\overline{U}^n_{i+1,j}-(D^n_{i,j}+D^n_{i-1,j})\overline{U}^n_{i,j}}{2\Delta x_{i,j}}$$
$$+\frac{(D^n_{i,j+1}+D^n_{i,j})\overline{V}^n_{i,j+1}-(D^n_{i,j}+D^n_{i,j-1})\overline{V}^n_{i,j}}{2\Delta y_{i,j}}+\frac{\eta^{n+1}_{i,j}-\eta^{n-1}_{i,j}}{2\Delta t_E}=0, \tag{3.65}$$
$$\frac{\overline{U}^{n+1}_{i,j}(D^{n+1}_{i,j}+D^{n+1}_{i-1,j})-\overline{U}^{n-1}_{i,j}(D^{n-1}_{i,j}+D^{n-1}_{i-1,j})}{4\Delta t_E}+\sum_{k=1}^{kb-1}\left[\frac{1}{4(\Delta x_{i,j}+\Delta x_{i-1,j})}\right.$$
$$\times\left[\left(U^n_{i+1,j,k}(D^n_{i+1,j}+D^n_{i,j})+U^n_{i,j,k}(D^n_{i,j}+D^n_{i-1,j})\right)(U^n_{i+1,j,k}+U^n_{i,j,k})\right.$$
$$\left.\left.-\left(U^n_{i,j,k}(D^n_{i,j}+D^n_{i-1,j})+U^n_{i-1,j,k}(D^n_{i-1,j}+D^n_{i-2,j})\right)(U^n_{i,j,k}+U^n_{i-1,j,k})\right]\Delta\sigma_k$$
$$+\sum_{k=1}^{kb-1}\left[\frac{1}{4(\Delta y_{i,j}+\Delta y_{i-1,j})}\left[\left(V^n_{i,j+1,k}(D^n_{i,j+1}+D^n_{i,j})+V^n_{i-1,j+1,k}(D^n_{i-1,j+1}+D^n_{i-1,j})\right)\right.\right.$$
$$\times(U^n_{i,j+1,k}+U^n_{i,j,k})-\left(V^n_{i,j,k}(D^n_{i,j}+D^n_{i,j-1})+V^n_{i-1,j,k}(D^n_{i-1,j}+D^n_{i-1,j-1})\right)$$
$$\left.\left.\times(U^n_{i,j,k}+U^n_{i,j-1,k})\right]\Delta\sigma_k\right.$$
$$-\sum_{k=1}^{kb-1}\left[\frac{\tilde{f}^n_{i,j,k}(V^n_{i,j+1,k}+V^n_{i,j,k})D^n_{i,j}+\tilde{f}^n_{i-1,j,k}(V^n_{i-1,j+1,k}+V^n_{i-1,j,k})D^n_{i-1,j}}{4}\right.$$
$$\left.-\frac{\hat{f}_{i,j}(\overline{V}^n_{i,j+1}+\overline{V}^n_{i,j})D^n_{i,j}+\hat{f}_{i-1,j}(\overline{V}^n_{i-1,j+1}+\overline{V}^n_{i-1,j})D^n_{i-1,j}}{4}\right]$$
$$+g(D^n_{i,j}+D^n_{i-1,j})\left(\frac{\eta^n_{i,j}-\eta^n_{i-1,j}}{\Delta x_{i,j}+\Delta x_{i-1,j}}\right)+\frac{g(D^n_{i,j}+D^n_{i-1,j})}{4\rho_0}\sum_{k=1}^{kb-1}\sum_{m=1}^{k}\left[(D^n_{i,j}+D^n_{i-1,j})\right.$$

$$\times\left(\frac{\rho^n_{i,j,k-1}-\rho^n_{i-1,j,k-1}+\rho^n_{i,j,k}-\rho^n_{i-1,j,k}}{\Delta x_{i,j}+\Delta x_{i-1,j}}\right)-(\sigma_{k-1/2}+\sigma_{k+1/2})$$
$$\times\left(\frac{D^n_{i,j}-D^n_{i-1,j}}{\Delta x_{i,j}+\Delta x_{i-1,j}}\right)\left(\frac{\rho^n_{i,j,k-1}+\rho^n_{i-1,j,k-1}-\rho^n_{i,j,k}-\rho^n_{i-1,j,k}}{\Delta\sigma_{k-1/2}}\right)\Bigg]\Delta\sigma_{k-1/2}\Delta\sigma_k$$
$$=-<wu(0)>_{i,j}+<wu(-1)>_{i,j}+\sum_{k=1}^{kb-1}(F_x)^{n-1}_{i,j,k}, \tag{3.66}$$

and

$$\frac{\overline{V}^{n+1}_{i,j}(D^{n+1}_{i,j}+D^{n+1}_{i,j-1})-\overline{V}^{n-1}_{i,j}(D^{n-1}_{i,j}+D^{n-1}_{i,j-1})}{4\Delta t_E}+\sum_{k=1}^{kb-1}\Bigg[\frac{1}{4(\Delta x_{i,j}+\Delta x_{i,j-1})}$$
$$\times\left[\left(U^n_{i+1,j,k}(D^n_{i+1,j}+D^n_{i,j})+U^n_{i+1,j-1,k}(D^n_{i+1,j-1}+D^n_{i,j-1})\right)(V^n_{i+1,j,k}+V^n_{i,j,k})\right.$$
$$\left.-\left(U^n_{i,j,k}(D^n_{i,j}+D^n_{i-1,j})+U^n_{i,j-1,k}(D^n_{i,j-1}+D^n_{i-1,j-1})\right)(V^n_{i,j,k}+V^n_{i-1,j,k})\right]\Delta\sigma_k$$
$$+\sum_{k=1}^{kb-1}\Bigg[\frac{1}{4(\Delta y_{i,j}+\Delta y_{i,j-1})}\left[\left(V^n_{i,j+1,k}(D^n_{i,j+1}+D^n_{i,j})+V^n_{i,j,k}(D^n_{i,j}+D^n_{i,j-1})\right)\right.$$
$$\left.\times(V^n_{i,j+1,k}+V^n_{i,j,k})-\left(V^n_{i,j,k}(D^n_{i,j}+D^n_{i,j-1})+V^n_{i,j-1,k}(D^n_{i,j-1}+D^n_{i,j-2})\right)\right.$$
$$\left.\times(V^n_{i,j,k}+V^n_{i,j-1,k})\right]\Delta\sigma_k$$
$$+\sum_{k=1}^{kb-1}\Bigg[\frac{\tilde{f}^n_{i,j,k}(U^n_{i+1,j,k}+U^n_{i,j,k})D^n_{i,j}+\tilde{f}^n_{i,j-1,k}(U^n_{i,j-1,k}+U^n_{i+1,j-1,k})D^n_{i,j-1}}{4}\Bigg]$$
$$+\frac{\hat{f}_{i,j}(\overline{U}^n_{i+1,j}+\overline{U}^n_{i,j})D^n_{i,j}+\hat{f}_{i,j-1}(\overline{U}^n_{i+1,j-1}+\overline{U}^n_{i,j-1})D^n_{i,j-1}}{4}$$
$$+g(D^n_{i,j}+D^n_{i,j-1})\left(\frac{\eta^n_{i,j}-\eta^n_{i,j-1}}{\Delta y_{i,j}+\Delta y_{i,j-1}}\right)+\frac{g(D^n_{i,j}+D^n_{i,j-1})}{4\rho_0}\sum_{k=1}^{kb-1}\sum_{m=1}^{k}\left[(D^n_{i,j}+D^n_{i,j-1})\right.$$
$$\times\left(\frac{\rho^n_{i,j,k-1}-\rho^n_{i,j-1,k-1}+\rho^n_{i,j,k}-\rho^n_{i,j-1,k}}{\Delta y_{i,j}+\Delta y_{i,j-1}}\right)-(\sigma_{k-1/2}+\sigma_{k+1/2})$$
$$\left.\times\left(\frac{D^n_{i,j}-D^n_{i,j-1}}{\Delta y_{i,j}+\Delta y_{i,j-1}}\right)\left(\frac{\rho^n_{i,j,k-1}+\rho^n_{i,j-1,k-1}-\rho^n_{i,j,k}-\rho^n_{i,j-1,k}}{\Delta\sigma_{k-1/2}}\right)\right]\Delta\sigma_{k-1/2}\Delta\sigma_k$$
$$=-<wv(0)>_{i,j}+<wv(-1)>_{i,j}+\sum_{k=1}^{kb-1}(F_y)^{n-1}_{i,j,k}, \tag{3.67}$$

respectively, where Δt_E is the external time step.

3.10.2 Solution Algorithm

All variables in the finite difference equations for internal and external modes are known at the time level $n-1$ and n. All algorithms of solving the primitive equations using the finite difference method are shown in Fig. 3.59. The calculation of finite difference equations for external mode in order to determine the surface elevation, η, and vertical mean of current velocities, $\overline{U}$ and $\overline{V}$, is entirely explicit. On the other hand, the calculation of finite difference equations for internal mode is mixed between implicit and explicit. The calculation of variables for internal mode equations is separated into an advection plus horizontal diffusion time step and a vertical diffusion time step. The former is explicit and the latter is implicit. To illustrate, consider the conservation equation for temperature,

$$\begin{aligned}
&\frac{T^{n+1}_{i,j,k}D^{n+1}_{i,j}-T^{n-1}_{i,j,k}D^{n-1}_{i,j}}{2\Delta t_I}\\
&+\frac{(T^{n}_{i+1,j,k}+T^{n}_{i,j,k})U^{n}_{i+1,j,k}(D^{n}_{i+1,j}+D^{n}_{i,j})+(T^{n}_{i,j,k}+T^{n}_{i-1,j,k})U^{n}_{i,j,k}(D^{n}_{i,j}+D^{n}_{i-1,j})}{4\Delta x_{i,j}}\\
&+\frac{(T^{n}_{i,j+1,k}+T^{n}_{i,j,k})V^{n}_{i,j+1,k}(D^{n}_{i,j+1}+D^{n}_{i,j})+(T^{n}_{i,j,k}+T^{n}_{i,j-1,k})V^{n}_{i,j,k}(D^{n}_{i,j}+D^{n}_{i,j-1})}{4\Delta y_{i,j}}\\
&+\frac{(T^{n}_{i,j,k-1}+T^{n}_{i,j,k})\omega^{n}_{i,j,k}-(T^{n}_{i,j,k}+T^{n}_{i,j,k+1})\omega^{n}_{i,j,k+1}}{2\Delta\sigma_k}\\
&=\frac{1}{D^{n+1}_{i,j}\Delta\sigma_k}\left[(K_H)^{n}_{i,j,k}\frac{(T^{n+1}_{i,j,k-1}-T^{n+1}_{i,j,k})}{\Delta\sigma_{k-1/2}}-(K_H)^{n}_{i,j,k+1}\frac{(T^{n+1}_{i,j,k}-T^{n+1}_{i,j,k+1})}{\Delta\sigma_{k+1/2}}\right]+(F_T)^{n-1}_{i,j,k}.
\end{aligned}\tag{3.68}$$

The solution is carried out in two steps. The advection and horizontal diffusion parts are

$$\begin{aligned}
&\frac{\tilde{T}\tilde{D}-T^{n-1}_{i,j,k}D^{n-1}_{i,j}}{2\Delta t_I}\\
&=-\frac{(T^{n}_{i+1,j,k}+T^{n}_{i,j,k})U^{n}_{i+1,j,k}(D^{n}_{i+1,j}+D^{n}_{i,j})+(T^{n}_{i,j,k}+T^{n}_{i-1,j,k})U^{n}_{i,j,k}(D^{n}_{i,j}+D^{n}_{i-1,j})}{4\Delta x_{i,j}}\\
&-\frac{(T^{n}_{i,j+1,k}+T^{n}_{i,j,k})V^{n}_{i,j+1,k}(D^{n}_{i,j+1}+D^{n}_{i,j})+(T^{n}_{i,j,k}+T^{n}_{i,j-1,k})V^{n}_{i,j,k}(D^{n}_{i,j}+D^{n}_{i,j-1})}{4\Delta y_{i,j}}\\
&-\frac{(T^{n}_{i,j,k-1}+T^{n}_{i,j,k})\omega^{n}_{i,j,k}-(T^{n}_{i,j,k}+T^{n}_{i,j,k+1})\omega^{n}_{i,j,k+1}}{2\Delta\sigma_k}+(F_T)^{n-1}_{i,j,k}.
\end{aligned}\tag{3.69}$$

The vertical diffusion part is

$$\begin{aligned}
&\frac{T^{n+1}_{i,j,k}D^{n+1}_{i,j}-\tilde{T}\tilde{D}}{2\Delta t_I}\\
&=\frac{1}{D^{n+1}_{i,j}\Delta\sigma_k}\left[(K_H)^{n}_{i,j,k}\frac{(T^{n+1}_{i,j,k-1}-T^{n+1}_{i,j,k})}{\Delta\sigma_{k-1/2}}-(K_H)^{n}_{i,j,k+1}\frac{(T^{n+1}_{i,j,k}-T^{n+1}_{i,j,k+1})}{\Delta\sigma_{k+1/2}}\right].
\end{aligned}\tag{3.70}$$

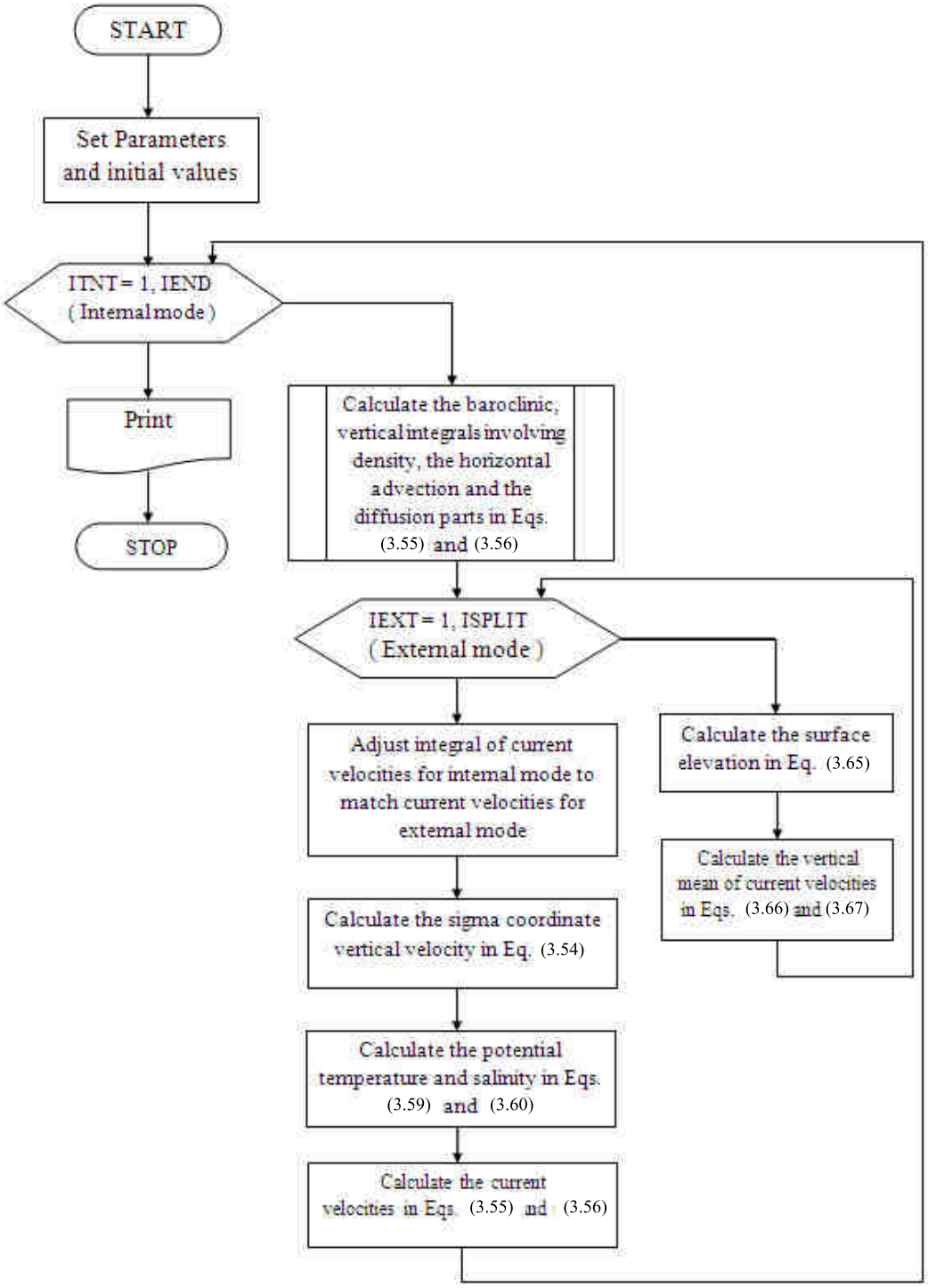

Figure 3.59 The algorithms of solving the primitive equations.

Note that $\tilde{T}\tilde{D}$ can be any three-dimensional variables. For solving the primitive equations, the variable $\tilde{D}$ in the advection and horizontal diffusion part and vertical diffusion part is set to be $D_{i,j}^{n+1}$.

Thus, the equation (3.70) is rewritten as

$$T_{i,j,k}^{n+1} - \tilde{T} = \frac{2\Delta t_I}{(D_{i,j}^{n+1})^2 \Delta\sigma_k}$$

$$\times \left[(K_H)_{i,j,k}^{n} \frac{(T_{i,j,k-1}^{n+1} - T_{i,j,k}^{n+1})}{\Delta\sigma_{k-1/2}} - (K_H)_{i,j,k+1}^{n} \frac{(T_{i,j,k}^{n+1} - T_{i,j,k+1}^{n+1})}{\Delta\sigma_{k+1/2}} \right]. \tag{3.71}$$

The equation (3.71) can now be written as

$$-T_{i,j,k+1}^{n+1} a_k + T_{i,j,k}^{n}(a_k + c_k - 1) - T_{i,j,k-1}^{n} c_k = d_k \tag{3.72}$$

where

$$a_k = -\frac{2\Delta t_I (K_H)_{i,j,k+1}^{n}}{(D_{i,j}^{n+1})^2 \Delta\sigma_k \Delta\sigma_{k+1/2}}, \tag{3.73}$$

$$c_k = -\frac{2\Delta t_I (K_H)_{i,j,k}^{n}}{(D_{i,j}^{n+1})^2 \Delta\sigma_k \Delta\sigma_{k-1/2}}, \tag{3.74}$$

and

$$d_k = -\tilde{T}. \tag{3.75}$$

A solution is assumed in the form of

$$T_{i,j,k}^{n+1} = ee_k T_{i,j,k+1}^{n+1} + gg_k. \tag{3.76}$$

Substituting $T_{i,j,k-1}^{n+1}$ from Eq. (3.76) into Eq. (3.72), the variables ee_k and gg_k yield

$$ee_k = \frac{a_k}{a_k + c_k(1 - ee_{k-1}) - 1} \tag{3.77}$$

and

$$gg_k = \frac{c_k gg_{k-1} + d_k}{a_k + c_k(1 - ee_{k-1}) - 1}. \tag{3.78}$$

To apply the surface boundary conditions, it is obtain from substituting $k = 1$ into Eq. (3.71), and then write in the form of Eq. (3.76), which is

$$ee_1 = \frac{a_1}{a_1 - 1} \tag{3.79}$$

and

$$gg_1 = \left(\frac{2\Delta t_I}{(D_{i,j}^{n+1})^2 \Delta\sigma_k} < wt(0) > -\tilde{T} \right) \left(\frac{a_1}{a_1 - 1} \right). \tag{3.80}$$

The solution is smoothed at each time step according to

$$(T_s)_{i,j,k}^{n} = T_{i,j,k}^{n} + \frac{\alpha}{2}(T_{i,j,k}^{n+1} - 2T_{i,j,k}^{n} + T_{i,j,k}^{n-1}) \tag{3.81}$$

where α is the parameter in the temporal smoother.

3.10.3 Time Step Constraints

The Courant-Friedrichs-Levy (CFL) computational stability conditions for internal and external modes are expressed as

$$\Delta t_I \leq \frac{1}{C_T}\left(\frac{1}{\Delta x^2}-\frac{1}{\Delta y^2}\right)^{-1/2} \tag{3.82}$$

and

$$\Delta t_E \leq \frac{1}{C_t}\left(\frac{1}{\Delta x^2}-\frac{1}{\Delta y^2}\right)^{-1/2} \tag{3.83}$$

where $C_T = 2C + U_{max}$ is the maximum internal gravity wave speed based on the gravest mode; U_{max} is the expected maximum velocity, and $C_t = 2(gH)^{1/2} + U_{max}$.

3.10.4 Parameters

The entire parameters and initial values used for solving the primitive equations are shown in Table 3.2.

Table 3.2 The parameters used in this research.

Parameter	Variable	Value	Unit
The reference seawater density	ρ_0	1025	kg/m^3
The gravitational acceleration	g	9.806	m/s^2
The roughness parameter [27]	z_0	0.01	-
The coefficient of the Smagorinsky diffusivity [19;20]	C	0.2	-
The expected maximum velocity	U_{max}	10	m/s
The initial value of the horizontal kinematic viscosity	A_M	500	-
The von Karman constant [27]	κ	0.4	-
The parameter in the temporal smoother [16]	α	0.1	-

3.11 Model Initialization

All above-mentioned methodologies are executed using an Ocean Circulation Model (OCM). The Princeton Ocean Model (POM) is applied in this research. It is used to solve the primitive equations in order to determine the current velocities, temperature, salinity, and density. The model is run until the time series of total kinetic energy (EK), total potential energy (EA), and total surface potential energy (EAS) reach a steady state. The formula for calculating the total kinetic energy (EK), total potential energy (EA), and total surface potential energy (EAS) are

$$EK = \frac{1}{2}\int\int\int \rho_0(U^2+V^2)dxdydz, \tag{3.84}$$

$$EA = -\frac{1}{2}g\int\int\int \frac{(\rho-\tilde{\rho})^2}{\frac{d\tilde{\rho}}{dz}}dxdydz, \tag{3.85}$$

and

$$EAS = \frac{1}{2}\int\int \rho_0 g\eta^2 dxdy \tag{3.86}$$

where $\tilde{\rho}$ is the horizontal averaging of the density field.

3.12 Heat Content of Volume and Transport Equations

The objective of this research is to investigate the heat content of volume, heat, freshwater, and water mass transports. The formula for the heat content is

$$Q = mc_pT \tag{3.87}$$

where

Q is the heat content (Joules, J);
m is the mass (kg);
c_p is the specific heat capacity (J/(kg $^\circ$ C)), and
T is the potential temperature ($^\circ$ C).

Since the density is the mass per unit volume, we can write their relationship as

$$\rho = \frac{m}{\hat{V}}$$

or

$$m = \rho\hat{V} \tag{3.88}$$

where

ρ is the seawater density (kg/m^3) and
$\hat{V}$ is the volume (m^3).

The formula for finding the volume is

$$\hat{V} = \iiint_{\hat{V}} dv. \tag{3.89}$$

Substituting Eq. (3.89) into Eq. (3.88), that is

$$m = \iiint_{\hat{V}} \rho dv. \tag{3.90}$$

Substituting Eq. (3.90) into Eq. (3.87), the heat content of volume is

$$Q = c_p \iiint_{\hat{V}} \rho T dv. \tag{3.91}$$

The integrated heat transport across an ocean basin of width L and depth $H(x)$ is

$$F_Q = c_p \int_0^L \int_{-H(x)}^0 \rho VT dz dx \tag{3.92}$$

where V is the current velocity in y direction.

The integrated freshwater transport across an ocean basin of width L and depth $H(x)$ is

$$F_W = \int_0^L \int_{-H(x)}^0 \rho V(1-S) dz dx \tag{3.93}$$

where S is the salinity.

The water mass transport of volume across an ocean basin of width L and depth $H(x)$ is

$$H_V = \int_0^L \int_{-H(x)}^0 V dz dx. \tag{3.94}$$

3.12.1 Discretization

Since the values of simulated current velocities, temperature, salinity, and density depend on grid locations, the equations of heat content of volume and heat, freshwater, and water mass transports, Eqs. (3.91) to (3.94), have to be discretized before calculation, which are expressed as

$$Q = c_p \sum_{k=1}^{kb-1} \sum_{i=1}^{im} \sum_{j=1}^{jm} \rho_{i,j,k} \Delta x_{i,j} \Delta y_{i,j} \Delta \sigma_k H_{i,j} T_{i,j,k}, \tag{3.95}$$

$$F_Q = c_p \sum_{k=1}^{kb-1} \sum_{i=1}^{im} \rho_{i,j,k} \left(\frac{V_{i,j,k} + V_{i,j+1,k}}{2} \right) \Delta x_{i,j} \Delta \sigma_k H_{i,j} T_{i,j,k}, \tag{3.96}$$

$$F_W = \sum_{k=1}^{kb-1} \sum_{i=1}^{im} \rho_{i,j,k} \left(\frac{V_{i,j,k} + V_{i,j+1,k}}{2} \right) (1 - S_{i,j,k}) \Delta x_{i,j} \Delta \sigma_k H_{i,j}, \tag{3.97}$$

and

$$H_V = \sum_{k=1}^{kb-1} \sum_{i=1}^{im} \left(\frac{V_{i,j,k} + V_{i,j+1,k}}{2} \right) \Delta x_{i,j} \Delta \sigma_k H_{i,j} \tag{3.98}$$

where

im and jm are the total number of grid points in x and y directions, respectively;
kb is the total number of levels in the sigma coordinate;
Δx and Δy are the grid spacing in x and y directions, respectively;
$\Delta \sigma$ is the difference of the value σ in the sigma coordinate, and
H is the bottom topography.

The equations (3.95) to (3.98) are used to calculate the heat content of volume and heat, freshwater, and water mass transports, respectively. In this research, we use the value of the specific heat capacity, c_p, as 3898 J/(kg °C)[18].

CHAPTER 4 RESULTS

Our main goals in this research are to investigate heat content of volume and transports of heat, freshwater, and water mass, which are calculated using the simulated current velocities, temperature, salinity, and density. Thus, the first step of this research is to simulate the current velocities, temperature, salinity, and density from the primitive equations using an Ocean Circulation Model (OCM). In this research, we use the Princeton Ocean Model (POM) to solve the primitive equations in order to determine the simulated current velocities, temperature, salinity, and density. The model is run until the time series of total kinetic energy (EK), total potential energy (EA), and total surface potential energy (EAS) reach a steady state. The time series of total kinetic energy, total potential energy, and total surface potential energy for each month are shown in Fig. 4.1 to 4.36.

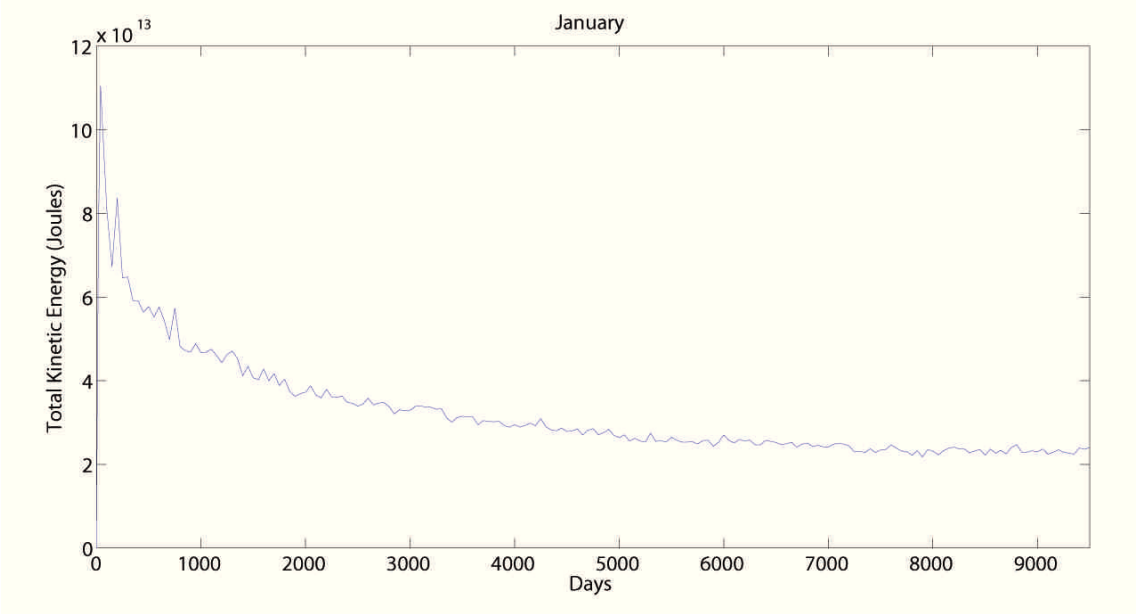

Figure 4.1 The time series of total kinetic energy in January.

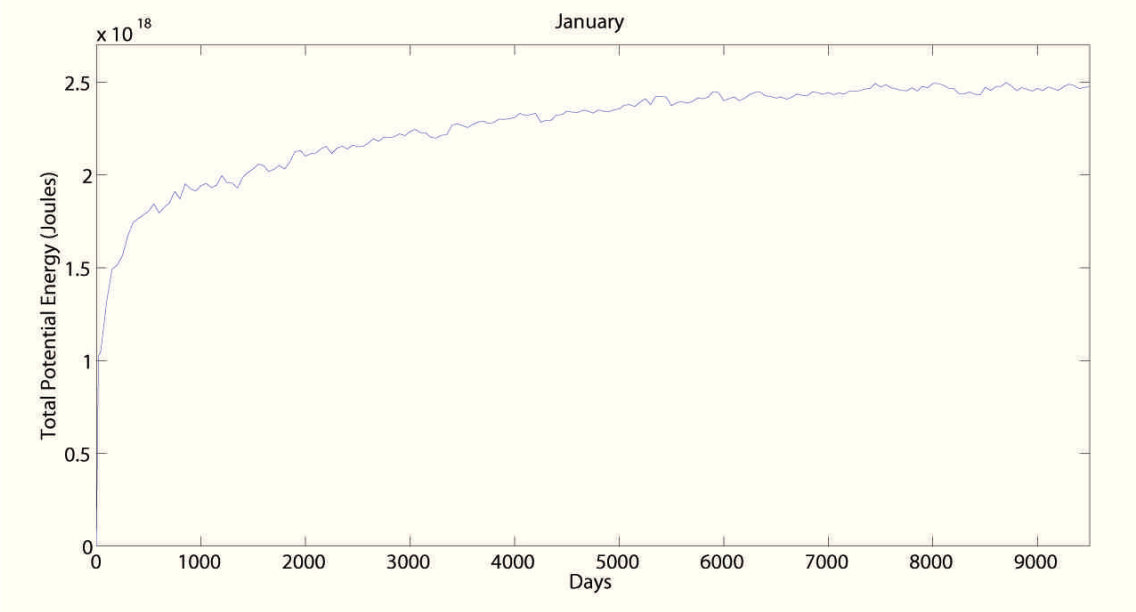

Figure 4.2 The time series of total potential energy in January.

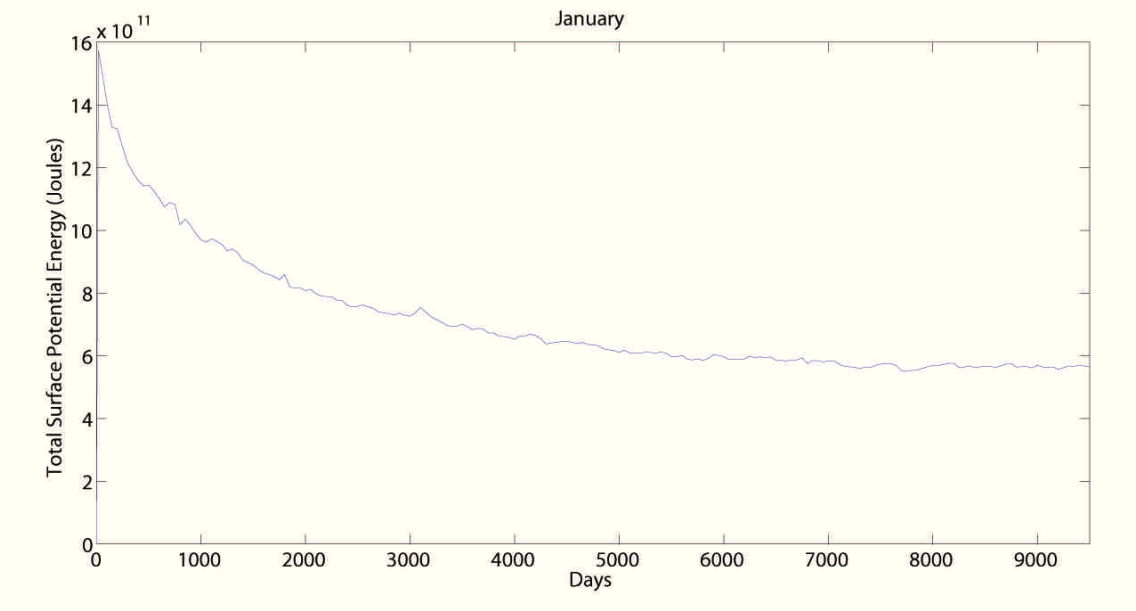

Figure 4.3 The time series of total surface potential energy in January.

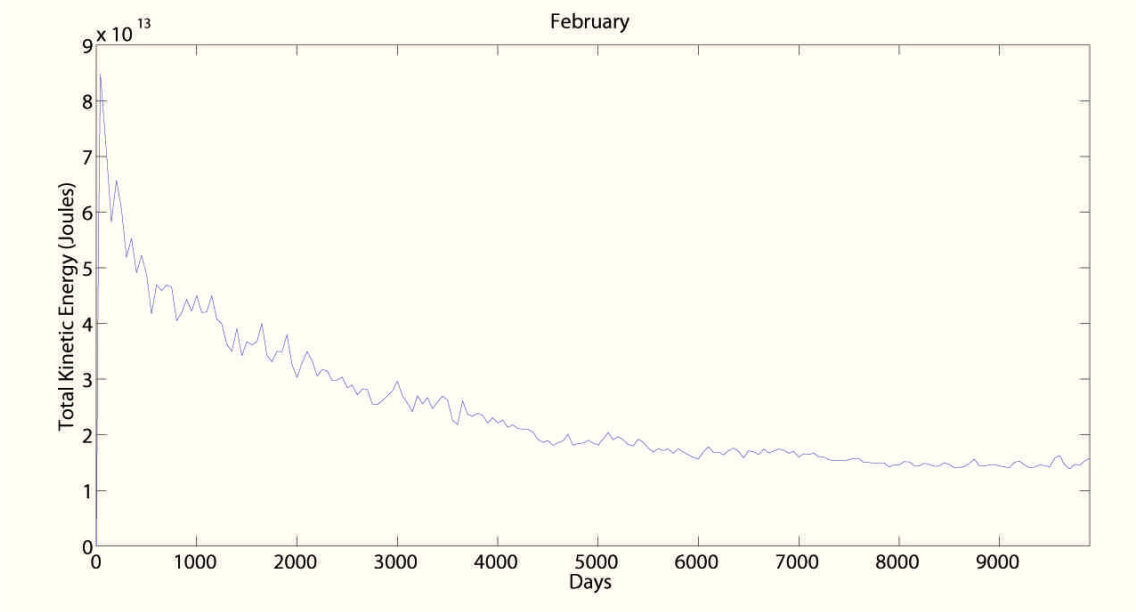

Figure 4.4 The time series of total kinetic energy in February.

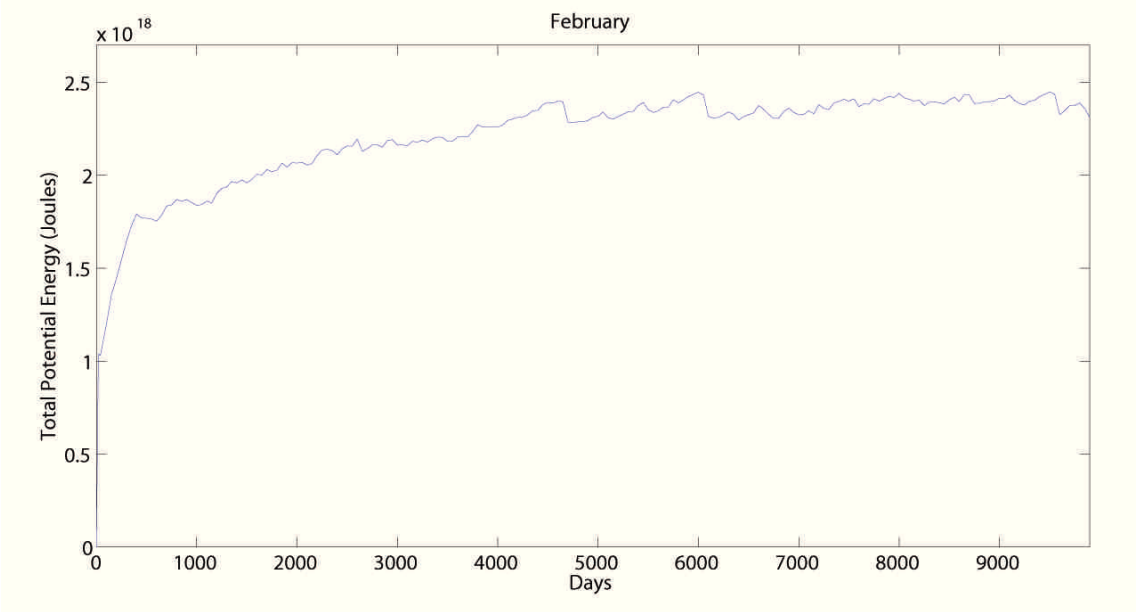

Figure 4.5 The time series of total potential energy in February.

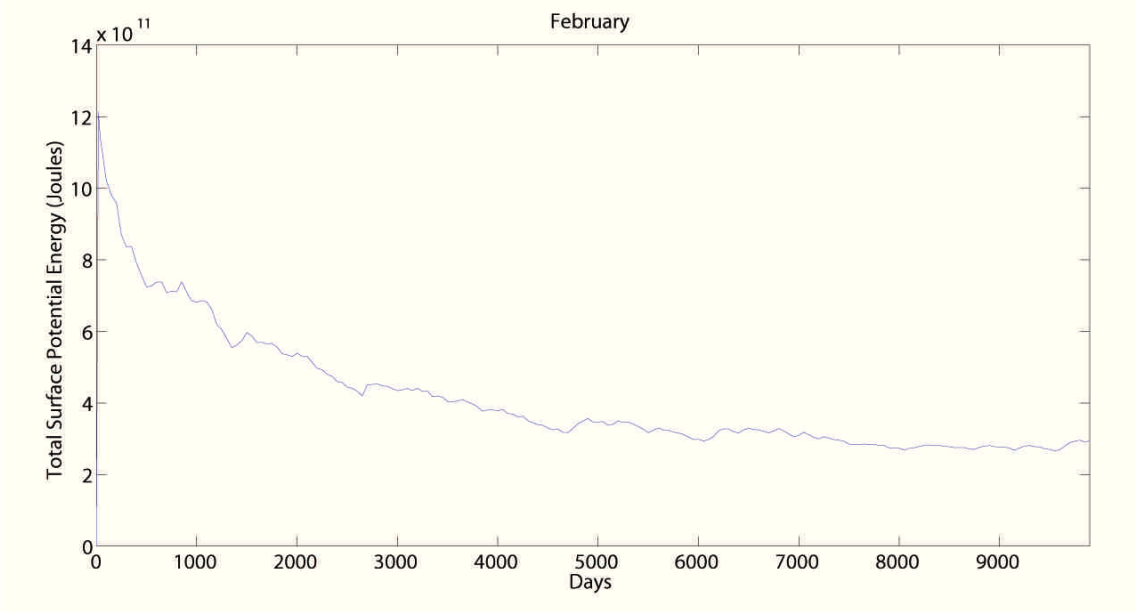

Figure 4.6 The time series of total surface potential energy in February.

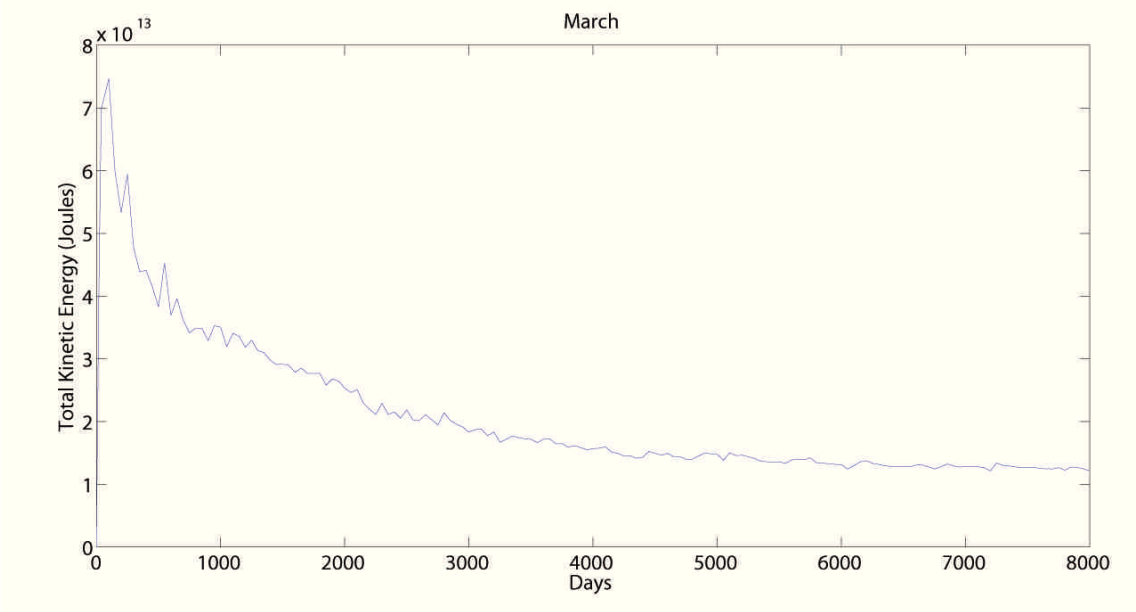

Figure 4.7 The time series of total kinetic energy in March.

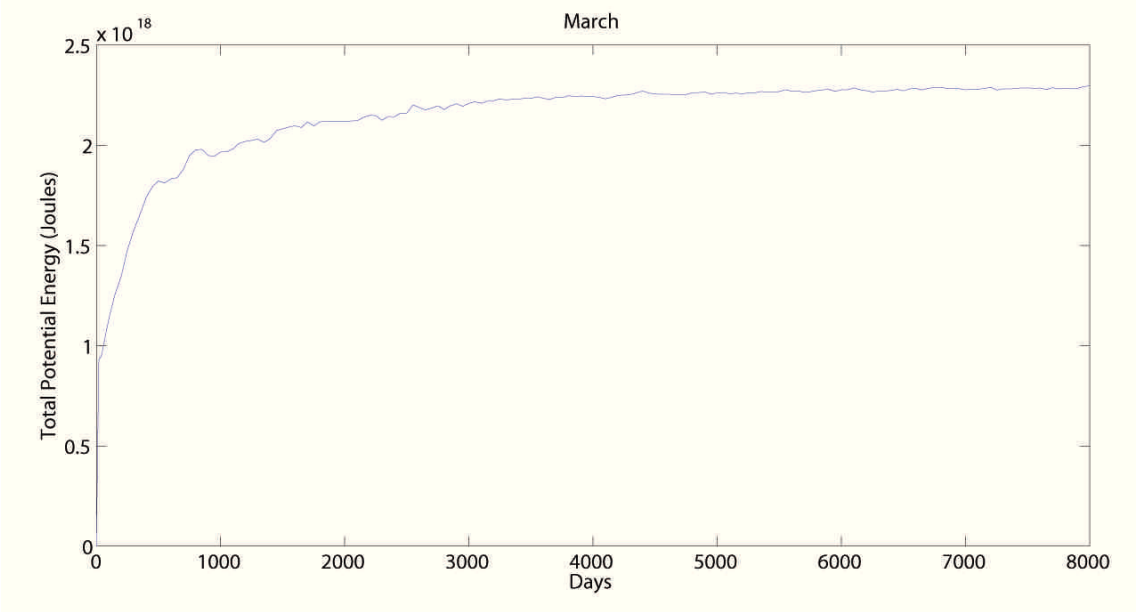

Figure 4.8 The time series of total potential energy in March.

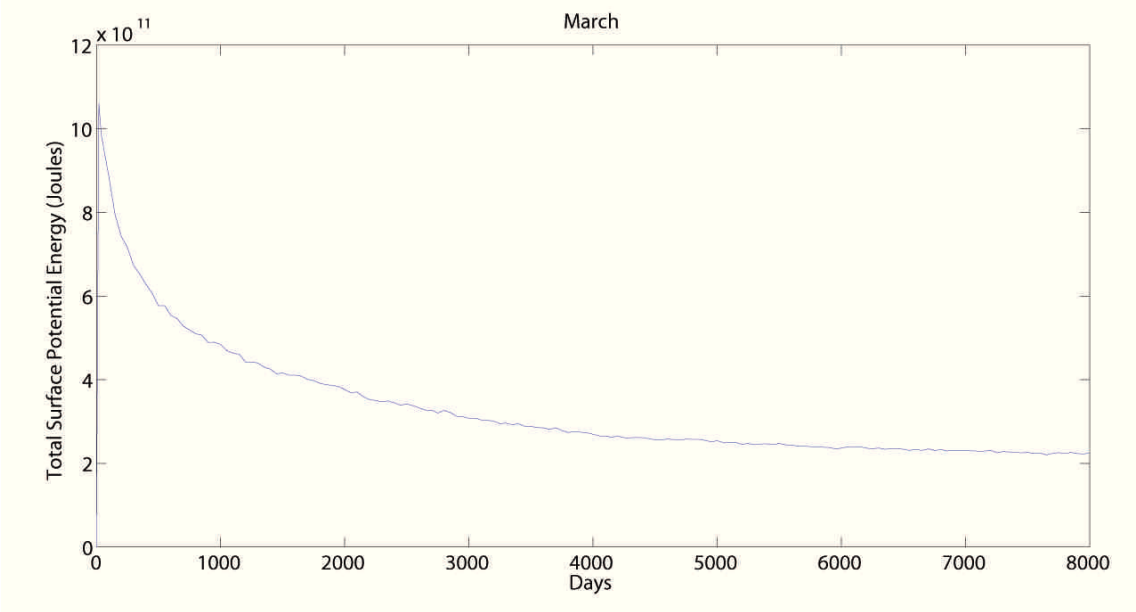

Figure 4.9 The time series of total surface potential energy in March.

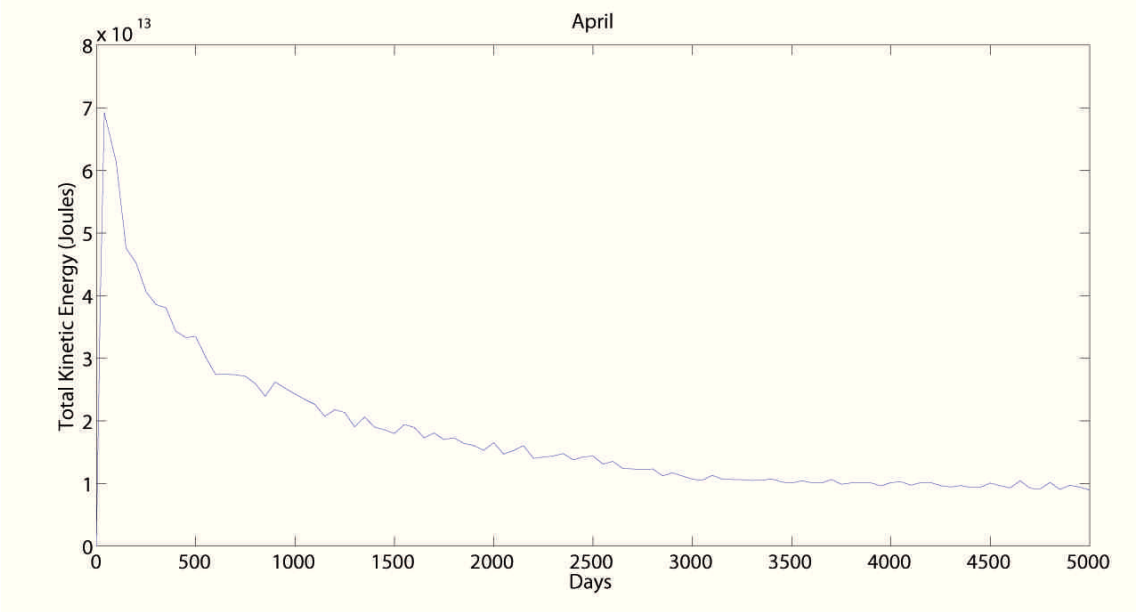

Figure 4.10 The time series of total kinetic energy in April.

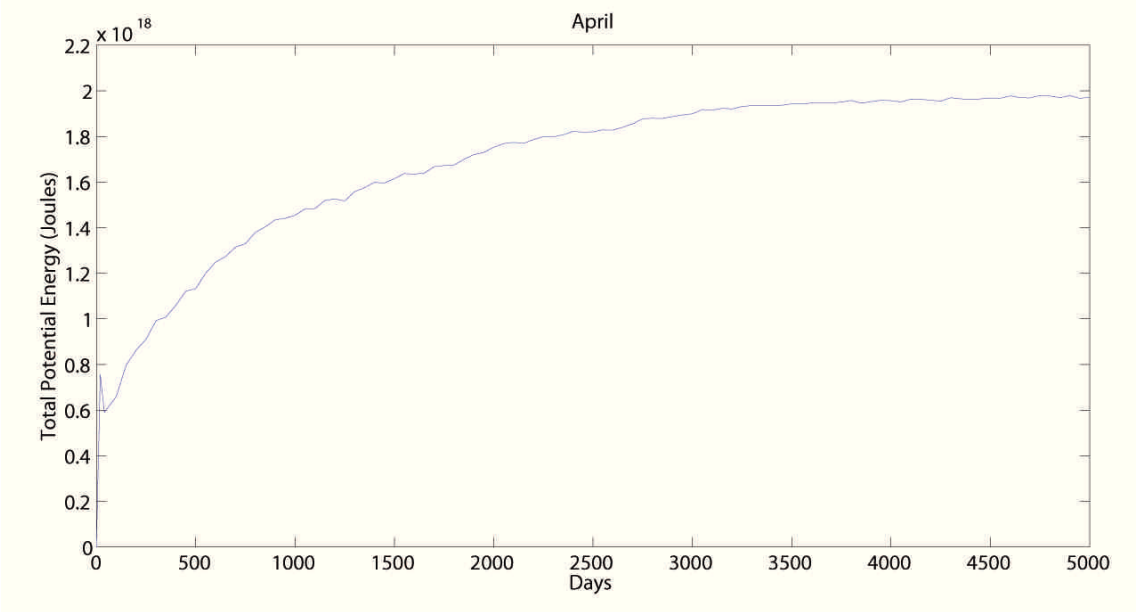

Figure 4.11 The time series of total potential energy in April.

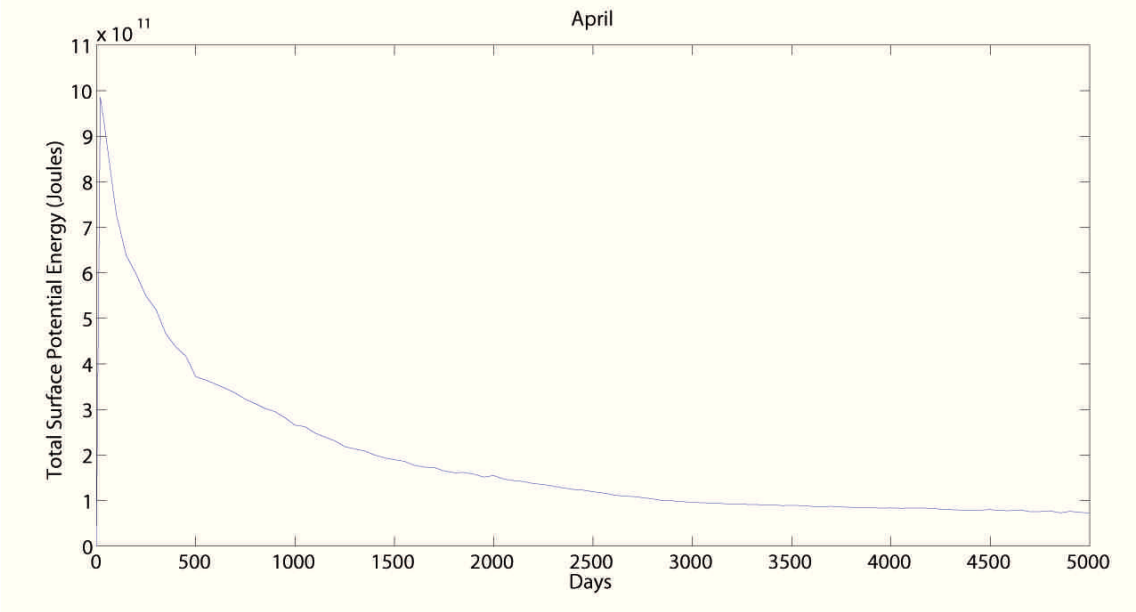

Figure 4.12 The time series of total surface potential energy in April.

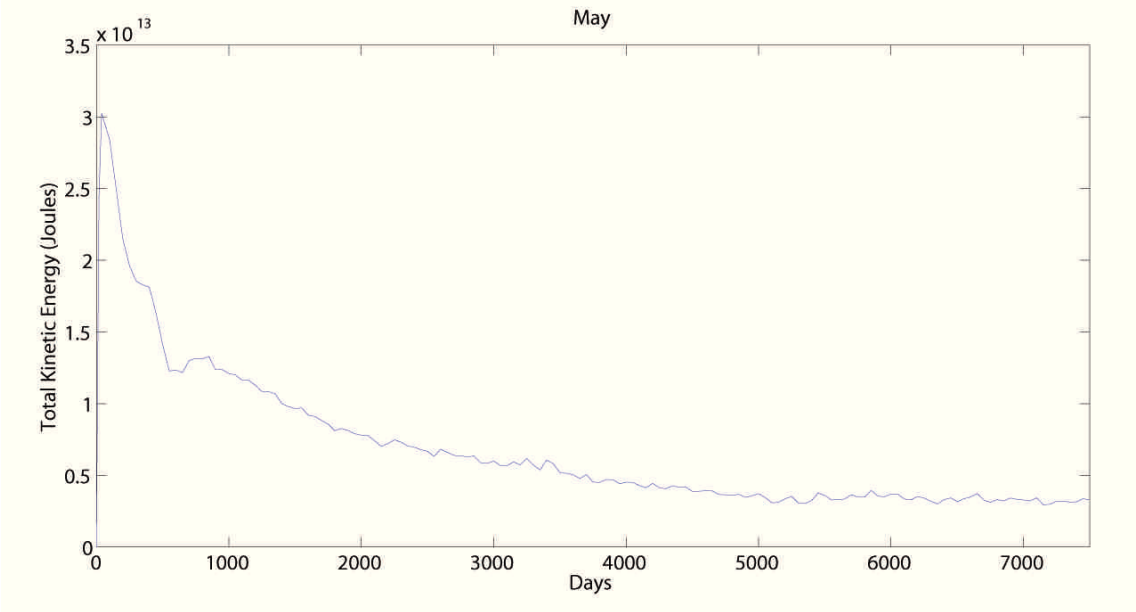

Figure 4.13 The time series of total kinetic energy in May.

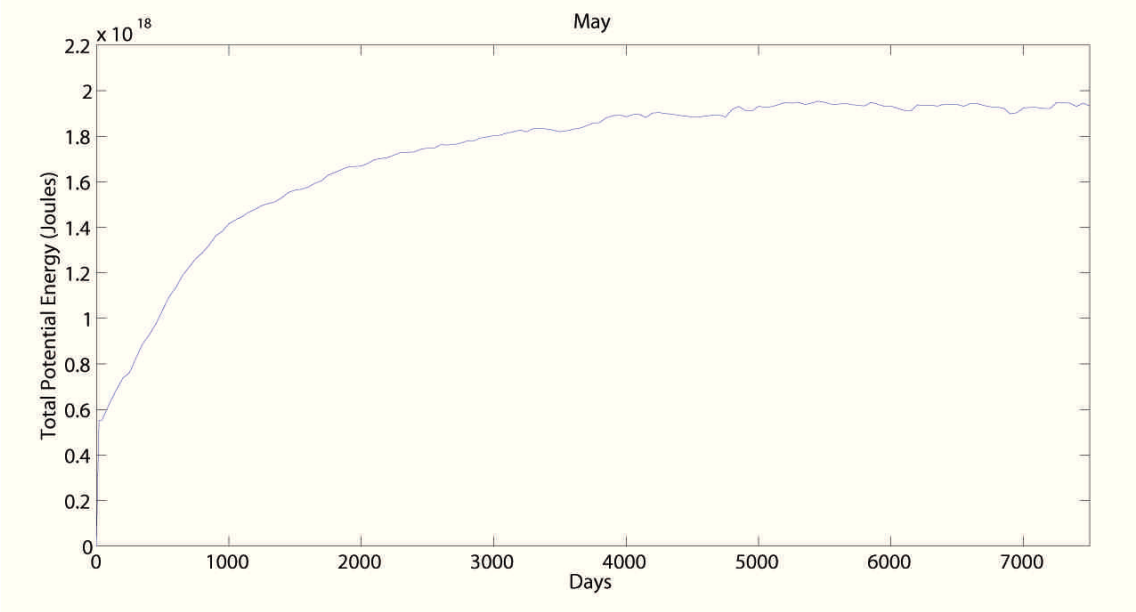

Figure 4.14 The time series of total potential energy in May.

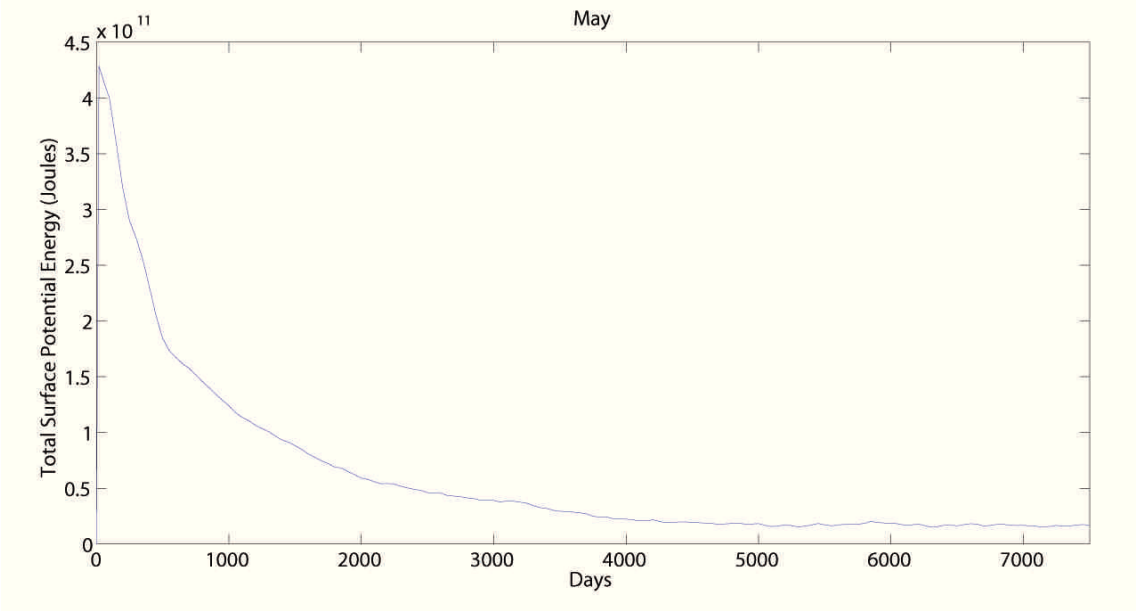

Figure 4.15 The time series of total surface potential energy in May.

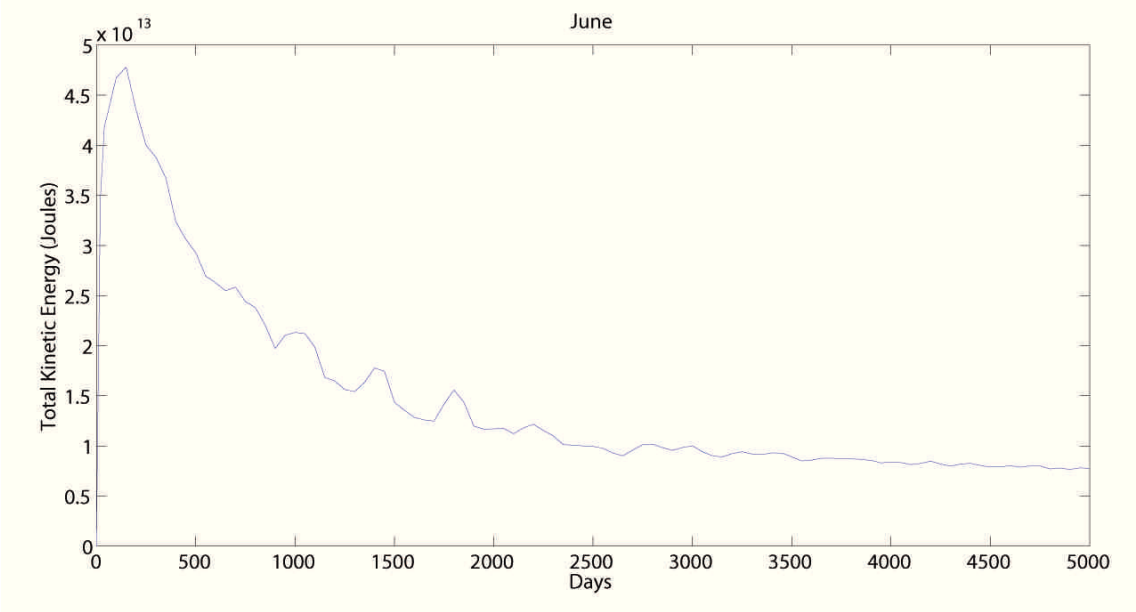

Figure 4.16 The time series of total kinetic energy in June.

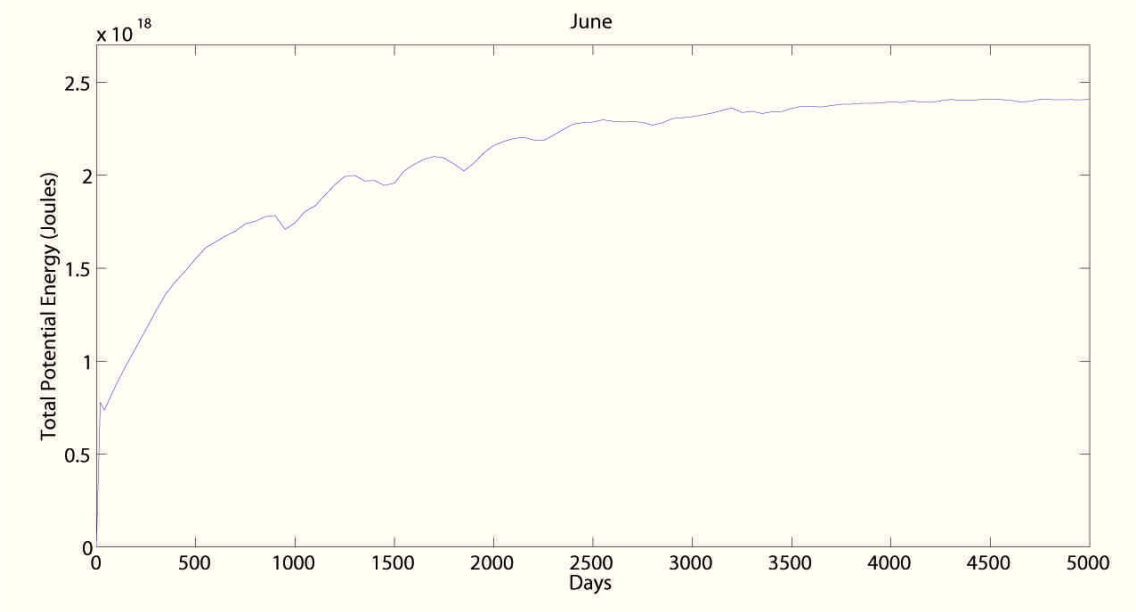

Figure 4.17 The time series of total potential energy in June.

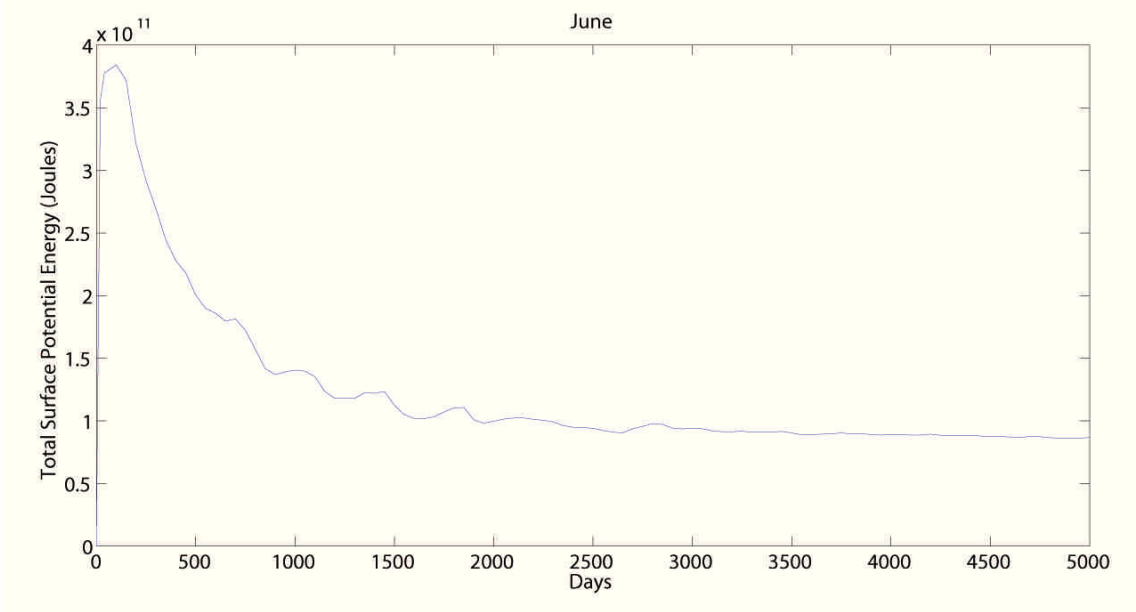

Figure 4.18 The time series of total surface potential energy in June.

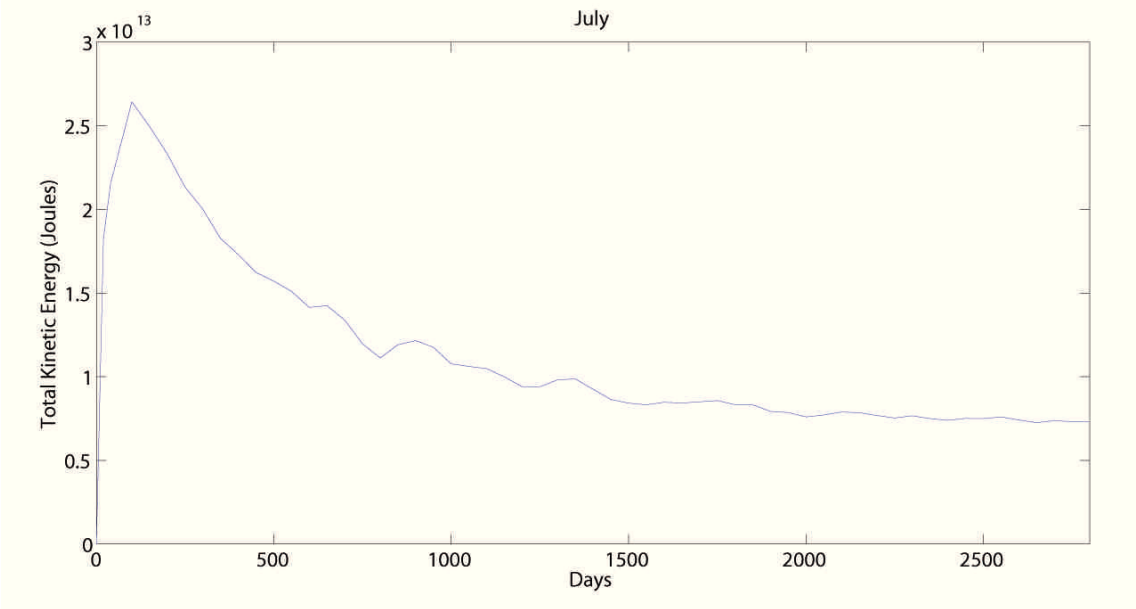

Figure 4.19 The time series of total kinetic energy in July.

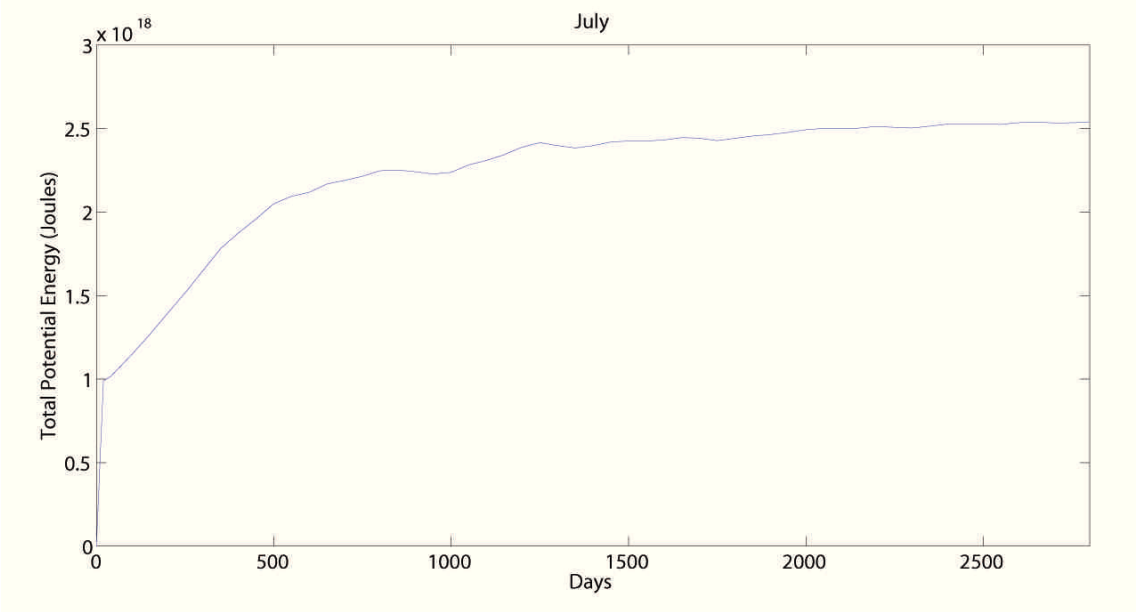

Figure 4.20 The time series of total potential energy in July.

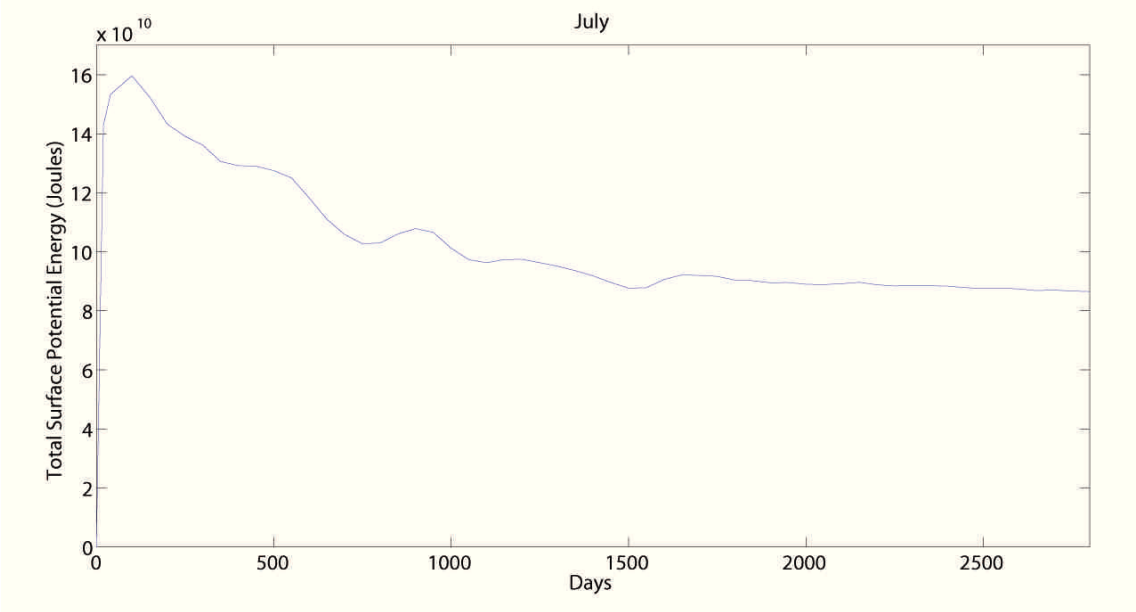

Figure 4.21 The time series of total surface potential energy in July.

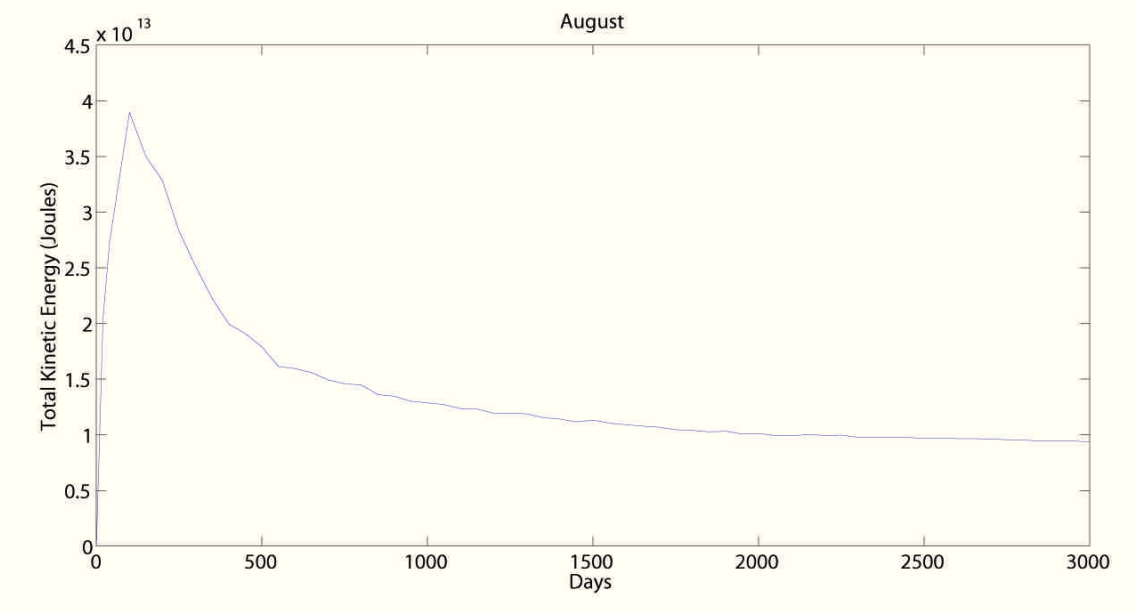

Figure 4.22 The time series of total kinetic energy in August.

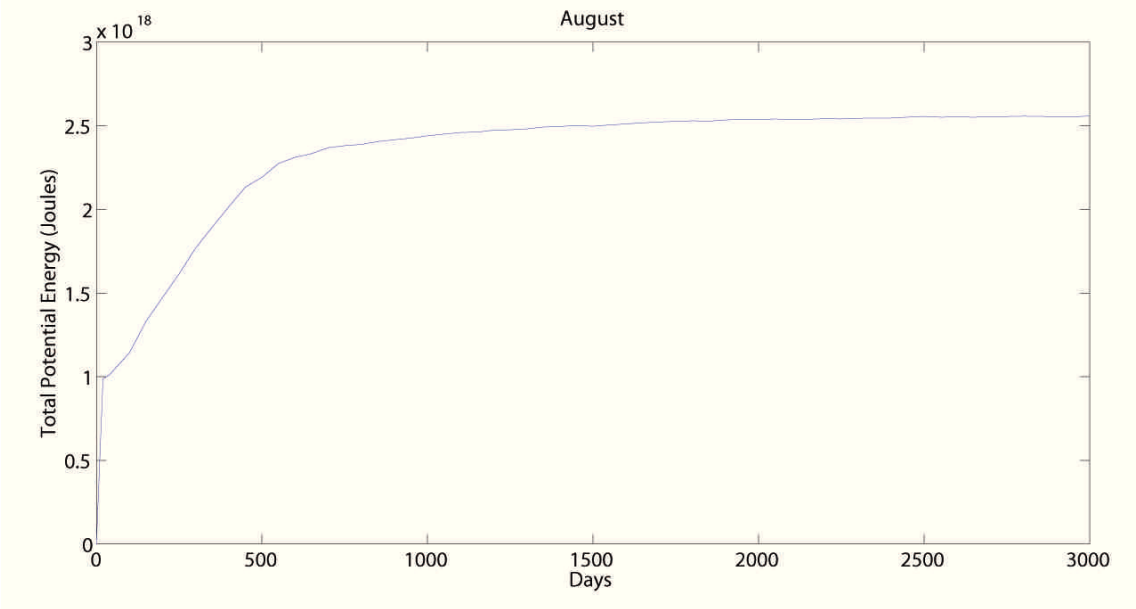

Figure 4.23 The time series of total potential energy in August.

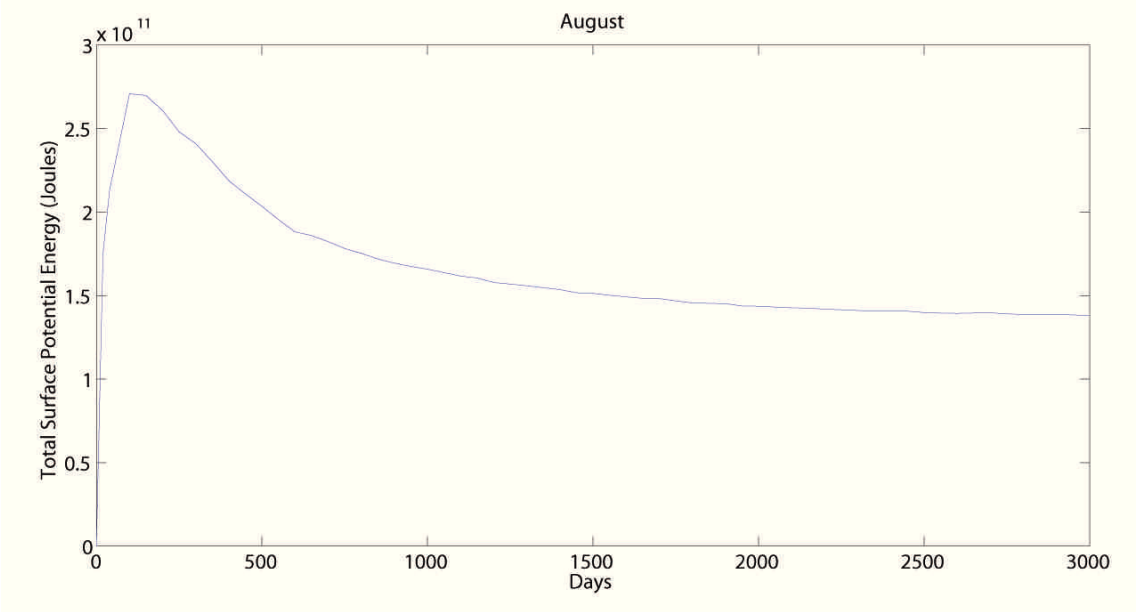

Figure 4.24 The time series of total surface potential energy in August.

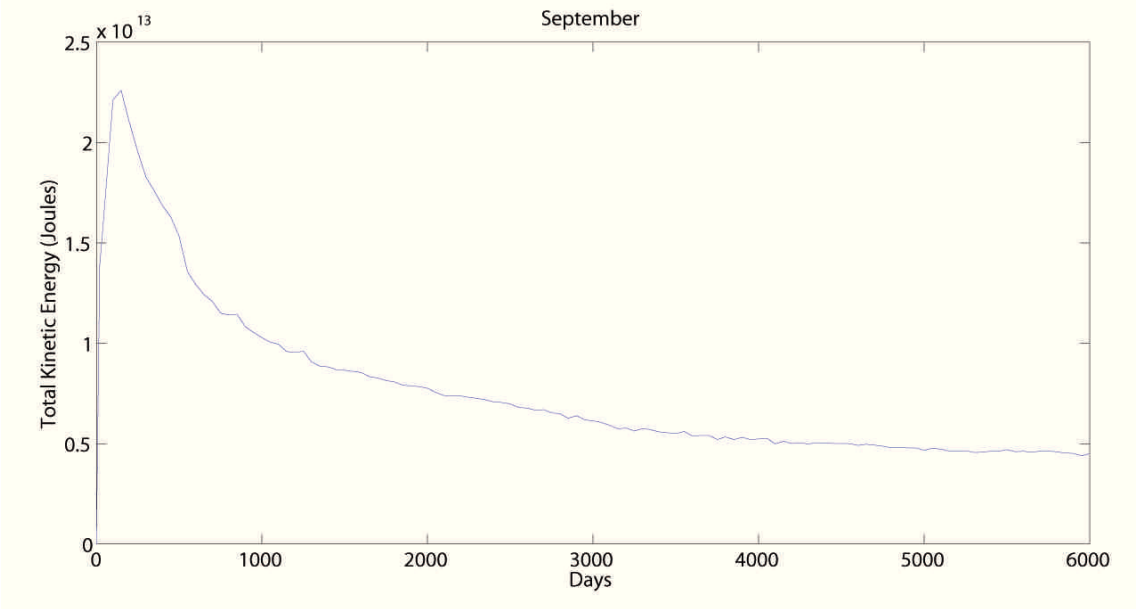

Figure 4.25 The time series of total kinetic energy in September.

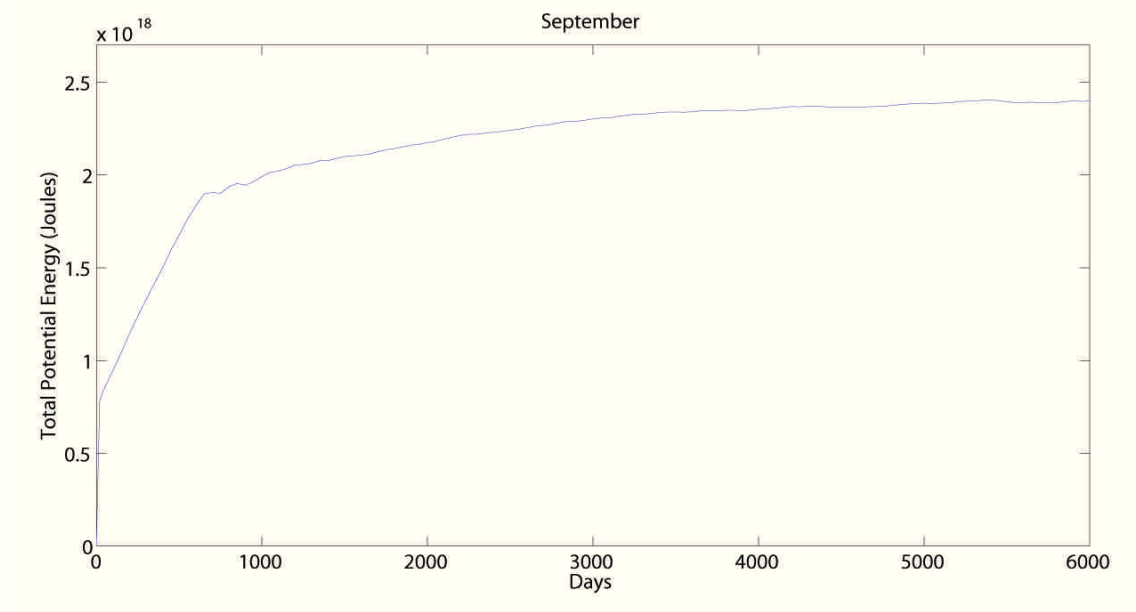

Figure 4.26 The time series of total potential energy in September.

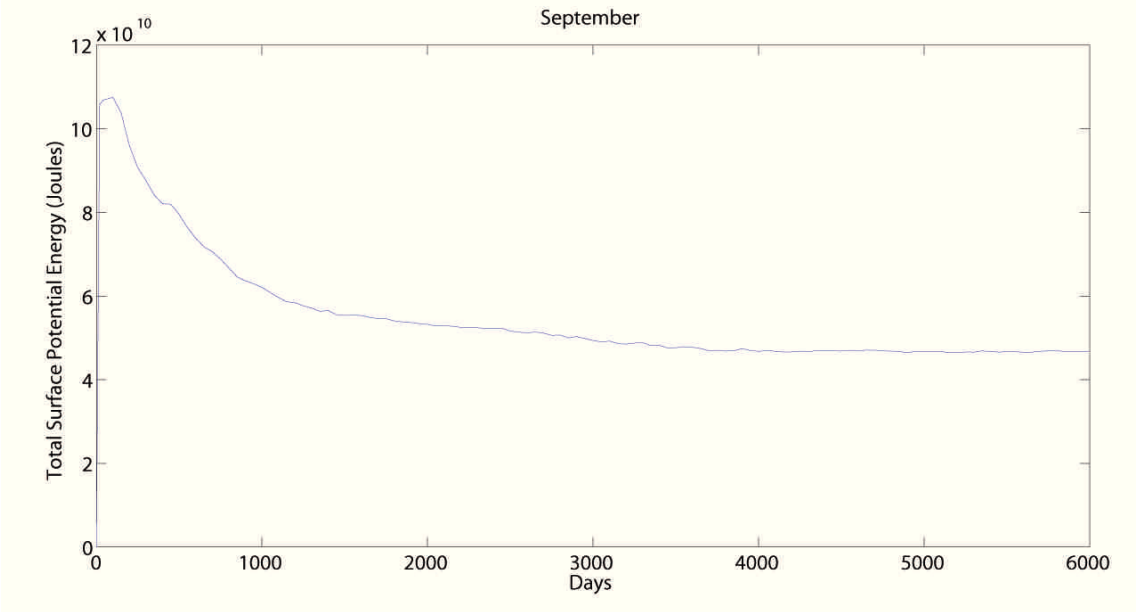

Figure 4.27 The time series of total surface potential energy in September.

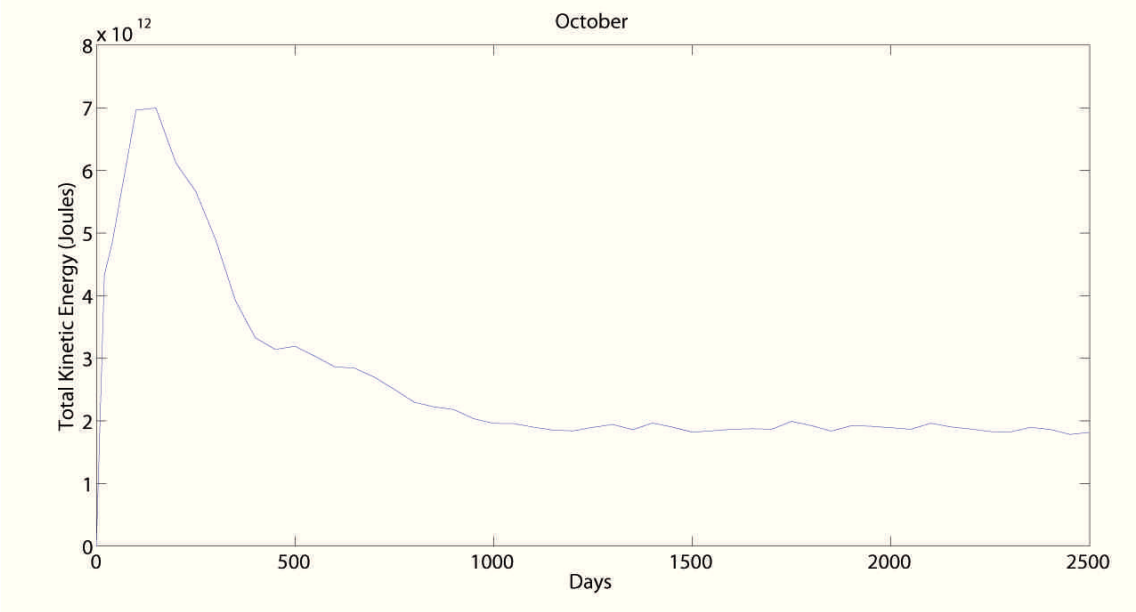

Figure 4.28 The time series of total kinetic energy in October.

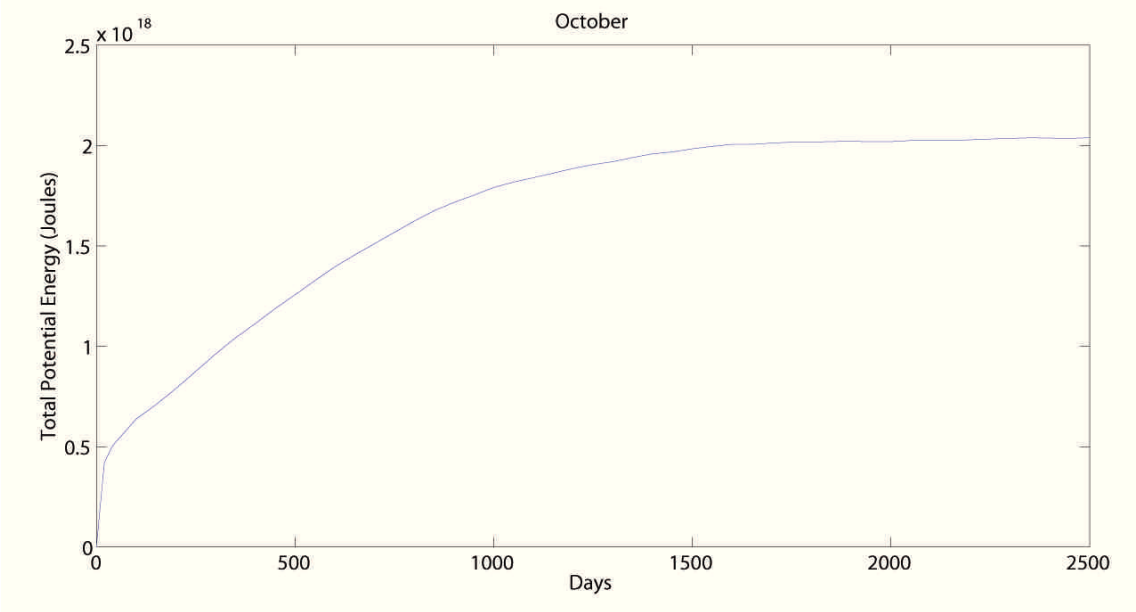

Figure 4.29 The time series of total potential energy in October.

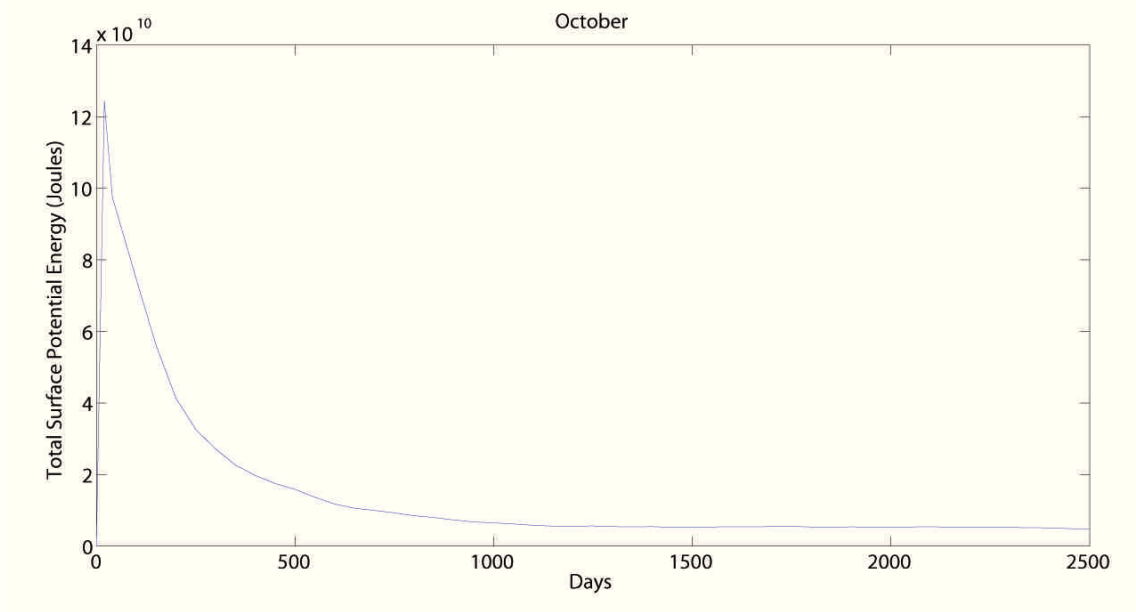

Figure 4.30 The time series of total surface potential energy in October.

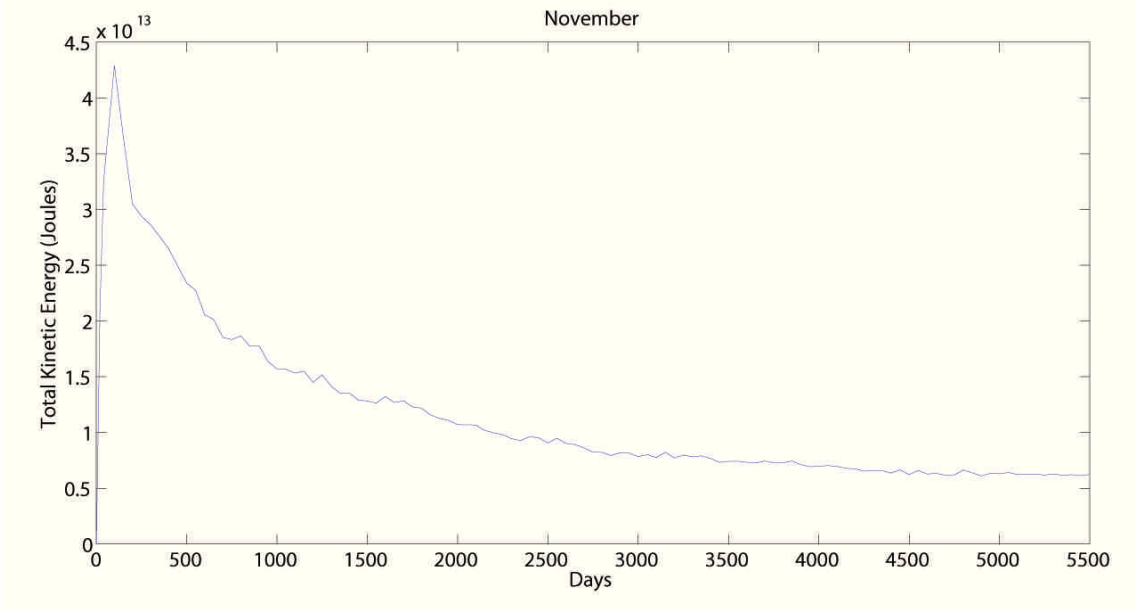

Figure 4.31 The time series of total kinetic energy in November.

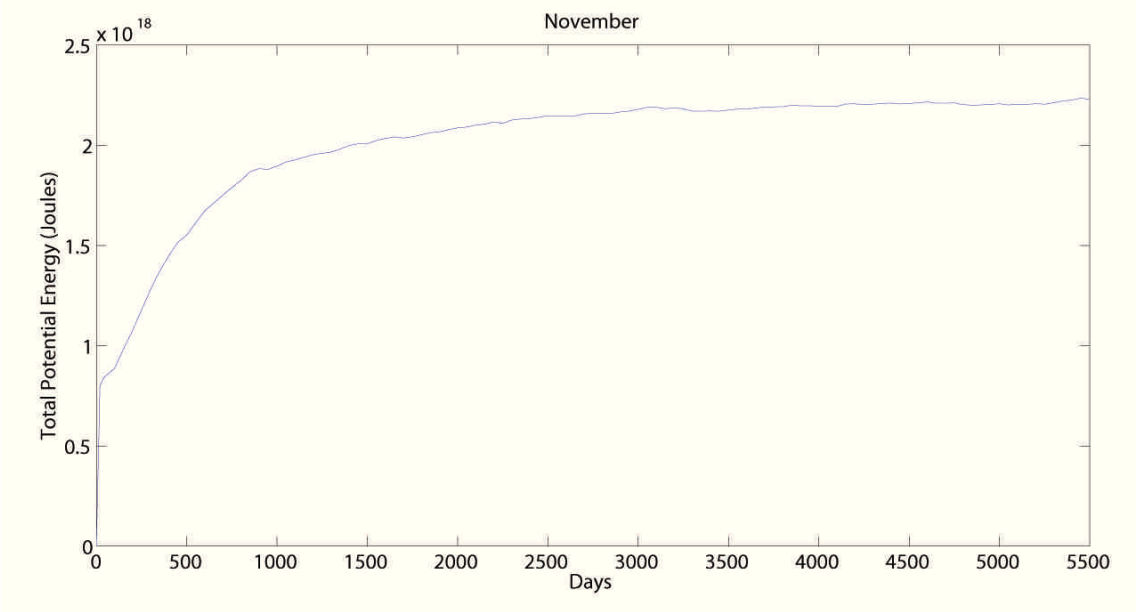

Figure 4.32 The time series of total potential energy in November.

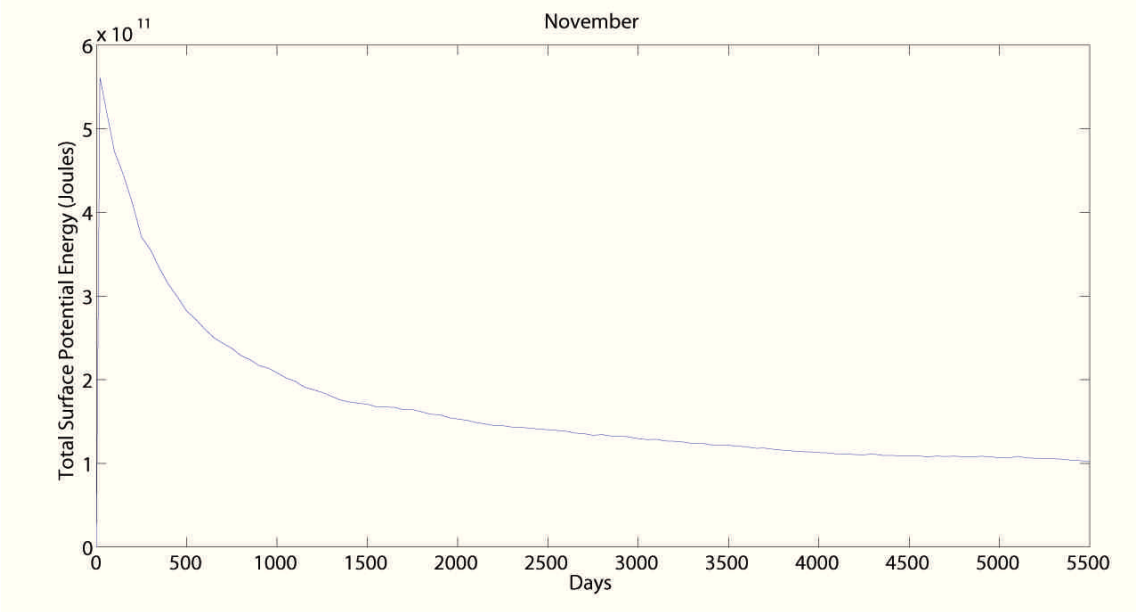

Figure 4.33 The time series of total surface potential energy in November.

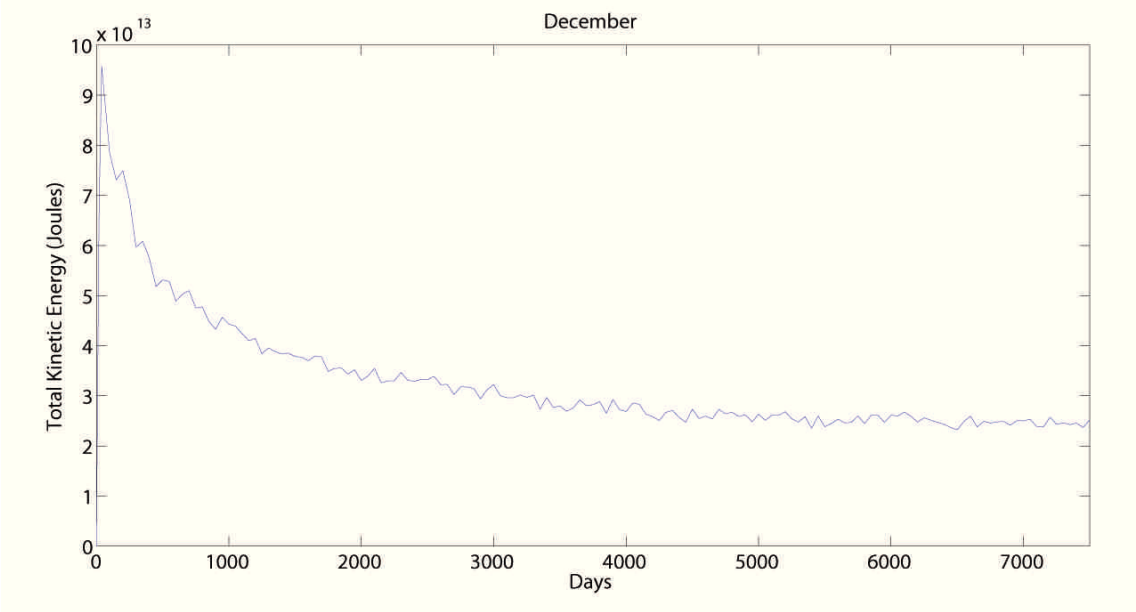

Figure 4.34 The time series of total kinetic energy in December.

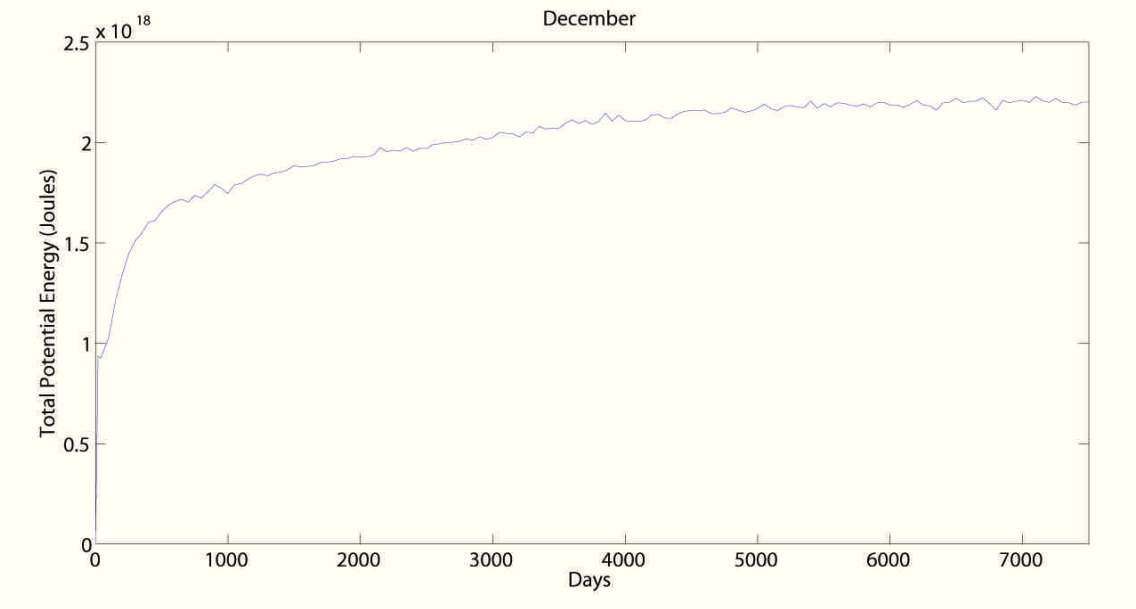

Figure 4.35 The time series of total potential energy in December.

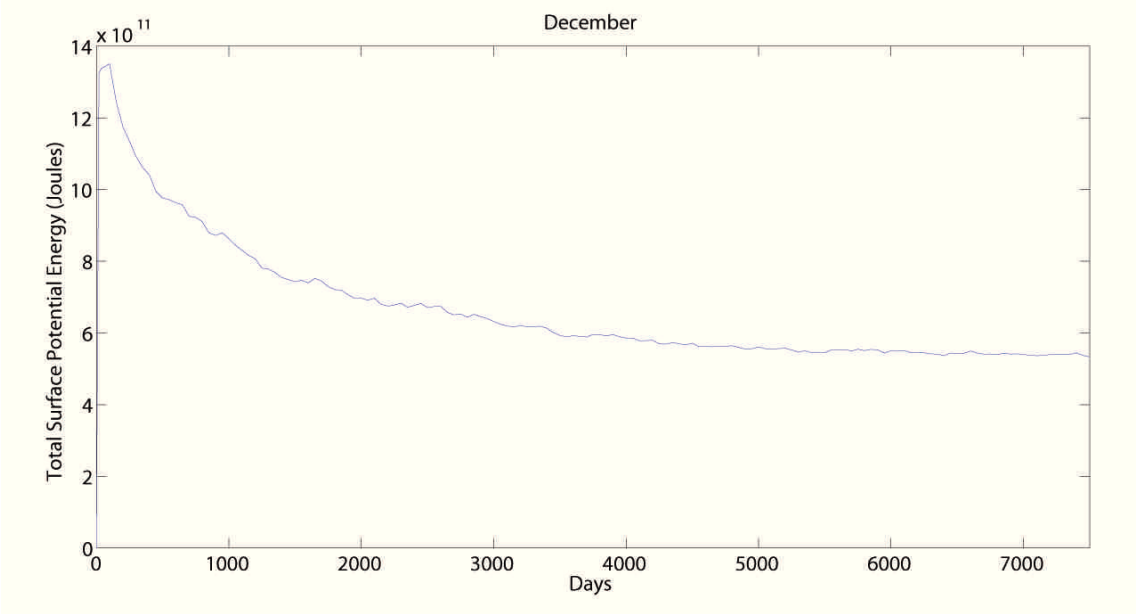

Figure 4.36 The time series of total surface potential energy in December.

It can be seen that the time series of total kinetic energy and total surface potential energy have the same trend. Their values increase rapidly in the first one hundred days, and then decrease slowly until the steady state. For the time-series of total potential energy, its value increases slowly until the steady state. The numbers of days used in the model run for each month are shown in Table 4.1.

Table 4.1 The numbers of days used in the model run for each month.

Month	Days
January	9500
February	9900
March	8000
April	5000
May	7500
June	5000
July	2800
August	3000
September	6000
October	2500
November	5500
December	7500

At the specified time in Table 4.1 of the model run, the simulated current velocities, potential temperature, salinity, and seawater density are used to be results for this research. The example results of simulated current circulation, potential temperature and salinity from the Princeton Ocean Model are shown in Figs. 4.37 to 4.144.

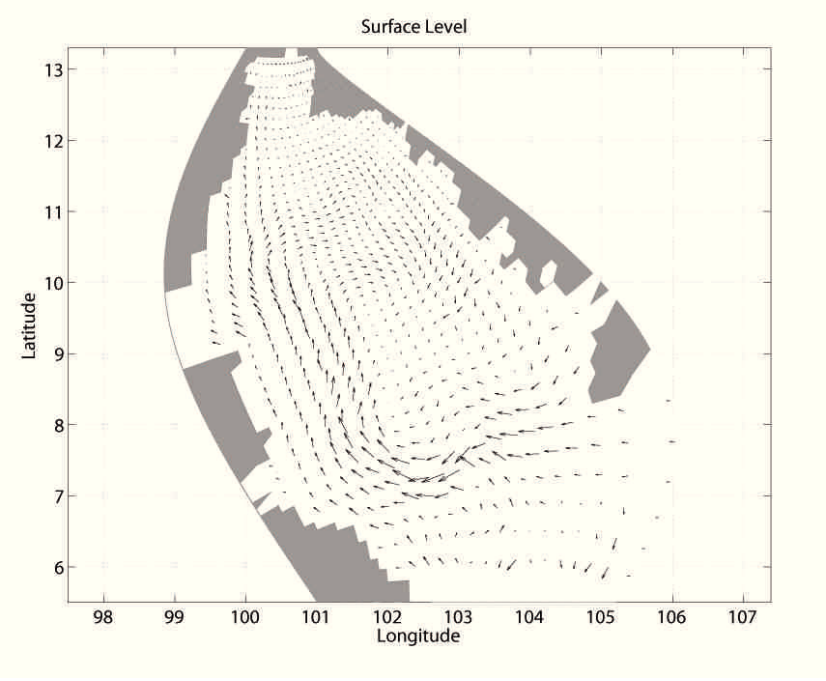

Figure 4.37 The simulated current circulation at surface level in January.

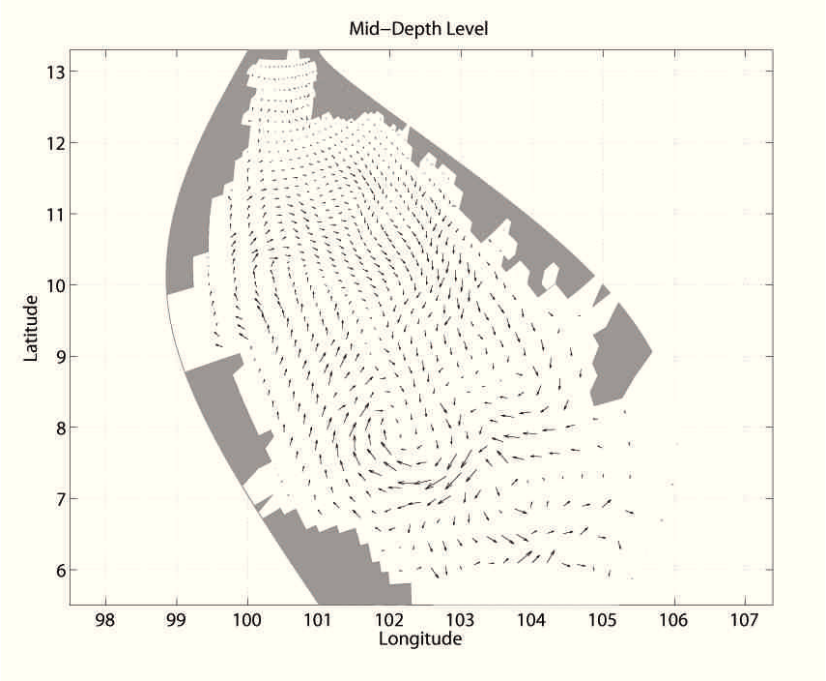

Figure 4.38 The simulated current circulation at mid-depth level in January.

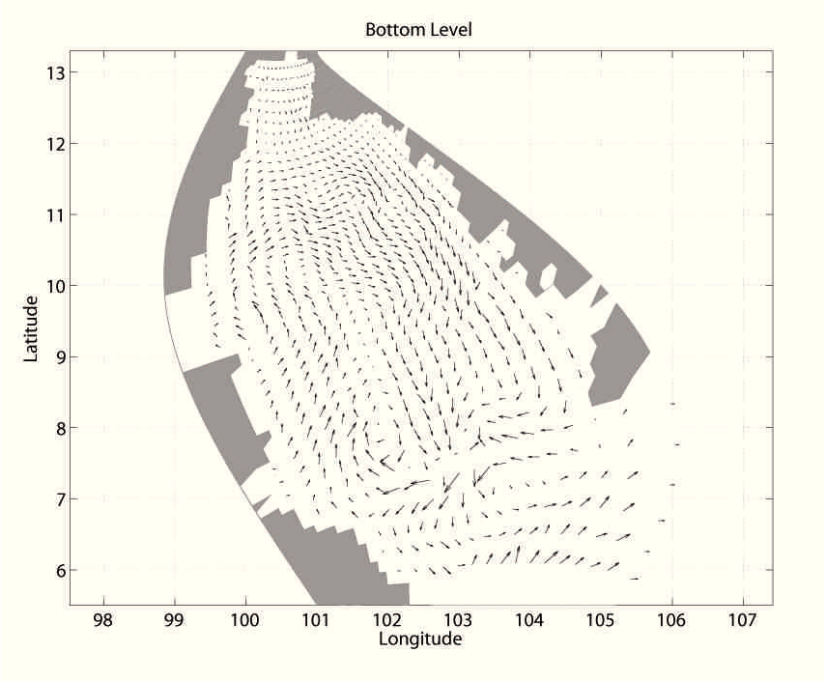

Figure 4.39 The simulated current circulation at bottom level in January.

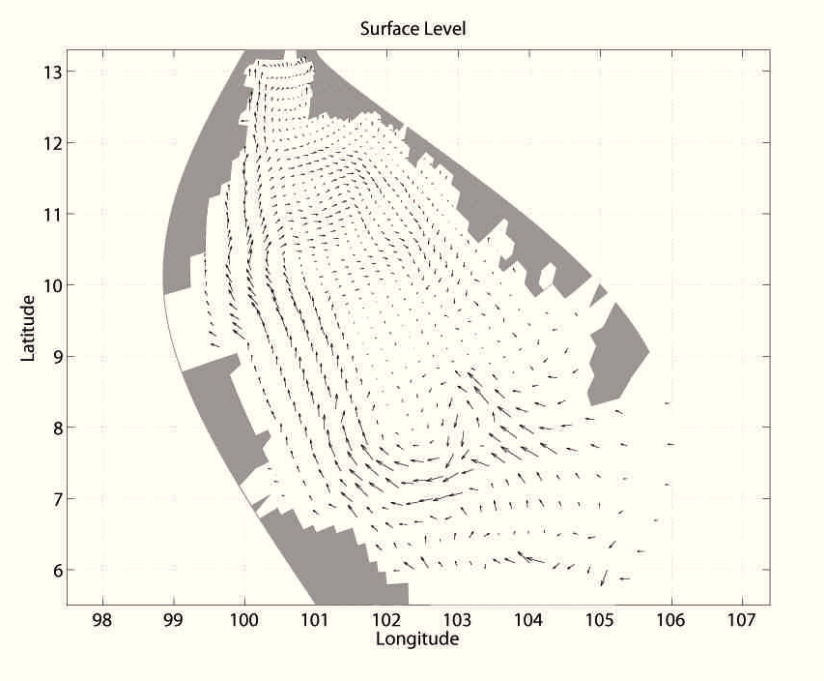

Figure 4.40 The simulated current circulation at surface level in February.

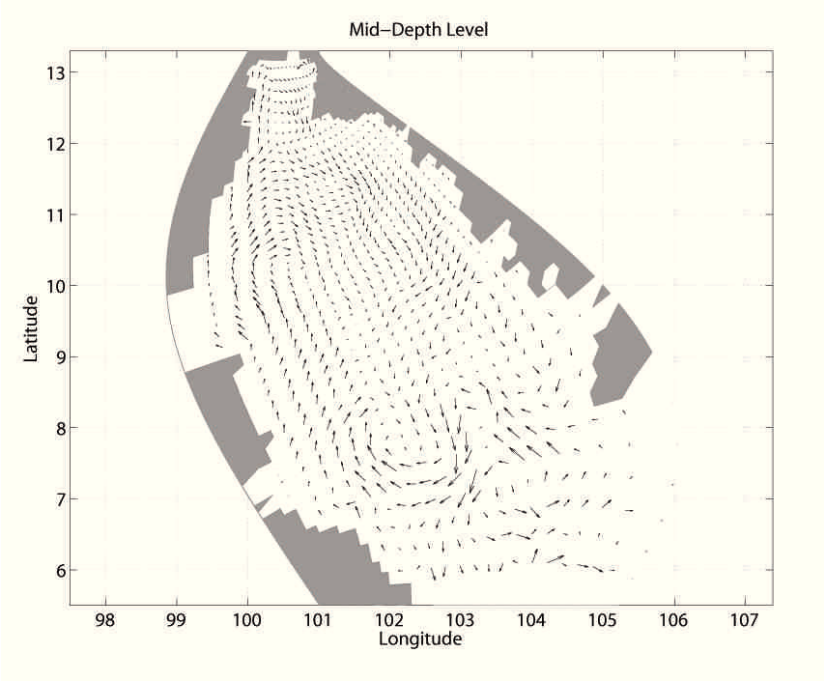

Figure 4.41 The simulated current circulation at mid-depth level in February.

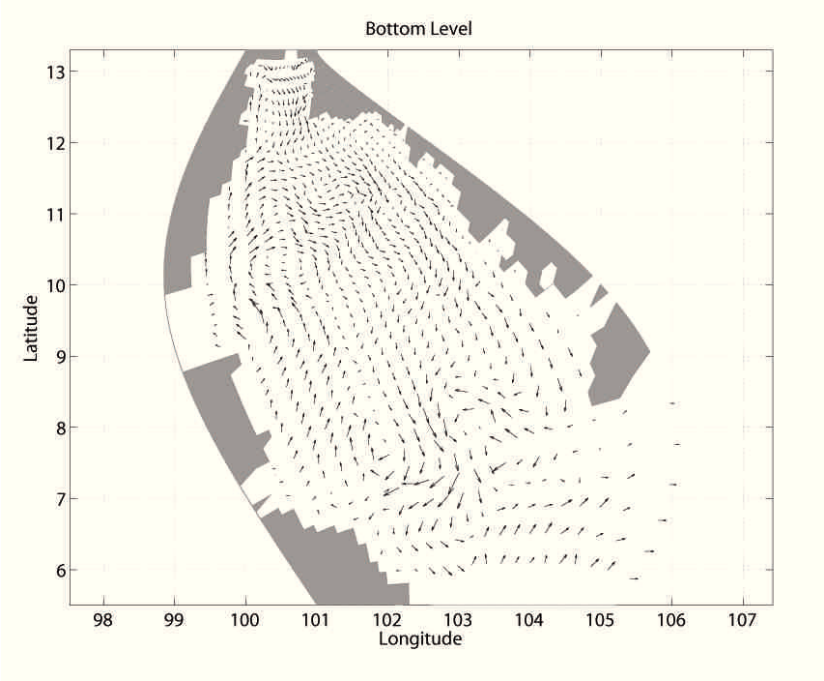

Figure 4.42 The simulated current circulation at bottom level in February.

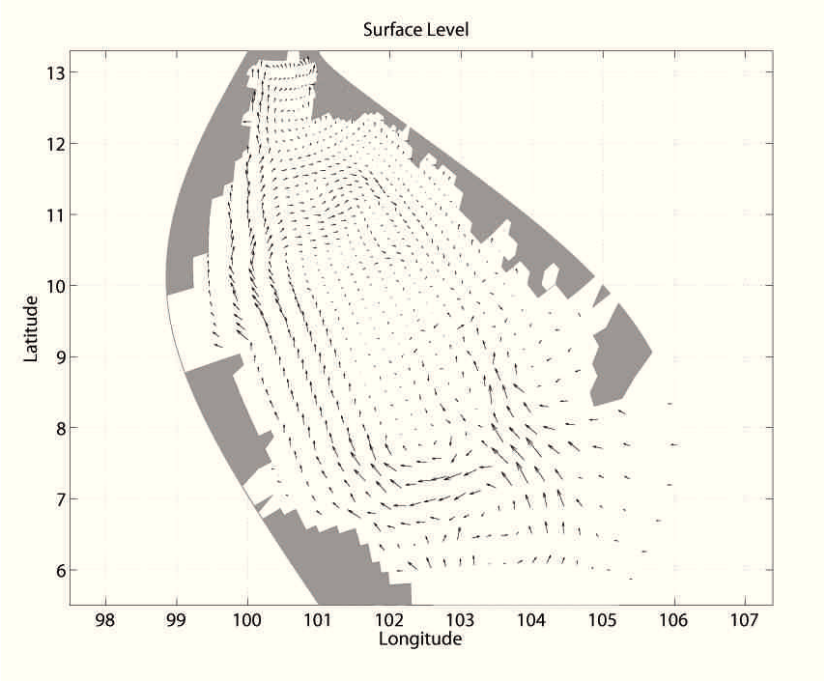

Figure 4.43 The simulated current circulation at surface level in March.

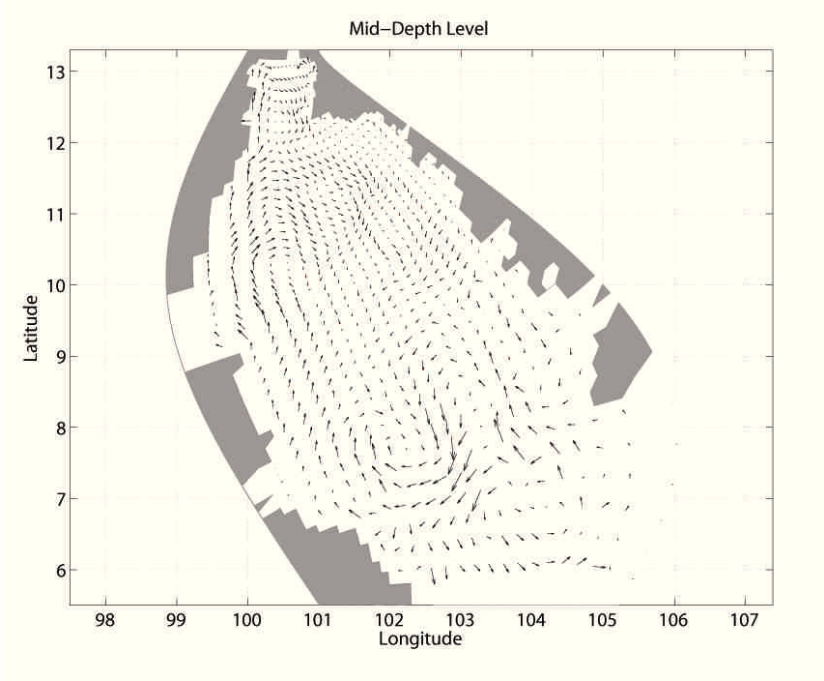

Figure 4.44 The simulated current circulation at mid-depth level in March.

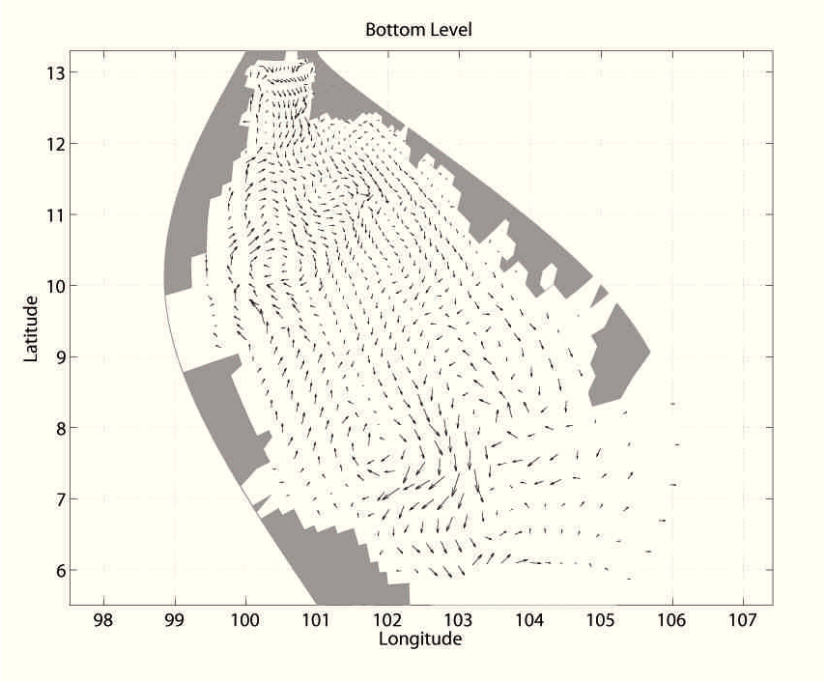

Figure 4.45 The simulated current circulation at bottom level in March.

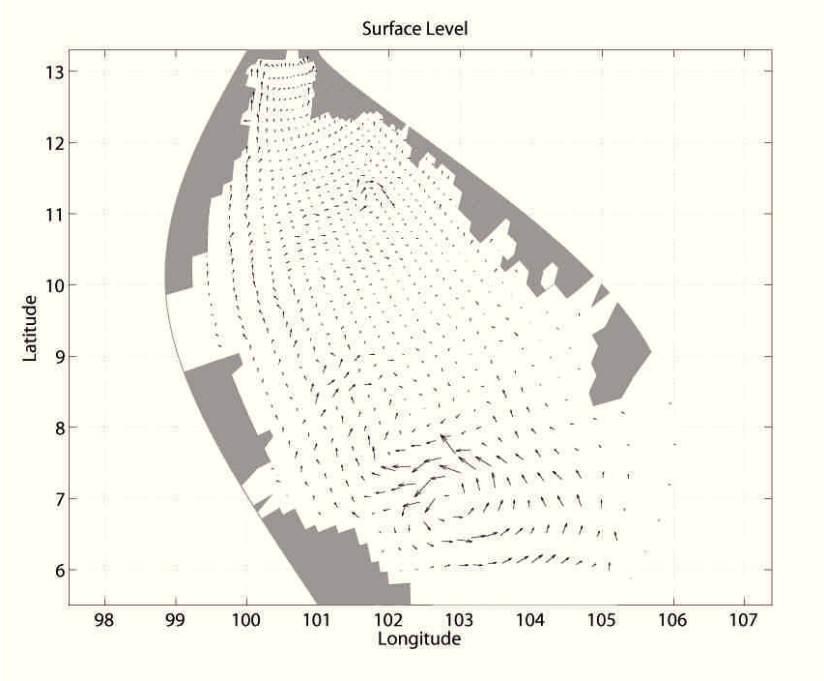

Figure 4.46 The simulated current circulation at surface level in April.

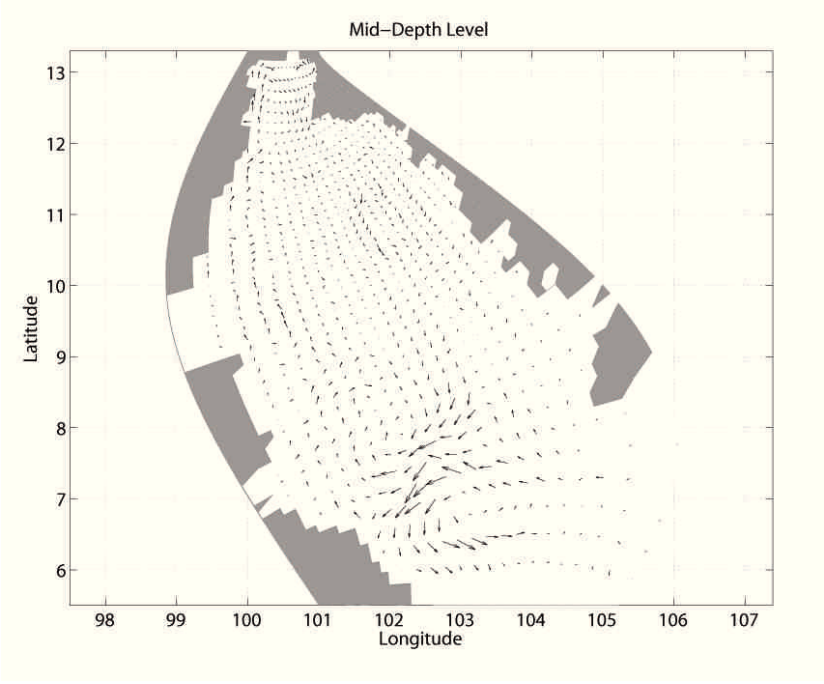

Figure 4.47 The simulated current circulation at mid-depth level in April.

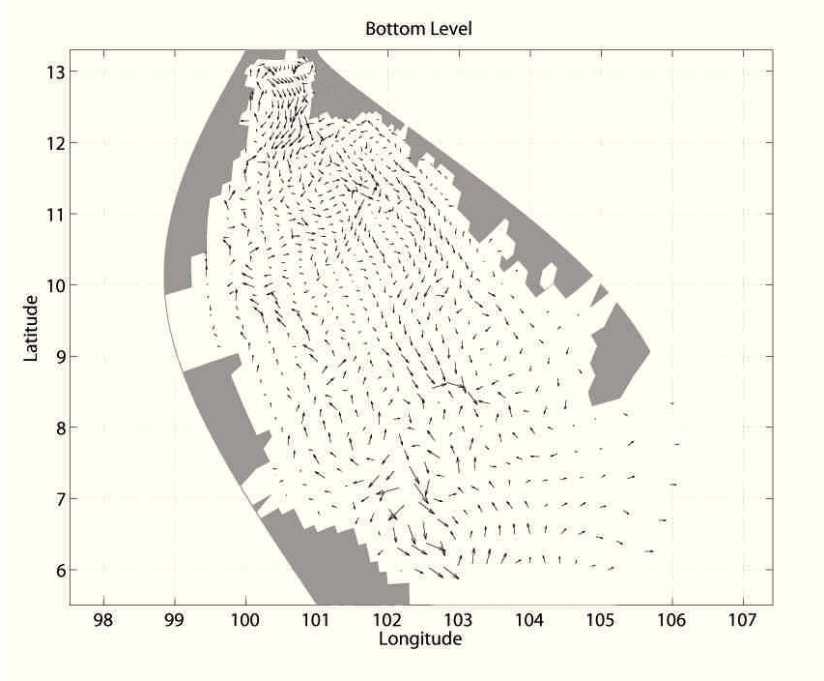

Figure 4.48 The simulated current circulation at bottom level in April.

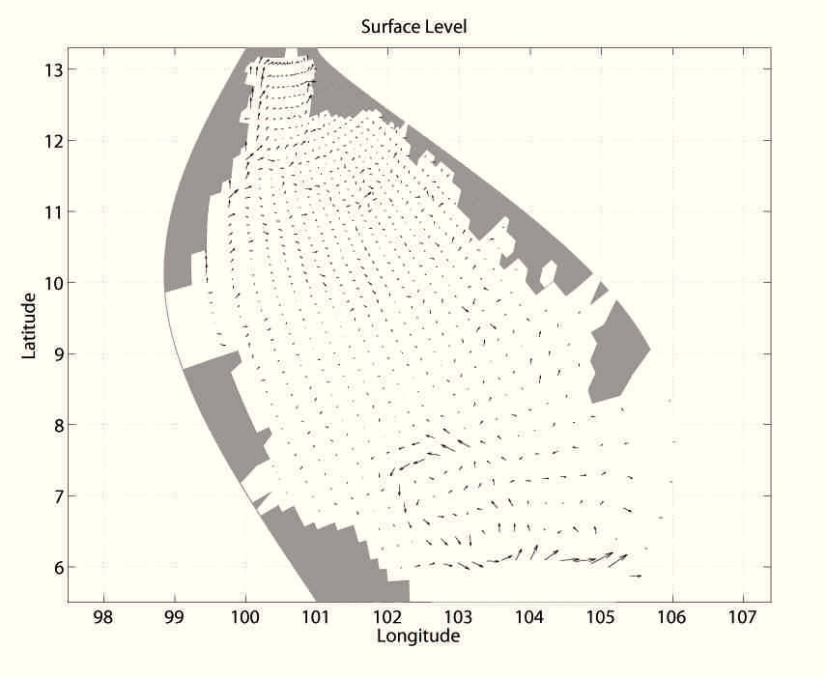

Figure 4.49 The simulated current circulation at surface level in May.

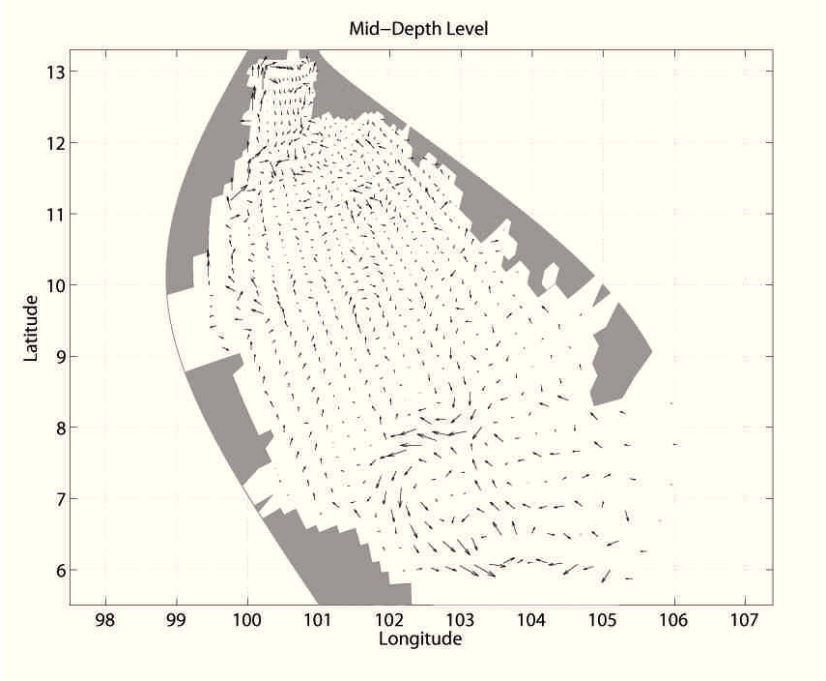

Figure 4.50 The simulated current circulation at mid-depth level in May.

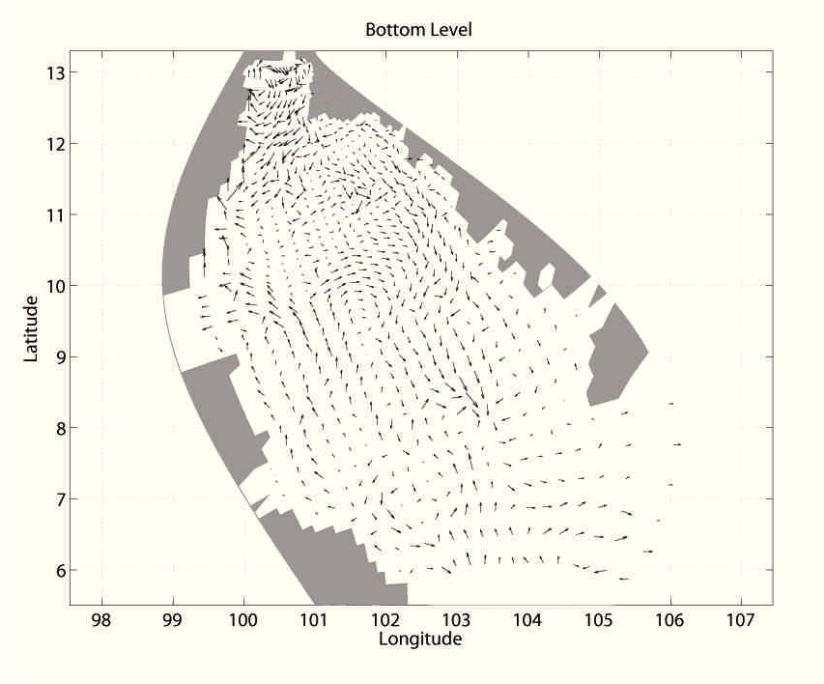

Figure 4.51 The simulated current circulation at bottom level in May.

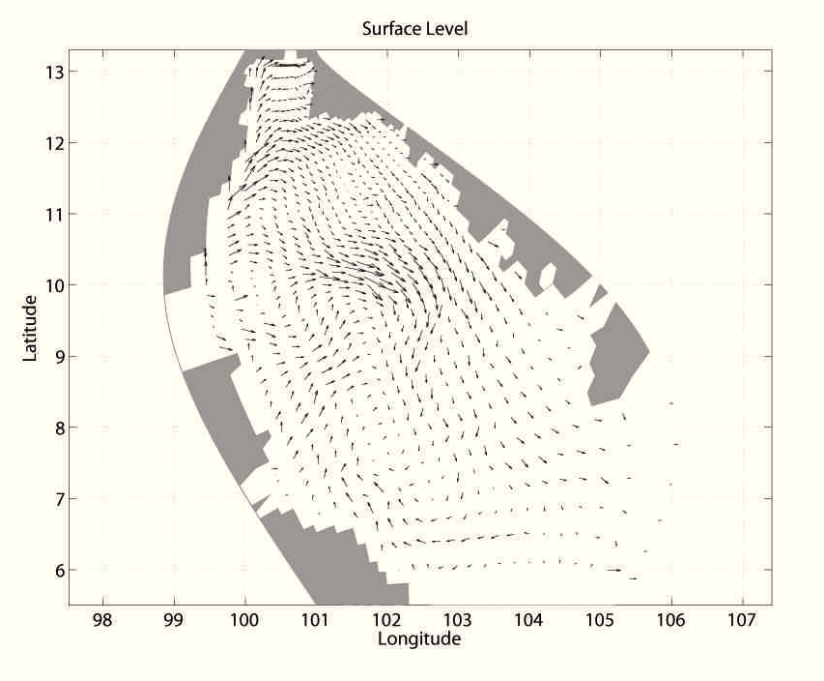

Figure 4.52 The simulated current circulation at surface level in June.

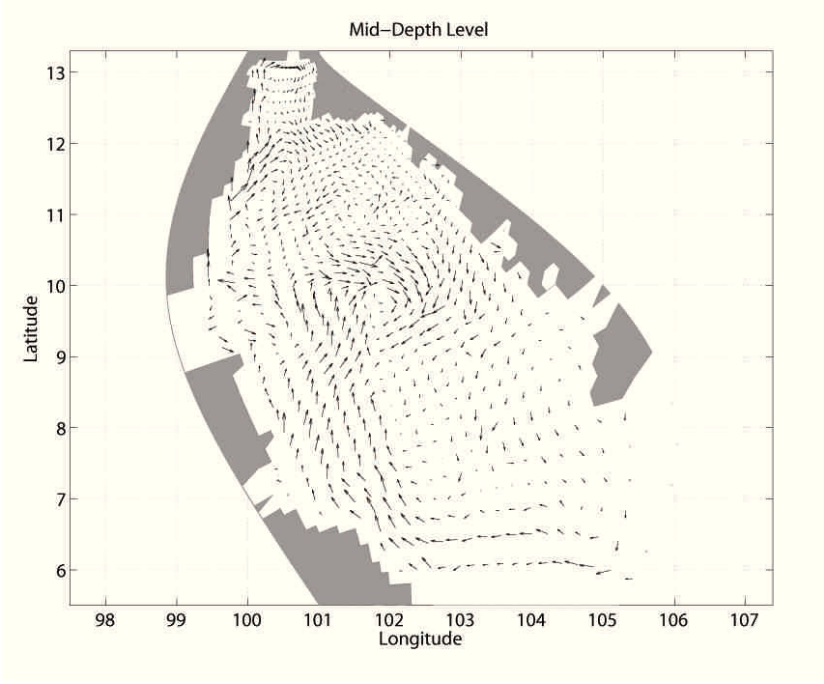

Figure 4.53 The simulated current circulation at mid-depth level in June.

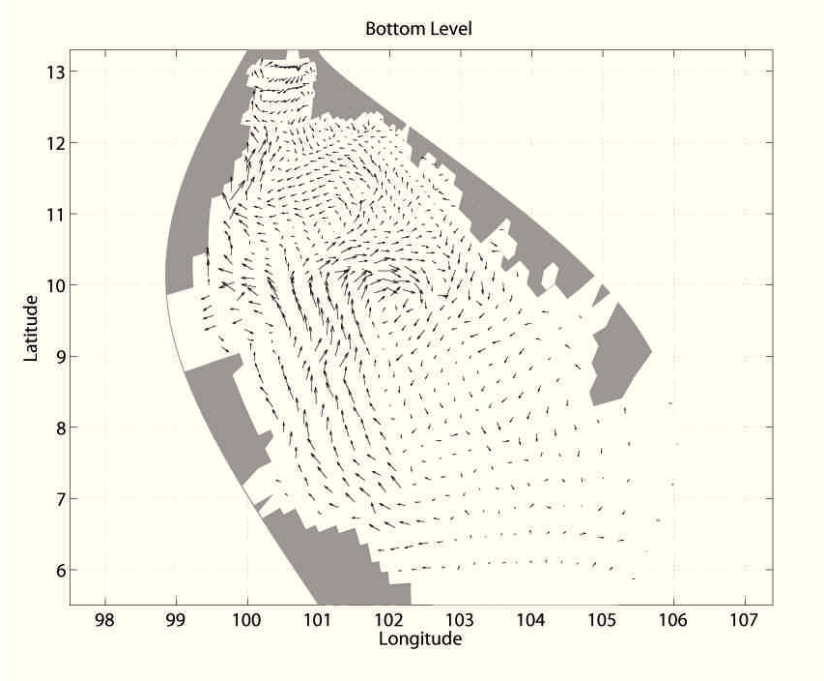

Figure 4.54 The simulated current circulation at bottom level in June.

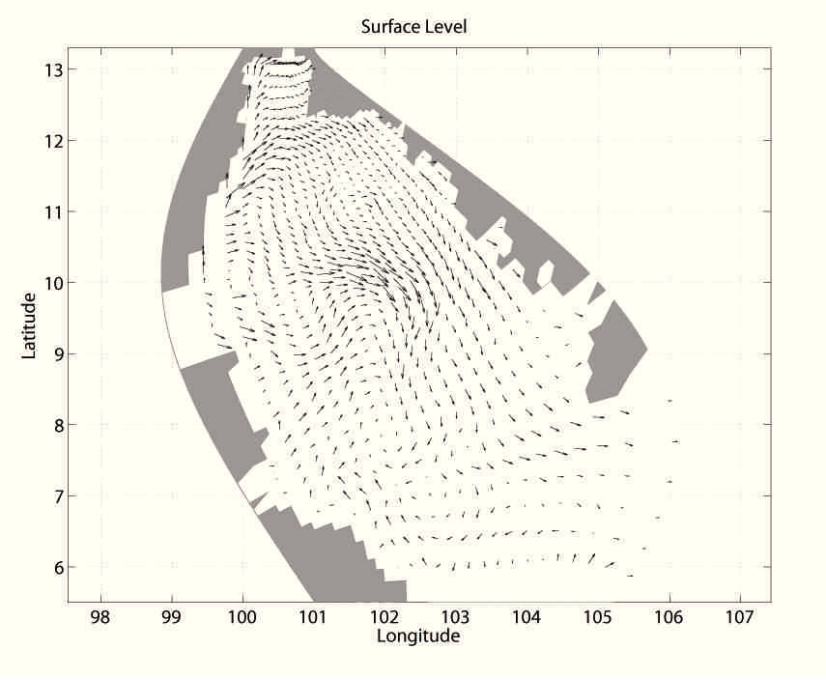

Figure 4.55 The simulated current circulation at surface level in July.

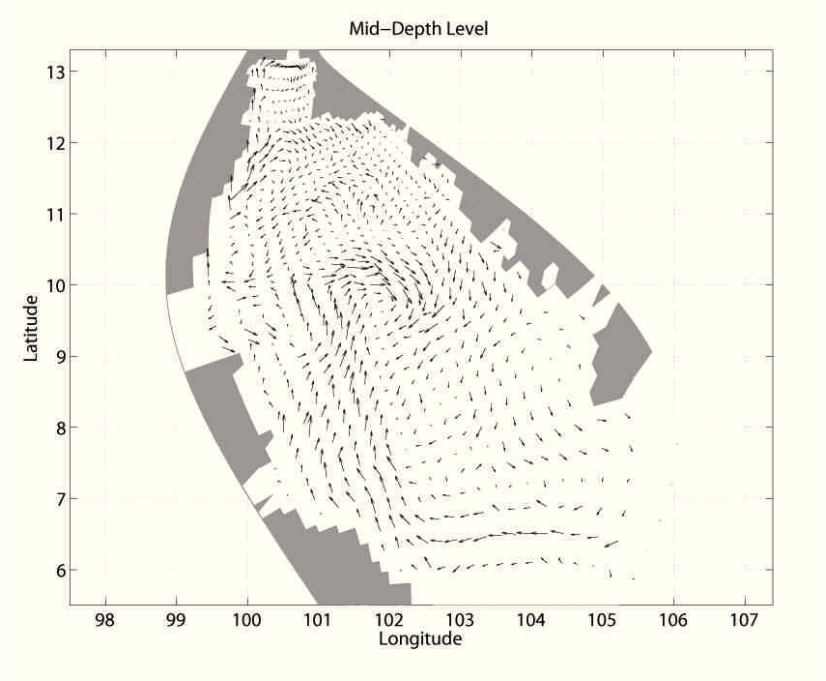

Figure 4.56 The simulated current circulation at mid-depth level in July.

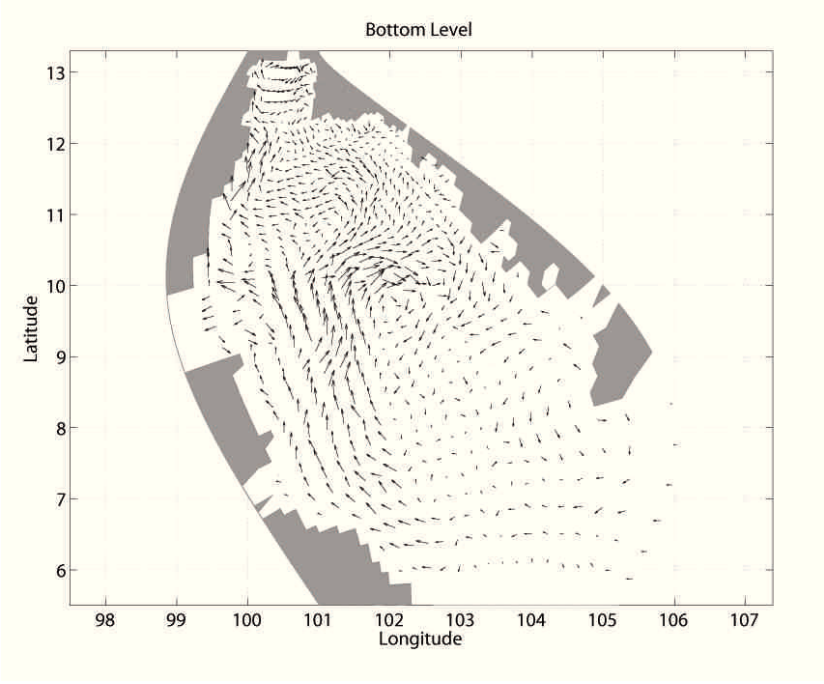

Figure 4.57 The simulated current circulation at bottom level in July.

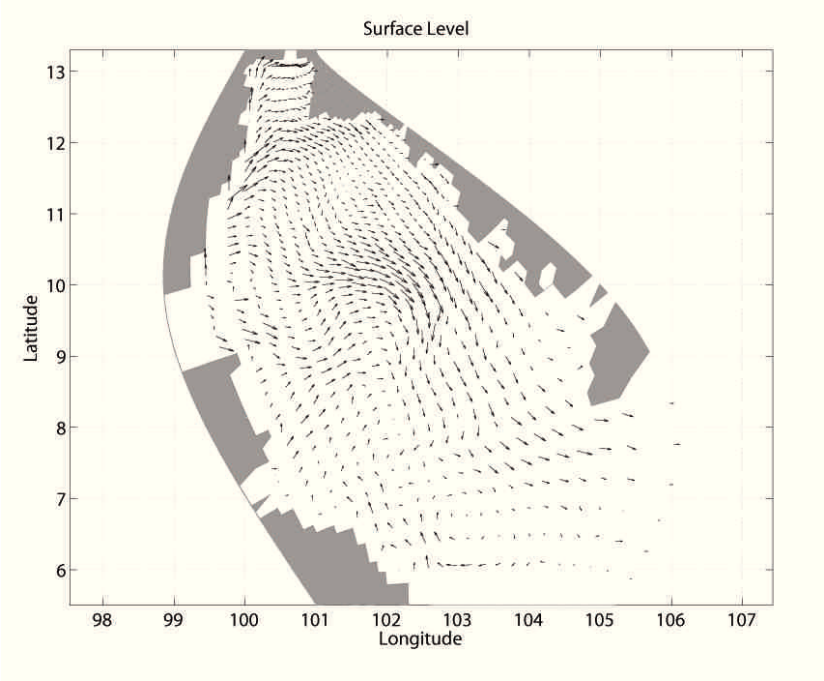

Figure 4.58 The simulated current circulation at surface level in August.

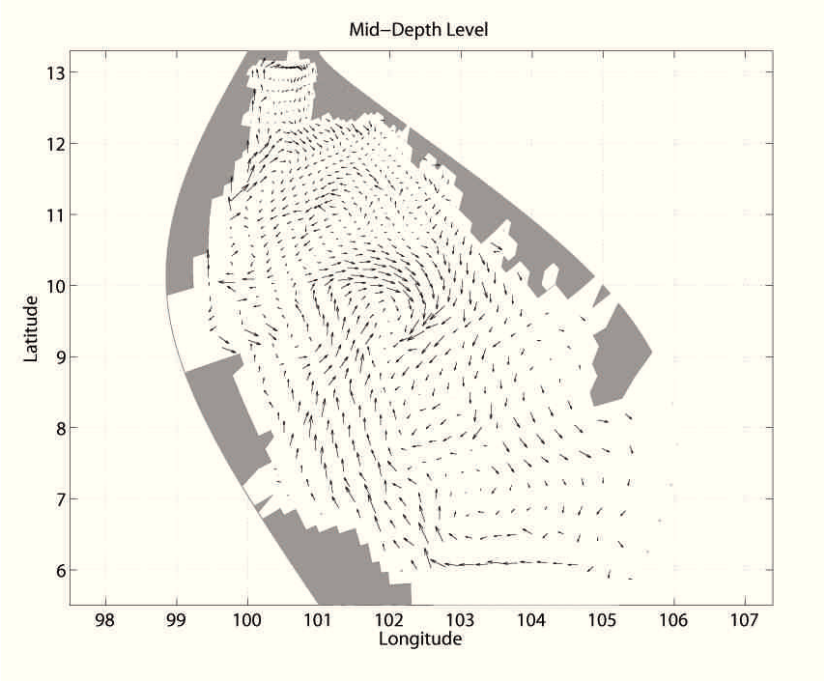

Figure 4.59 The simulated current circulation at mid-depth level in August.

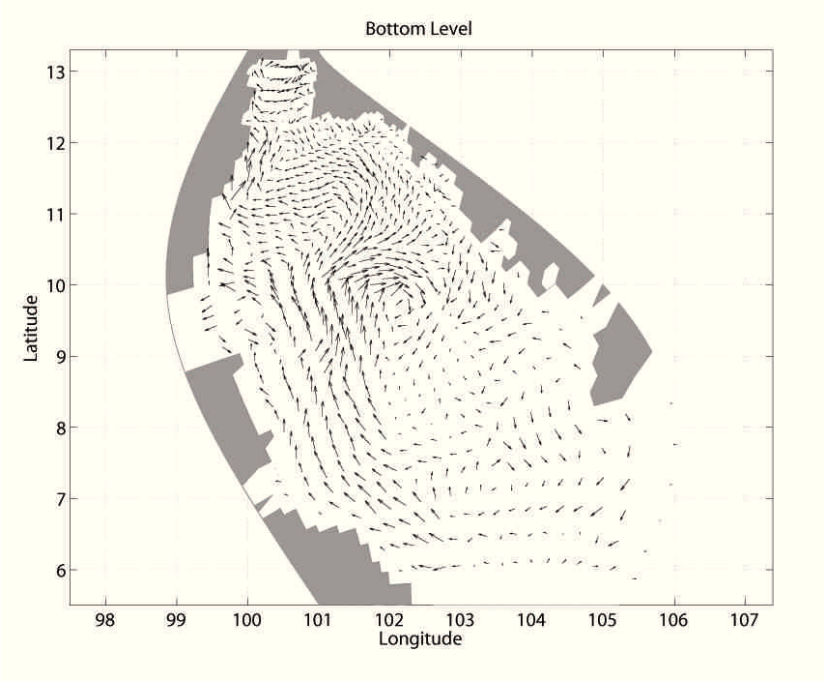

Figure 4.60 The simulated current circulation at bottom level in August.

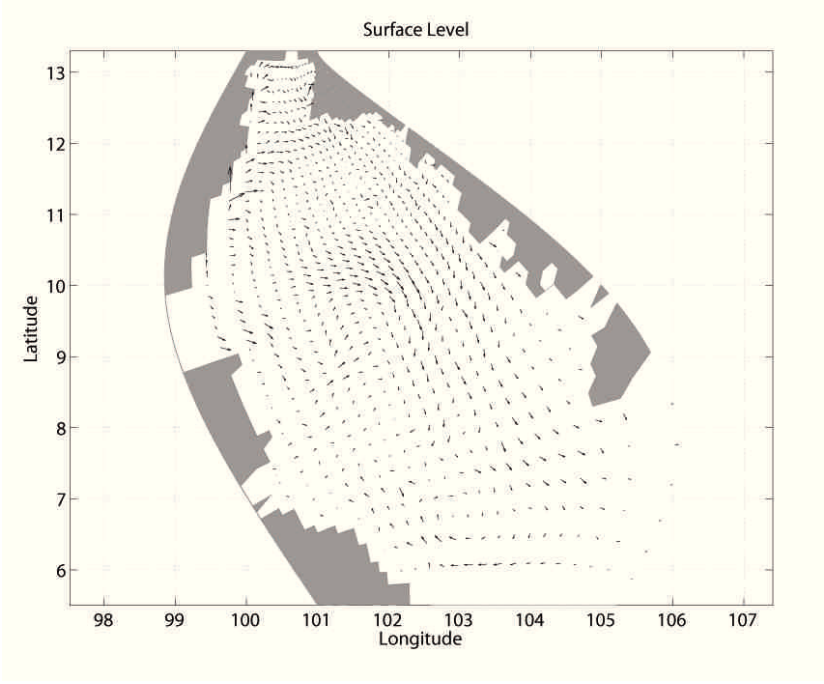

Figure 4.61 The simulated current circulation at surface level in September.

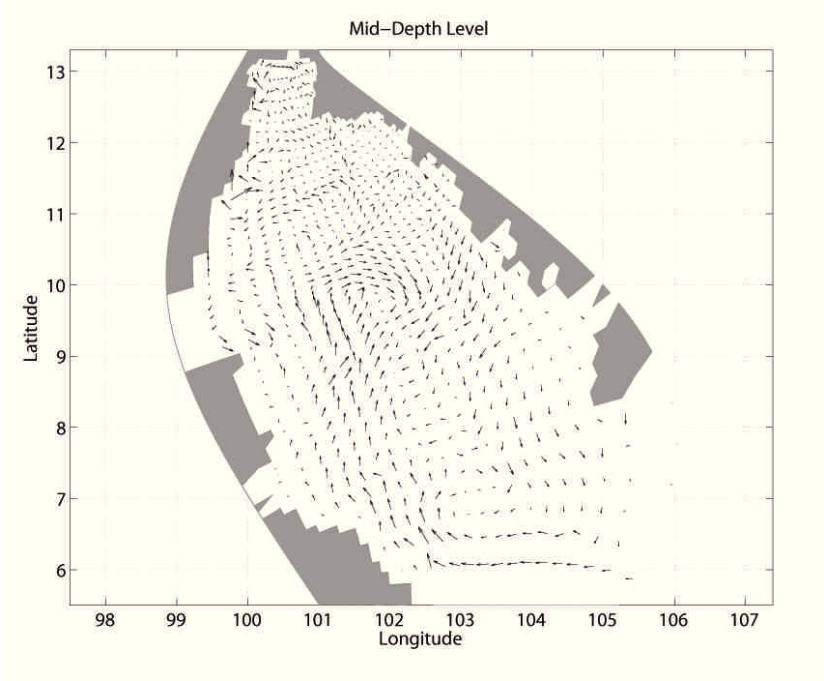

Figure 4.62 The simulated current circulation at mid-depth level in September.

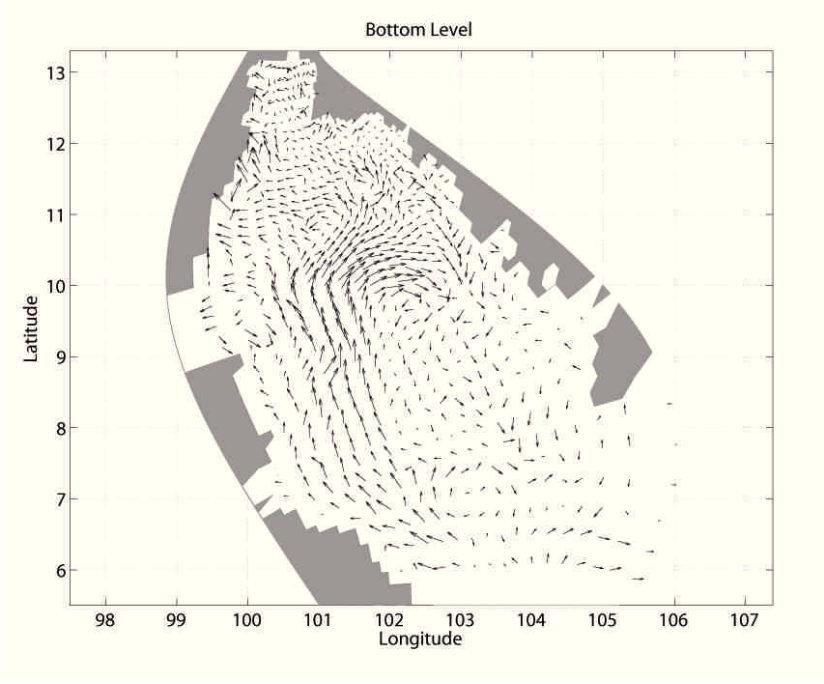

Figure 4.63 The simulated current circulation at bottom level in September.

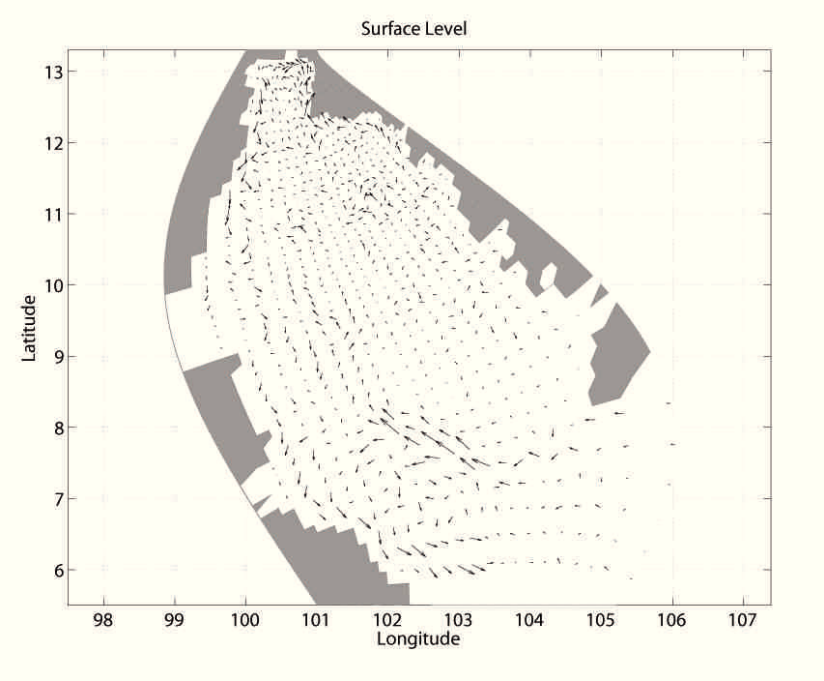

Figure 4.64 The simulated current circulation at surface level in October.

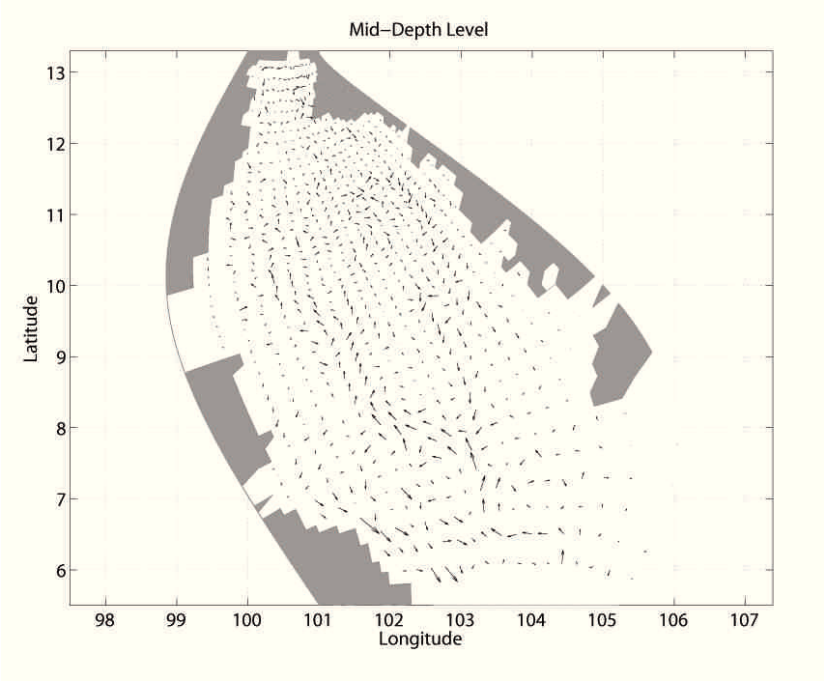

Figure 4.65 The simulated current circulation at mid-depth level in October.

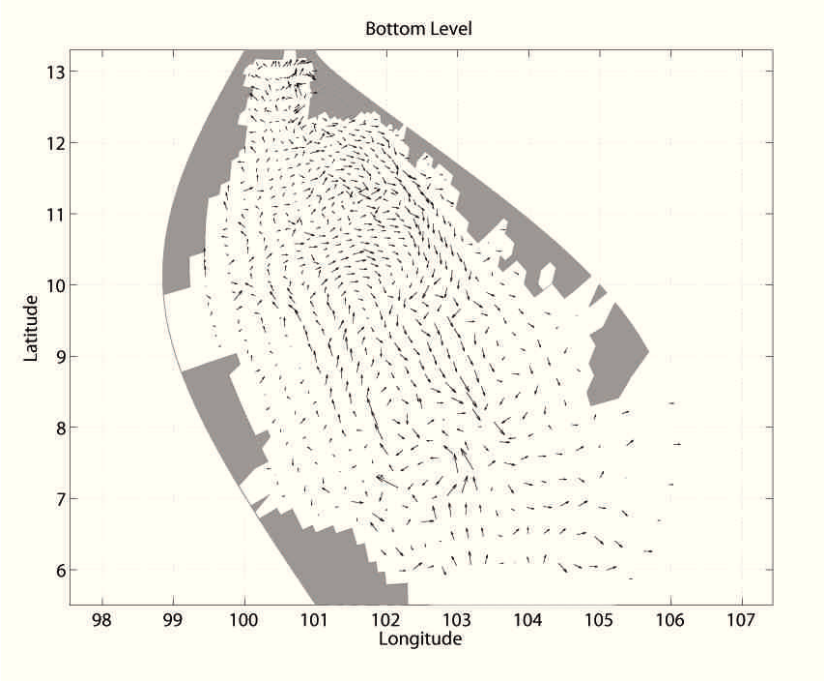

Figure 4.66 The simulated current circulation at bottom level in October.

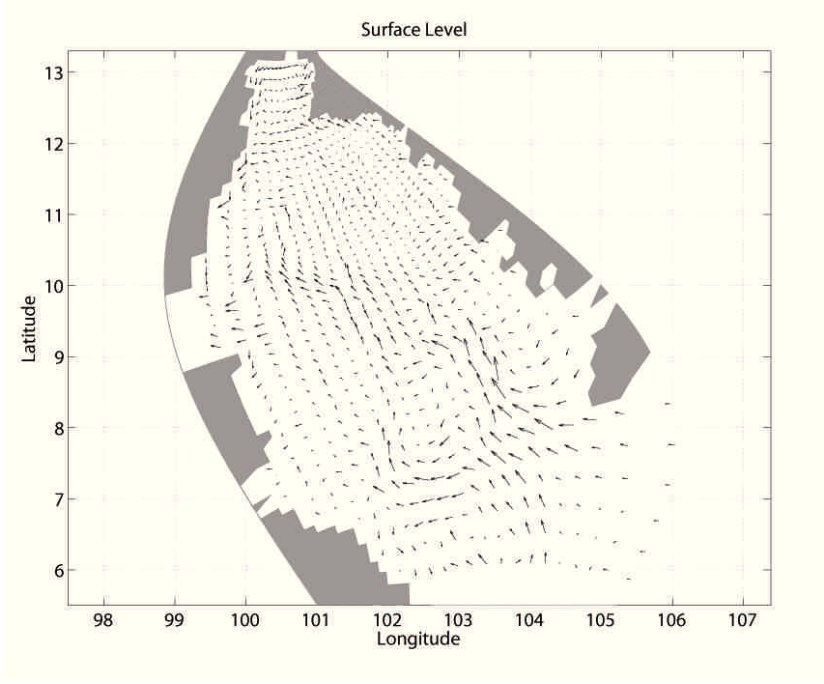

Figure 4.67 The simulated current circulation at surface level in November.

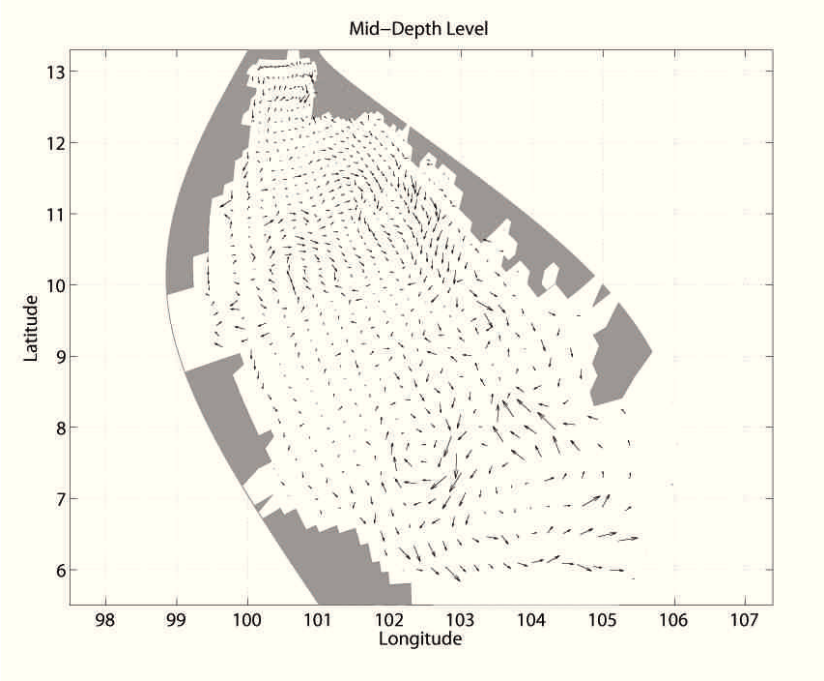

Figure 4.68 The simulated current circulation at mid-depth level in November.

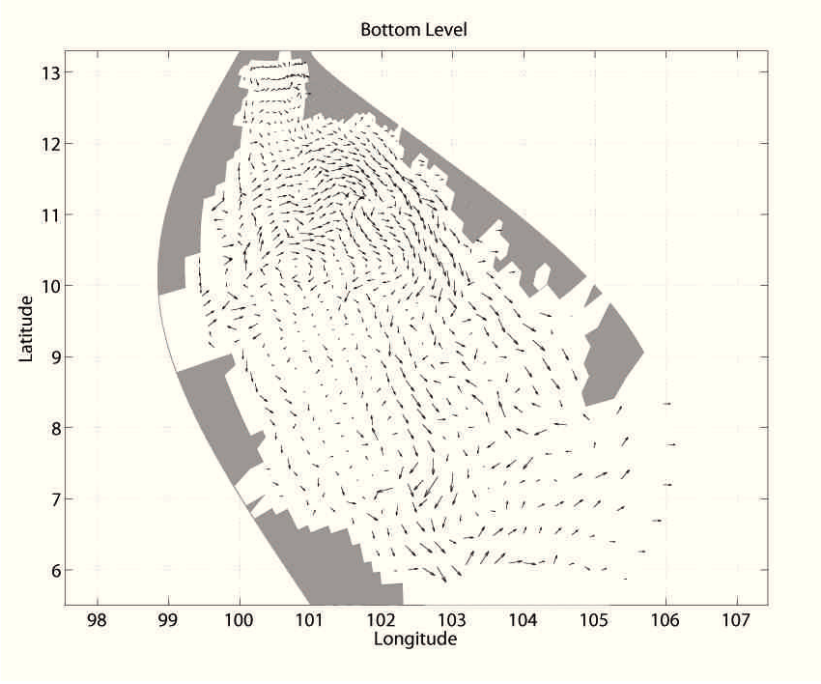

Figure 4.69 The simulated current circulation at bottom level in November.

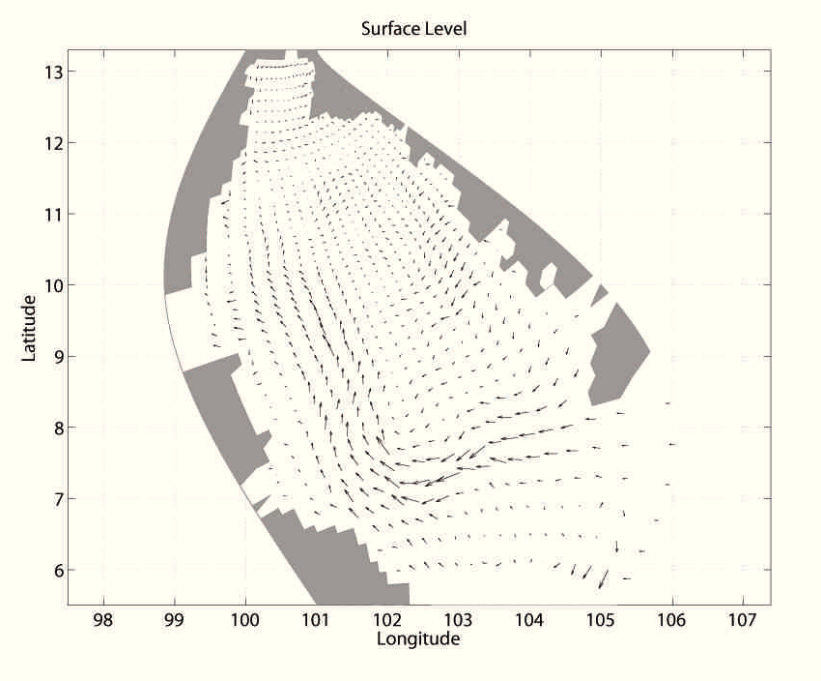

Figure 4.70 The simulated current circulation at surface level in December.

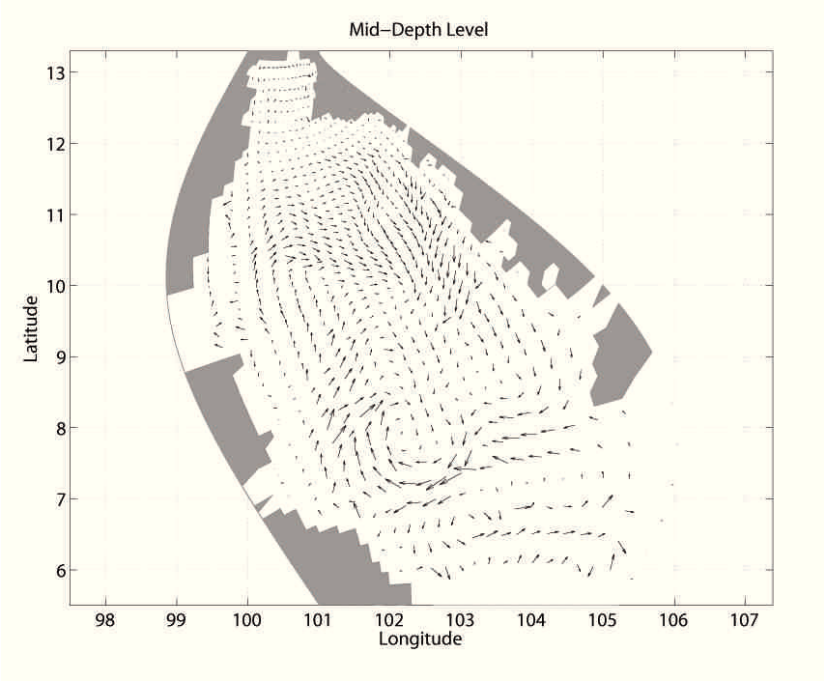

Figure 4.71 The simulated current circulation at mid-depth level in December.

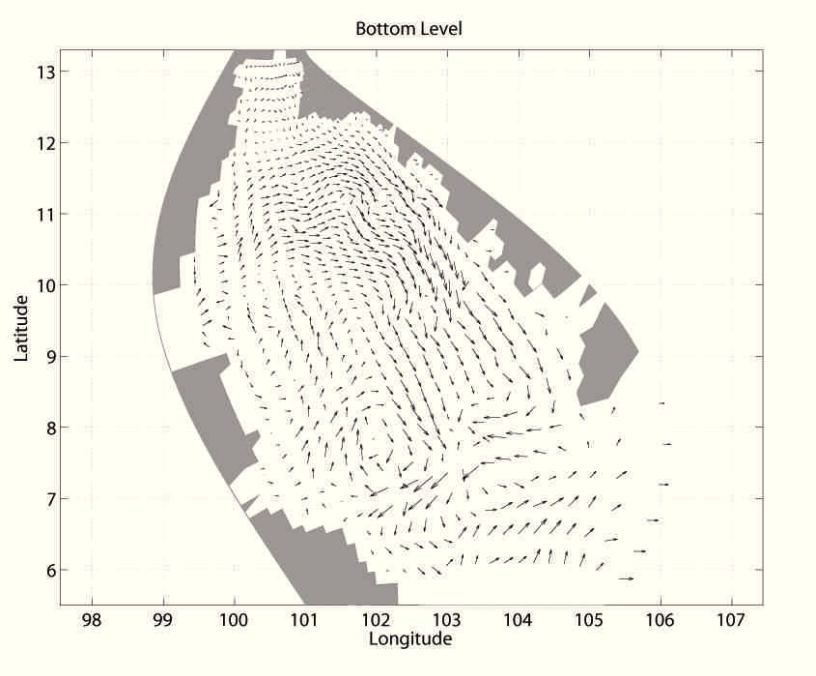

Figure 4.72 The simulated current circulation at bottom level in December.

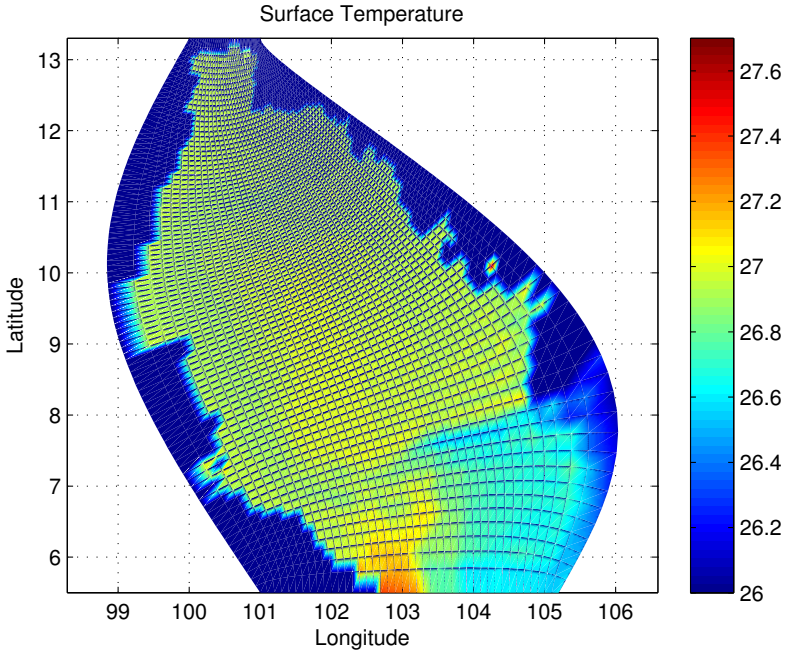

Figure 4.73 The simulated temperature (°C) at surface level in January.

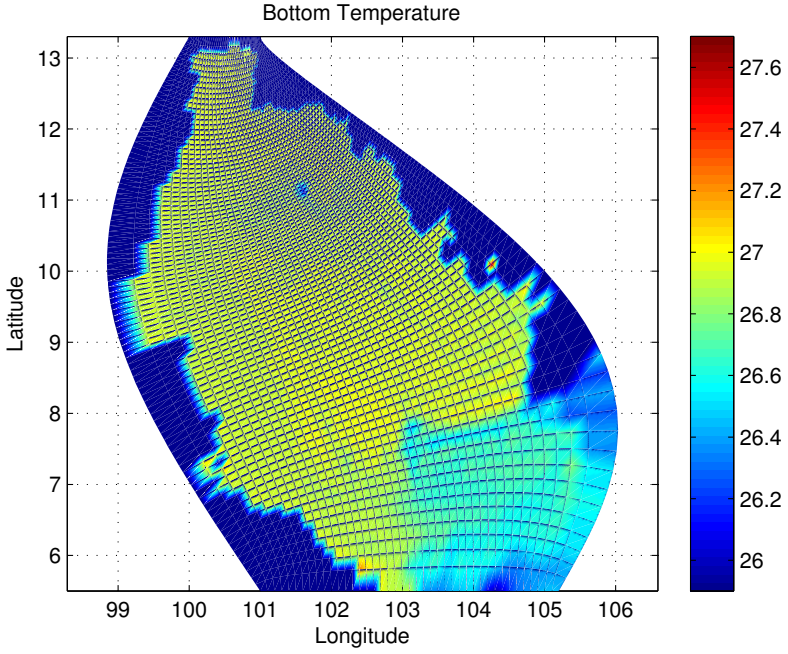

Figure 4.74 The simulated temperature (°C) at bottom level in January.

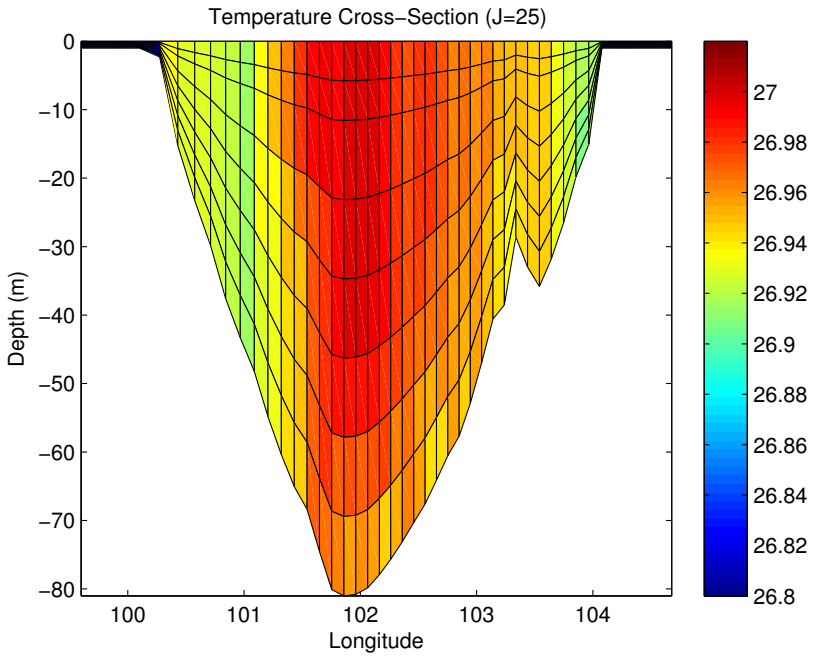

Figure 4.75 The simulated temperature cross-section (°C) in January.

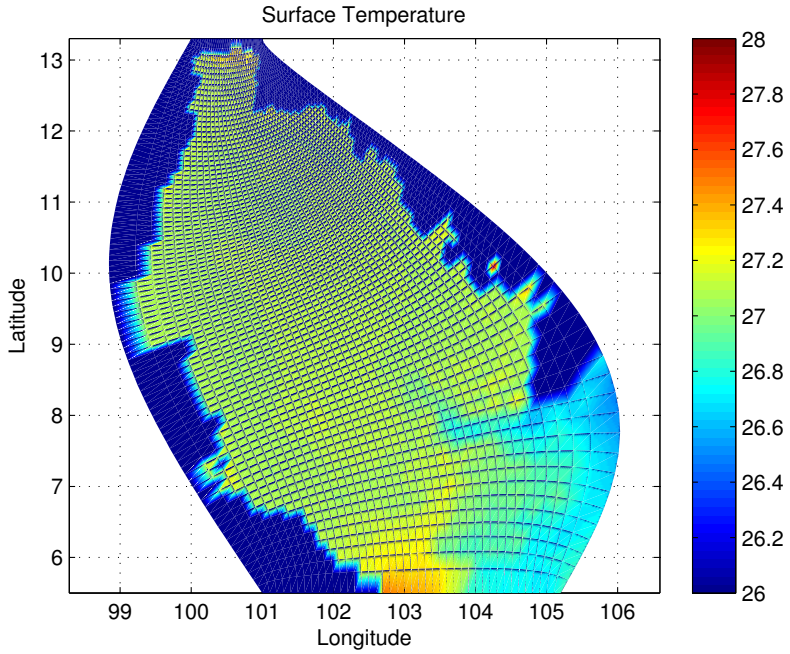

Figure 4.76 The simulated temperature (°C) at surface level in February.

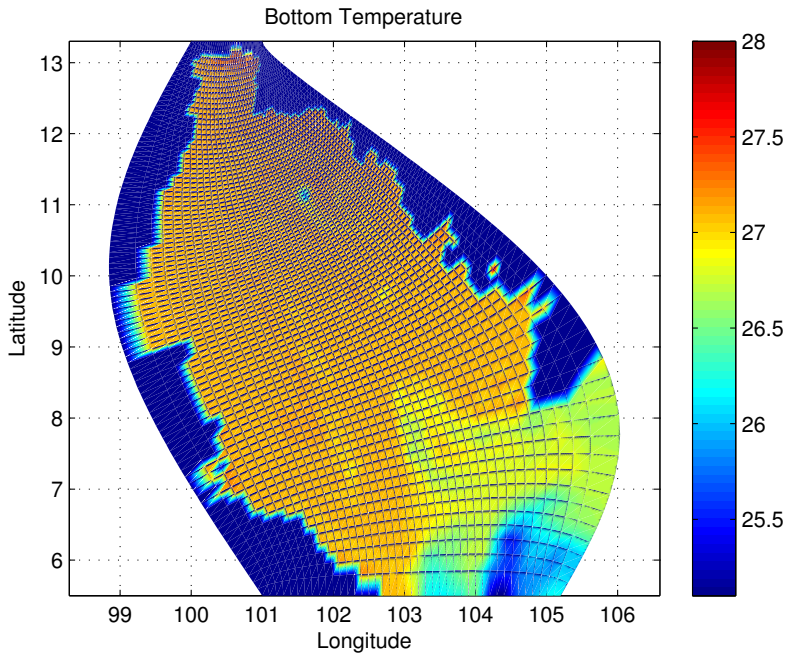

Figure 4.77 The simulated temperature (°C) at bottom level in February.

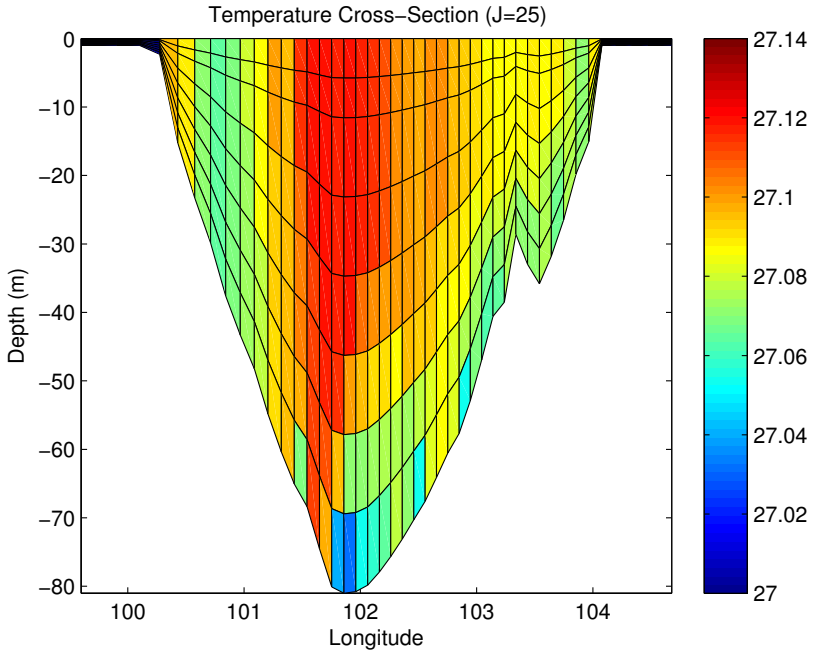

Figure 4.78 The simulated temperature cross-section (°C) in February.

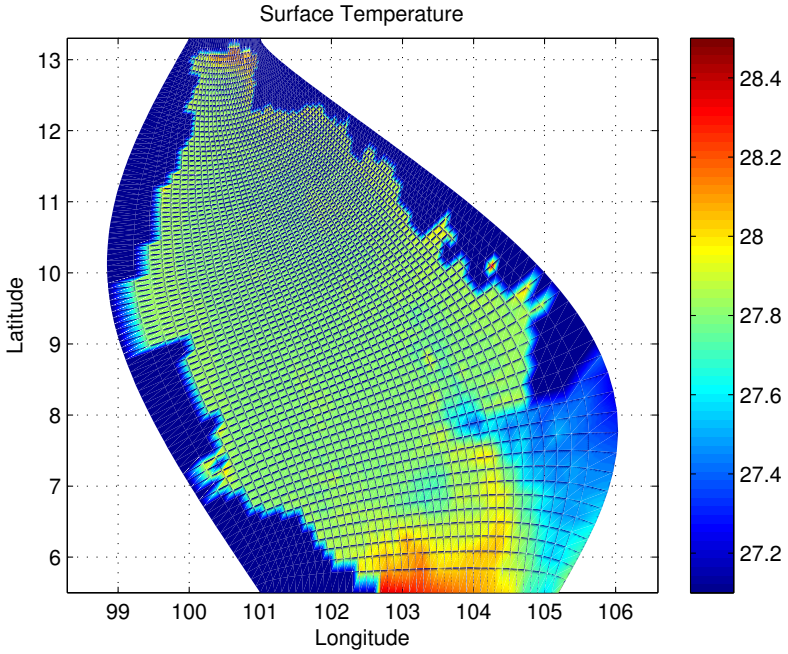

Figure 4.79 The simulated temperature (°C) at surface level in March.

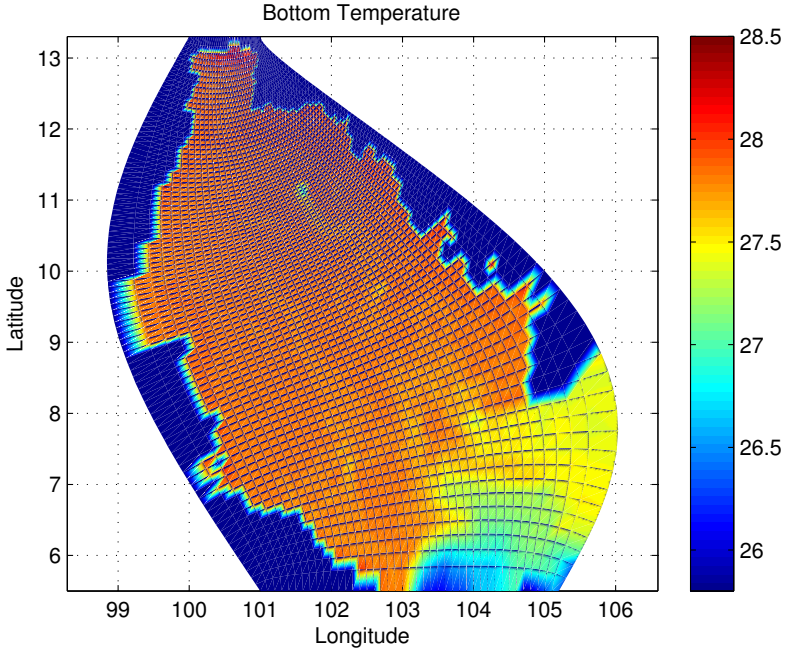

Figure 4.80 The simulated temperature (°C) at bottom level in March.

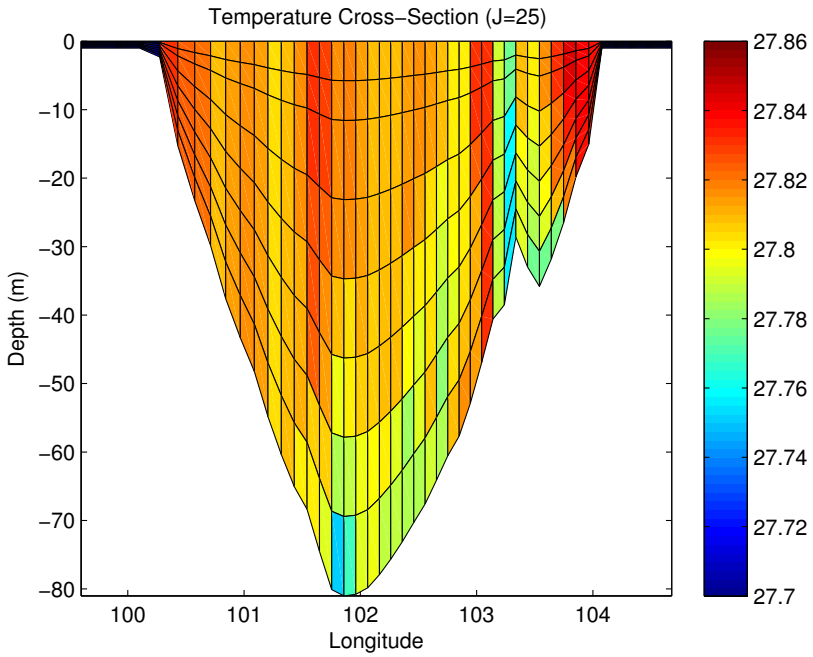

Figure 4.81 The simulated temperature cross-section (°C) in March.

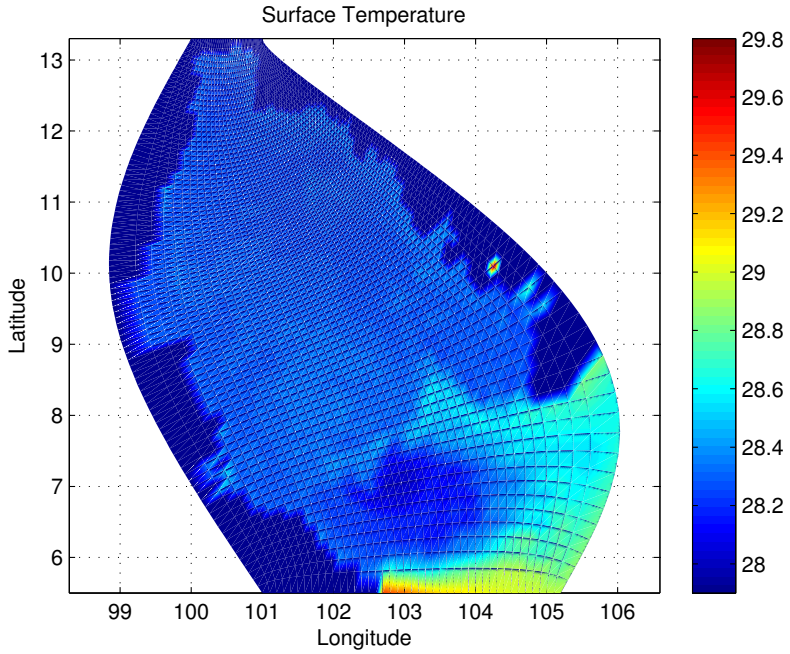

Figure 4.82 The simulated temperature (°C) at surface level in April.

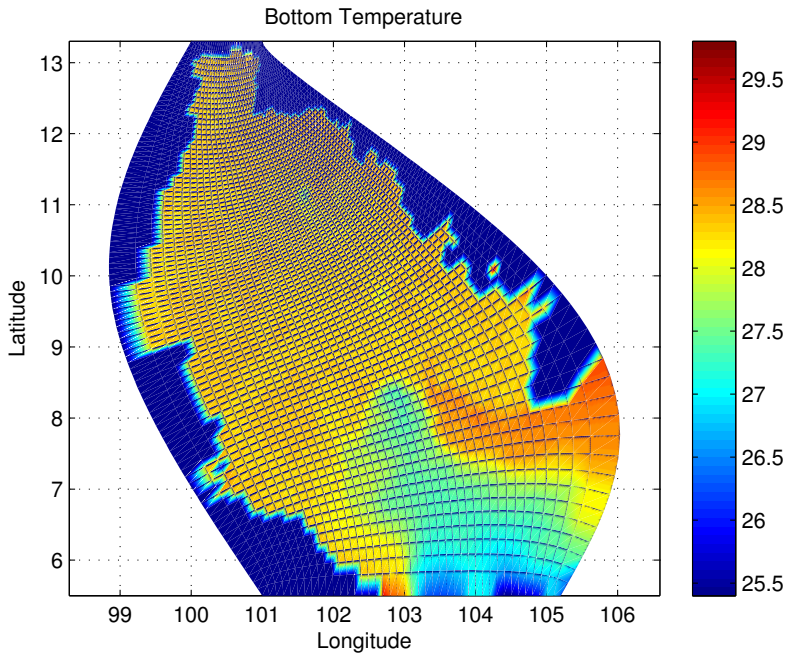

Figure 4.83 The simulated temperature (°C) at bottom level in April.

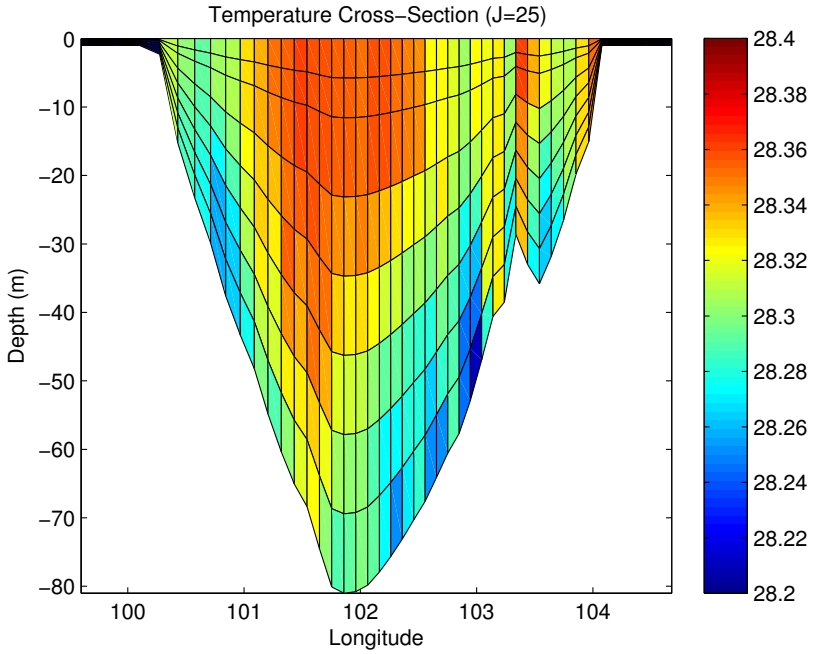

Figure 4.84 The simulated temperature cross-section (°C) in April.

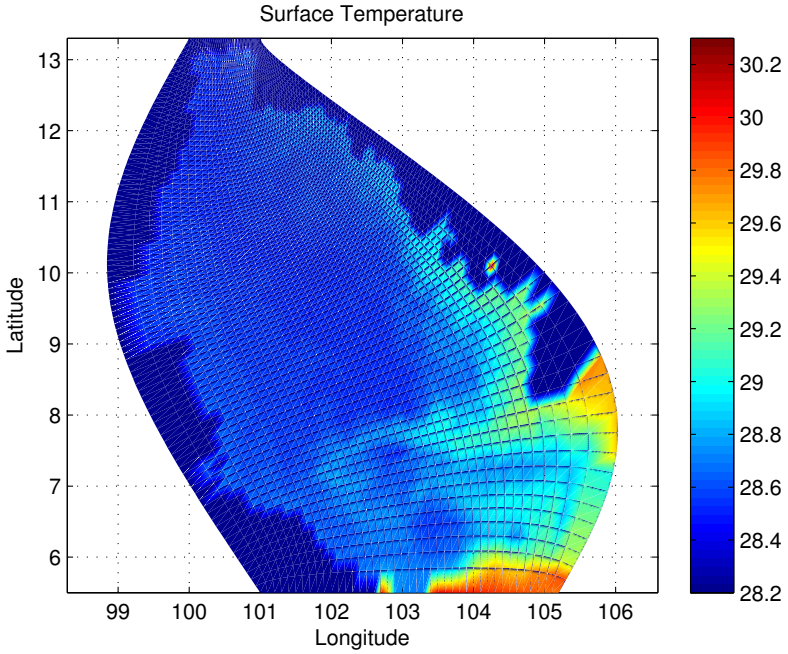

Figure 4.85 The simulated temperature (°C) at surface level in May.

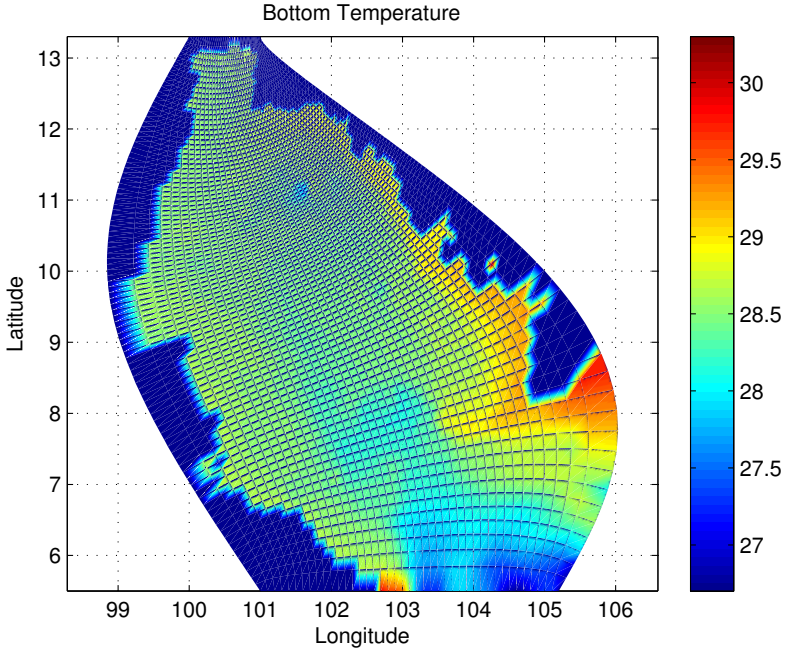

Figure 4.86 The simulated temperature (°C) at bottom level in May.

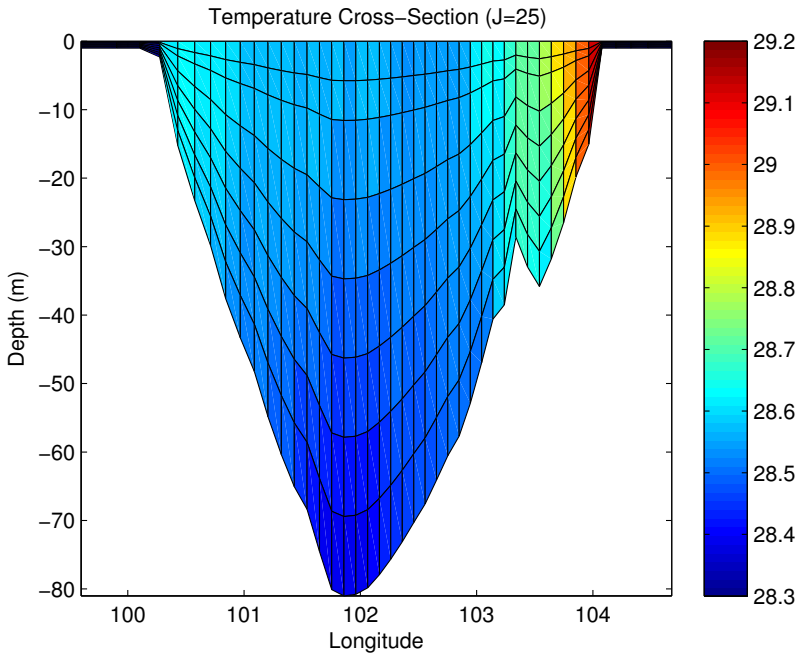

Figure 4.87 The simulated temperature cross-section (°C) in May.

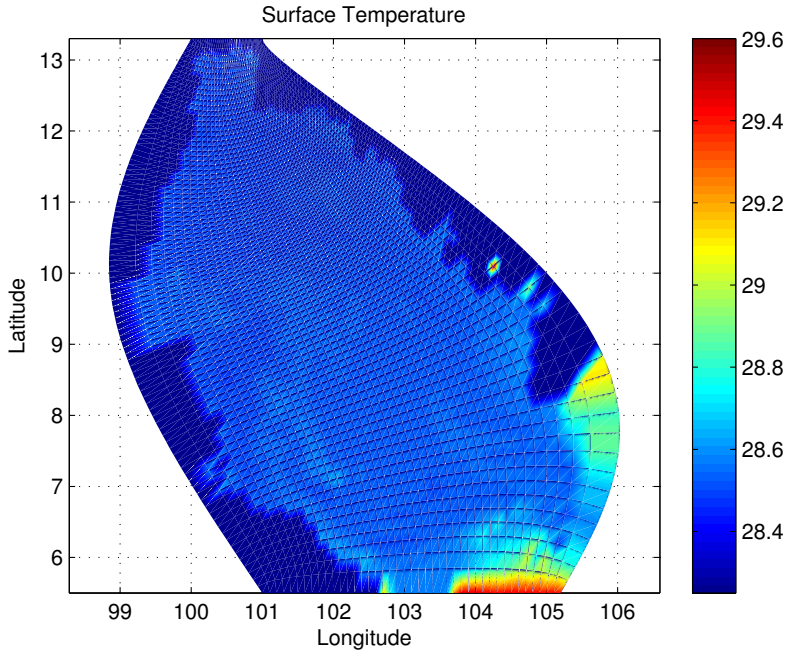

Figure 4.88 The simulated temperature (°C) at surface level in June.

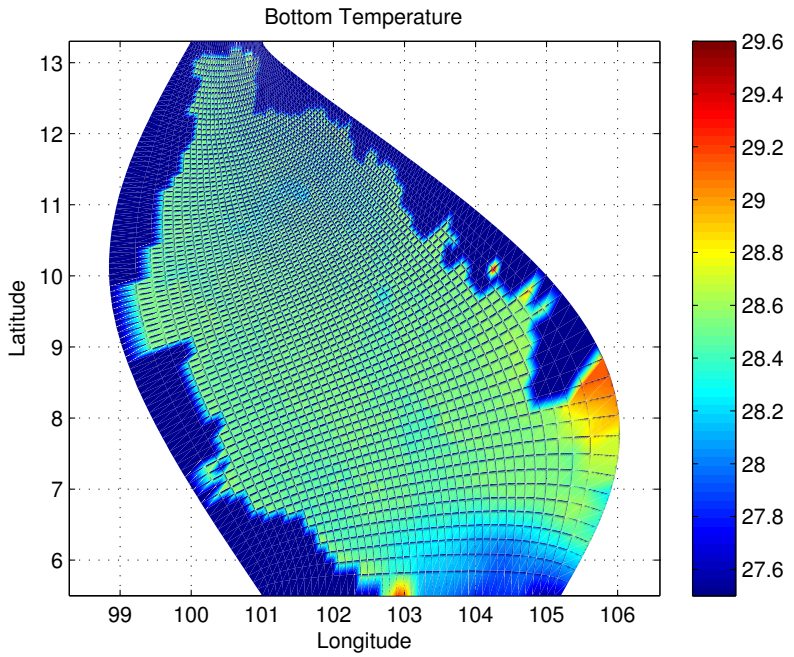

Figure 4.89 The simulated temperature (°C) at bottom level in June.

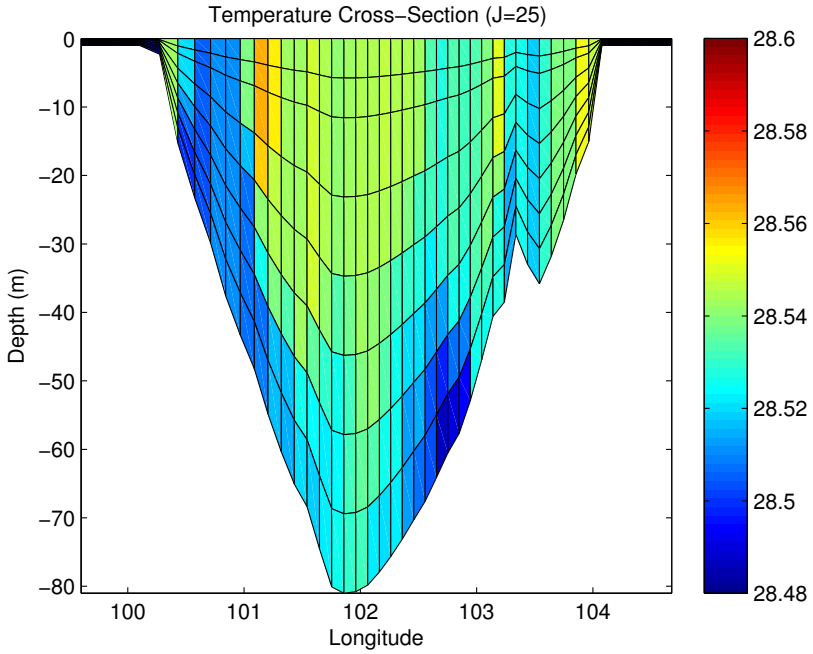

Figure 4.90 The simulated temperature cross-section (°C) in June.

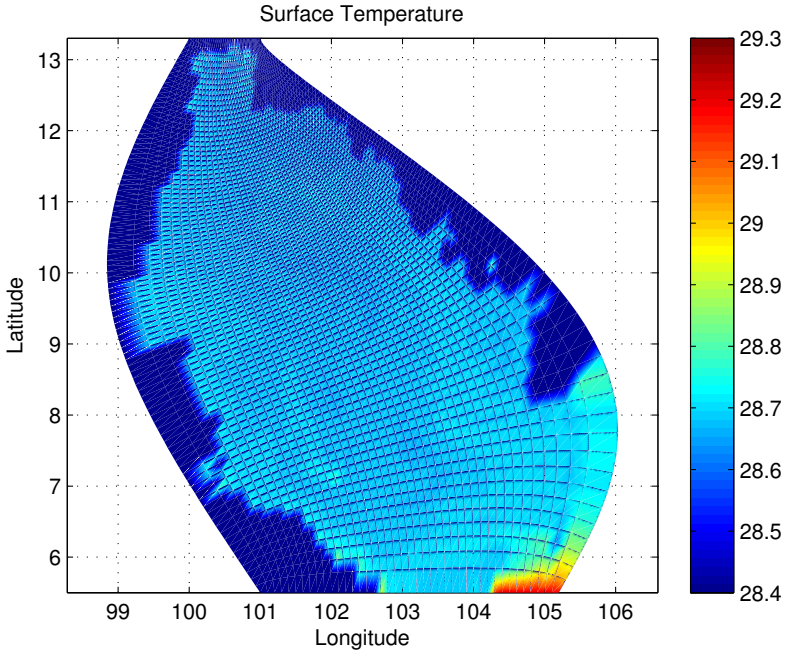

Figure 4.91 The simulated temperature (°C) at surface level in July.

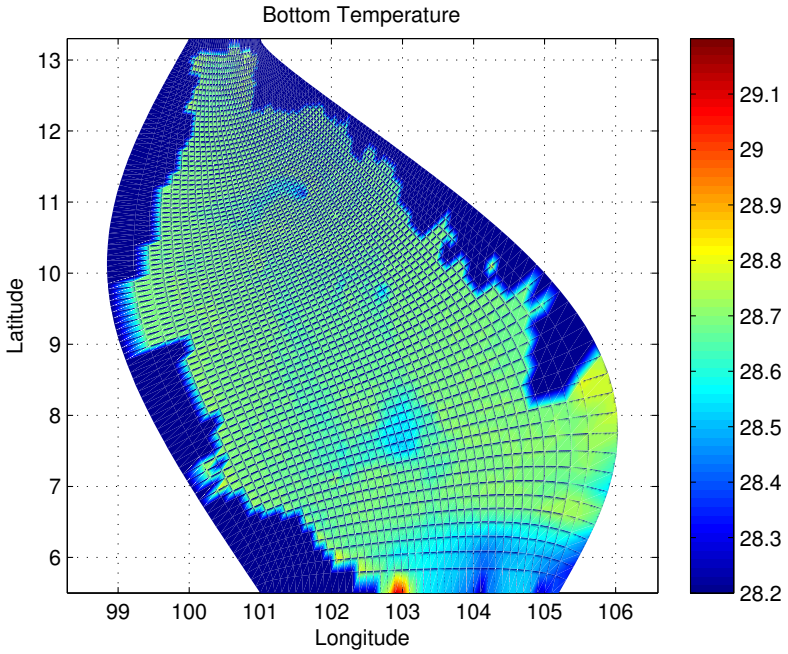

Figure 4.92 The simulated temperature (°C) at bottom level in July.

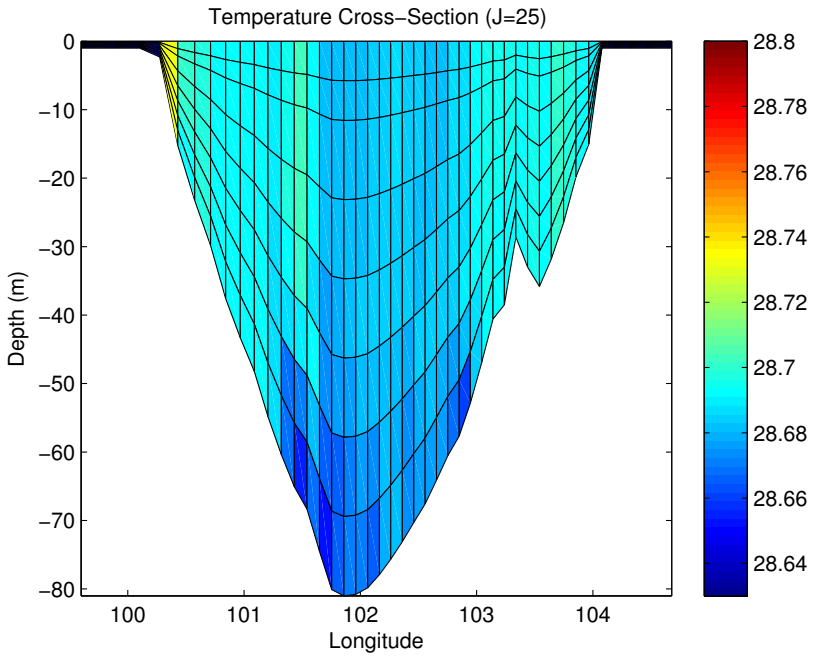

Figure 4.93 The simulated temperature cross-section (°C) in July.

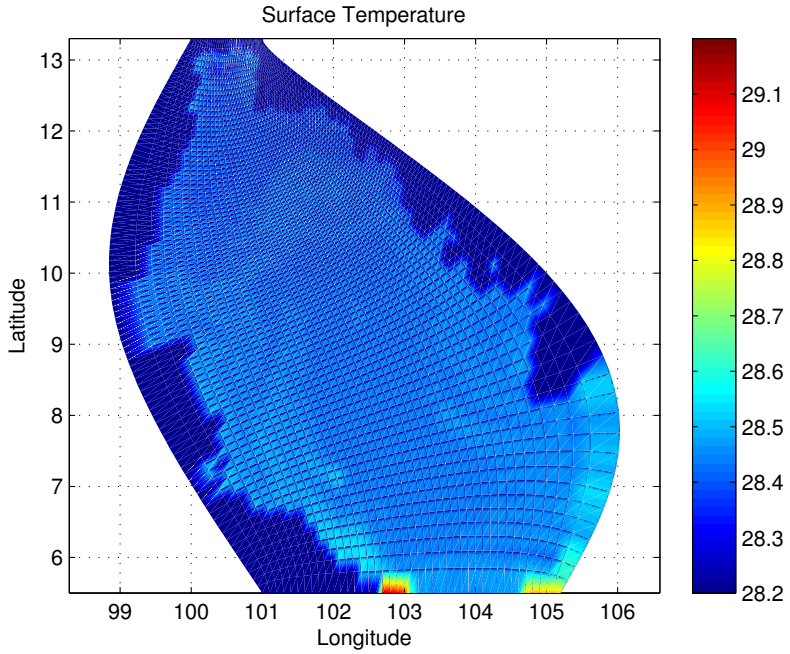

Figure 4.94 The simulated temperature (°C) at surface level in August.

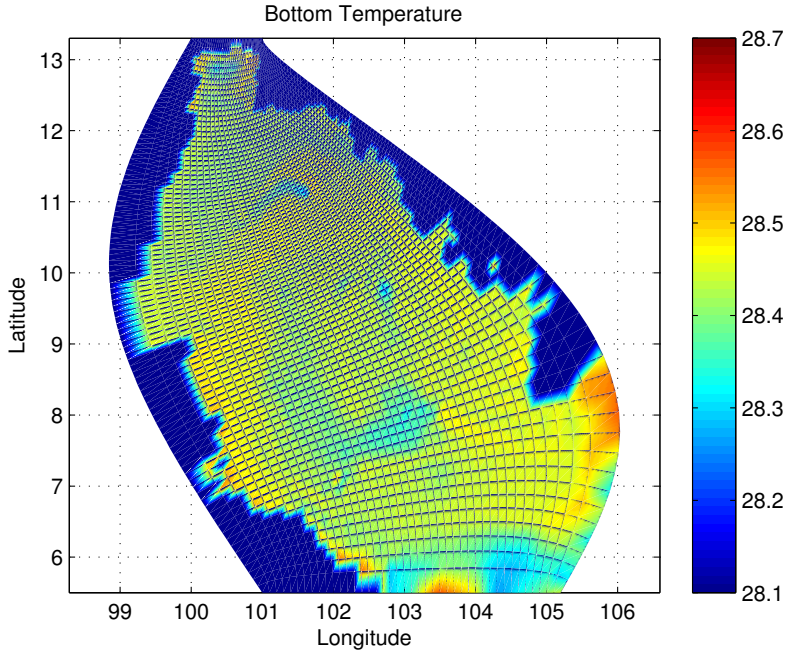

Figure 4.95 The simulated temperature (°C) at bottom level in August.

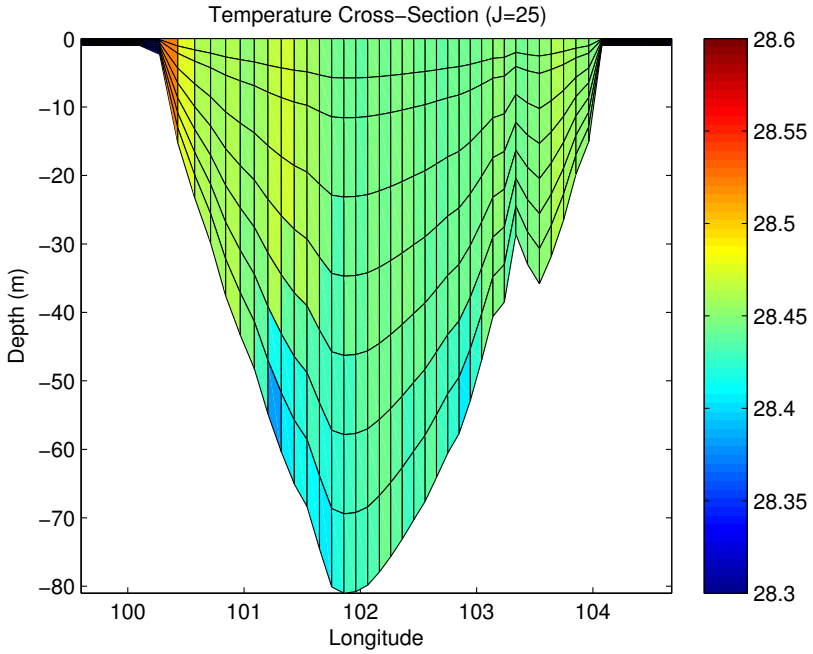

Figure 4.96 The simulated temperature cross-section (°C) in August.

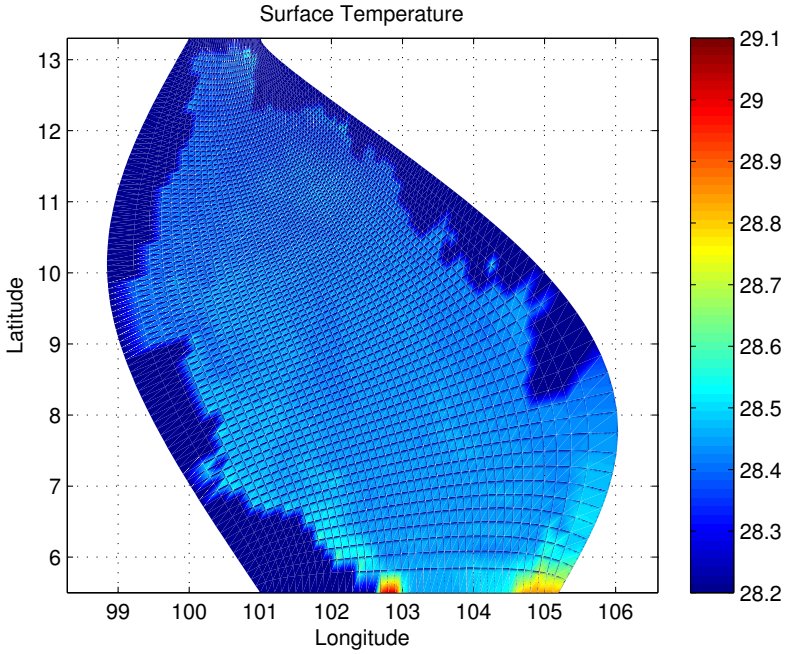

Figure 4.97 The simulated temperature (°C) at surface level in September.

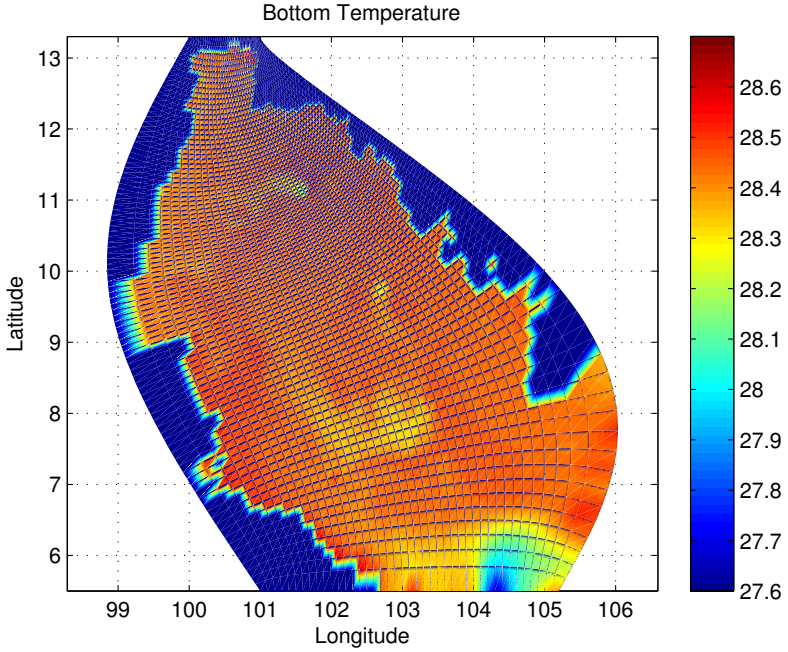

Figure 4.98 The simulated temperature (°C) at bottom level in September.

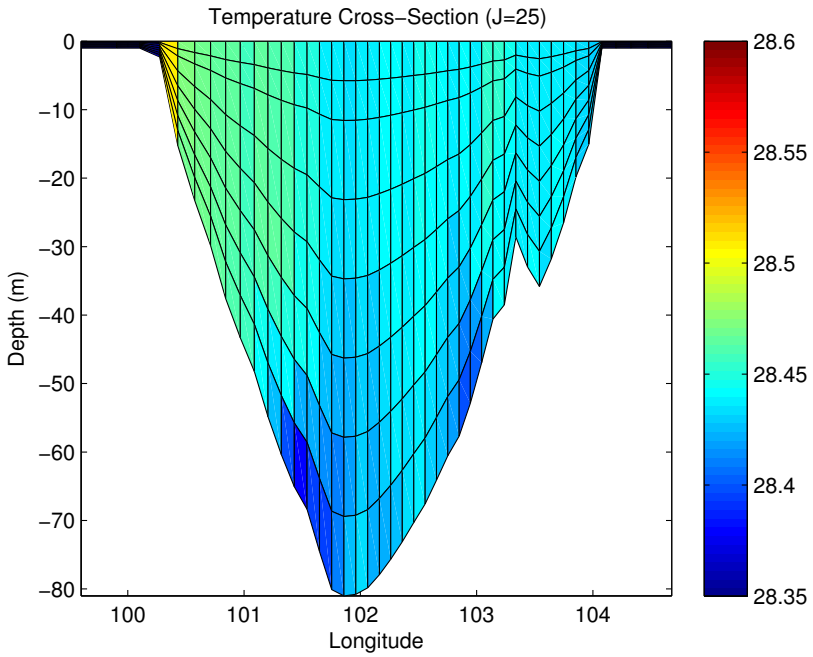

Figure 4.99 The simulated temperature cross-section (°C) in September.

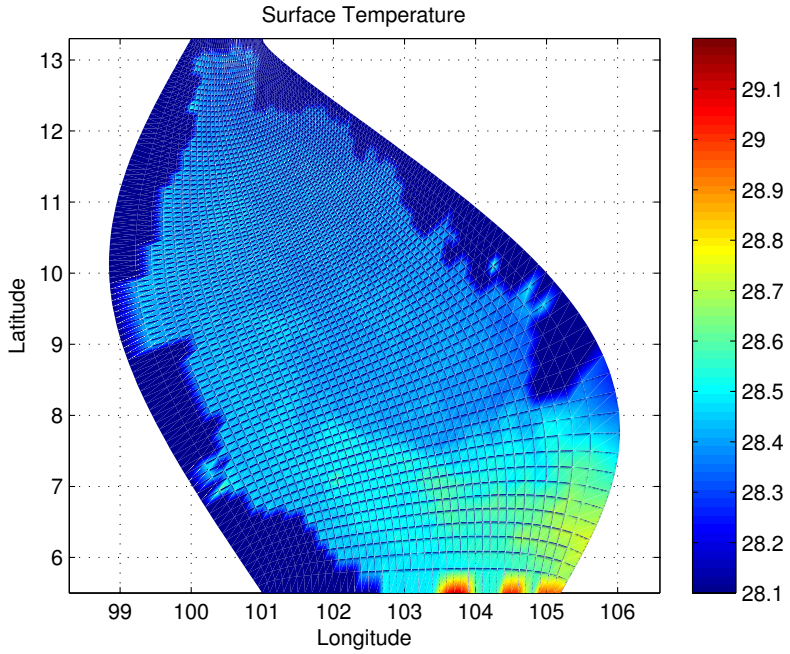

Figure 4.100 The simulated temperature (°C) at surface level in October.

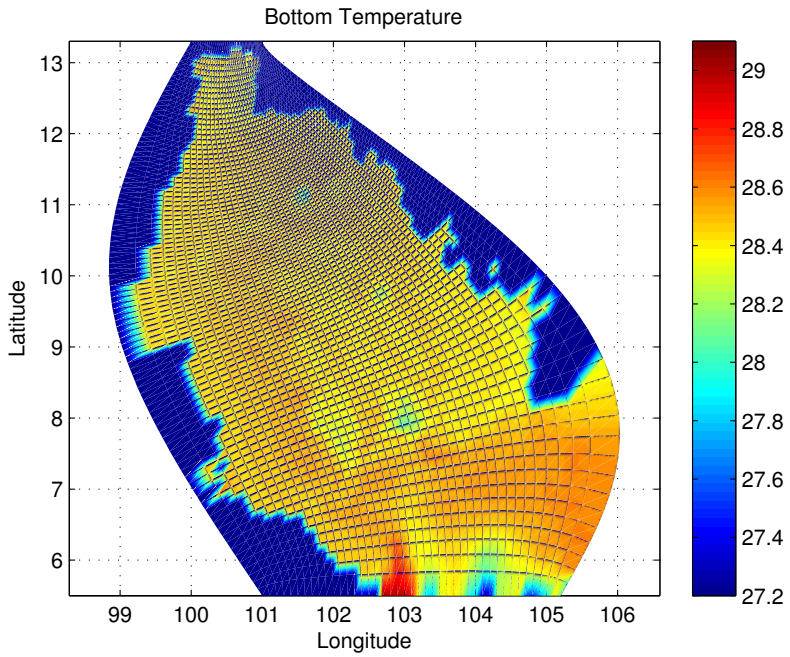

Figure 4.101 The simulated temperature (°C) at bottom level in October.

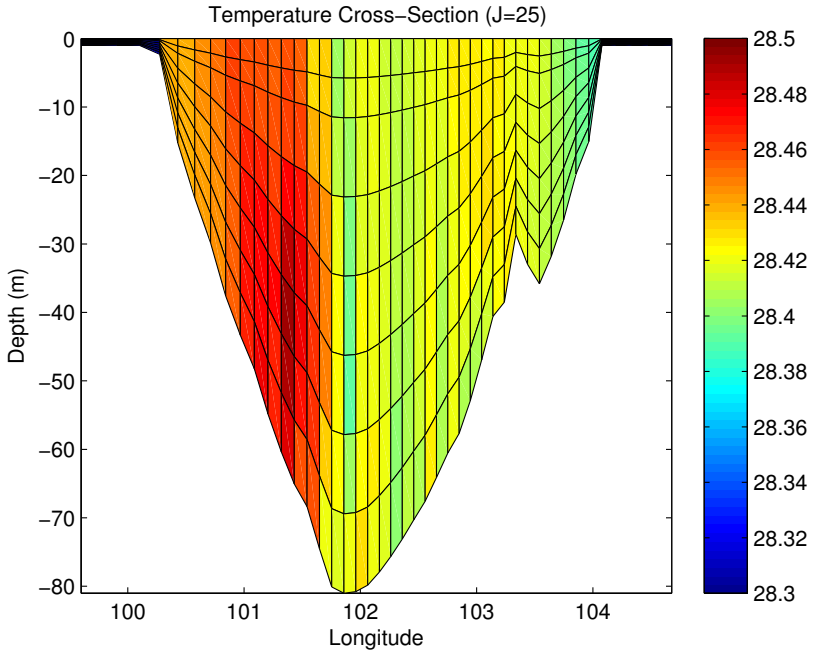

Figure 4.102 The simulated temperature cross-section (°C) in October.

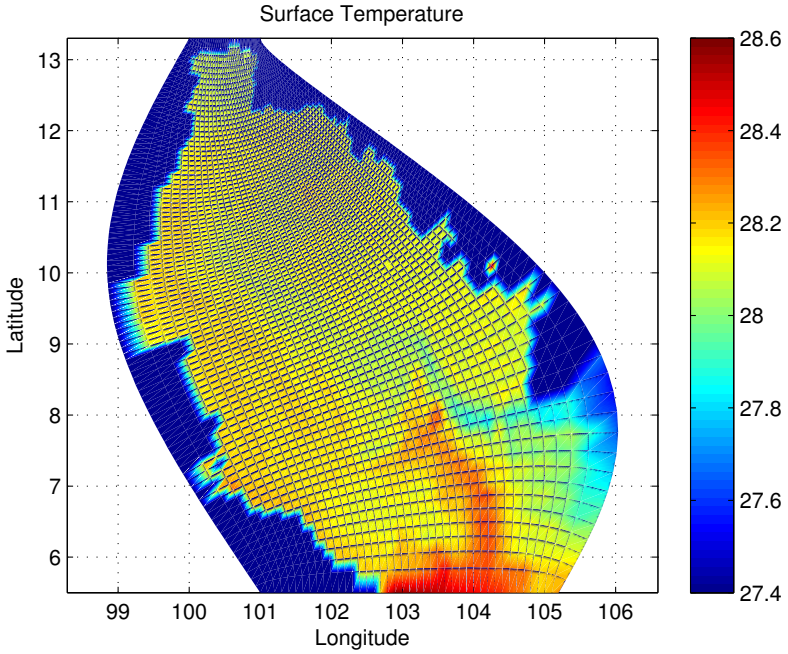

Figure 4.103 The simulated temperature (°C) at surface level in November.

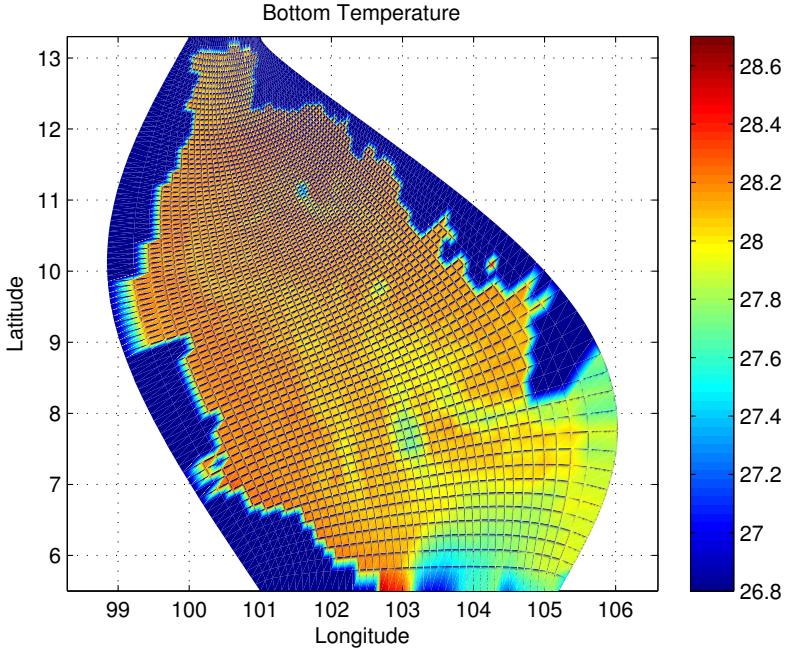

Figure 4.104 The simulated temperature (°C) at bottom level in November.

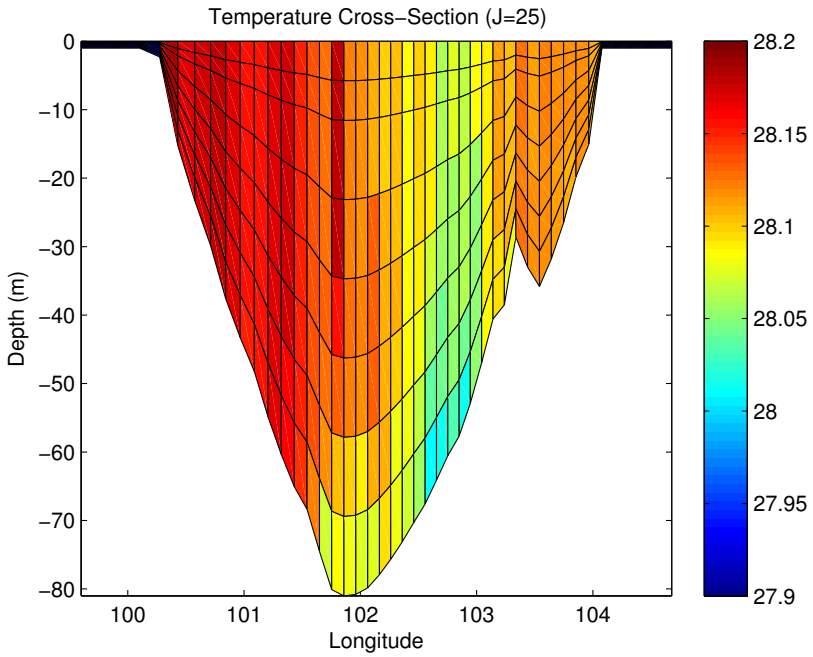

Figure 4.105 The simulated temperature cross-section (°C) in November.

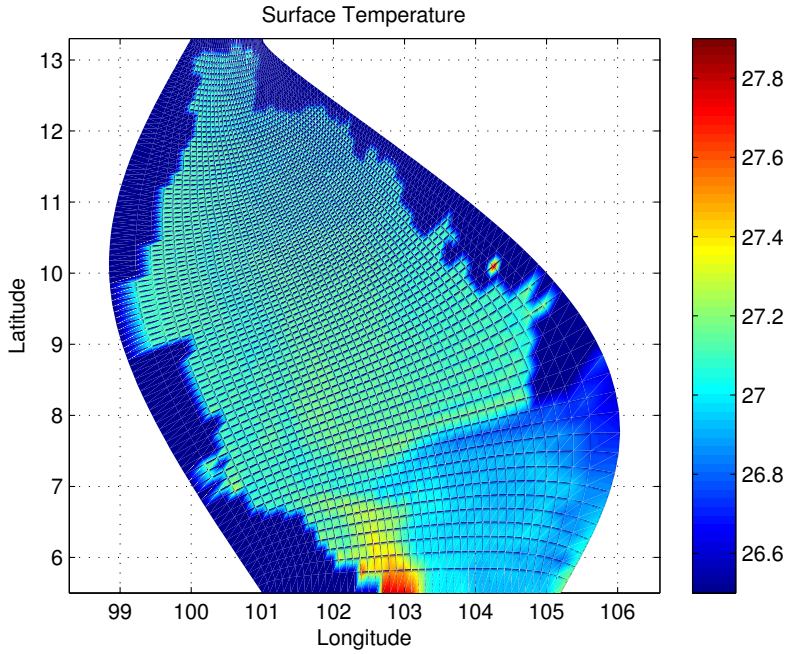

Figure 4.106 The simulated temperature (°C) at surface level in December.

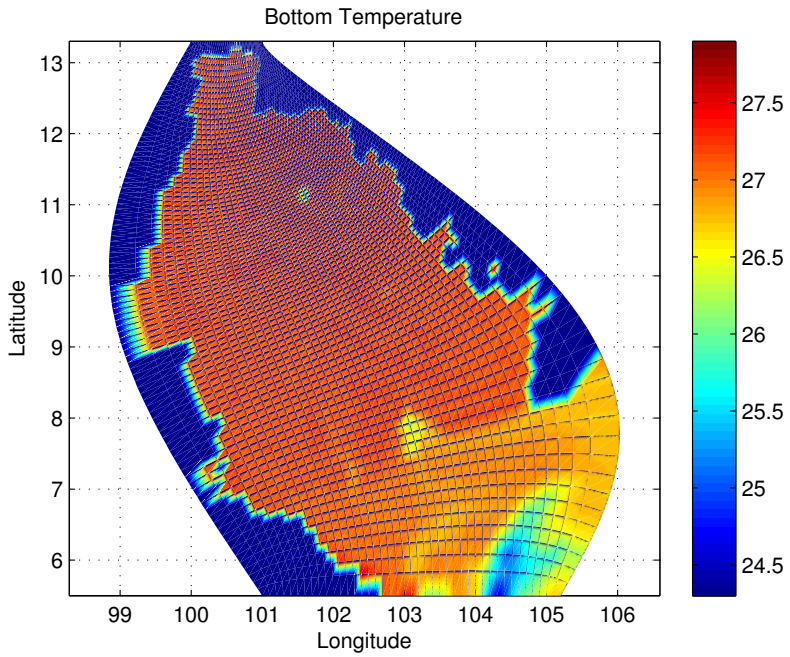

Figure 4.107 The simulated temperature (°C) at bottom level in December.

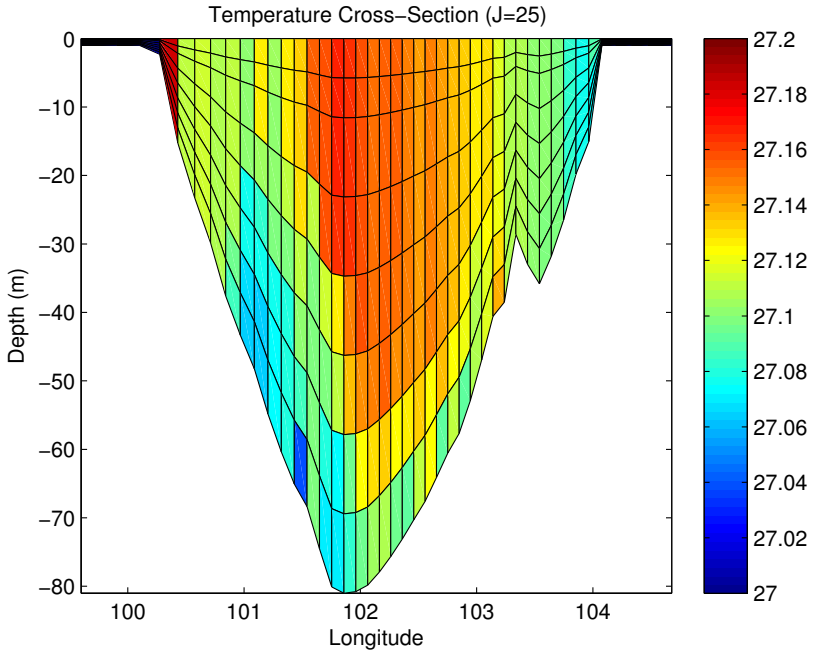

Figure 4.108 The simulated temperature cross-section (°C) in December.

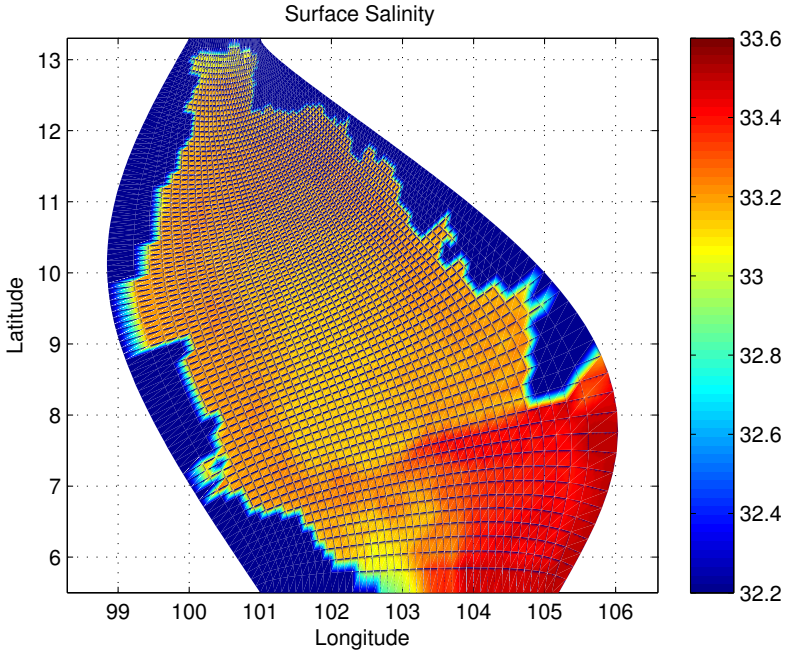

Figure 4.109 The simulated salinity (psu) at surface level in January.

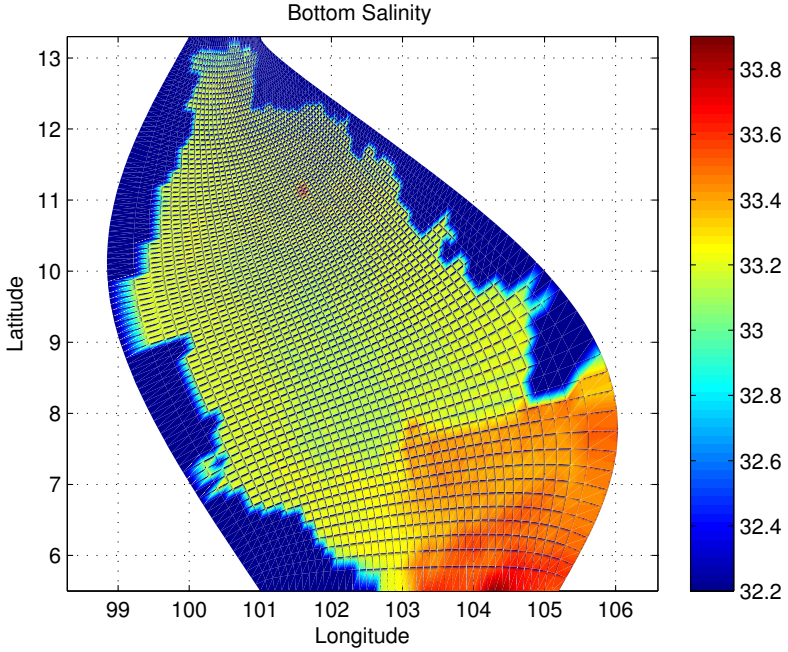

Figure 4.110 The simulated salinity (psu) at bottom level in January.

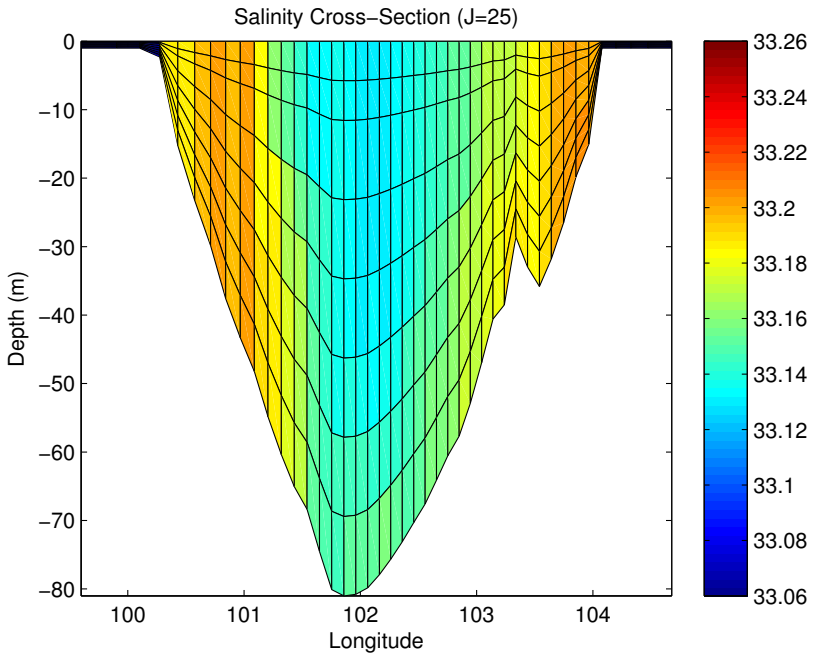

Figure 4.111 The simulated salinity cross-section (psu) in January.

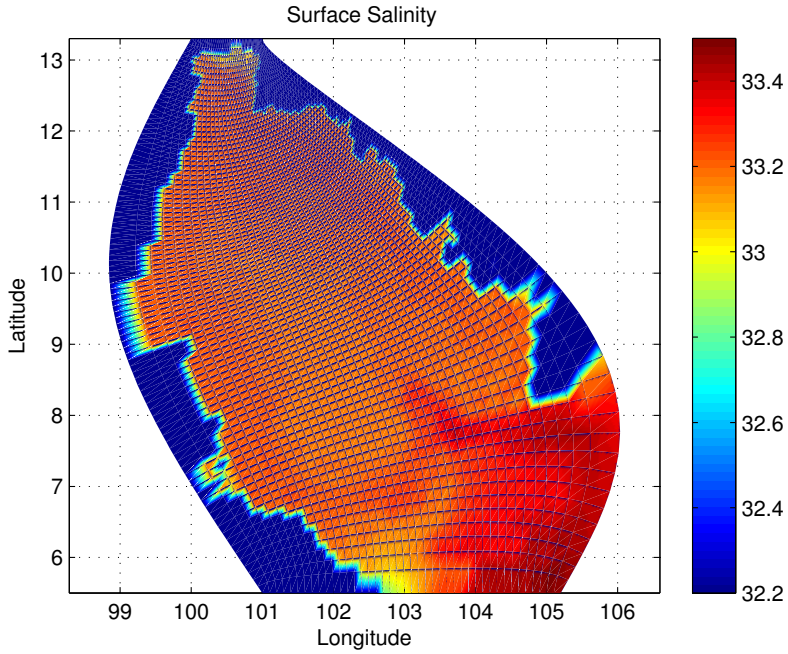

Figure 4.112 The simulated salinity (psu) at surface level in February.

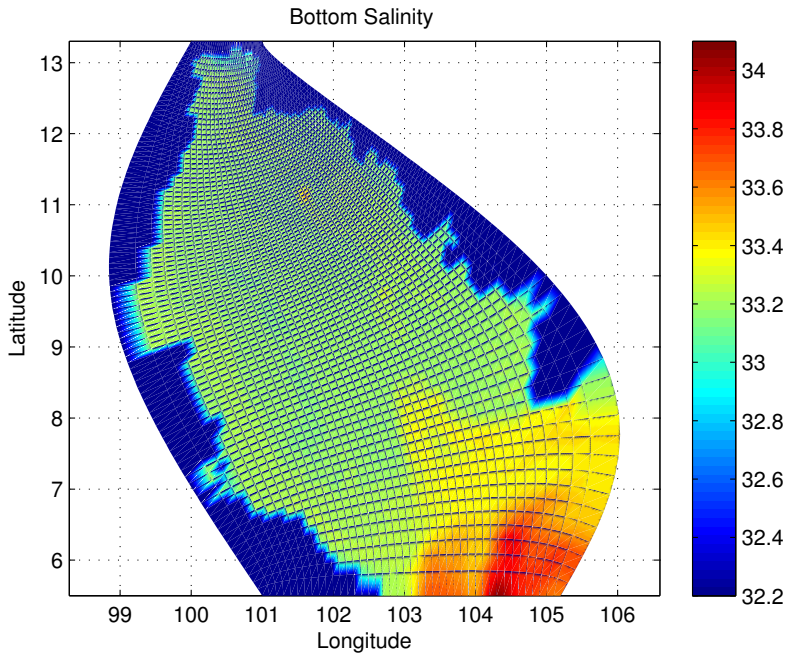

Figure 4.113 The simulated salinity (psu) at bottom level in February.

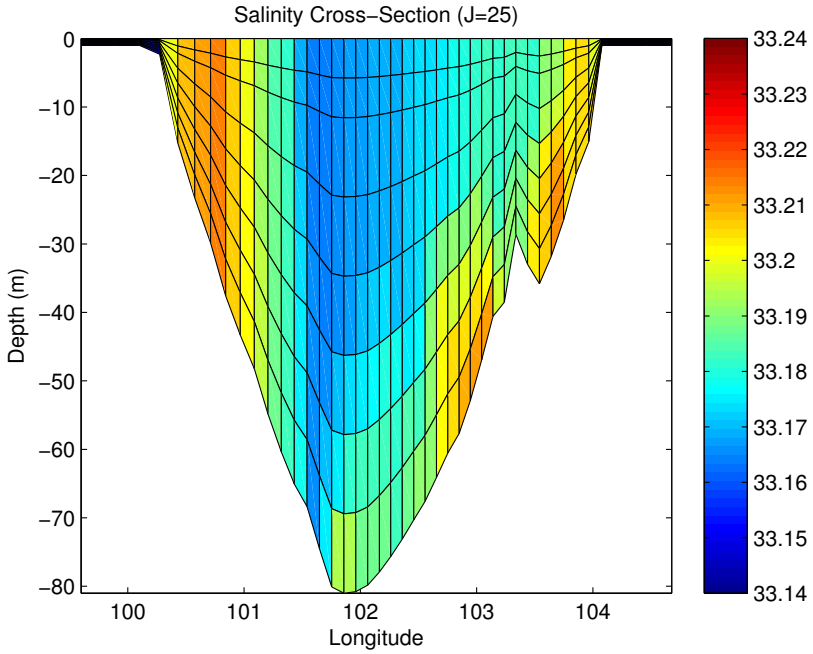

Figure 4.114 The simulated salinity cross-section (psu) in February.

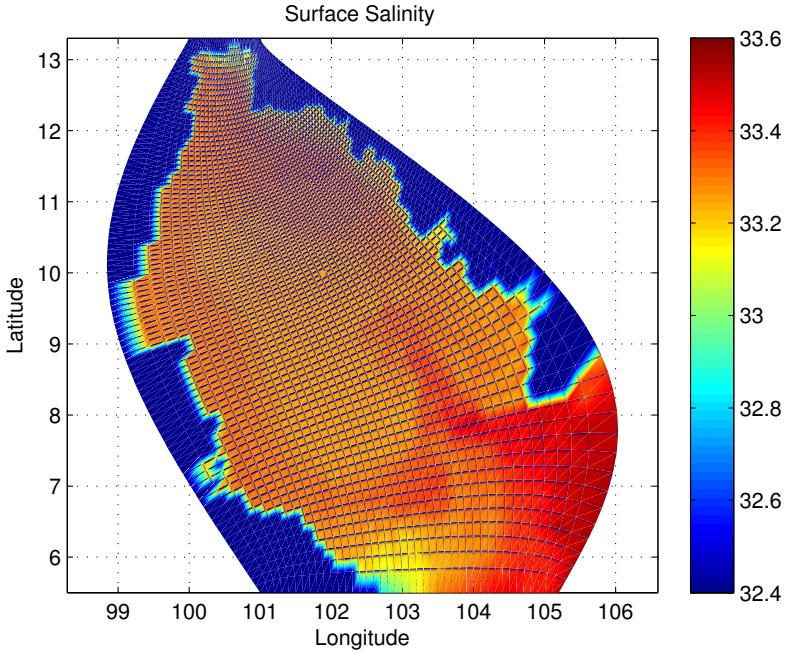

Figure 4.115 The simulated salinity (psu) at surface level in March.

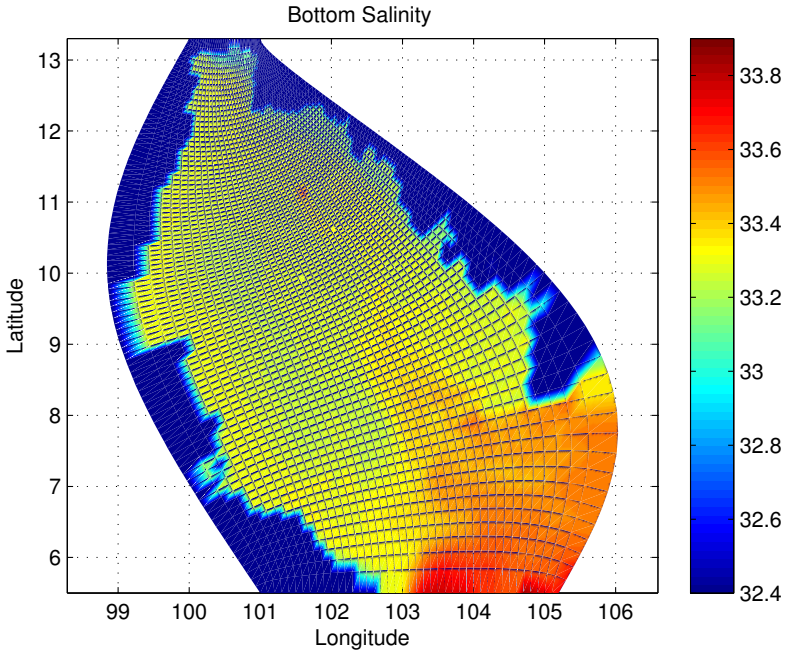

Figure 4.116 The simulated salinity (psu) at bottom level in March.

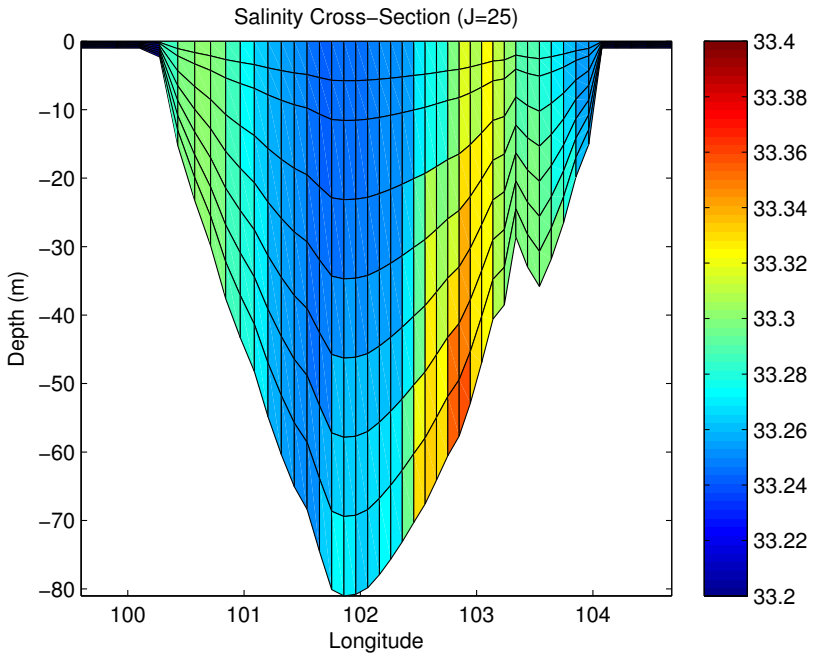

Figure 4.117 The simulated salinity cross-section (psu) in March.

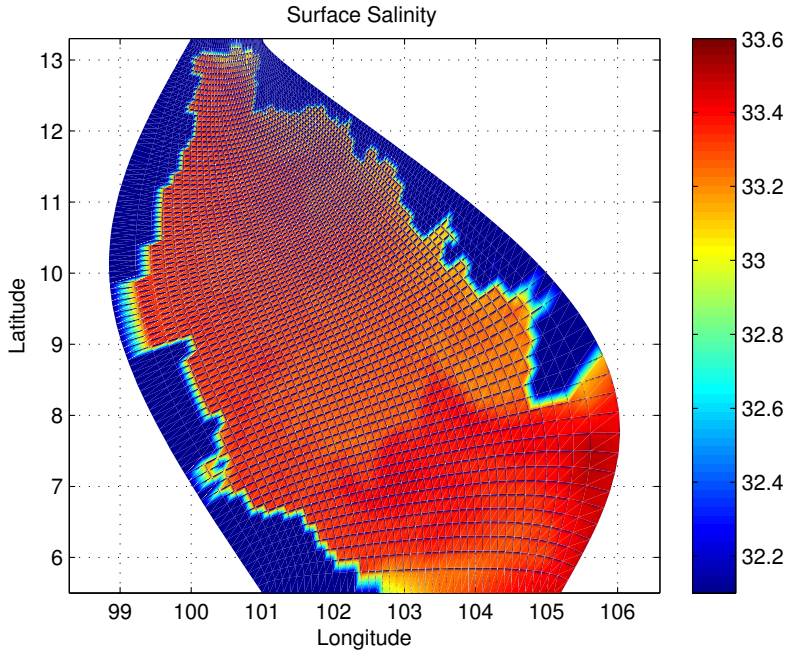

Figure 4.118 The simulated salinity (psu) at surface level in April.

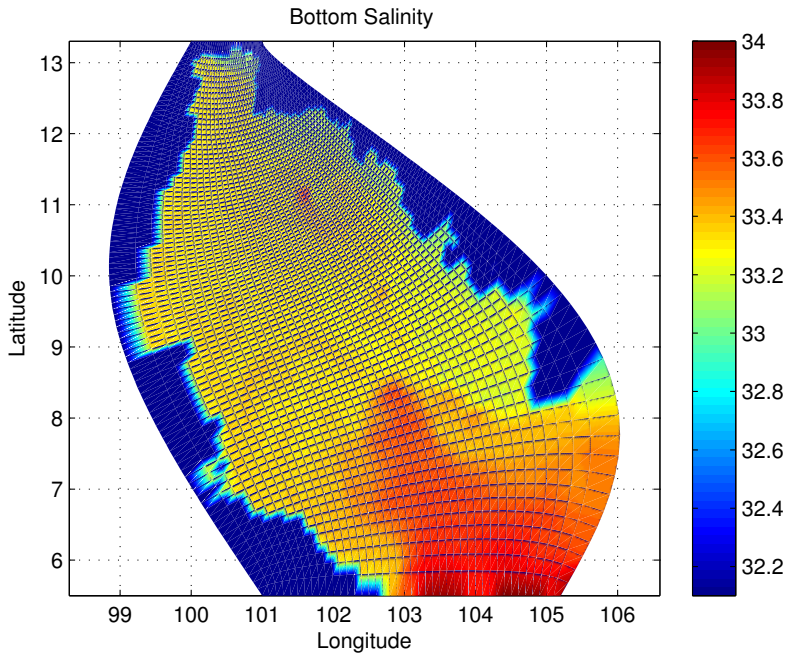

Figure 4.119 The simulated salinity (psu) at bottom level in April.

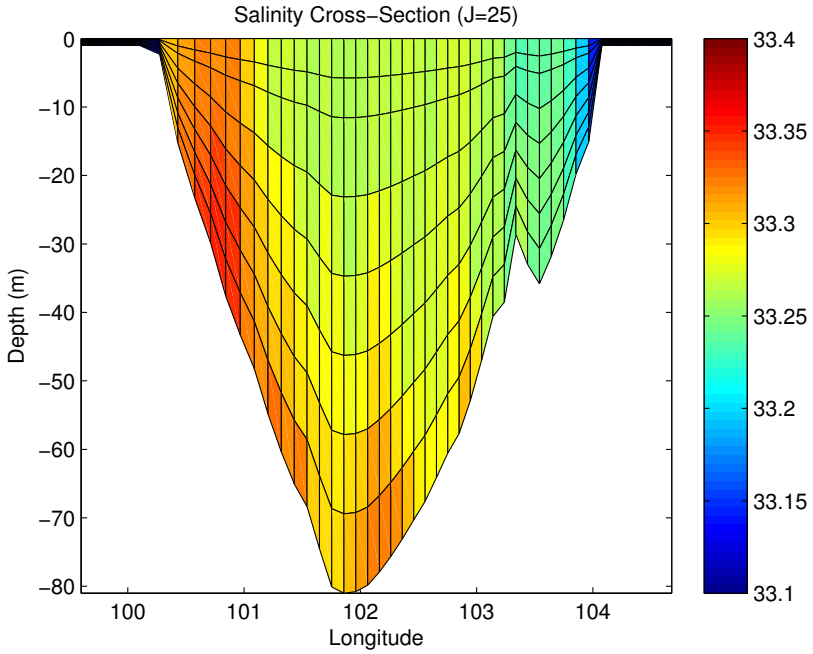

Figure 4.120 The simulated salinity cross-section (psu) in April.

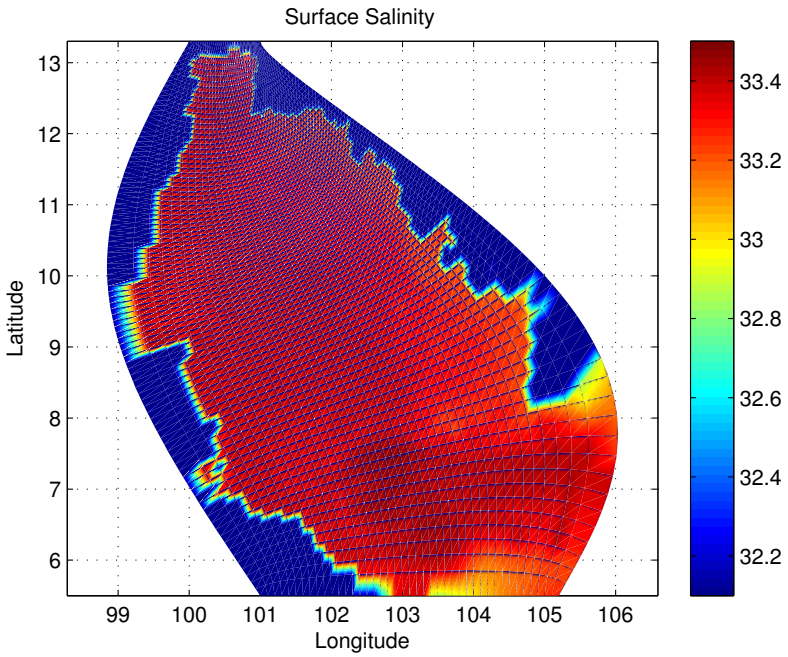

Figure 4.121 The simulated salinity (psu) at surface level in May.

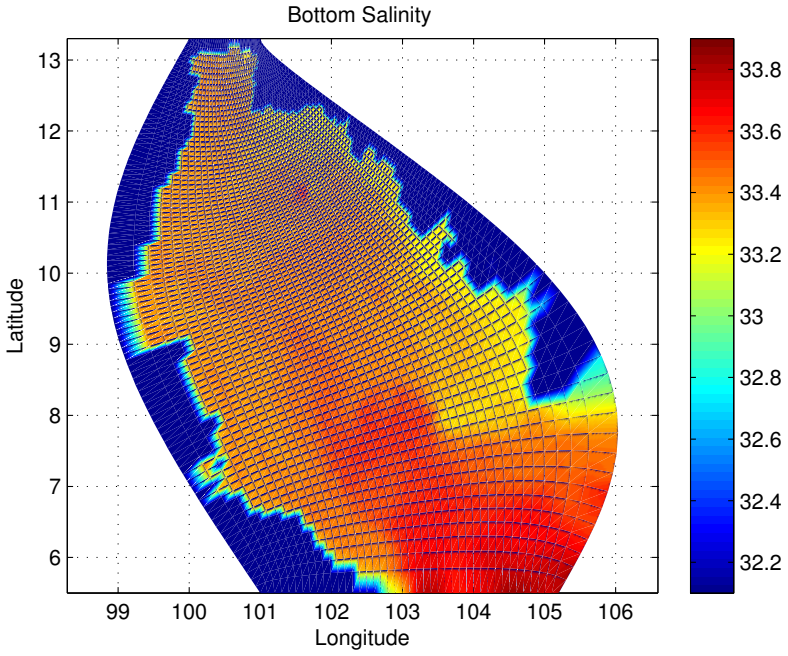

Figure 4.122 The simulated salinity (psu) at bottom level in May.

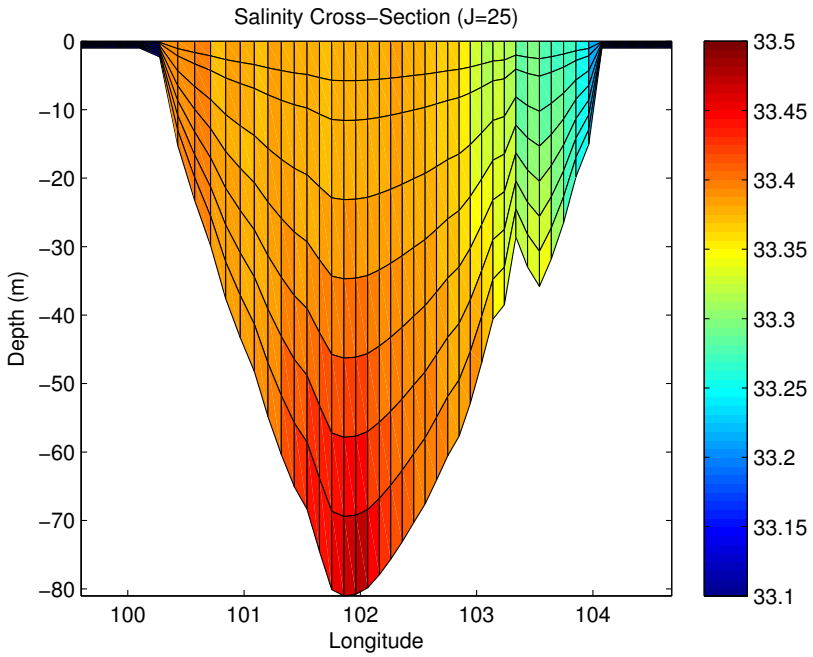

Figure 4.123 The simulated salinity cross-section (psu) in May.

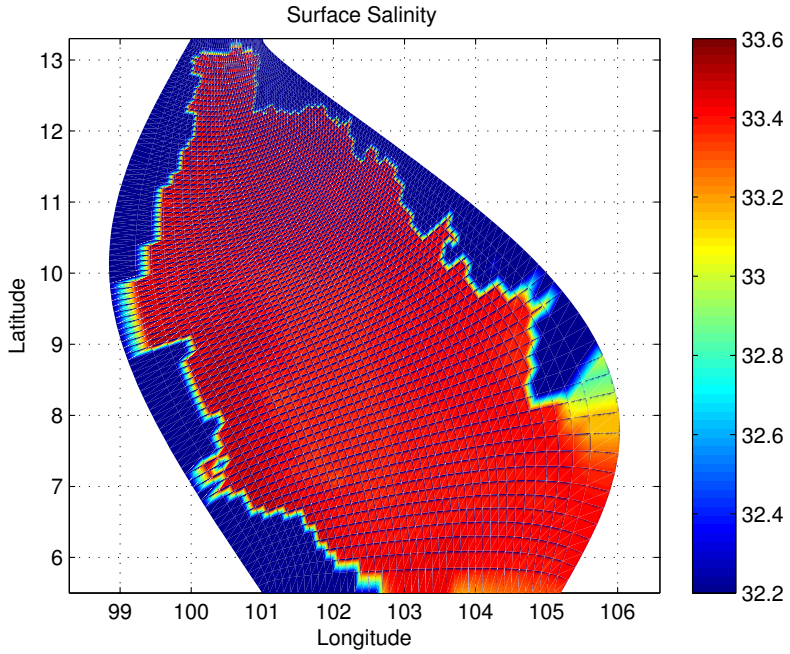

Figure 4.124 The simulated salinity (psu) at surface level in June.

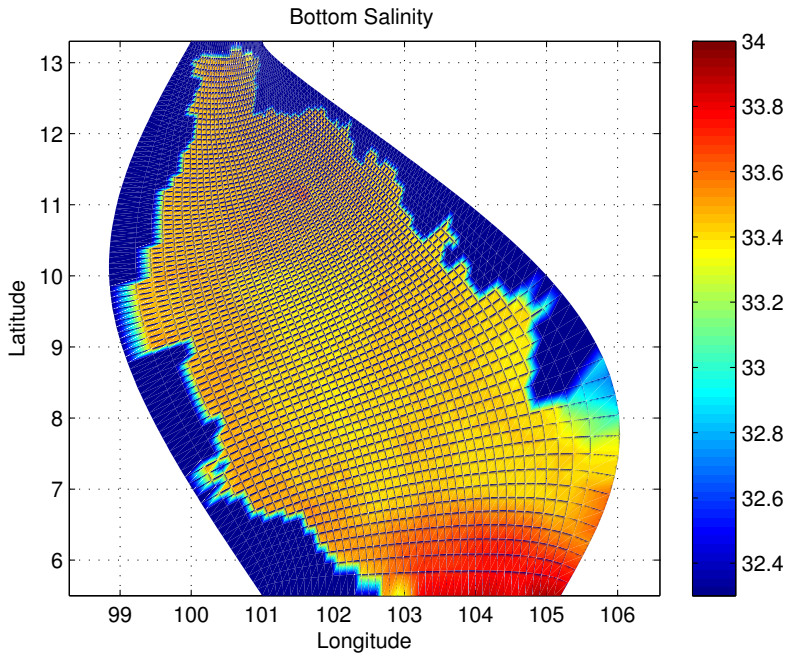

Figure 4.125 The simulated salinity (psu) at bottom level in June.

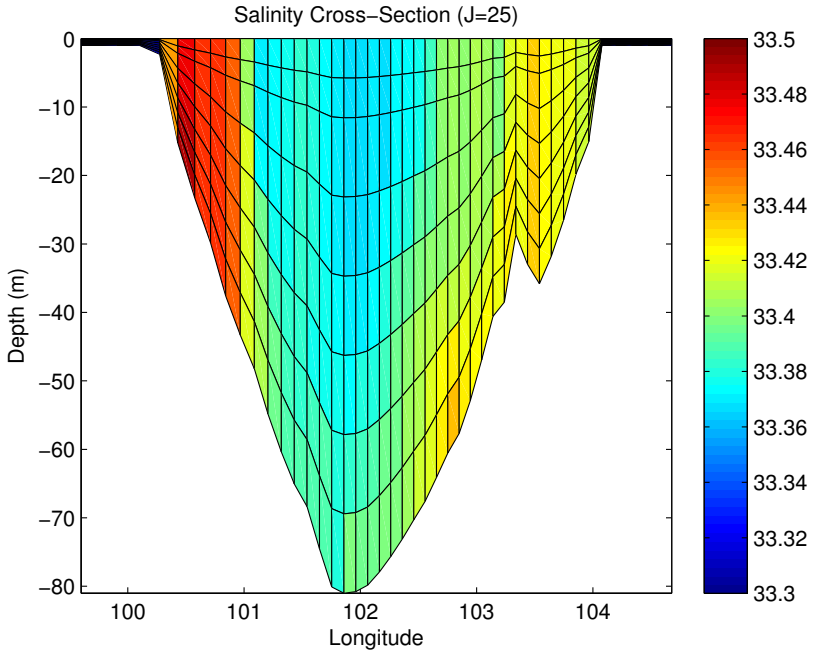

Figure 4.126 The simulated salinity cross-section (psu) in June.

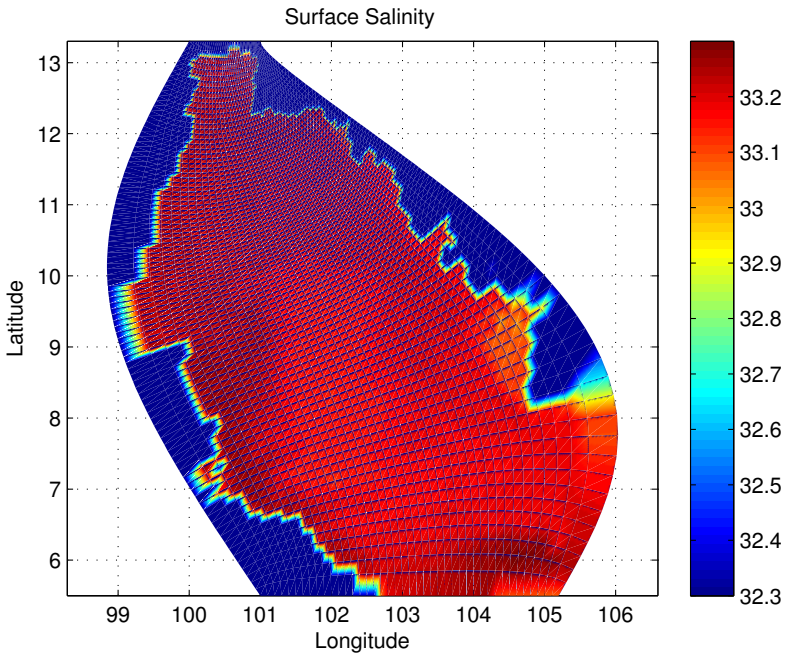

Figure 4.127 The simulated salinity (psu) at surface level in July.

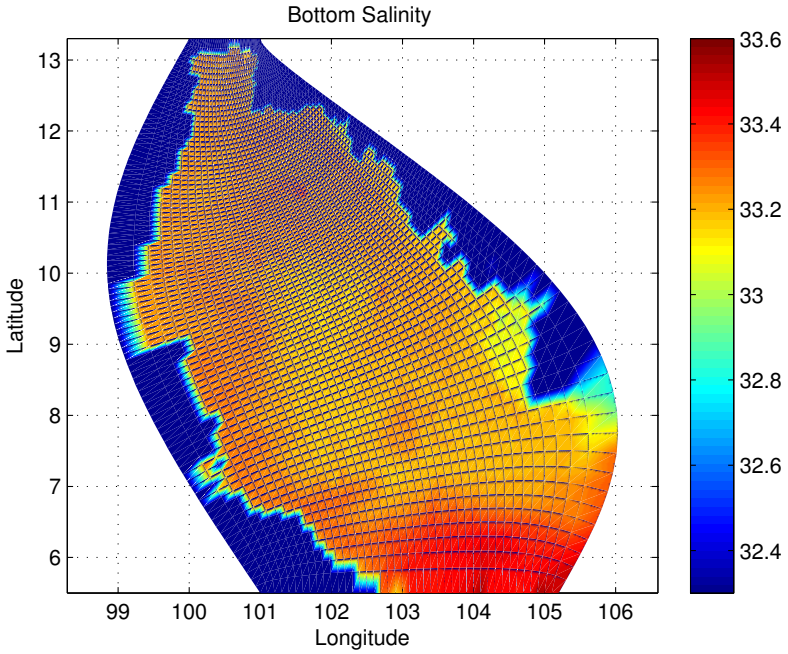

Figure 4.128 The simulated salinity (psu) at bottom level in July.

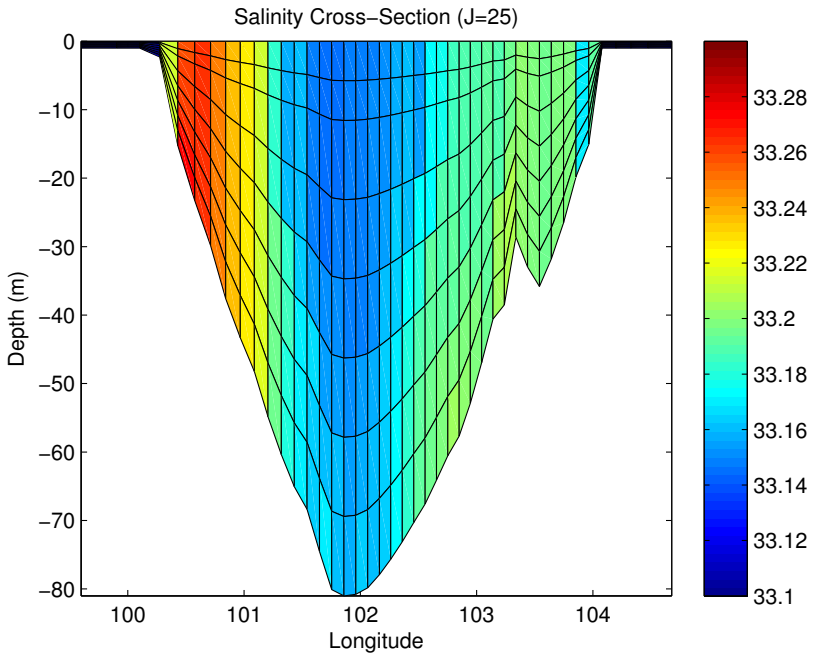

Figure 4.129 The simulated salinity cross-section (psu) in July.

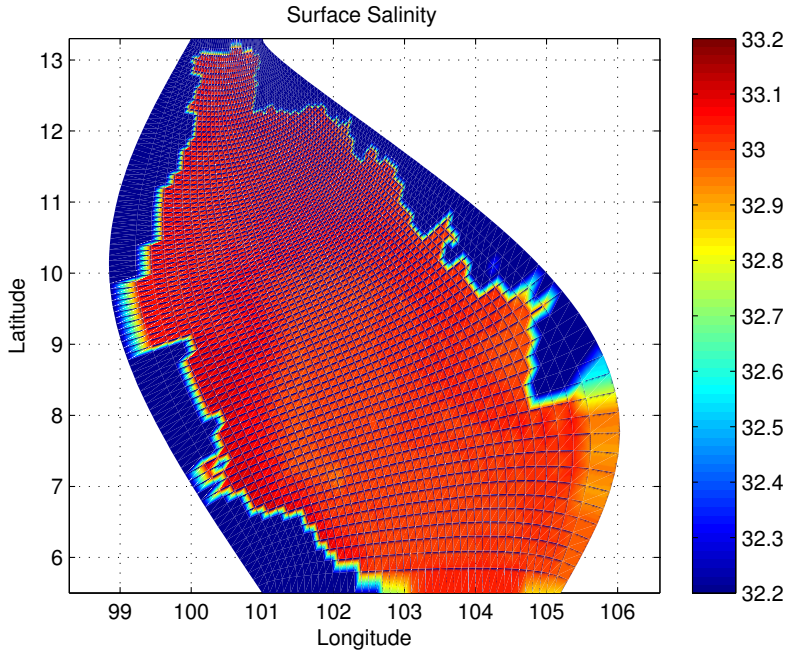

Figure 4.130 The simulated salinity (psu) at surface level in August.

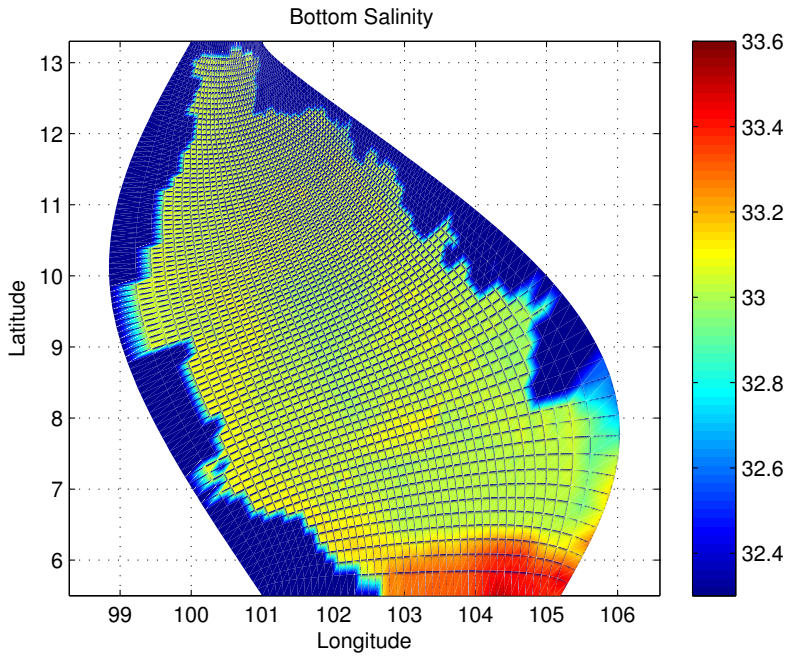

Figure 4.131 The simulated salinity (psu) at bottom level in August.

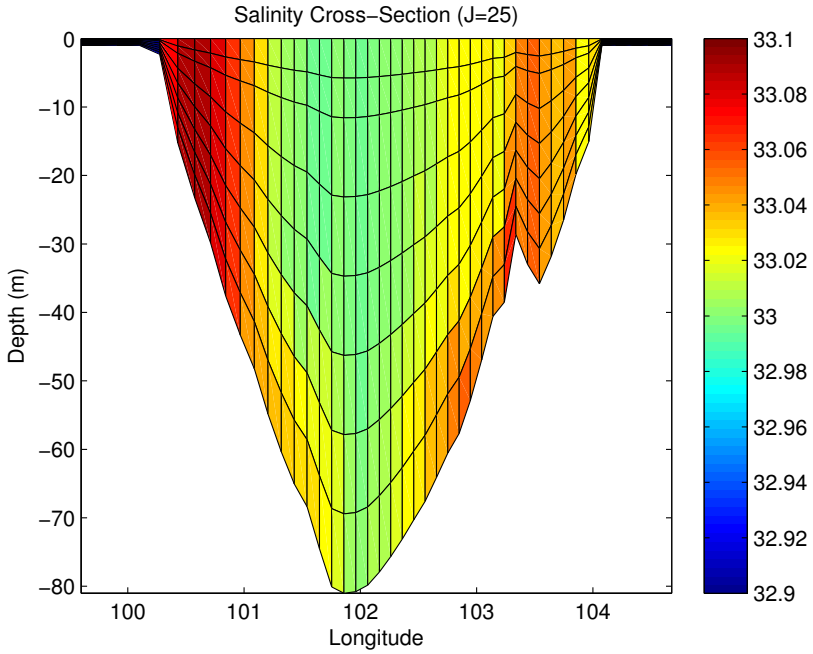

Figure 4.132 The simulated salinity cross-section (psu) in August.

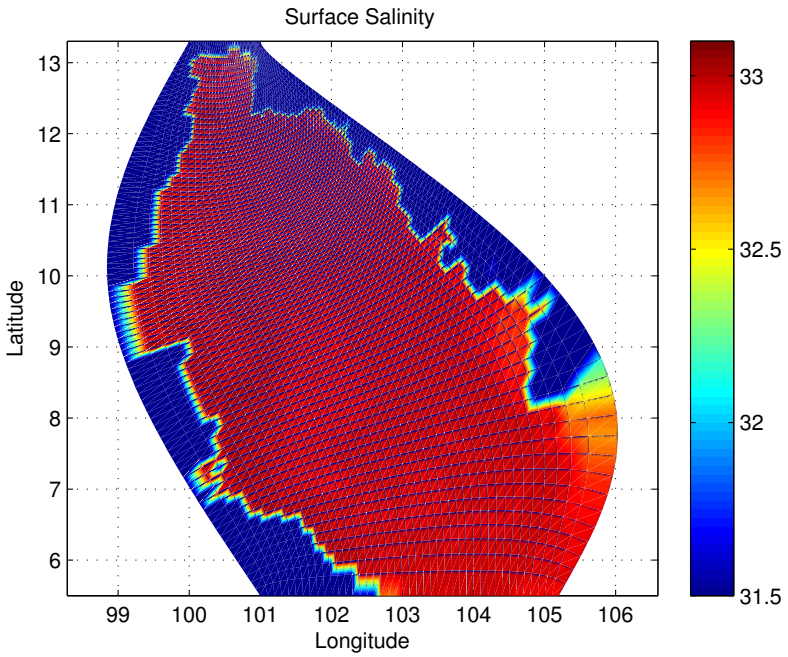

Figure 4.133 The simulated salinity (psu) at surface level in September.

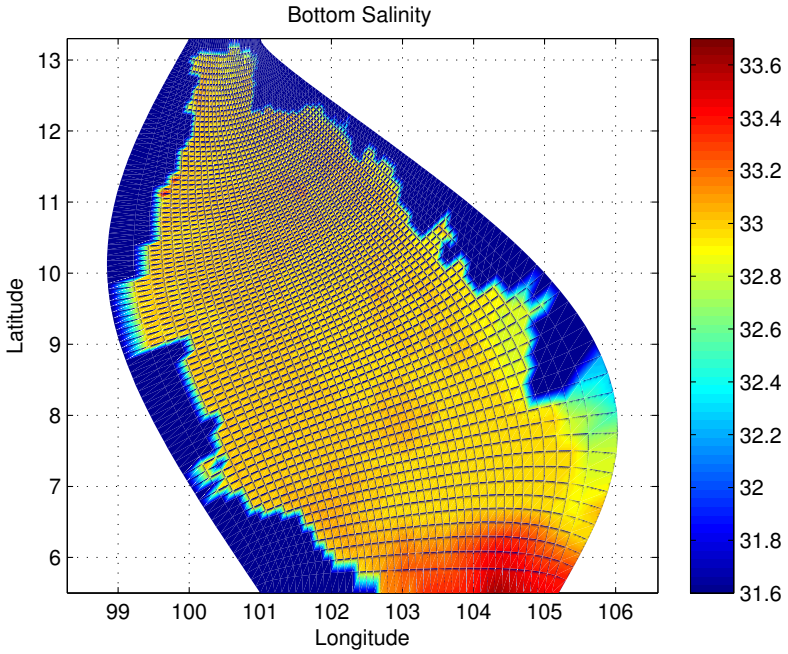

Figure 4.134 The simulated salinity (psu) at bottom level in September.

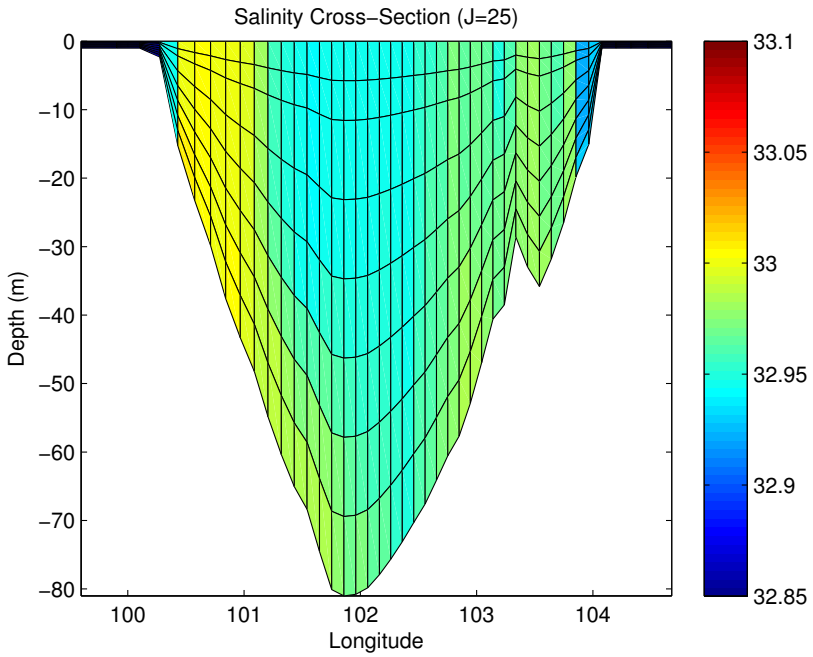

Figure 4.135 The simulated salinity cross-section (psu) in September.

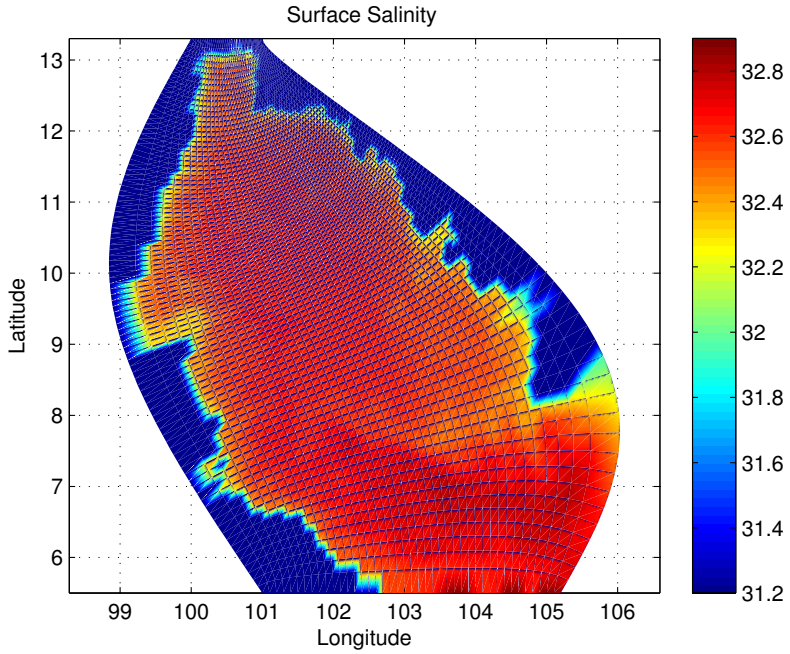

Figure 4.136 The simulated salinity (psu) at surface level in October.

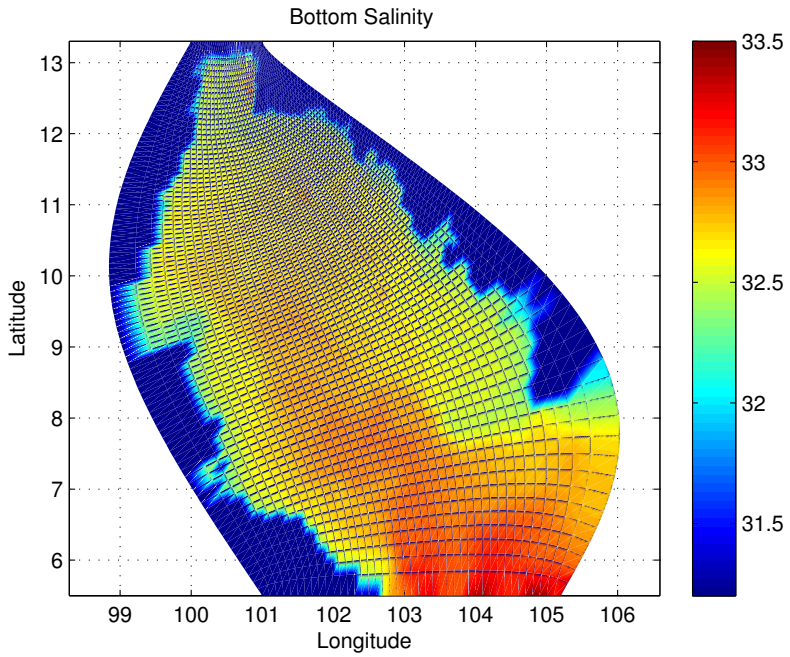

Figure 4.137 The simulated salinity (psu) at bottom level in October.

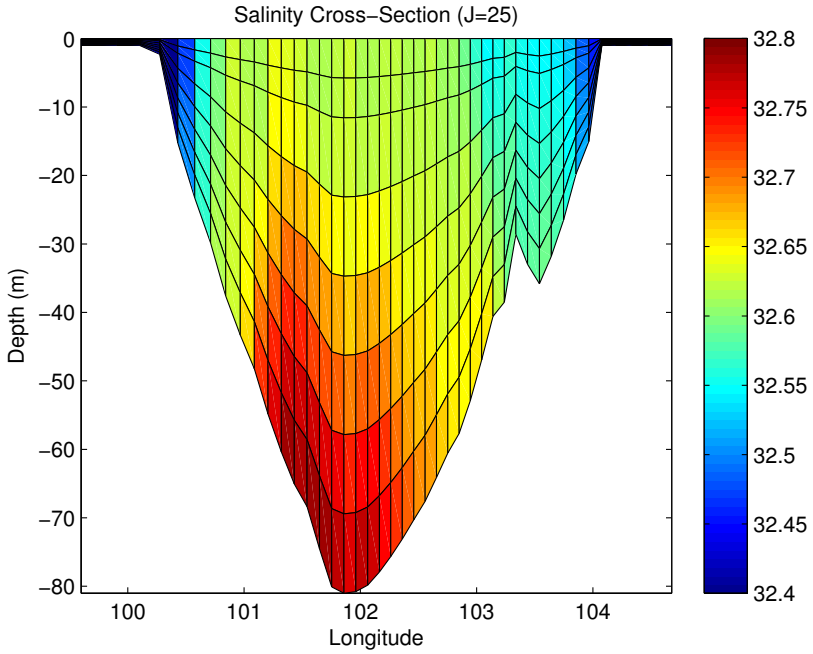

Figure 4.138 The simulated salinity cross-section (psu) in October.

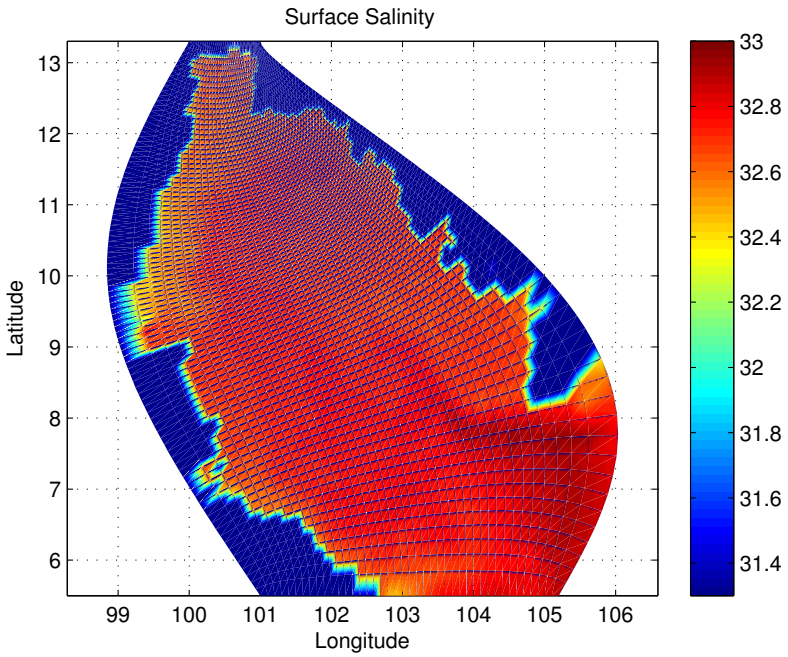

Figure 4.139 The simulated salinity (psu) at surface level in November.

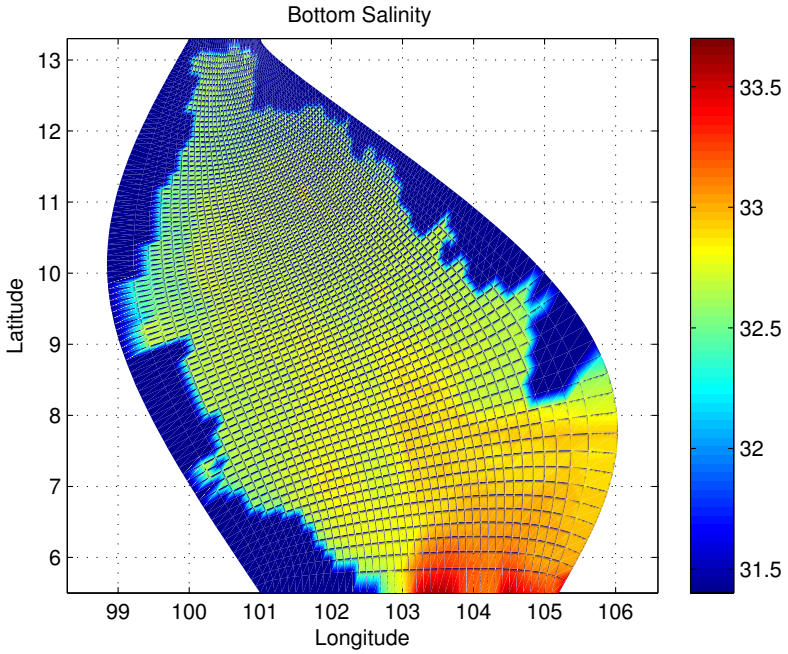

Figure 4.140 The simulated salinity (psu) at bottom level in November.

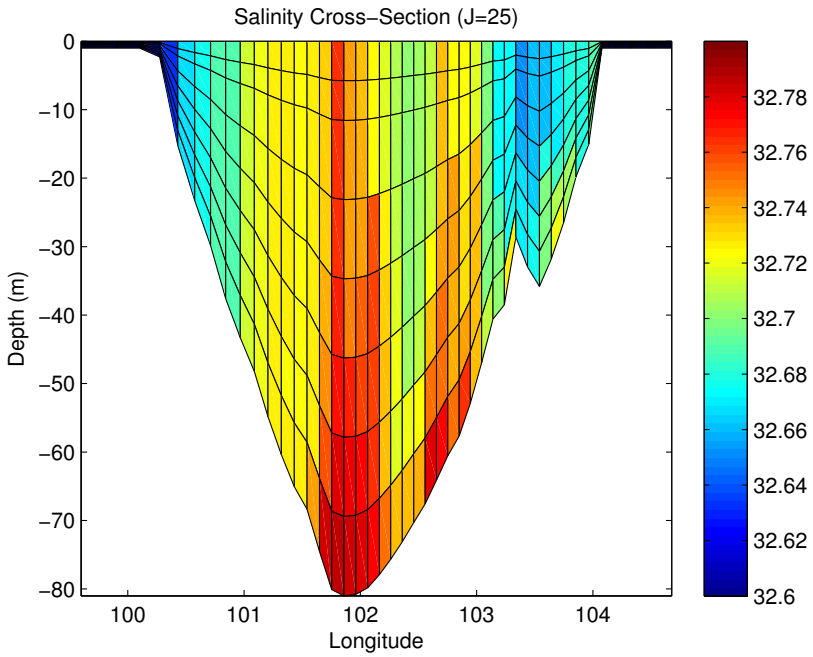

Figure 4.141 The simulated salinity cross-section (psu) in November.

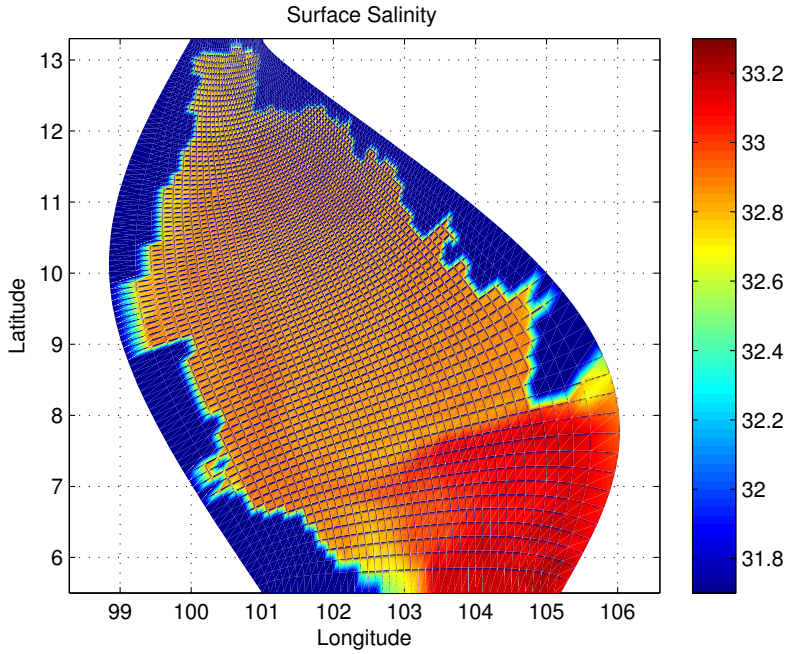

Figure 4.142 The simulated salinity (psu) at surface level in December.

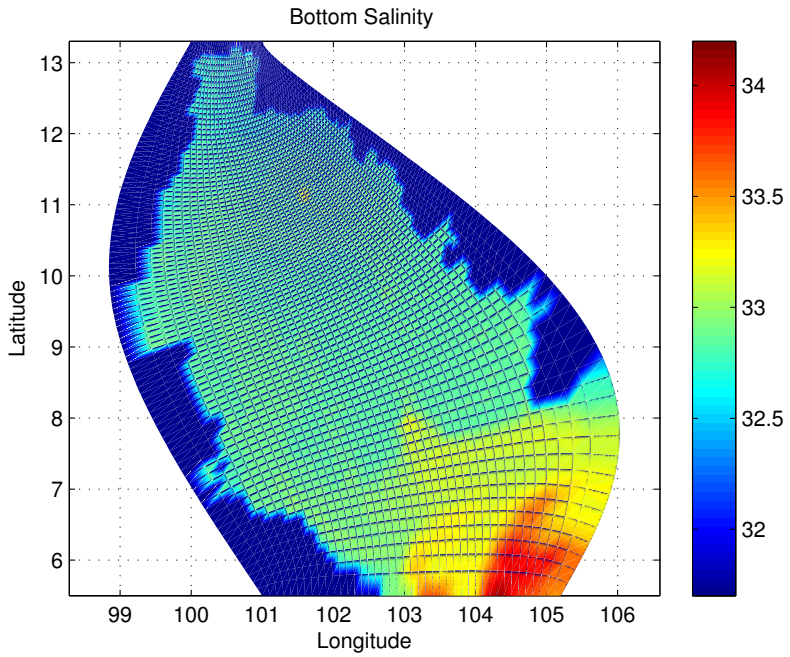

Figure 4.143 The simulated salinity (psu) at bottom level in December.

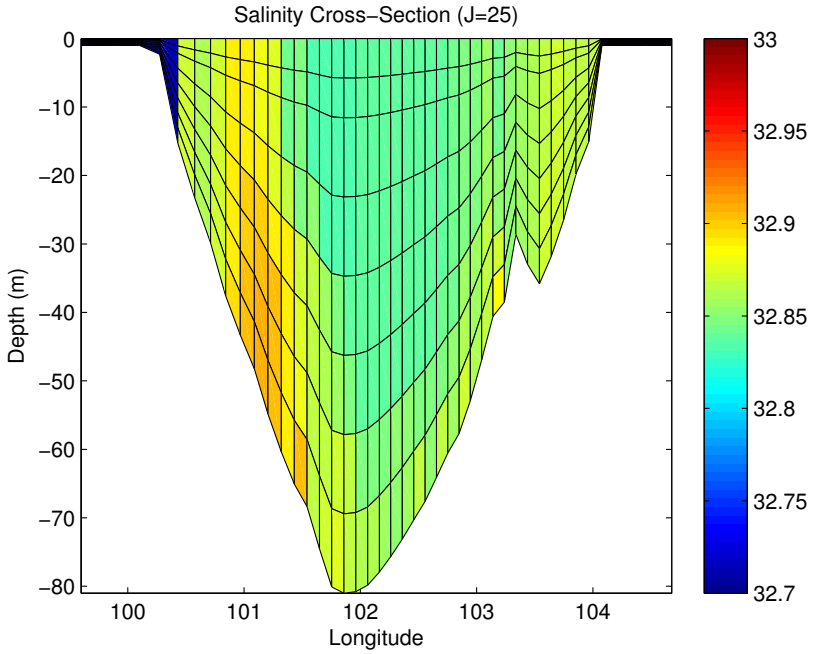

Figure 4.144 The simulated salinity cross-section (psu) in December.

Next, we will use the simulated current velocities, potential temperature, salinity, and seawater density to calculate the heat content of volume and transports of heat, freshwater, and water mass. The heat content of volume is calculated from Eq. (3.95) and the heat, freshwater, and water mass transports are calculated from Eqs. (3.96), (3.97), and (3.98), respectively. The result of heat content of volume in each layer is shown in Table 4.2.

Table 4.2 The heat content of volume ($\times 10^{20}$ Joules) in each layer, k=1, 2,..., 8, in the Gulf of Thailand.

Month	k=**1**	k=**2**	k=**3**	k=**4**	k=**5**	k=**6**	k=**7**	k=**8**
Jan	1.2674	1.2693	2.5351	2.5360	2.5343	2.5356	2.5328	2.5324
Feb	1.2750	1.2768	2.5499	2.5500	2.5478	2.5487	2.5444	2.5390
Mar	1.3107	1.3125	2.6206	2.6198	2.6170	2.6176	2.6126	2.6072
Apr	1.3378	1.3393	2.6710	2.6679	2.6624	2.6580	2.6481	2.6412
May	1.3547	1.3559	2.7054	2.7020	2.6957	2.6919	2.6817	2.6786
Jun	1.3469	1.3487	2.6924	2.6935	2.6892	2.6890	2.6844	2.6846
Jul	1.3524	1.3543	2.7048	2.7066	2.7042	2.7052	2.7022	2.7028
Aug	1.3407	1.3426	2.6813	2.6836	2.6810	2.6823	2.6799	2.6812
Sep	1.3404	1.3423	2.6809	2.6828	2.6803	2.6815	2.6780	2.6779
Oct	1.3412	1.3431	2.6828	2.6851	2.6835	2.6845	2.6809	2.6805
Nov	1.3255	1.3274	2.6509	2.6511	2.6485	2.6492	2.6452	2.6425
Dec	1.2763	1.2781	2.5528	2.5536	2.5516	2.5530	2.5486	2.5416

The Table 4.2 shows that the highest heat content of volume is in the third and fourth layers, and in the deeper layers the heat content of volume decreases continuously. Actually, the highest and lowest heat content of volume are at the sea surface, or the first layer, and the bottom, or the eighth layer, respectively, but in this research the first layer has low heat content of volumes as a result of small volumes.

The total heat content of volume in the Gulf of Thailand is shown in Fig. 4.145. From the figure, the red line is the total heat content of volume calculated from the simulated data of the Princeton Ocean Model and the blue line is the total heat content of volume calculated from observed data of Levitus94. The correlation coefficient is 0.9332. This means that the heat content of volume calculated from the simulated data from the model has trends that are the same as the heat content of volume calculated from observed data. We can see that the heat contents of volume are high in the Gulf of Thailand in the summer, April to June, and low in the winter, November to March.

For the heat, freshwater, and water mass transports, they are investigated in the Gulf of Thailand by choosing study regions from horizontal lines in the x direction of the model grid because these regions make us know that the heat, freshwater, and water mass are transported in or out of the Gulf of Thailand. The cross-section lines at j=14, j=20, j=27, j=35, j=44, j=54, j=54, j=74, and j=84 of the model grid are shown in Fig. 4.146. The results of heat, freshwater, and water mass transports in the Gulf of Thailand at each cross-section line are shown in Fig. 4.147 to Fig. 4. 4.173.

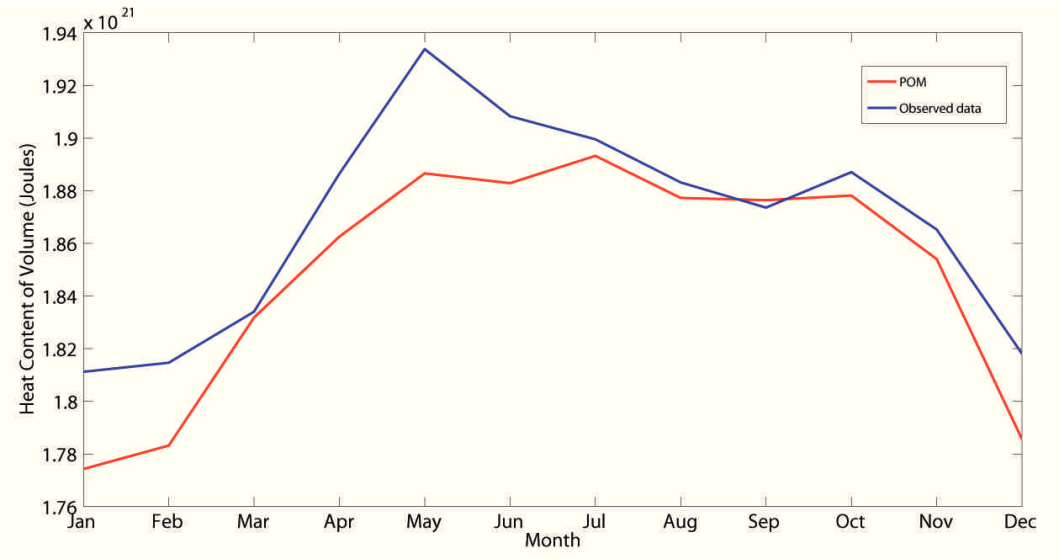

Figure 4.145 The total heat content of volume in the Gulf of Thailand.

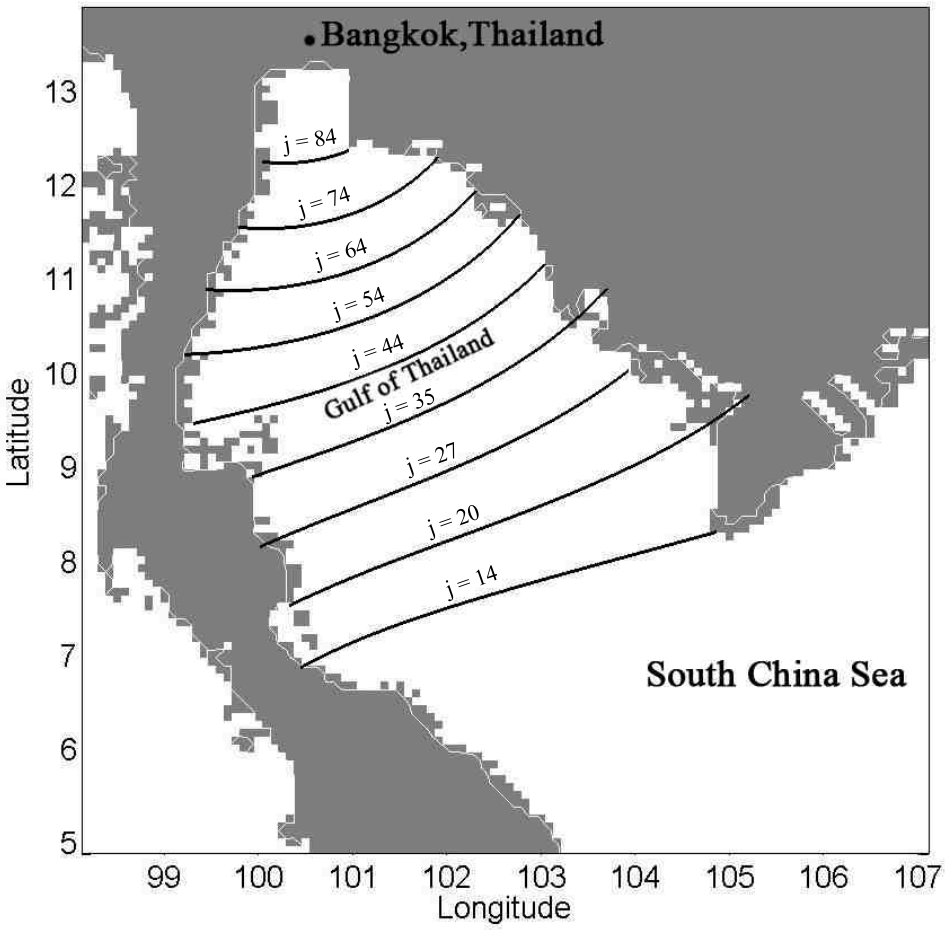

Figure 4.146 The cross-section lines in the Gulf of Thailand.

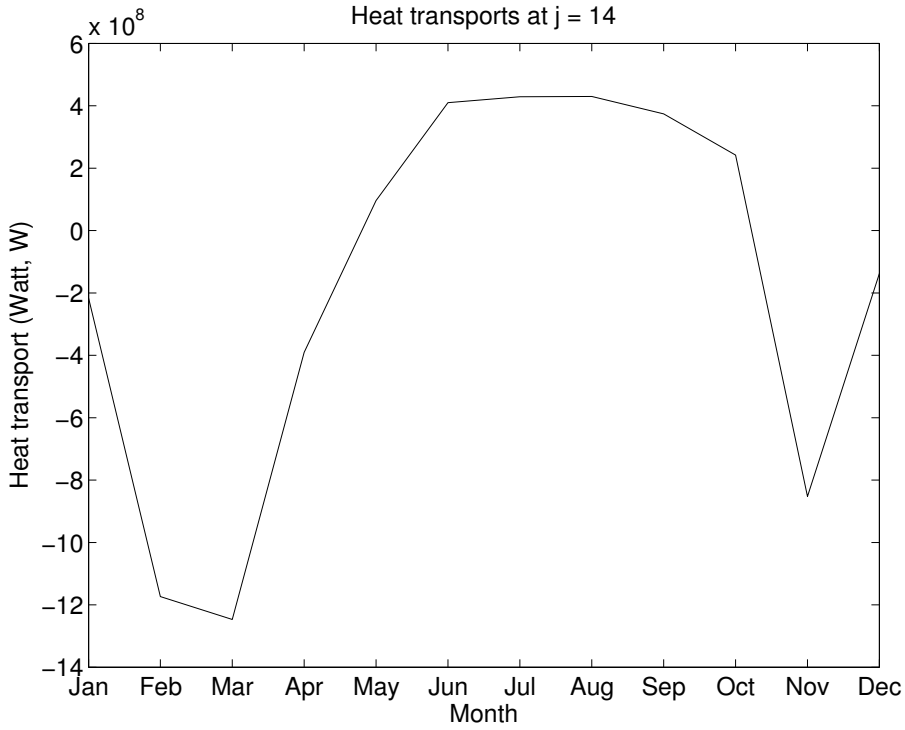

Figure 4.147 The values of heat transports at j=14 of the model grid.

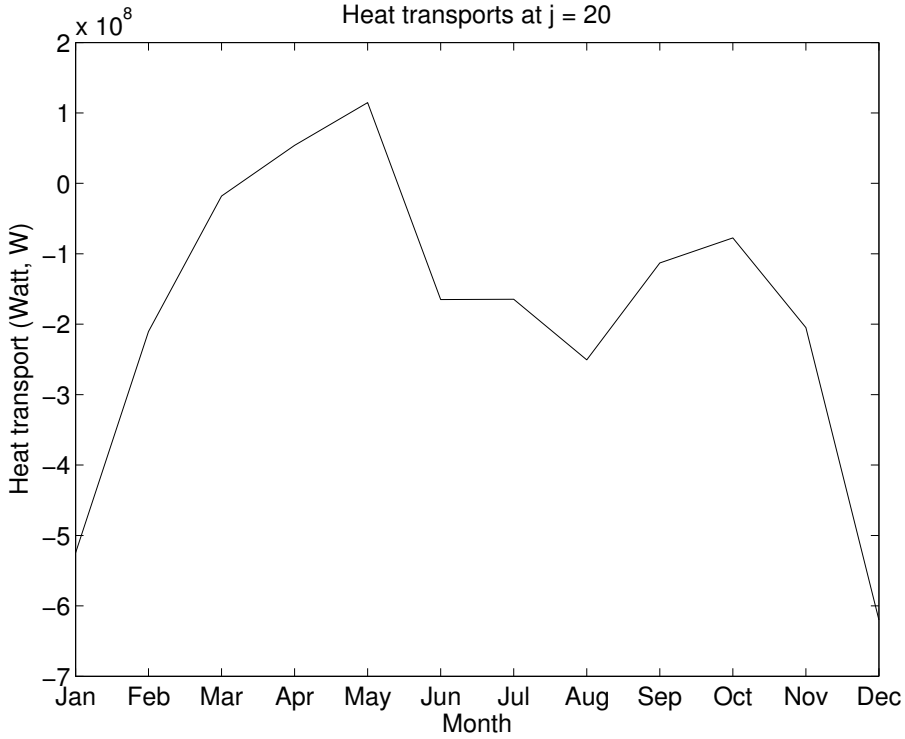

Figure 4.148 The values of heat transports at j=20 of the model grid.

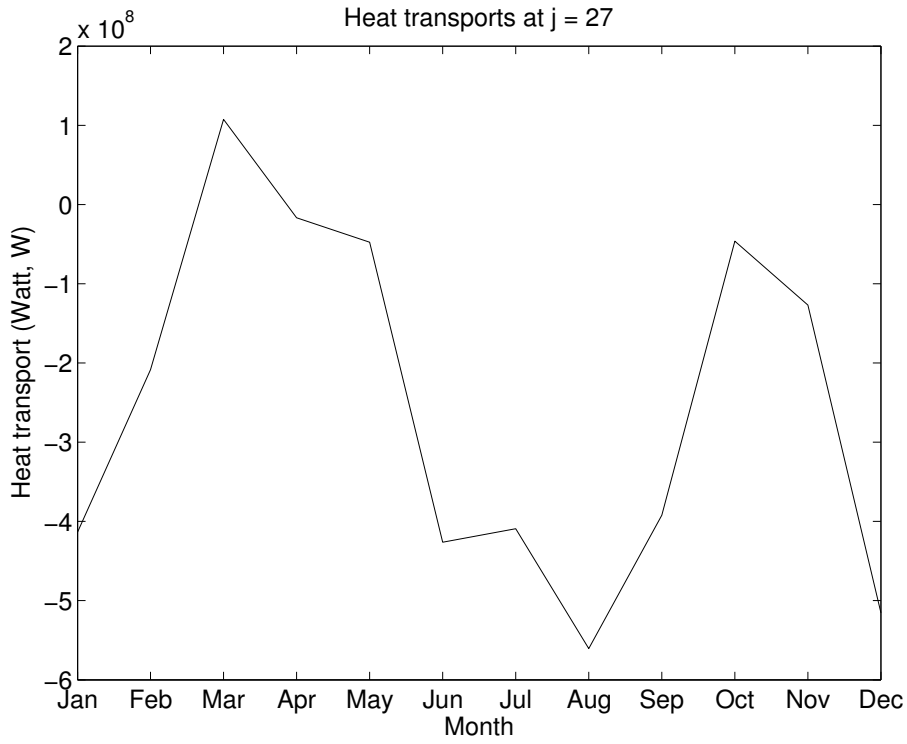

Figure 4.149 The values of heat transports at j=27 of the model grid.

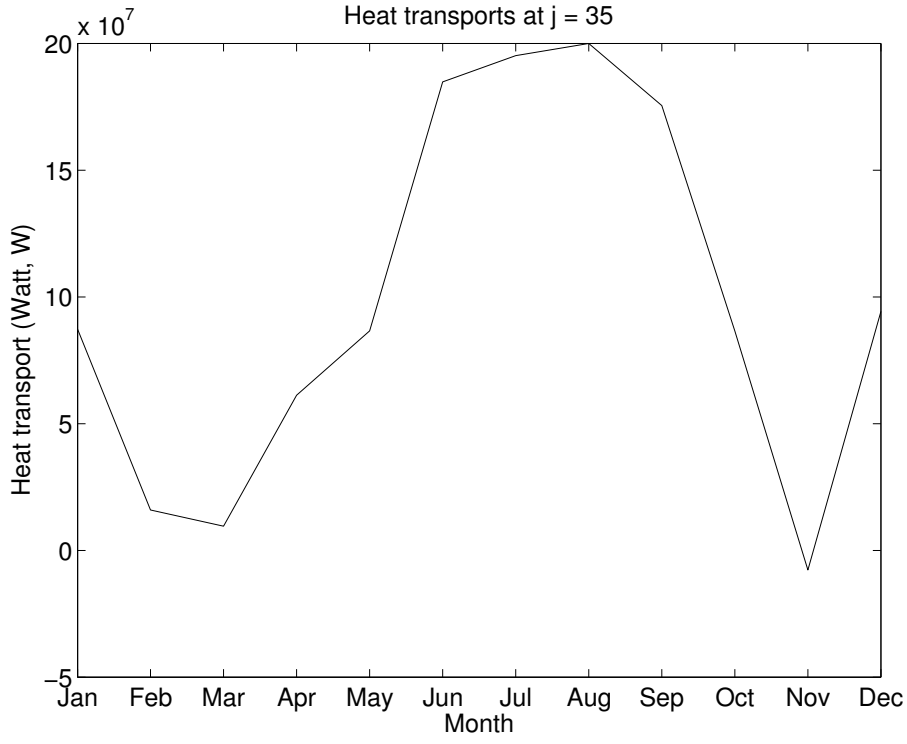

Figure 4.150 The values of heat transports at j=35 of the model grid.

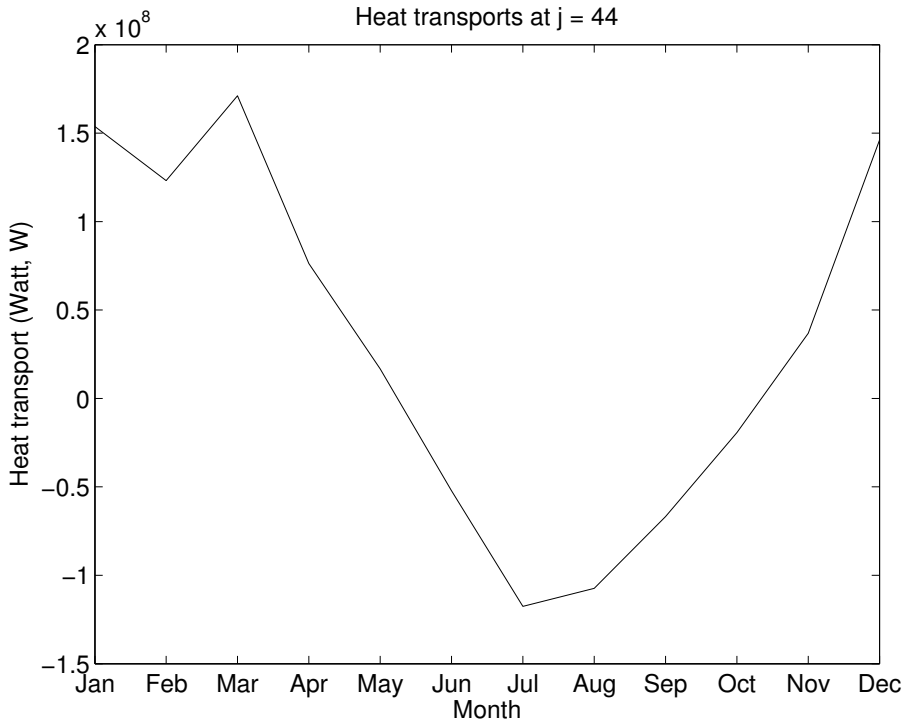

Figure 4.151 The values of heat transports at j=44 of the model grid.

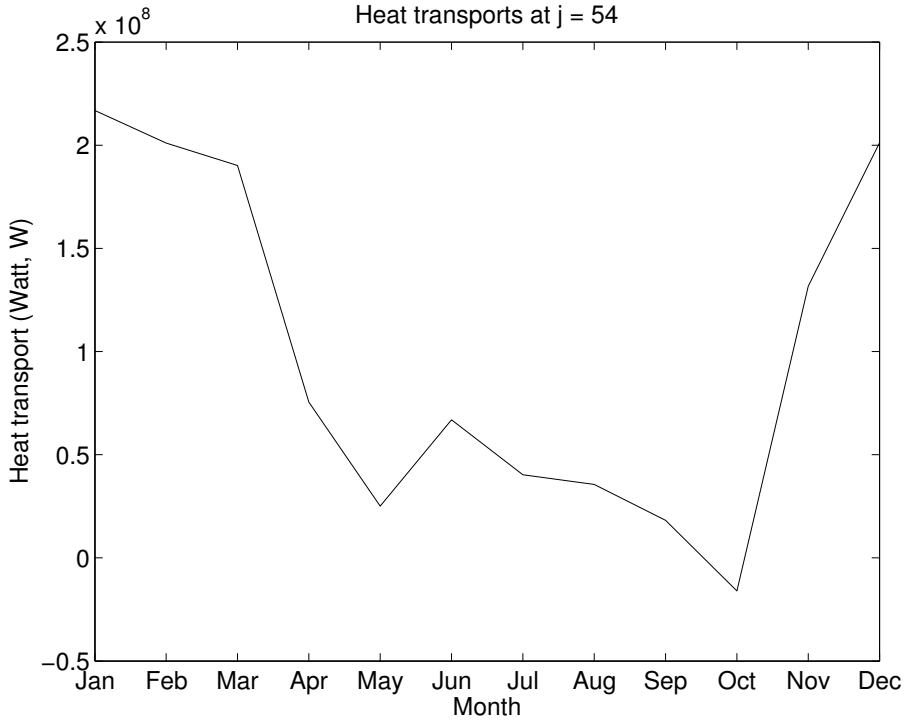

Figure 4.152 The values of heat transports at j=54 of the model grid.

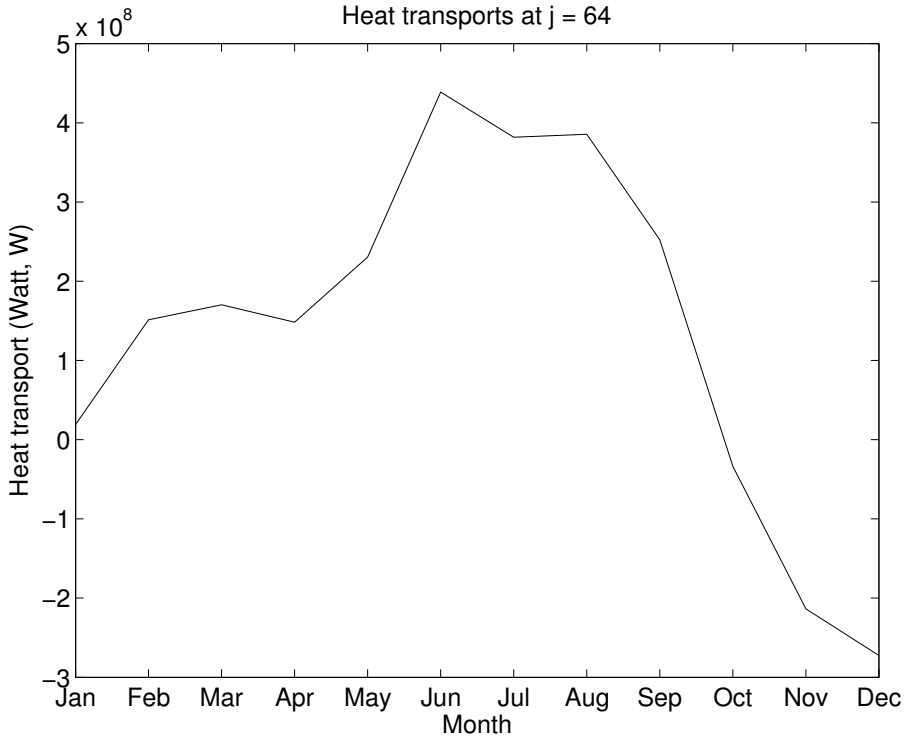

Figure 4.153 The values of heat transports at j=64 of the model grid.

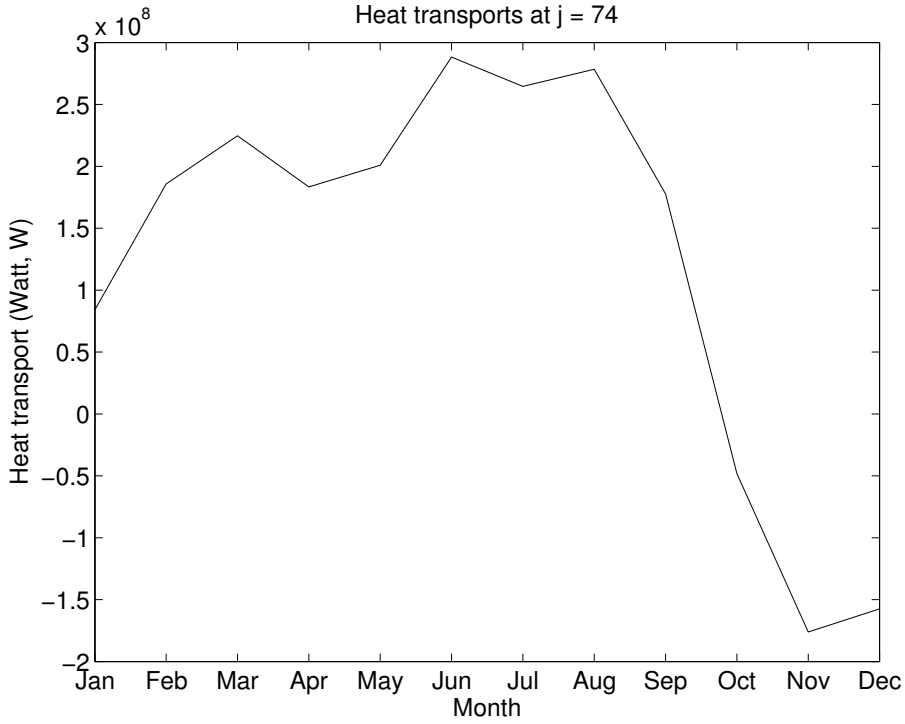

Figure 4.154 The values of heat transports at j=74 of the model grid.

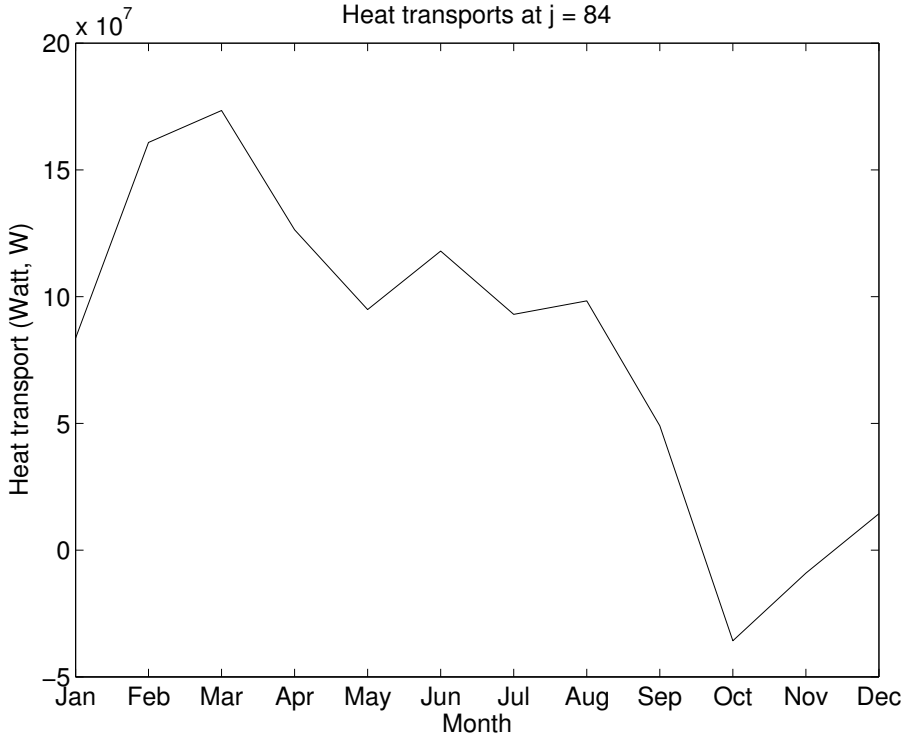

Figure 4.155 The values of heat transports at j=84 of the model grid.

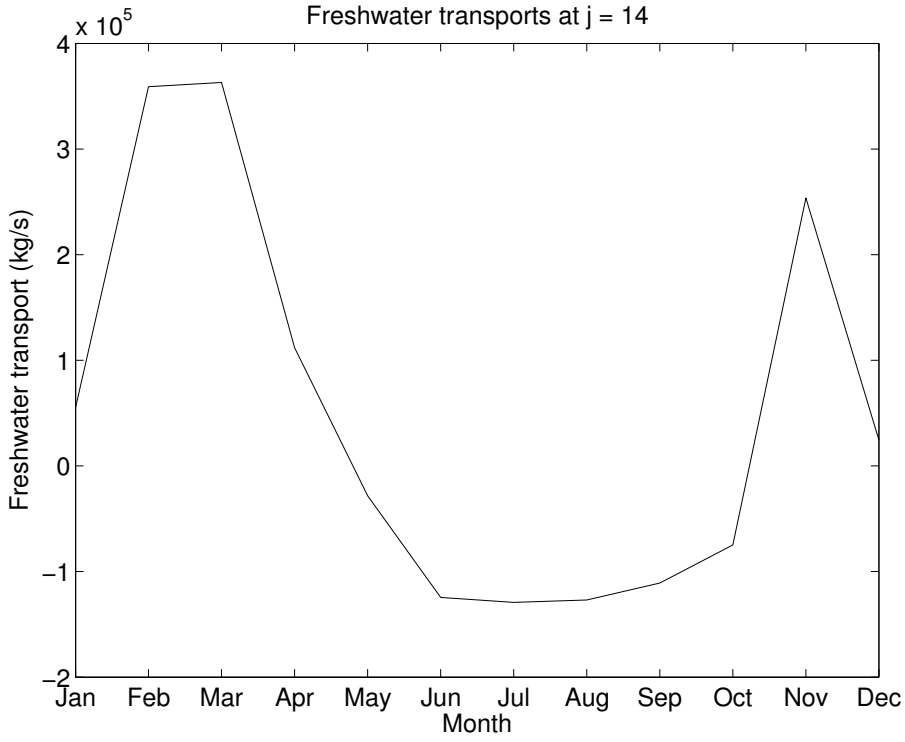

Figure 4.156 The values of freshwater transports at j=14 of the model grid.

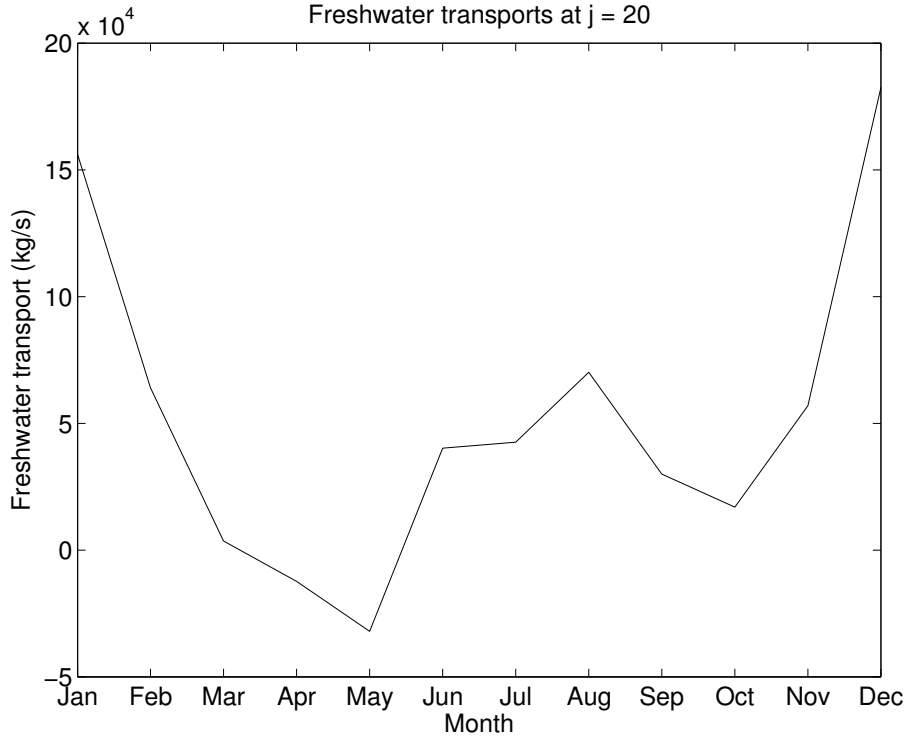

Figure 4.157 The values of freshwater transports at j=20 of the model grid.

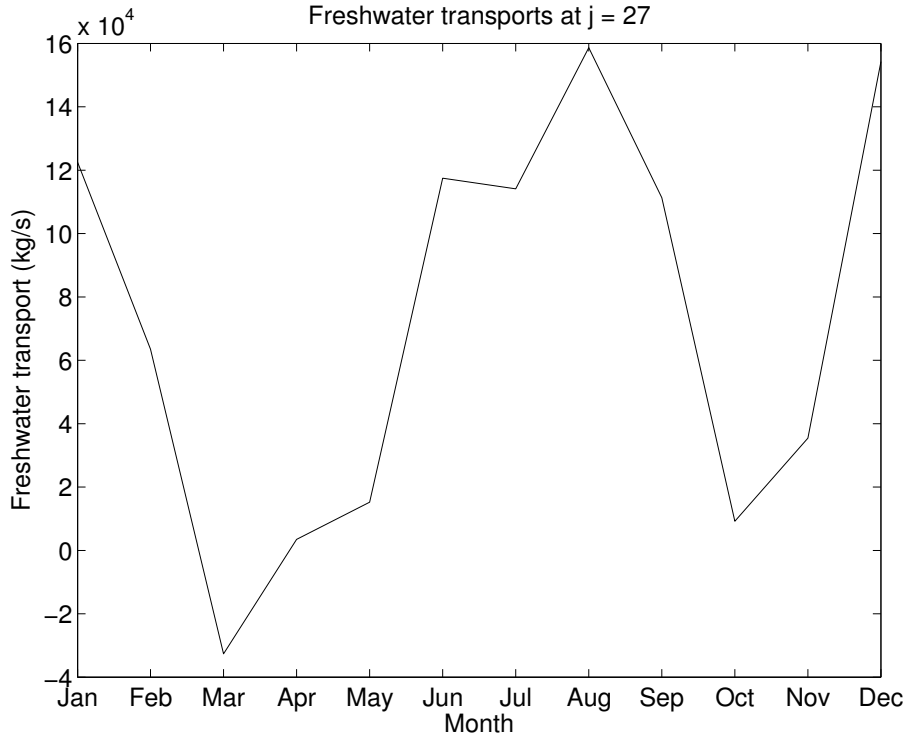

Figure 4.158 The values of freshwater transports at j=27 of the model grid.

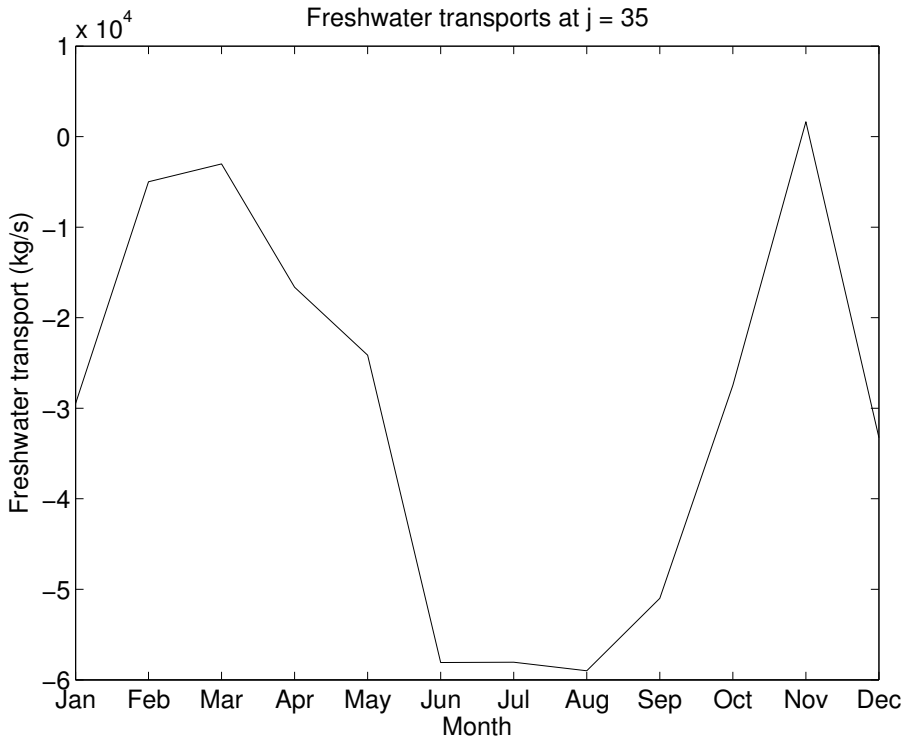

Figure 4.159 The values of freshwater transports at j=35 of the model grid.

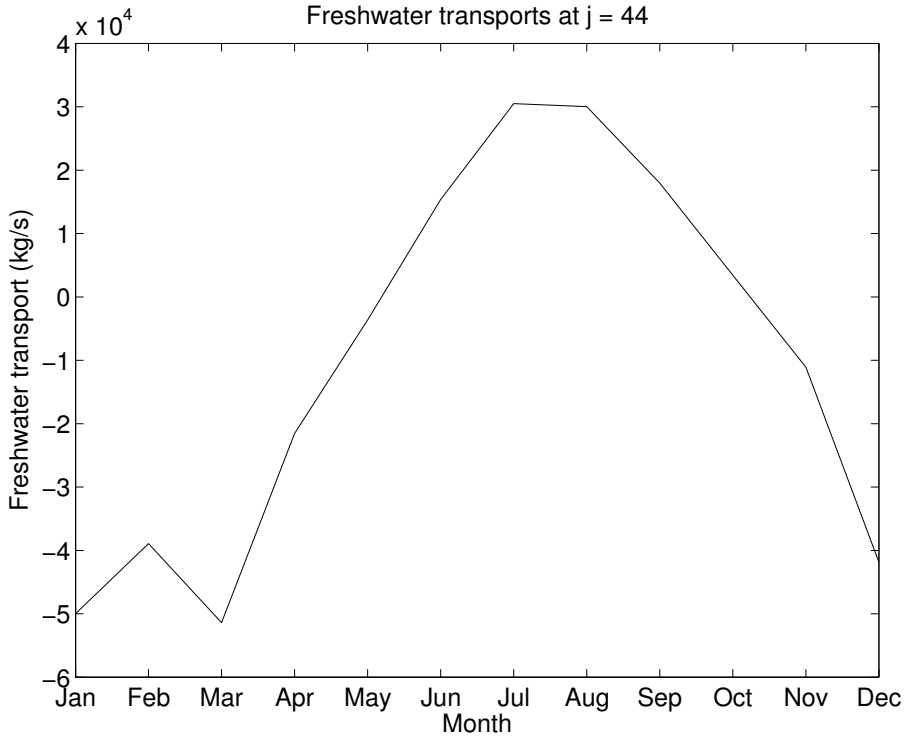

Figure 4.160 The values of freshwater transports at j=44 of the model grid.

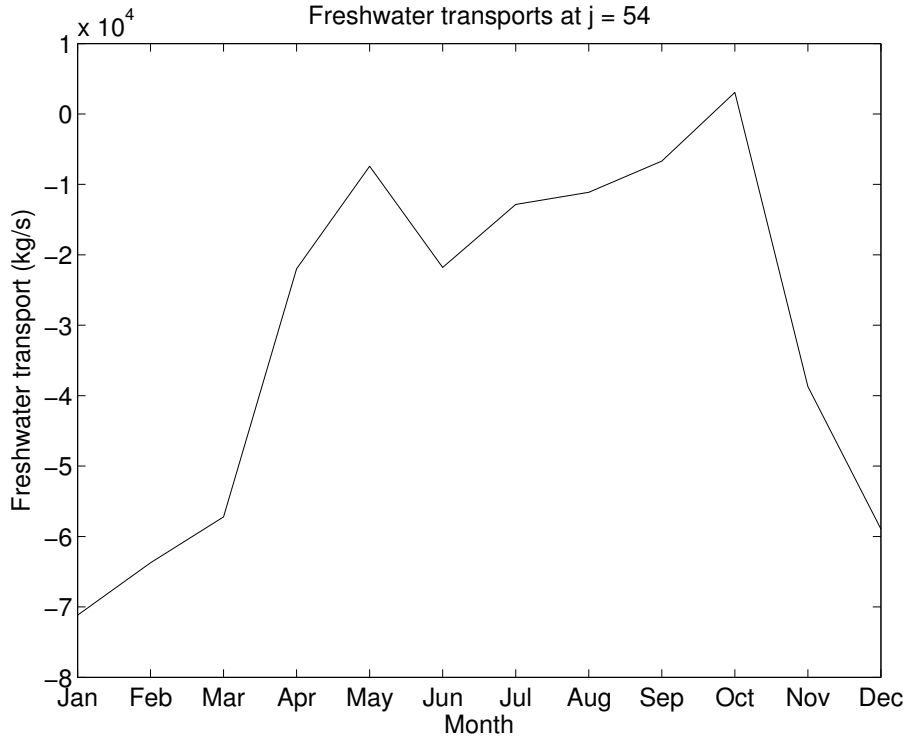

Figure 4.161 The values of freshwater transports at j=54 of the model grid.

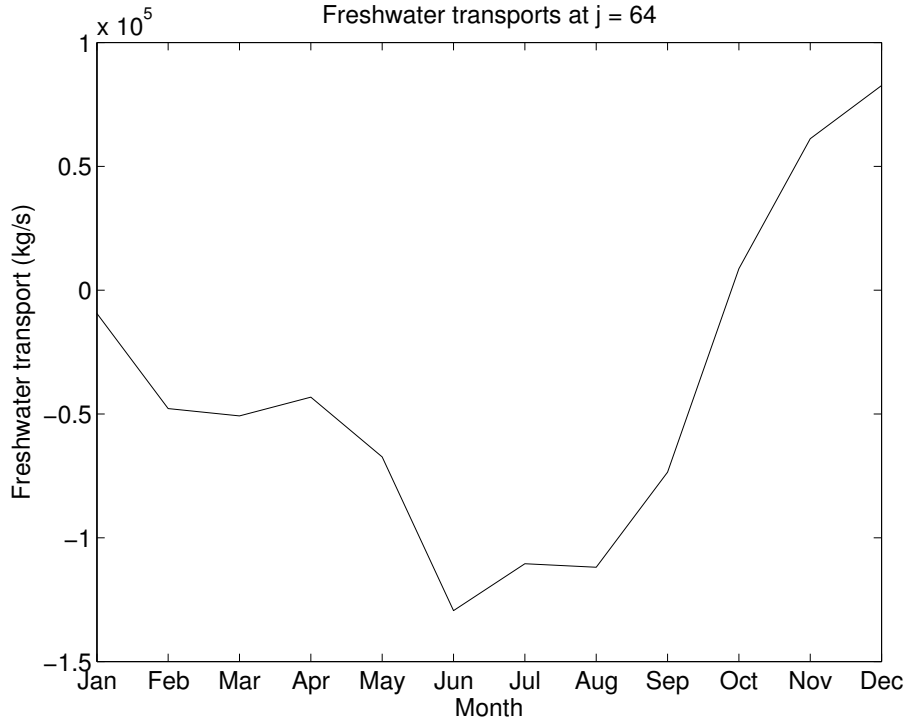

Figure 4.162 The values of freshwater transports at j=64 of the model grid.

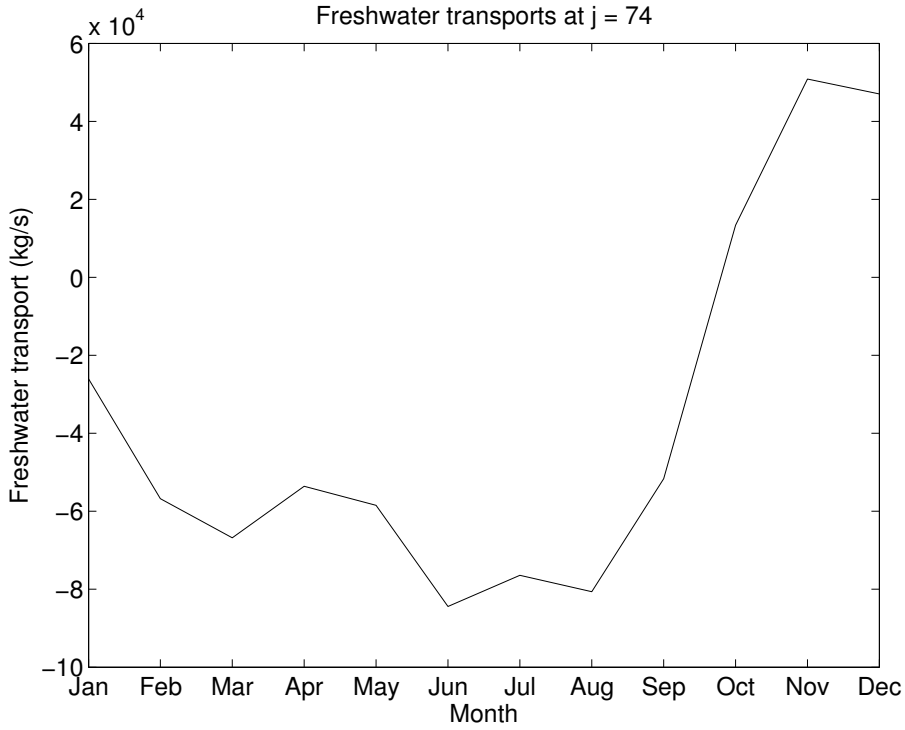

Figure 4.163 The values of freshwater transports at j=74 of the model grid.

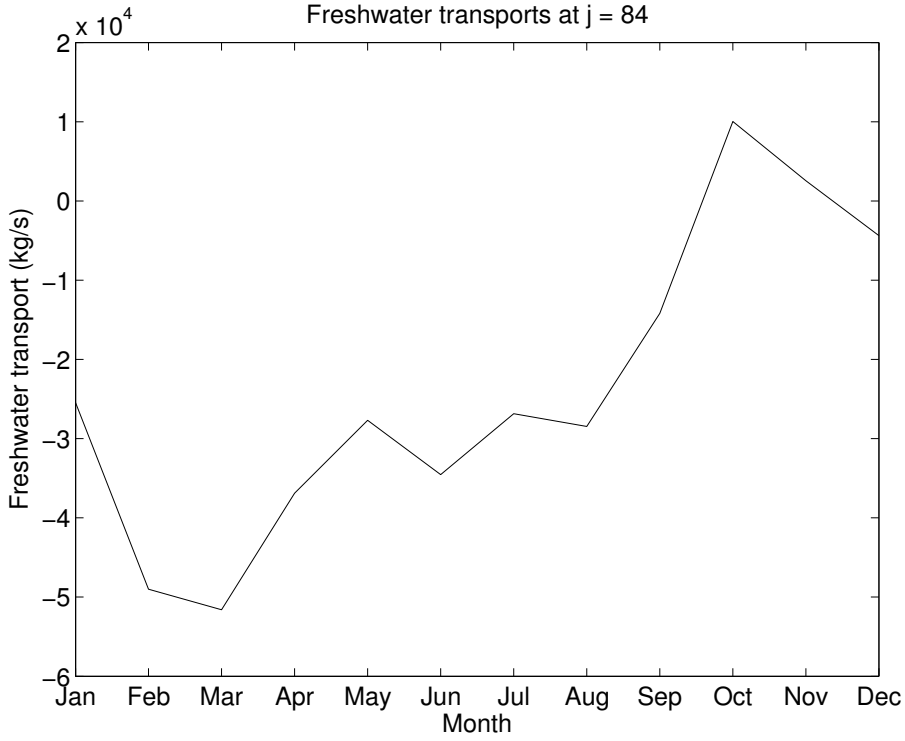

Figure 4.164 The values of freshwater transports at j=84 of the model grid.

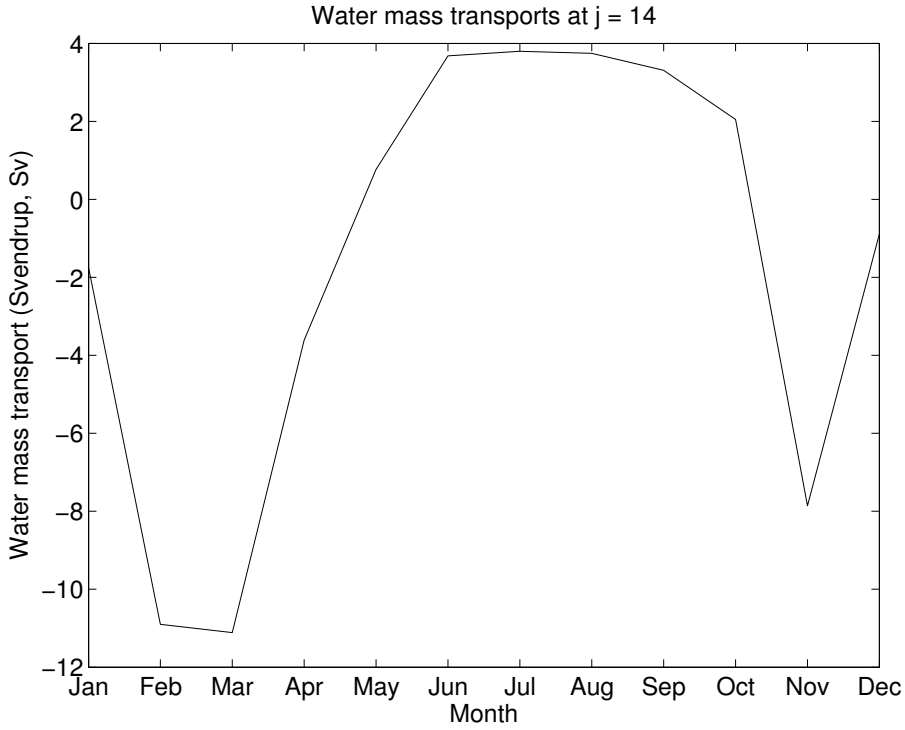

Figure 4.165 The values of water mass transports at j=14 of the model grid.

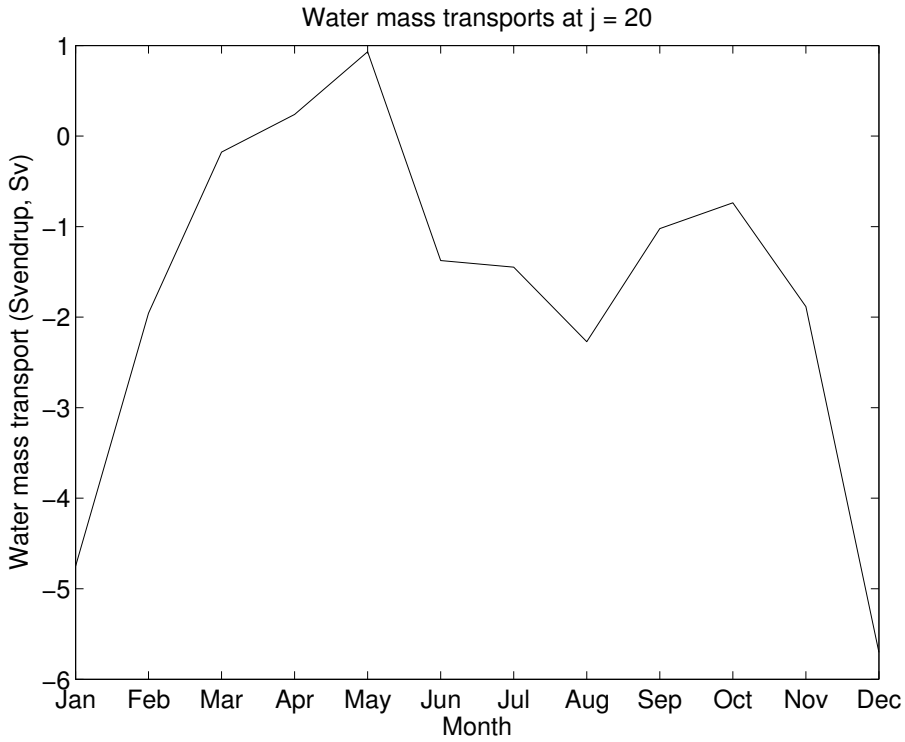

Figure 4.166 The values of water mass transports at j=20 of the model grid.

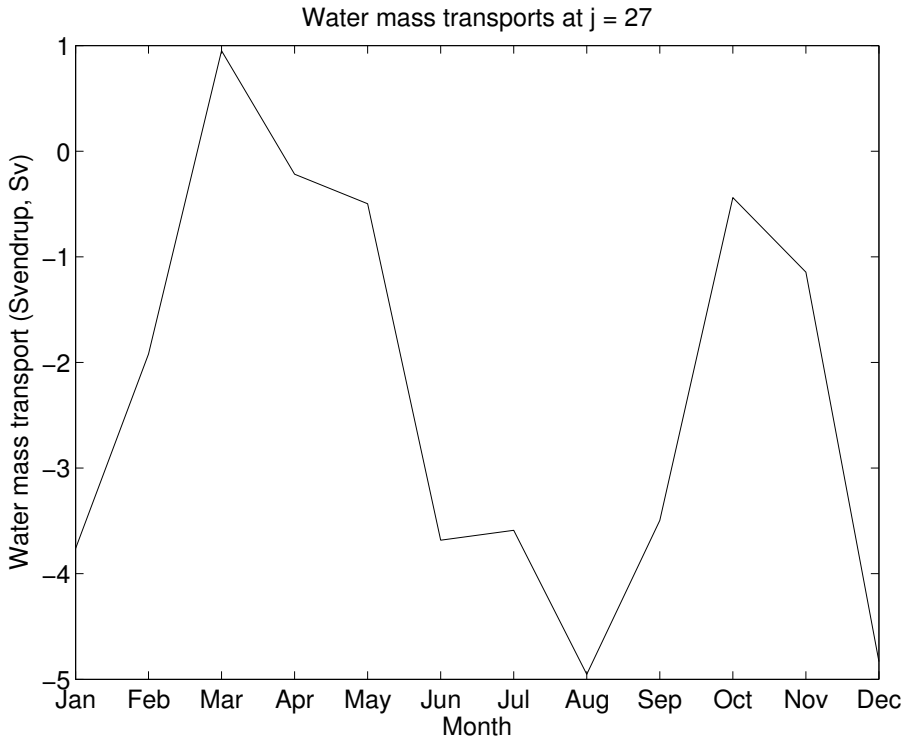

Figure 4.167 The values of water mass transports at j=27 of the model grid.

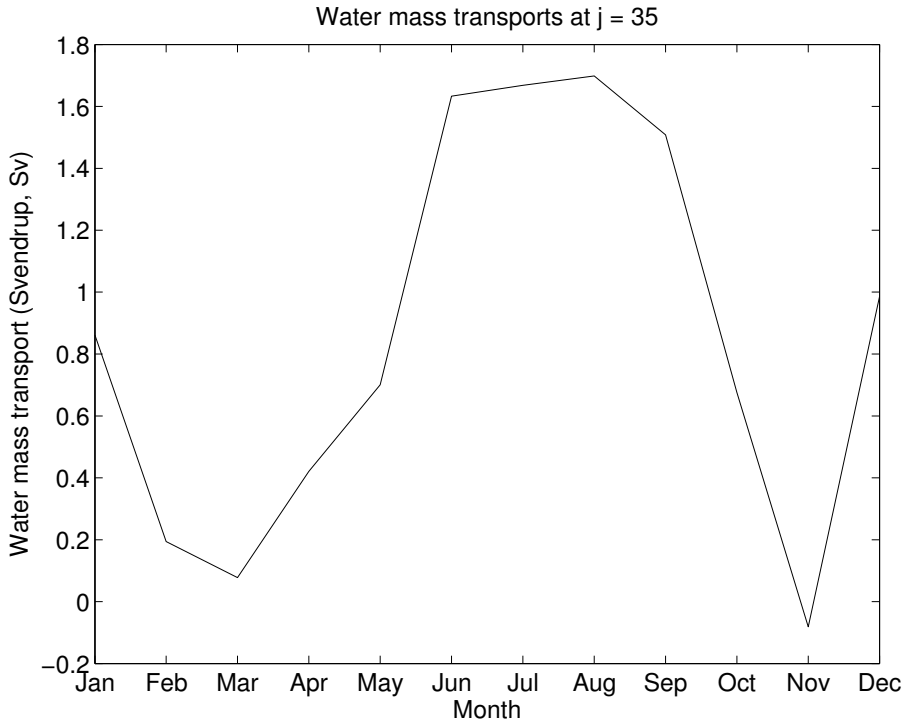

Figure 4.168 The values of water mass transports at j=35 of the model grid.

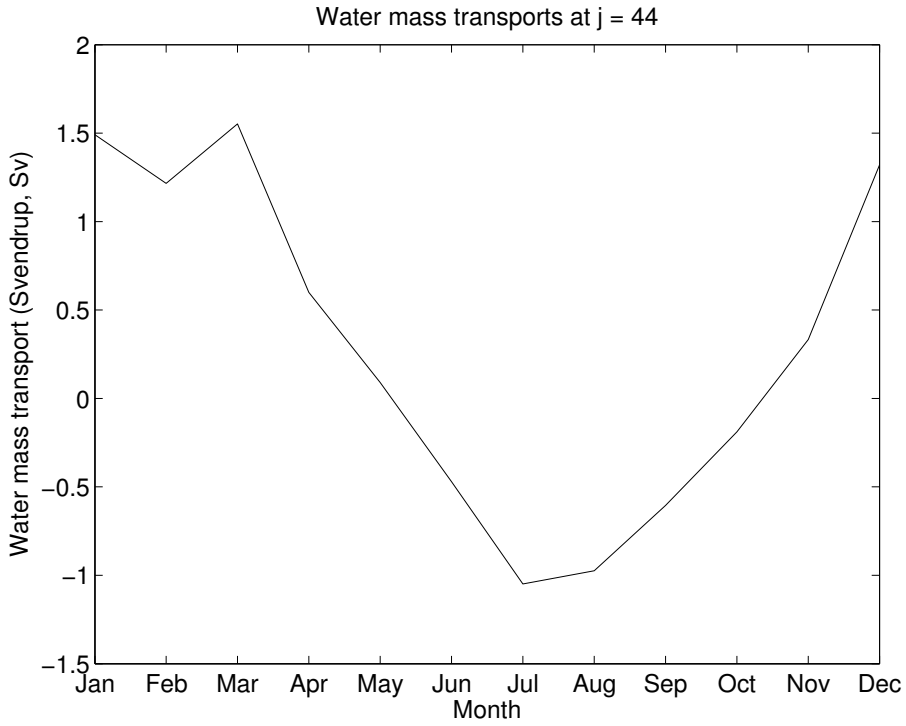

Figure 4.169 The values of water mass transports at j=44 of the model grid.

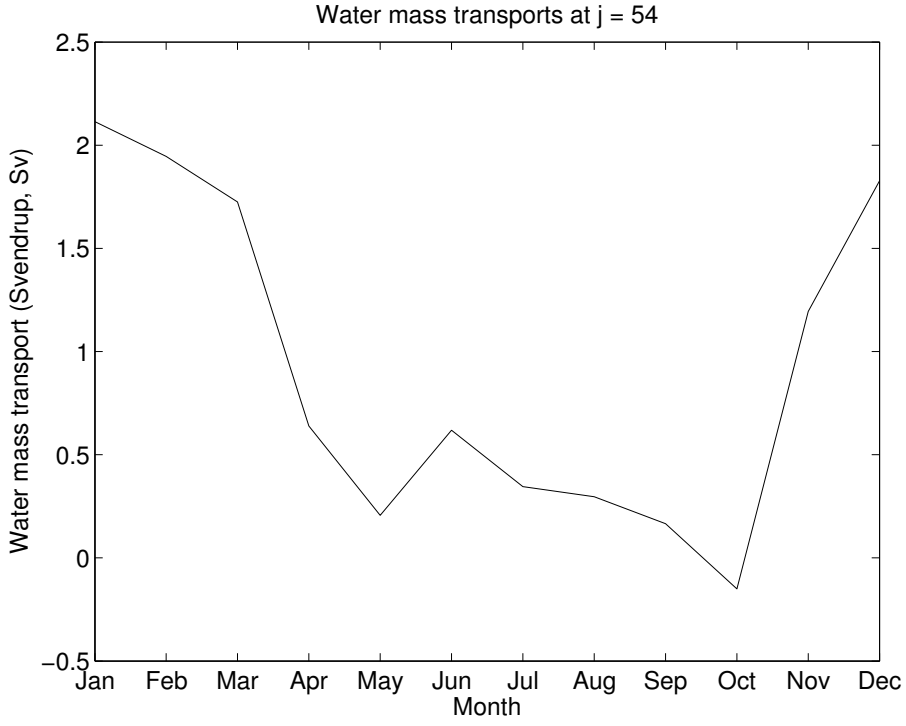

Figure 4.170 The values of water mass transports at j=54 of the model grid.

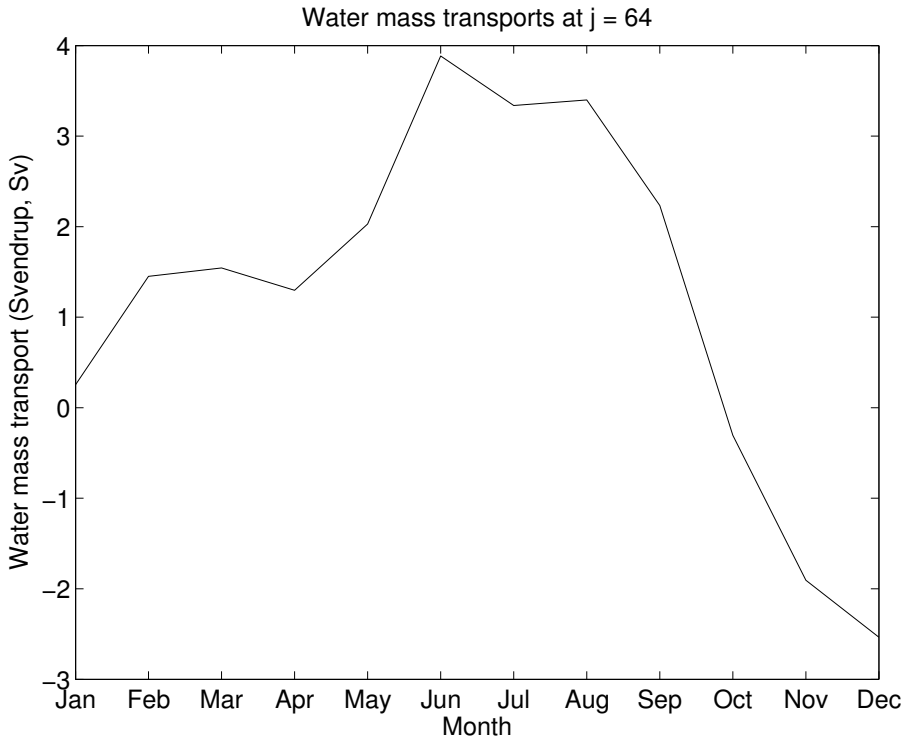

Figure 4.171 The values of water mass transports at j=64 of the model grid.

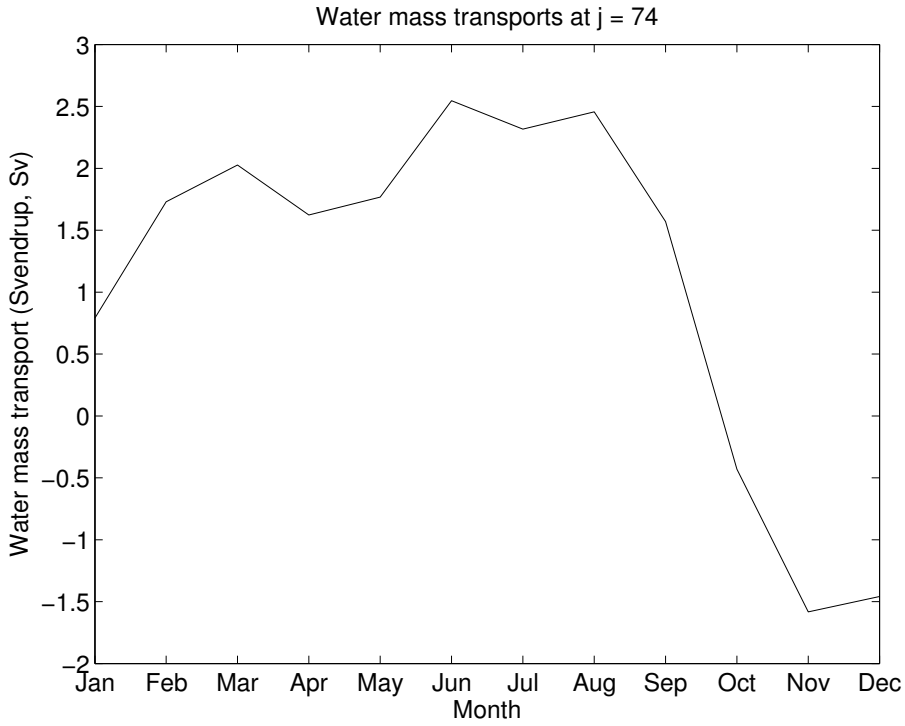

Figure 4.172 The values of water mass transports at j=74 of the model grid.

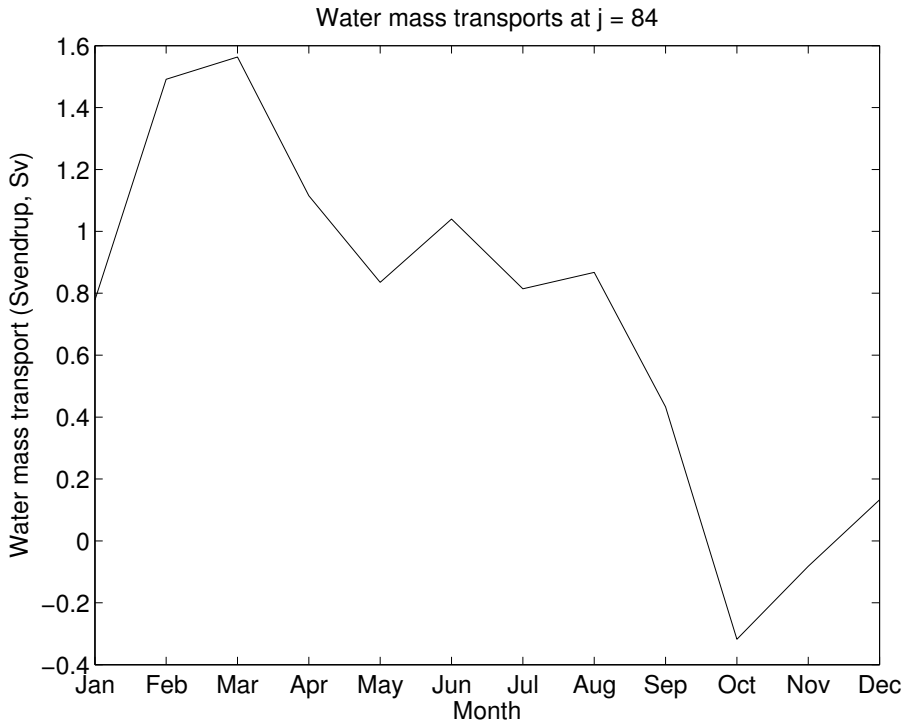

Figure 4.173 The values of water mass transports at j=84 of the model grid.

The results of the heat, freshwater, and water mass transports yield positive and negative values. Positive values mean the moving from the South China Sea into the Gulf of Thailand. On the other hand, the moving out of the Gulf of Thailand to the South China Sea produces negative values.

All results of heat, freshwater, and water mass transports can be displayed in the form of magnitudes and directions of heat, freshwater, and water mass transports in the Gulf of Thailand for each month, as shown in Fig. 4.174 to Fig. 4.209.

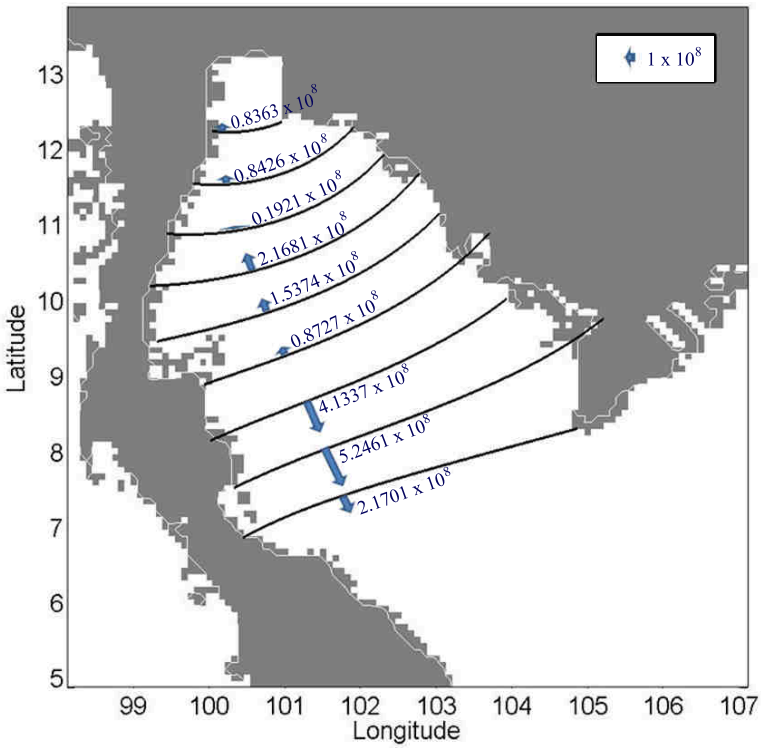

Figure 4.174 The heat transports (W) in the Gulf of Thailand for January.

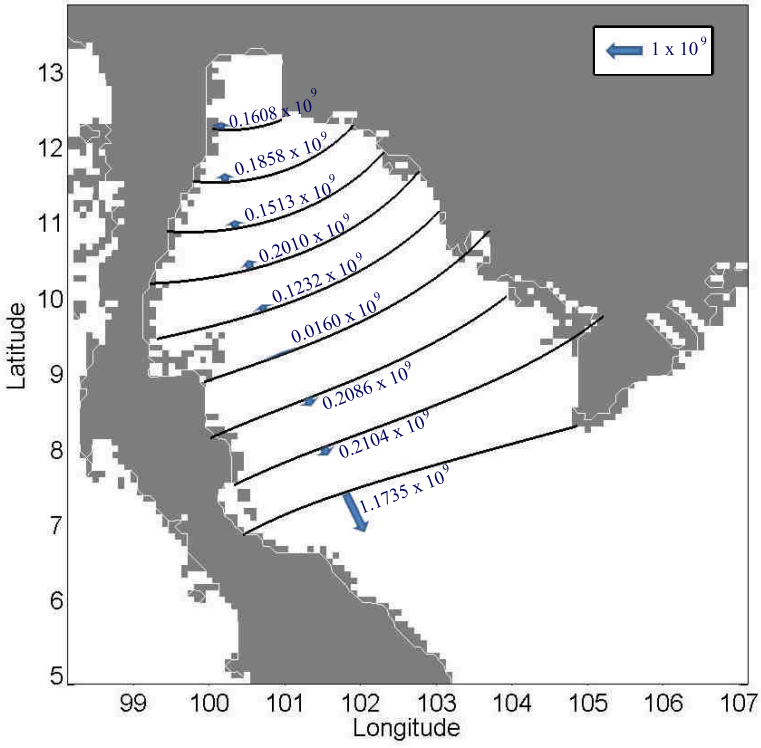

Figure 4.175 The heat transports (W) in the Gulf of Thailand for February.

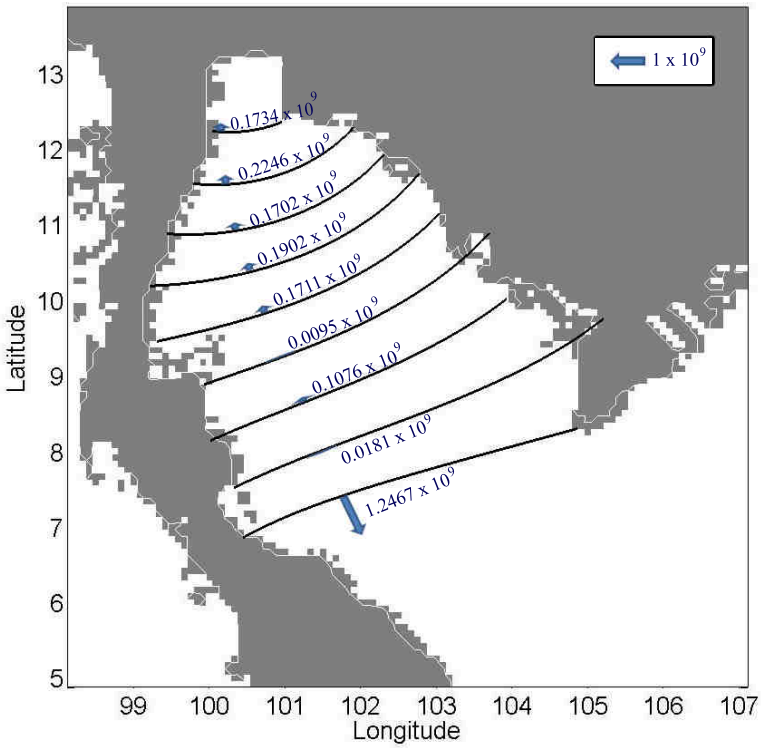

Figure 4.176 The heat transports (W) in the Gulf of Thailand for March.

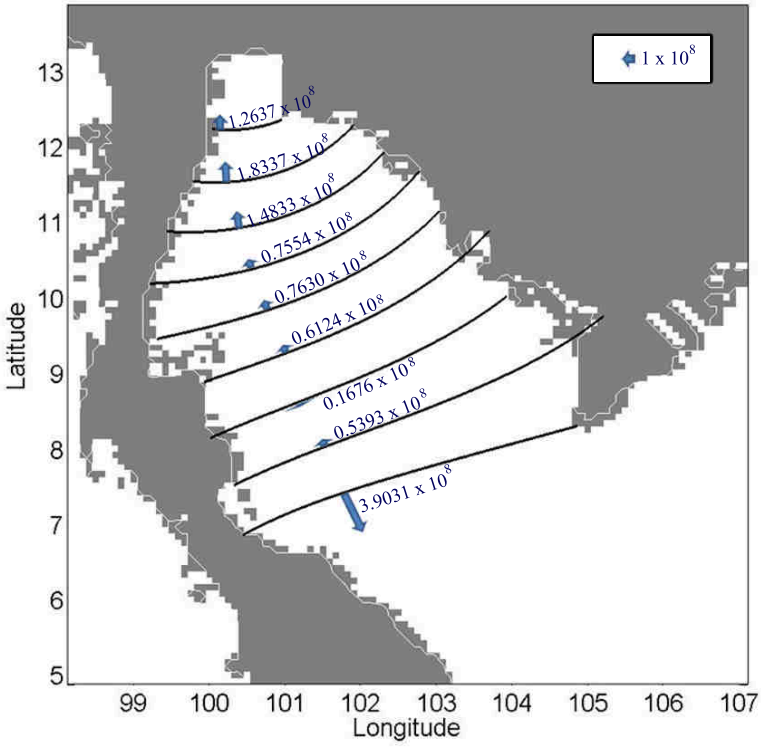

Figure 4.177 The heat transports (W) in the Gulf of Thailand for April.

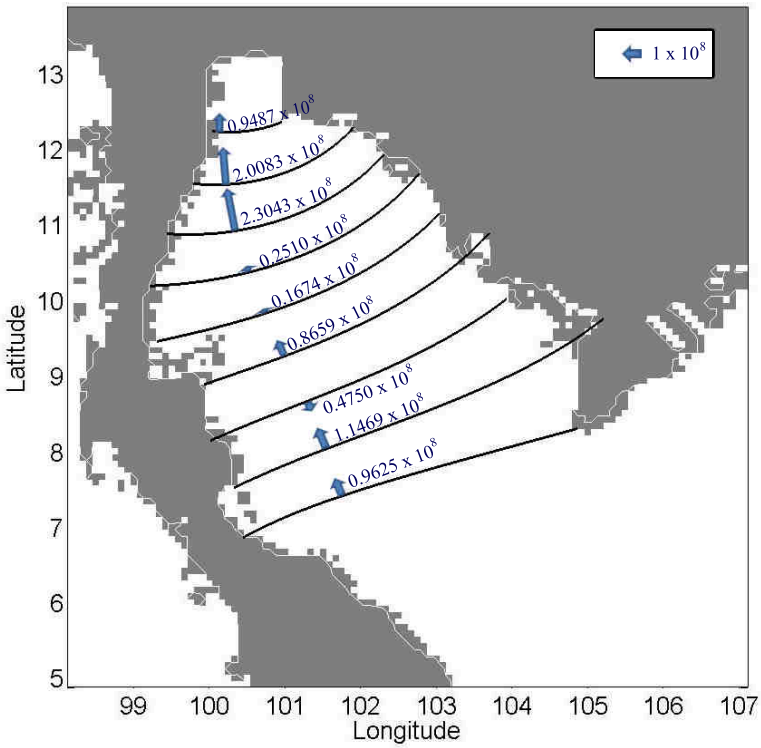

Figure 4.178 The heat transports (W) in the Gulf of Thailand for May.

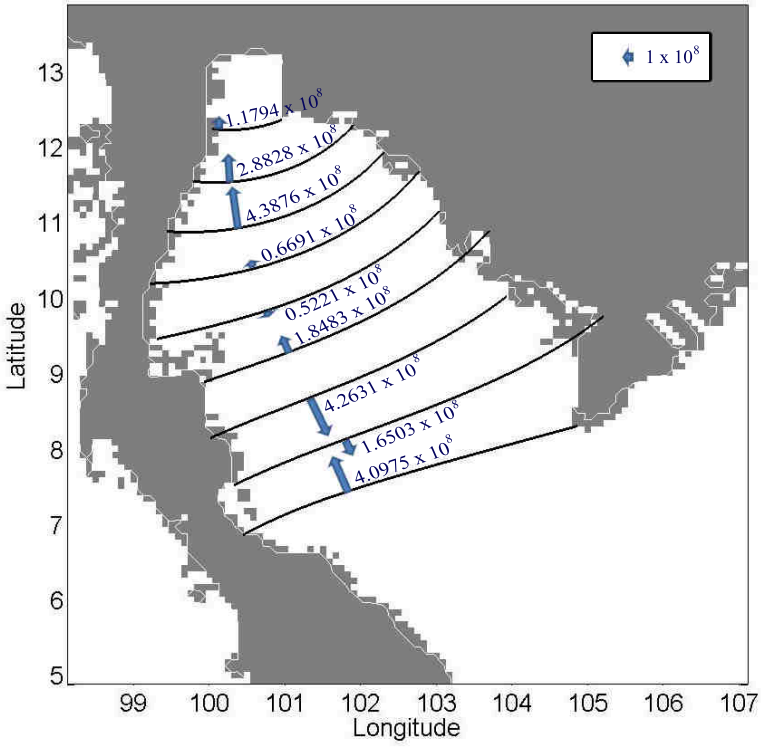

Figure 4.179 The heat transports (W) in the Gulf of Thailand for June.

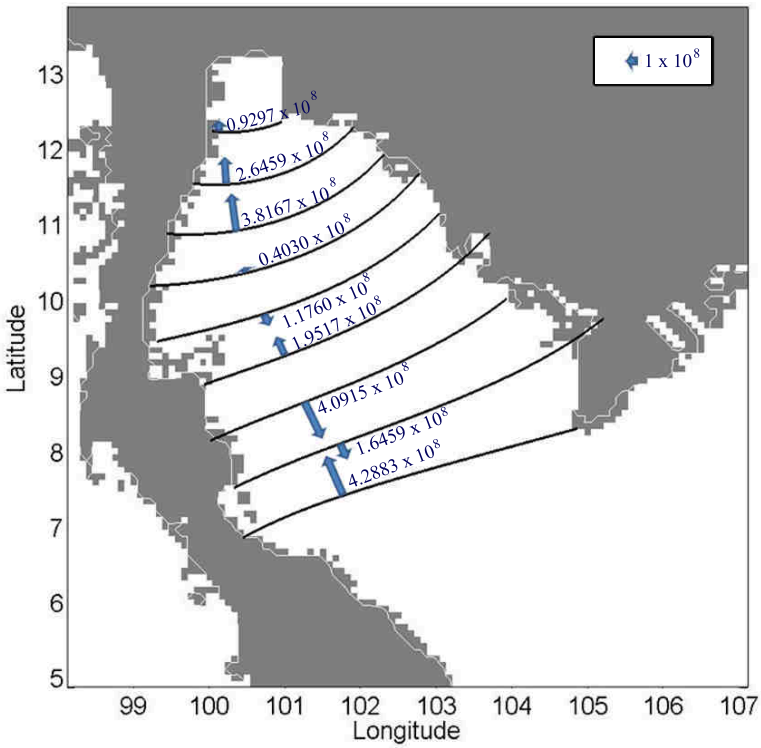

Figure 4.180 The heat transports (W) in the Gulf of Thailand for July.

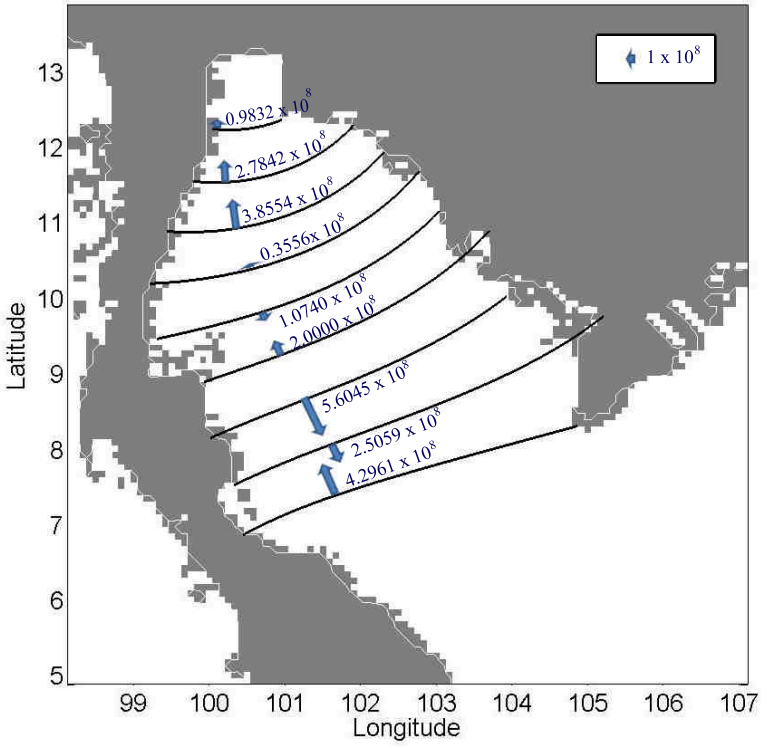

Figure 4.181 The heat transports (W) in the Gulf of Thailand for August.

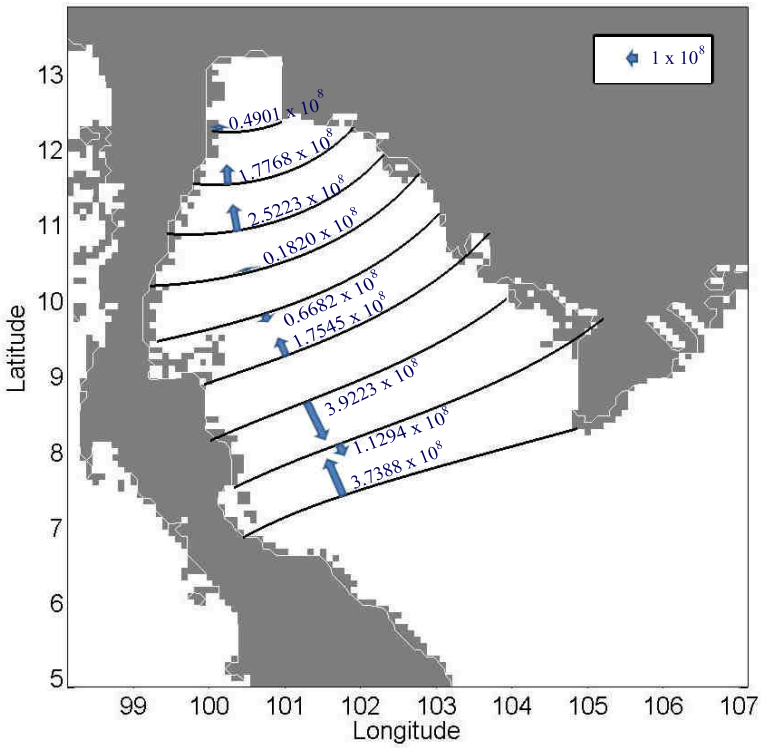

Figure 4.182 The heat transports (W) in the Gulf of Thailand for September.

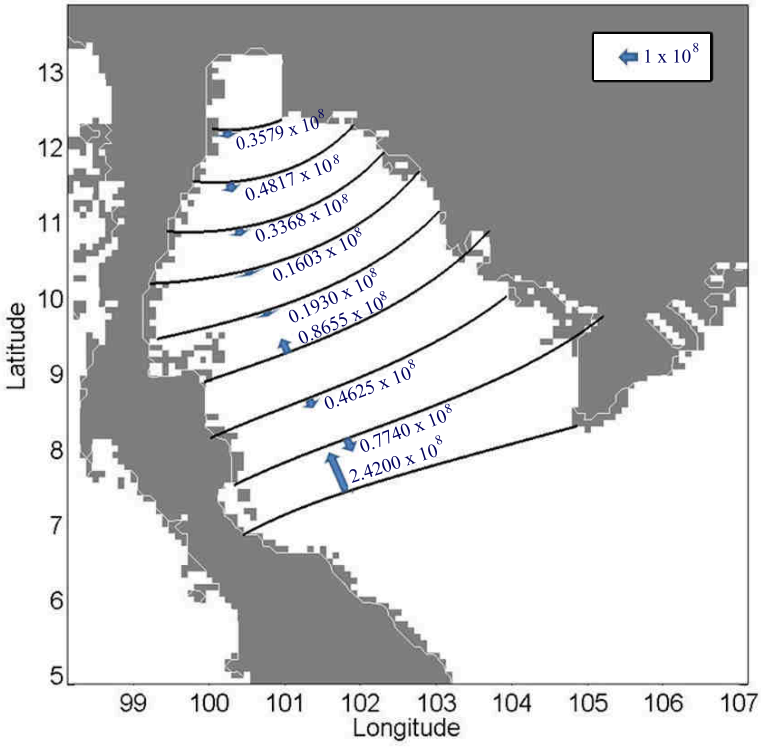

Figure 4.183 The heat transports (W) in the Gulf of Thailand for October.

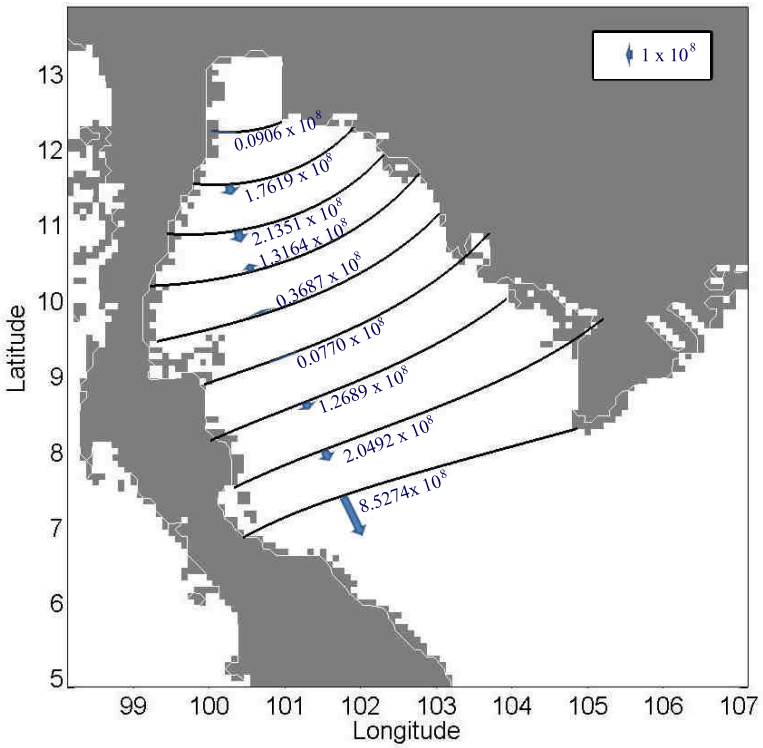

Figure 4.184 The heat transports (W) in the Gulf of Thailand for November.

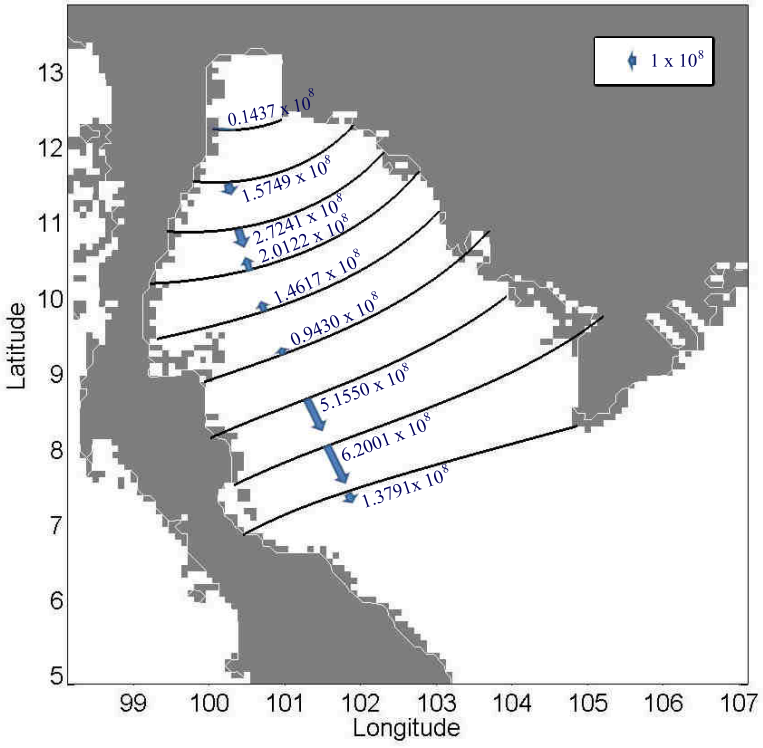

Figure 4.185 The heat transports (W) in the Gulf of Thailand for December.

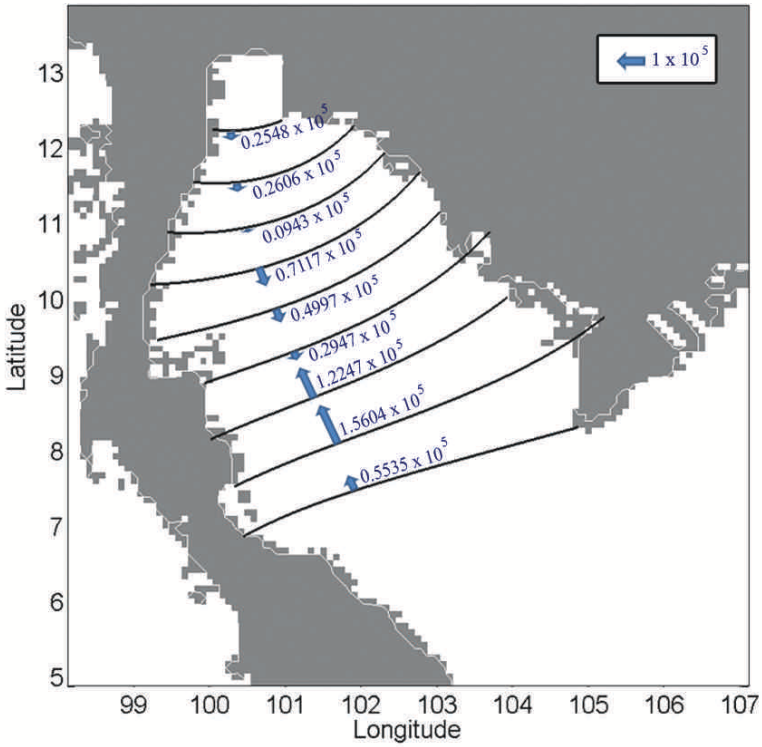

Figure 4.186 The freshwater transports (kg/s) in the Gulf of Thailand for January.

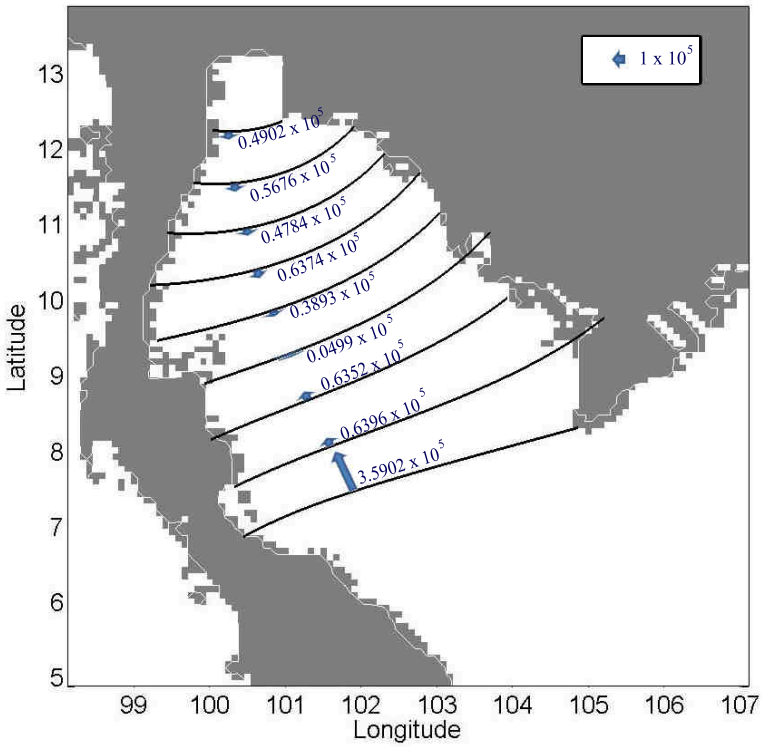

Figure 4.187 The freshwater transports (kg/s) in the Gulf of Thailand for February.

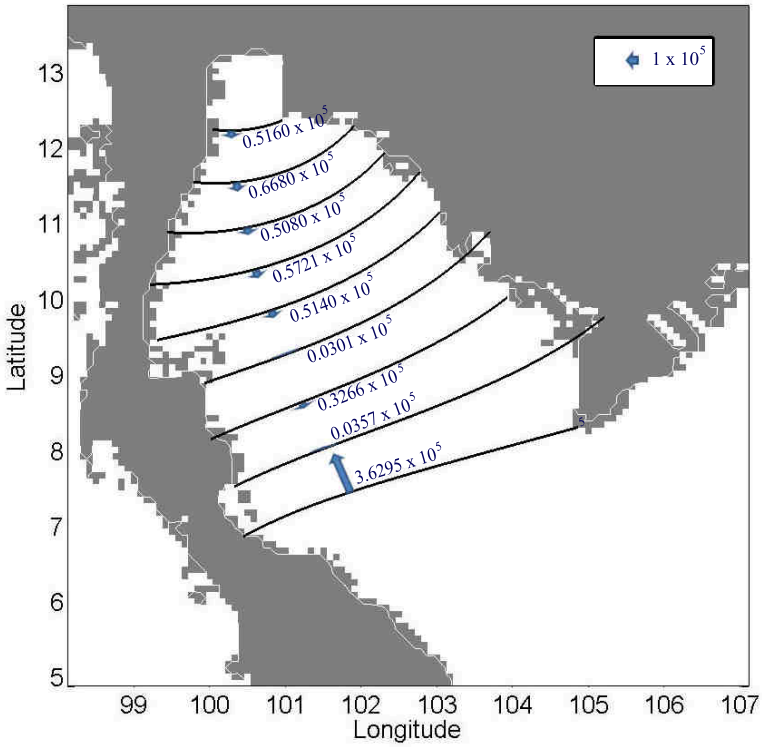

Figure 4.188 The freshwater transports (kg/s) in the Gulf of Thailand for March.

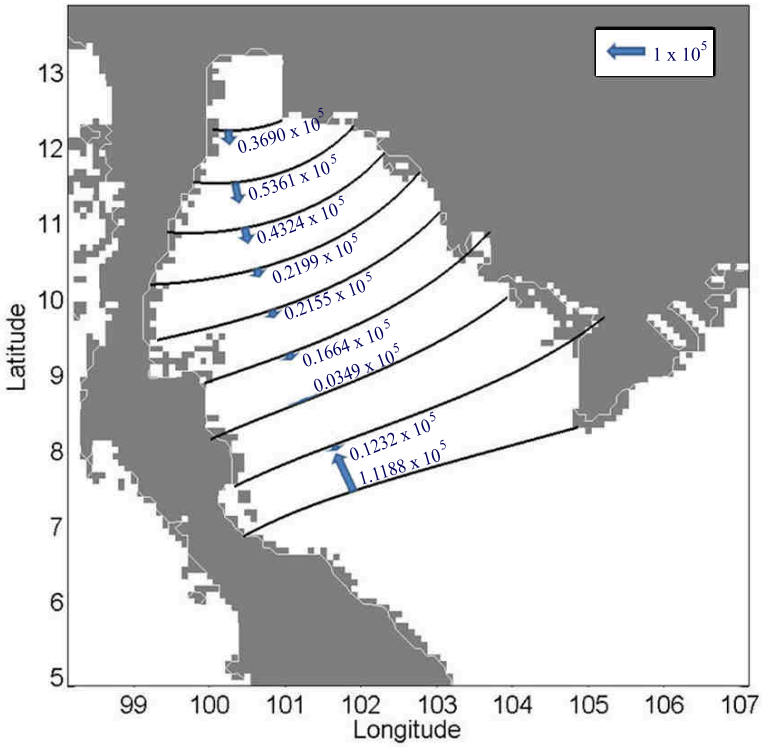

Figure 4.189 The freshwater transports (kg/s) in the Gulf of Thailand for April.

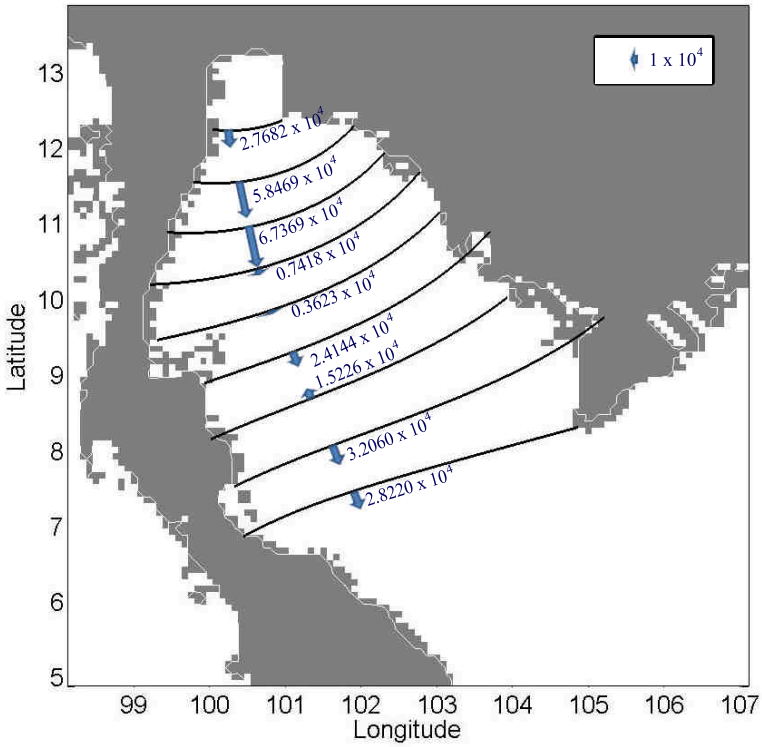

Figure 4.190 The freshwater transports (kg/s) in the Gulf of Thailand for May.

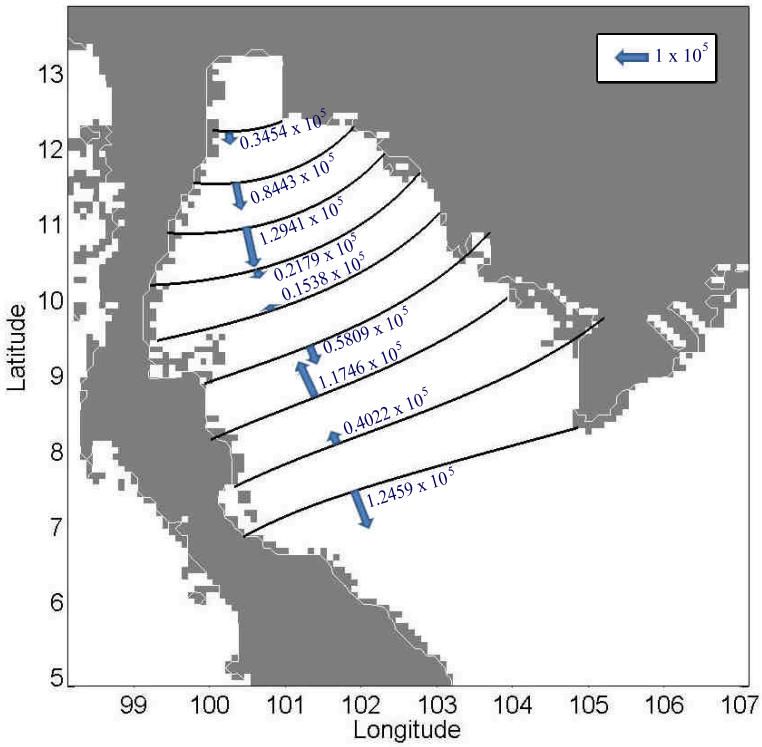

Figure 4.191 The freshwater transports (kg/s) in the Gulf of Thailand for June.

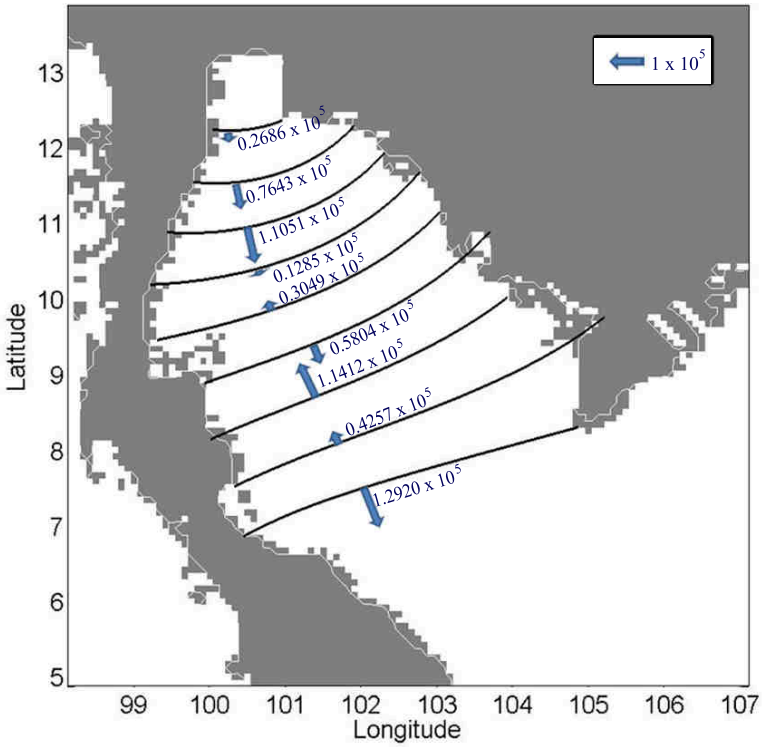

Figure 4.192 The freshwater transports (kg/s) in the Gulf of Thailand for July.

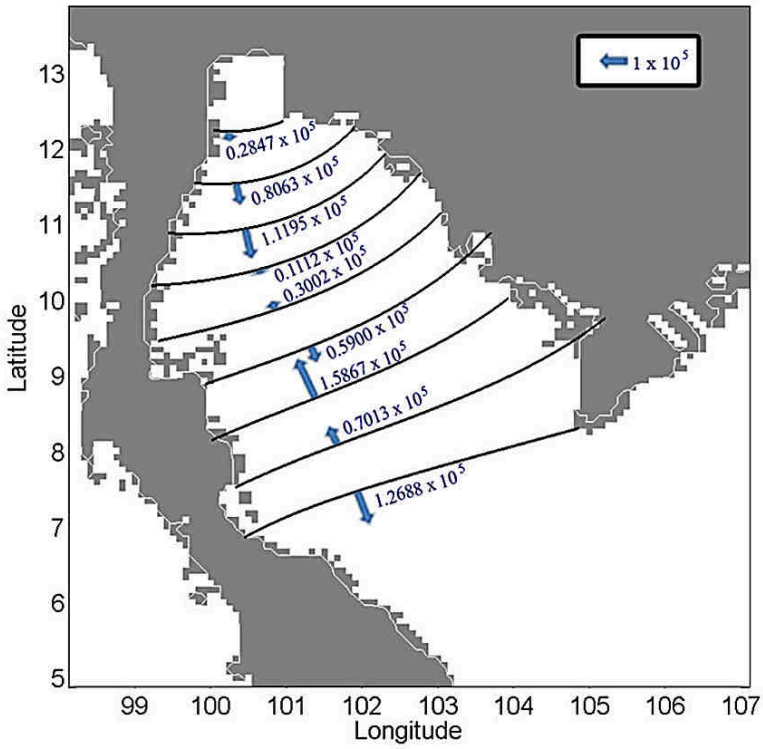

Figure 4.193 The freshwater transports (kg/s) in the Gulf of Thailand for August.

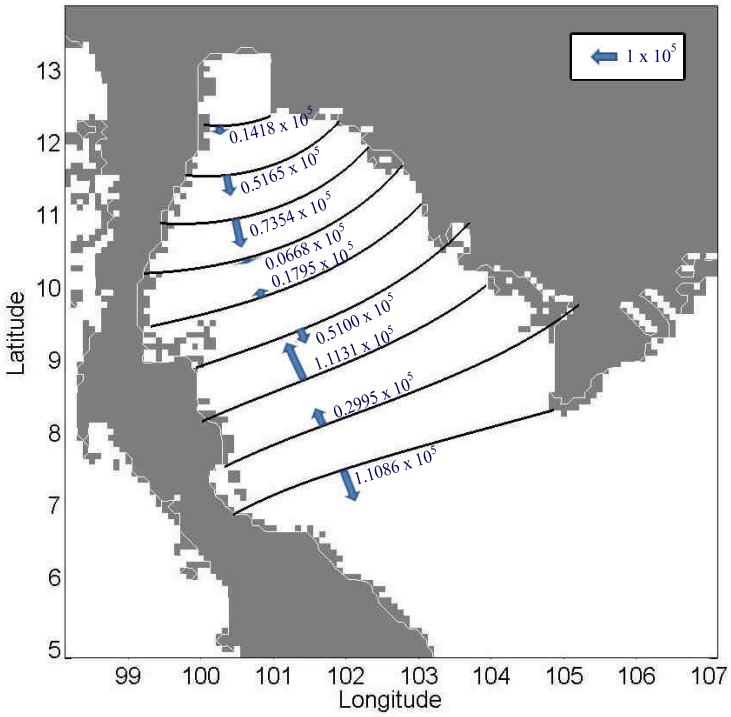

Figure 4.194 The freshwater transports (kg/s) in the Gulf of Thailand for September.

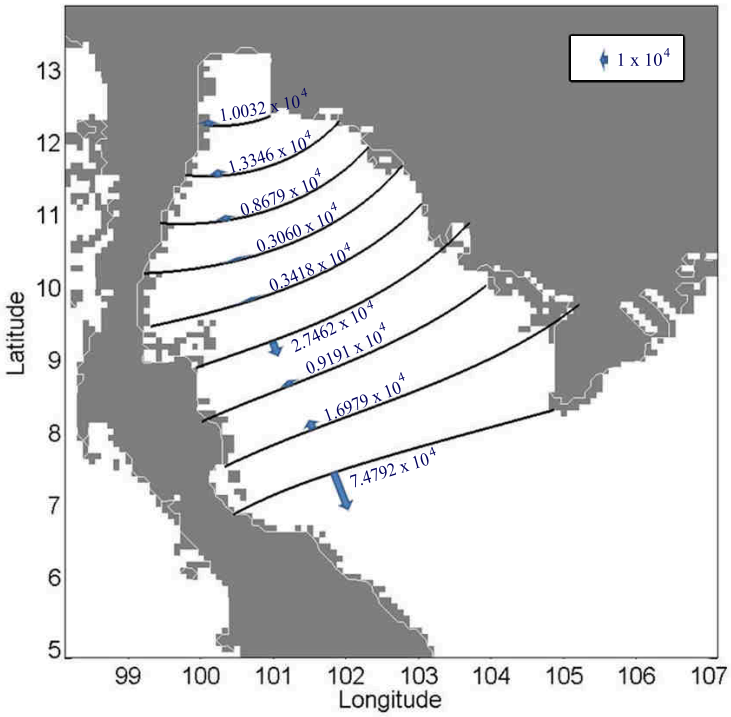

Figure 4.195 The freshwater transports (kg/s) in the Gulf of Thailand for October.

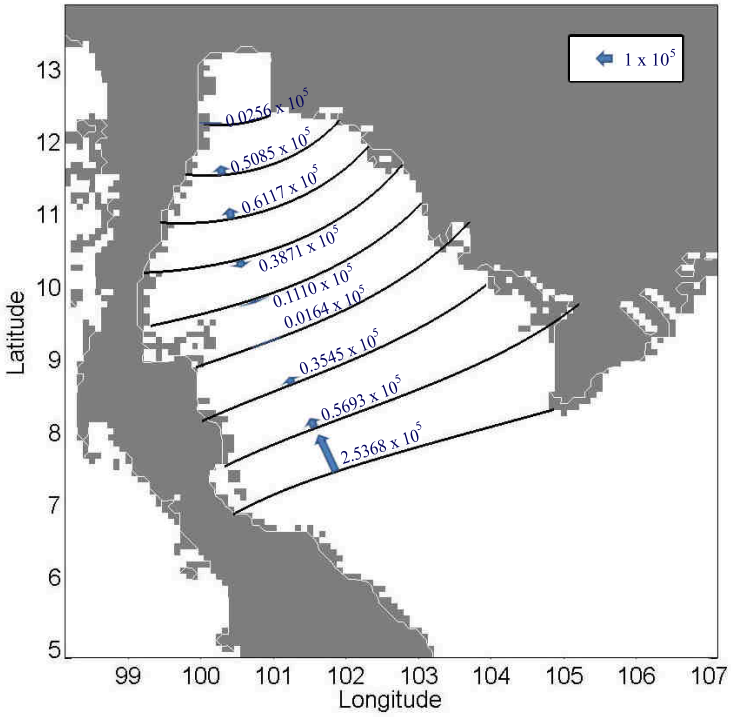

Figure 4.196 The freshwater transports (kg/s) in the Gulf of Thailand for November.

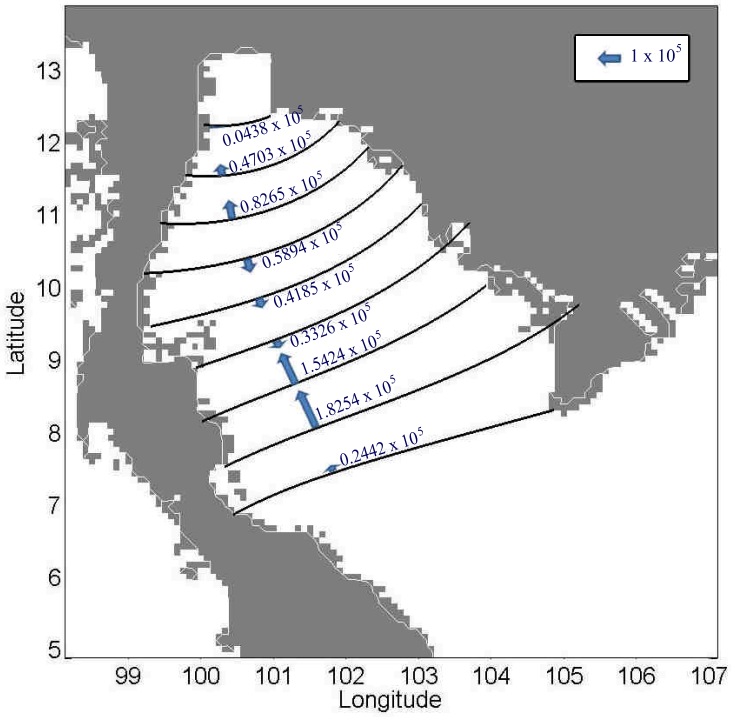

Figure 4.197 The freshwater transports (kg/s) in the Gulf of Thailand for December.

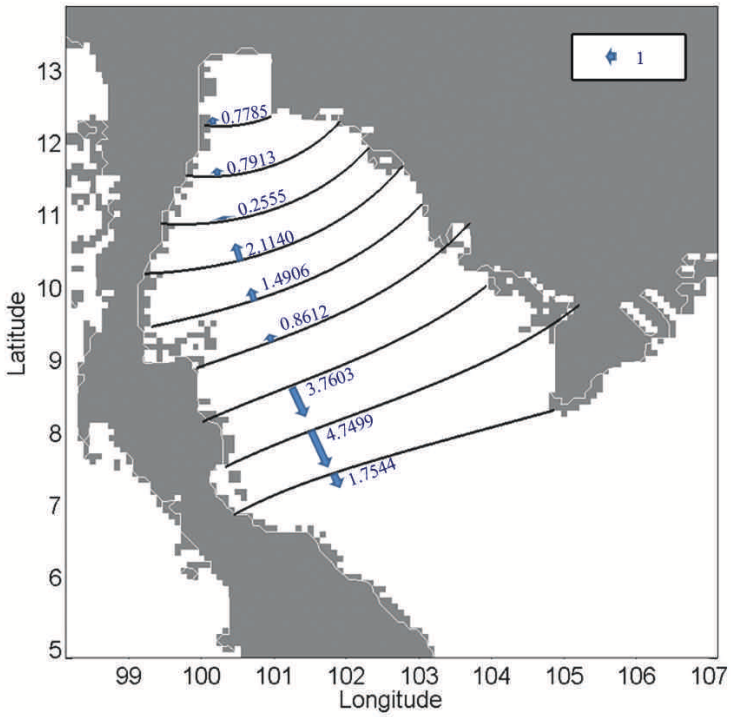

Figure 4.198 The water mass transports (Sv) in the Gulf of Thailand for January.

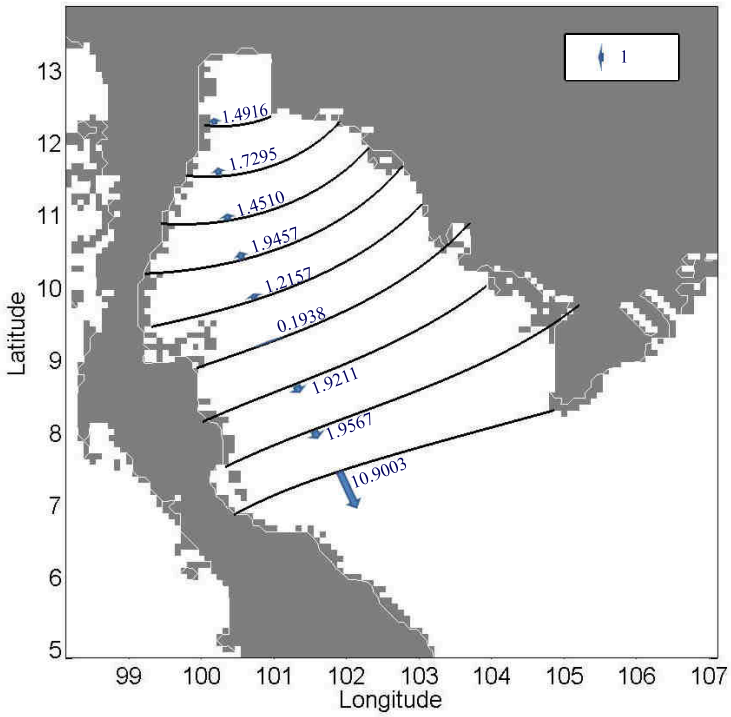

Figure 4.199 The water mass transports (Sv) in the Gulf of Thailand for February.

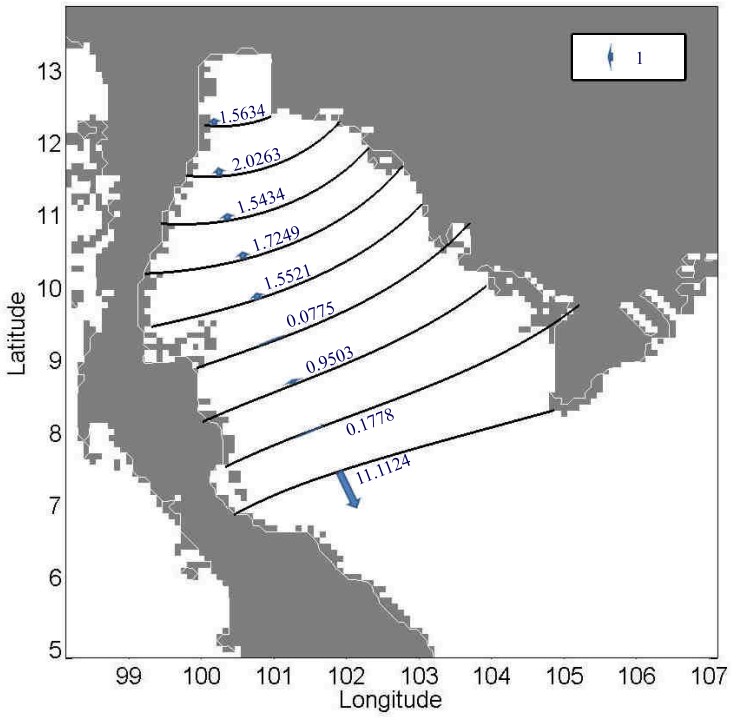

Figure 4.200 The water mass transports (Sv) in the Gulf of Thailand for March.

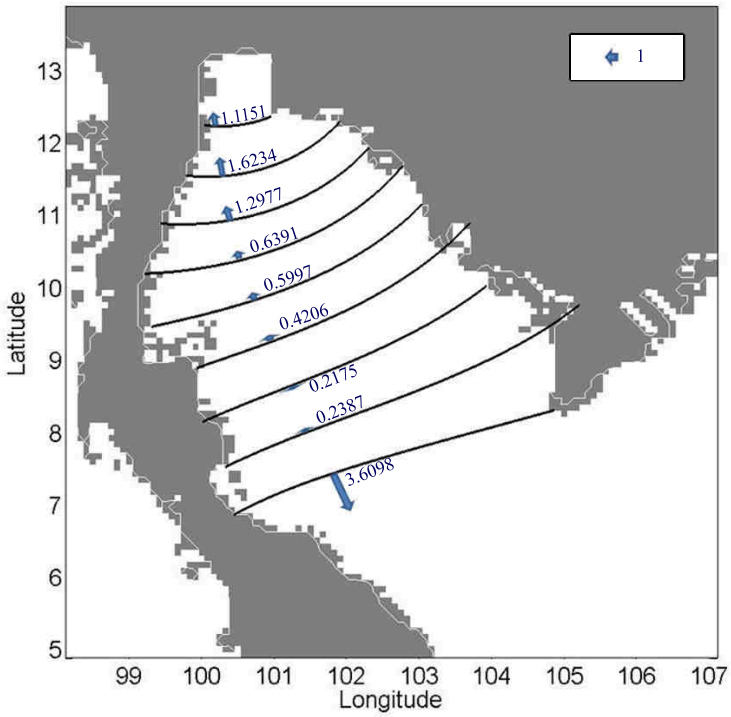

Figure 4.201 The water mass transports (Sv) in the Gulf of Thailand for April.

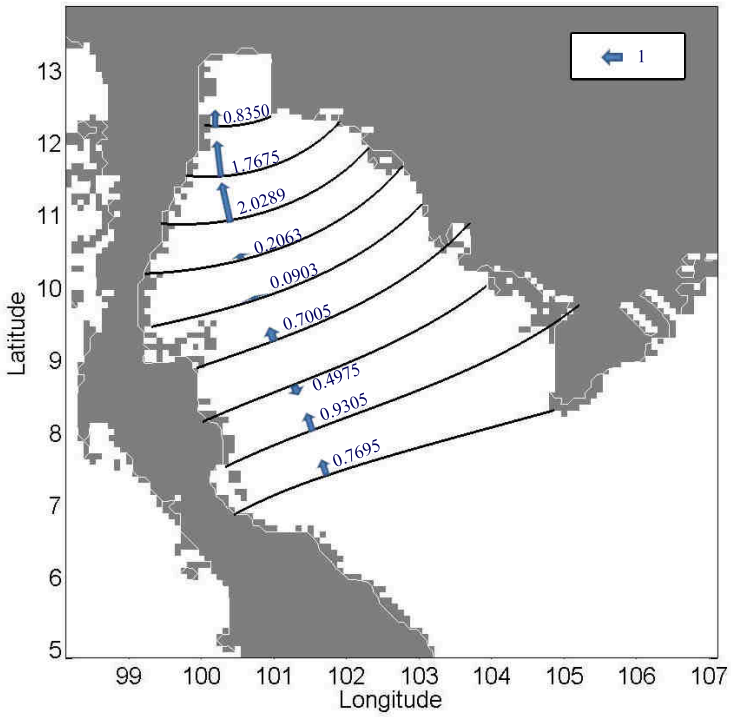

Figure 4.202 The water mass transports (Sv) in the Gulf of Thailand for May.

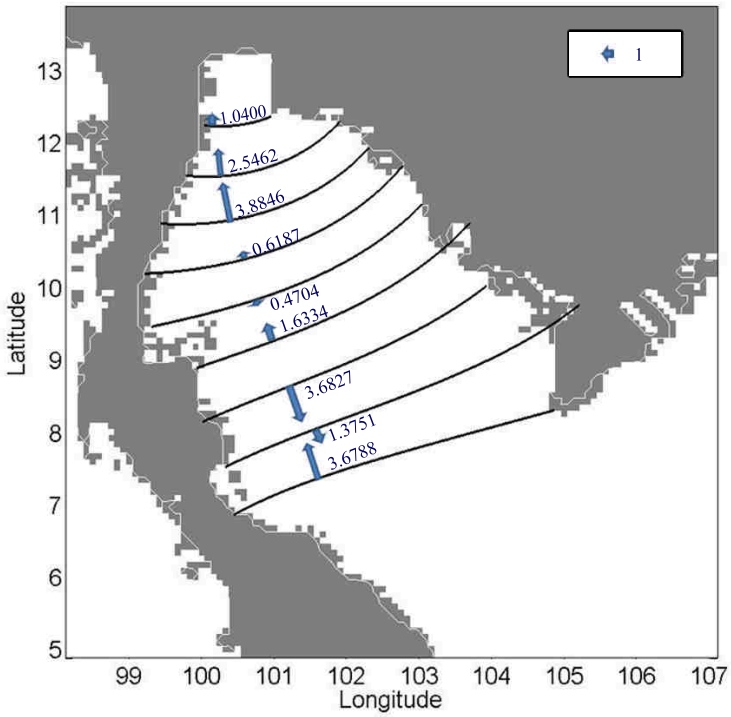

Figure 4.203 The water mass transports (Sv) in the Gulf of Thailand for June.

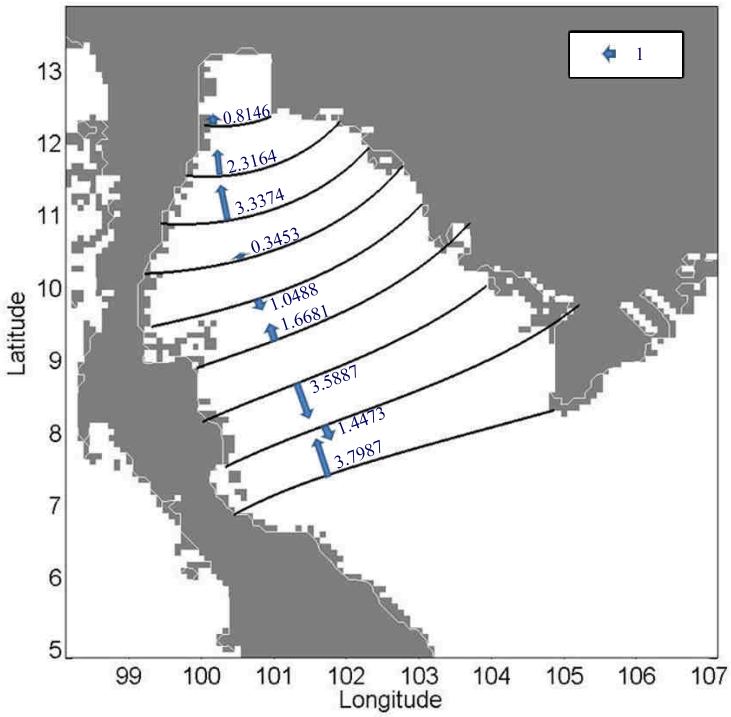

Figure 4.204 The water mass transports (Sv) in the Gulf of Thailand for July.

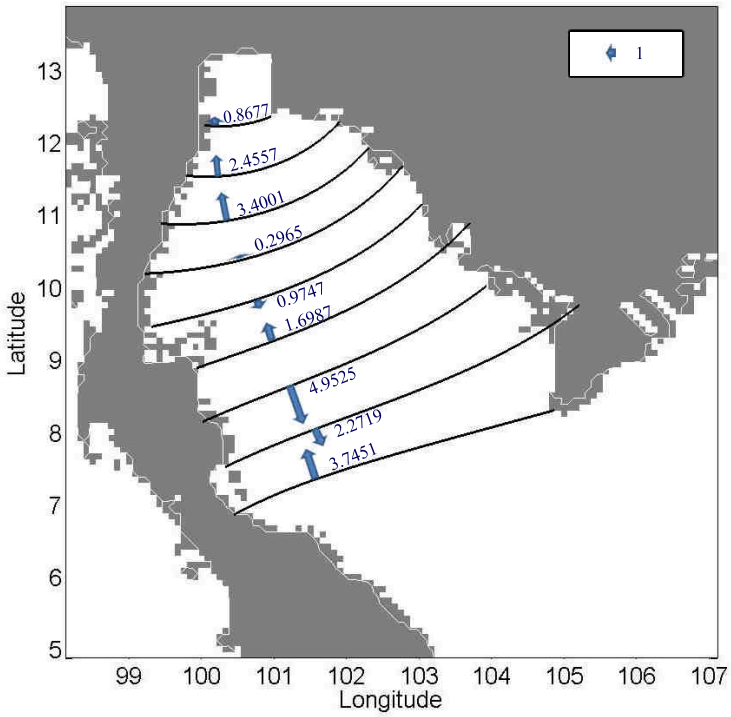

Figure 4.205 The water mass transports (Sv) in the Gulf of Thailand for August.

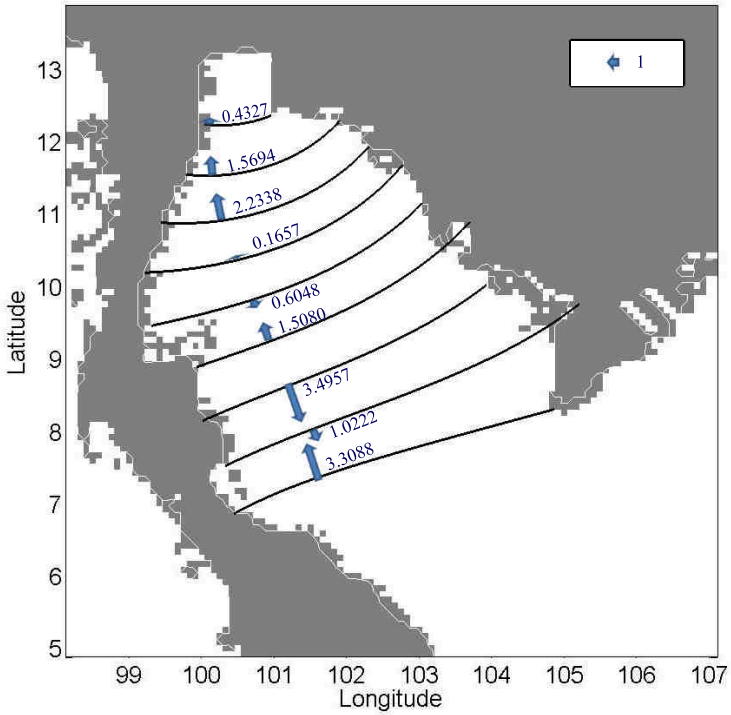

Figure 4.206 The water mass transports (Sv) in the Gulf of Thailand for September.

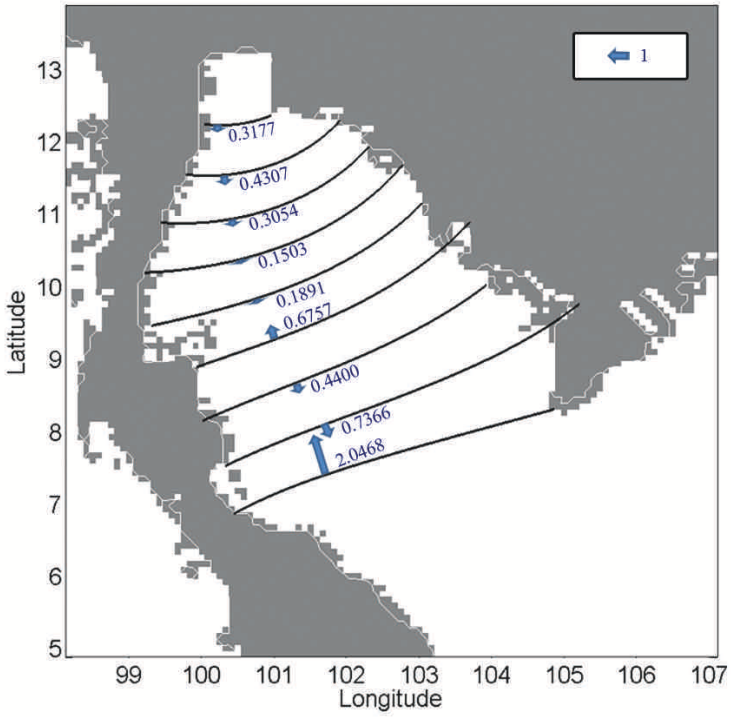

Figure 4.207 The water mass transports (Sv) in the Gulf of Thailand for October.

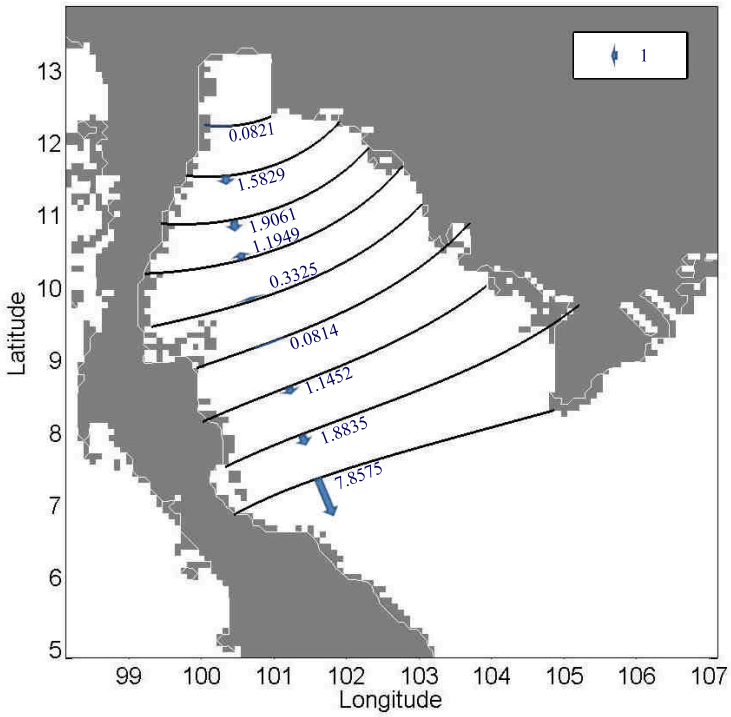

Figure 4.208 The water mass transports (Sv) in the Gulf of Thailand for November.

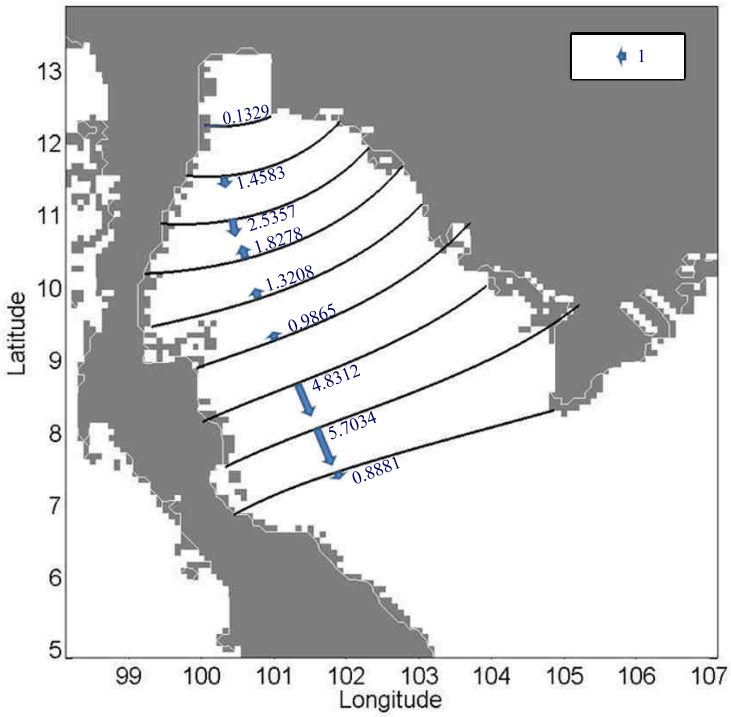

Figure 4.209 The water mass transports (Sv) in the Gulf of Thailand for December.

It can be seen that the highest and lowest values of heat, freshwater, and water mass transports in each month are at the same region. The heat and water mass transports have the same directions, while the freshwater transport has the opposite direction.

For the onset of the winter of Thailand, November to December, the values of heat, freshwater, and water mass transports are between 0.7×10^7 W to 8.6×10^8 W, 0.1×10^4 kg/s to 2.6×10^5 kg/s, and 0.08 Sv to 7.9 Sv, respectively. Their highest values occurred at the connection section between the Gulf of Thailand and the South China Sea are 8.5274×10^8 W, 2.5368×10^5 kg/s, and 7.8575 Sv, respectively, and their lowest values occurred at latitude 9°N are 0.77×10^7 W, 0.164×10^4 kg/s, and 0.0814 Sv, respectively. For the upper Gulf of Thailand which is upper than 9°N, the heat and water mass transports move northward and southward alternately, while they move out of the Gulf of Thailand in the lower Gulf of Thailand which is lower than 9°N.

For the end of the winter of Thailand, January to February, the values of heat, freshwater, and water mass transports are between 0.1×10^8 W to 1.2×10^9 W, 0.4×10^4 kg/s to 3.6×10^5 kg/s, and 0.1 Sv to 11.0 Sv, respectively. Their highest values occurred at the connection section between the Gulf of Thailand and the South China Sea are 1.1735×10^9 W, 3.5902×10^5 kg/s, and 10.9003 Sv, respectively, and their lowest values occurred at latitude 9°N are 0.160×10^8 W, 0.499×10^4 kg/s, and 0.1938 Sv, respectively. For the upper Gulf of Thailand which is upper than 9°N, the heat and water mass transports move northward, while they move out of the Gulf of Thailand in the lower Gulf of Thaialnd which is lower than 9°N.

For the summer of Thailand, March to May, the values of heat, freshwater, and water mass transports are between 0.9×10^7 W to 1.3×10^9 W, 0.3×10^4 kg/s to 3.7×10^5 kg/s, and 0.07 Sv to 11.2 Sv, respectively. Their highest values occurred at the connection section between the Gulf of Thailand and the South China Sea are 1.2467×10^9 W, 3.6295×10^5 kg/s, and 11.1124 Sv, respectively, and their lowest values occurred at latitude 9°N are 0.95×10^7 W, 0.301×10^4 kg/s, and 0.0775 Sv, respectively. For the upper Gulf of Thailand which is upper than 9°N, the heat and water mass transports move northward, while they move in and out of the Gulf of Thailand alternately in the lower Gulf of Thaialnd which is lower than 9°N.

For the rainy season of Thailand, June to September, the values of heat, freshwater, and water mass transports are between 0.1×10^8 W to 5.7×10^8 W, 0.6×10^4 kg/s to 1.6×10^5 kg/s, and 0.1 Sv to 5.0 Sv, respectively. Their highest values occurred between latitudes 8°N to 9°N are 5.6045×10^8 W, 1.5867×10^5 kg/s, and 4.9525 Sv, respectively, and their lowest values occurred between latitudes 10°N to 11°N are 0.1820×10^8 W, 0.668×10^4 kg/s, and 0.1657 Sv, respectively. For the upper Gulf of Thailand which is upper than 10°N, the heat and water mass transports move northward, while they move in and out of the Gulf of Thailand alternately in the lower Gulf of Thaialnd which is lower than 10°N.

For the end of the rainy season of Thailand, October, the values of heat, freshwater, and water mass transports are between 0.1×10^8 W to 2.5×10^8 W, 0.3×10^4 kg/s to

7.5×10^4 kg/s, and 0.1 Sv to 2.1 Sv, respectively. Their highest values occurred at the connection section between the Gulf of Thailand and the South China Sea are 2.4200×10^8 W, 7.4792×10^4 kg/s, and 2.0468 Sv, respectively, and their lowest values occurred between latitudes 10°N to 11°N are 0.1603×10^8 W, 0.3060×10^4 kg/s, and 0.1503 Sv, respectively. For the upper Gulf of Thailand which is upper than 9°N, the heat and water mass transports move southward, while they move in and out of the Gulf of Thailand alternately in the lower Gulf of Thaialnd which is lower than 9°N.

It can be summarized that the directions and magnitudes of volume, heat, and freshwater transports depend mainly on the current. The direction of transport arise from most current moving in a region greatly. While the magnitude of transport depends on the direction and speed of current. The high magnitude of transport results from the current has high speed and move in that region. On the other hand, the low magnitude of transport arise from the current at the region which has low speed.

In order to validate the results, the water mass transports for this research are compared with the water mass transports obtained from Wyrtki (1961), who studied water mass transport of the Southeast Asian Waters. Although he did not study sections in the Gulf of Thailand directly, his research is close enough to compare with our results because it is the nearest region. The boundary line between the Gulf of Thailand and the South China Sea is connected from the point (100.448°E, 6.857°N) to the point (104.870°E, 8.297°N). The results of heat, freshwater, and water mass transports across the connection section between the Gulf of Thailand and the South China Sea for each month are shown in Table 4.3.

Table 4.3 The values of heat, freshwater, and water mass transports across the connection section between the Gulf of Thailand and the South China Sea for each month.

Month	**Heat transports** ($\times 10^9$ W)	**Freshwater transports** ($\times 10^5$ kg/s)	**Water mass transports** (Sv)
January	-0.2170	0.5535	-1.7544
February	-1.1735	3.5902	-10.9003
March	-1.2467	3.6295	-11.1124
April	-0.3903	1.1188	-3.6098
May	0.0962	-0.2822	0.7695
June	0.4097	-1.2459	3.6788
July	0.4288	-1.2920	3.7987
August	0.4296	-1.2688	3.7451
September	0.3739	-1.1086	3.3088
October	0.2420	-0.7479	2.0468
November	-0.8527	2.5368	-7.8575
December	-0.1379	0.2442	-0.8881

From Table 4.3, we can see that heat and water mass are transported from the South China Sea into the Gulf of Thailand during May to October, while freshwater

is transported from the Gulf of Thailand into the South China Sea. For the rest of the year, heat and water mass are transported from the Gulf of Thailand into the South China Sea and freshwater is transported from the South China Sea into the Gulf of Thailand.

Wyrtki only studied the direction of water mass transports of the Southeast Asian Waters in June and December, as shown in Figs. 4.210 and 4.211, respectively, and the values of water mass transports near the Vietnam coast in February, April, June, August, and October, as shown in Table 4.4.

Table 4.4 The values of the water mass transports in the Southeast Asian Waters near the Vietnam coast from Wyrtki (1961).

Month	**Water mass transports (Sv)**
February	-5.0
April	-1.5
June	3.5
August	3.0
October	-2.0
December	-5.0

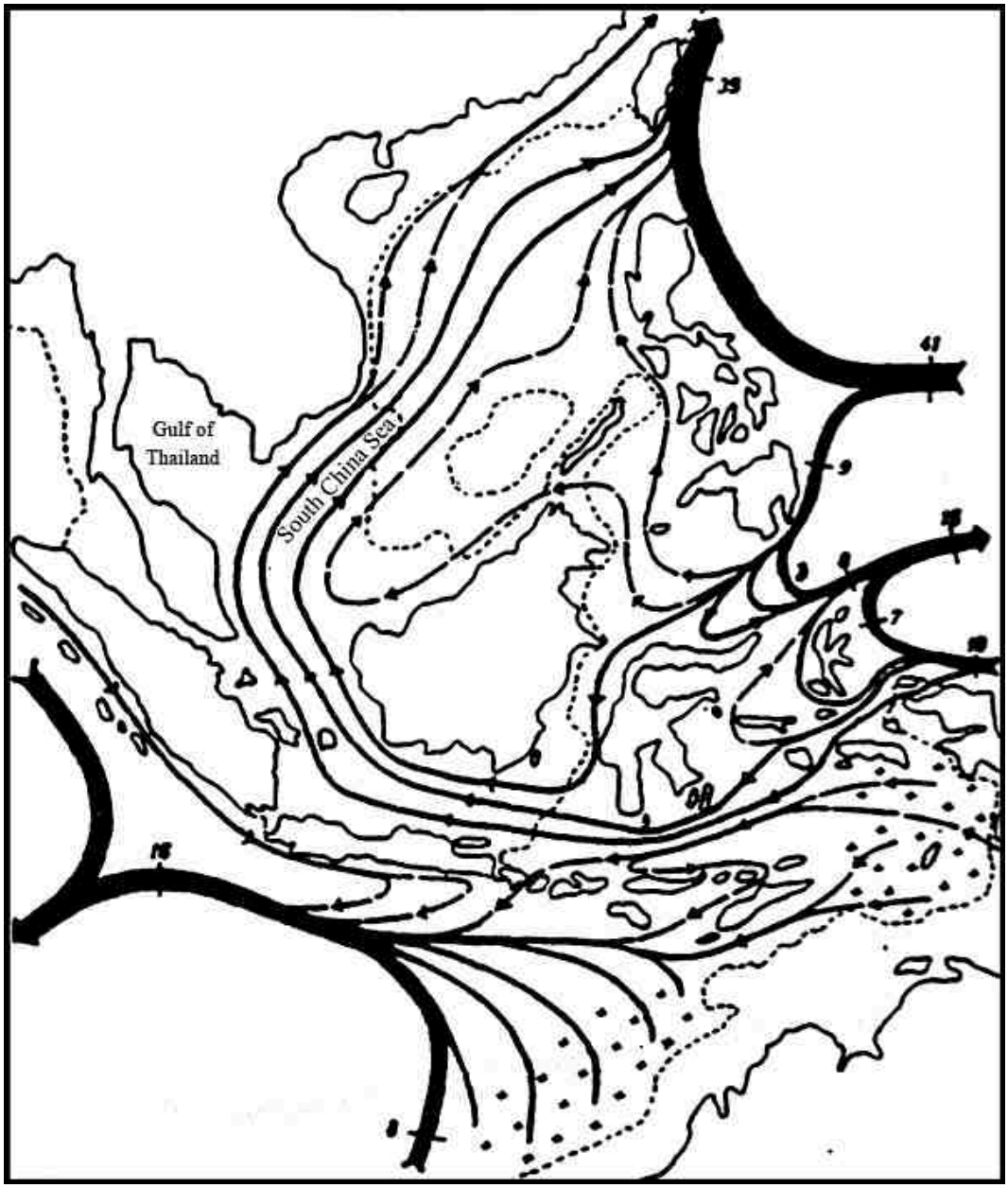

Figure 4.210 The directions of water mass transports of the Southeast Asian Waters in June from Wyrtki (1961).

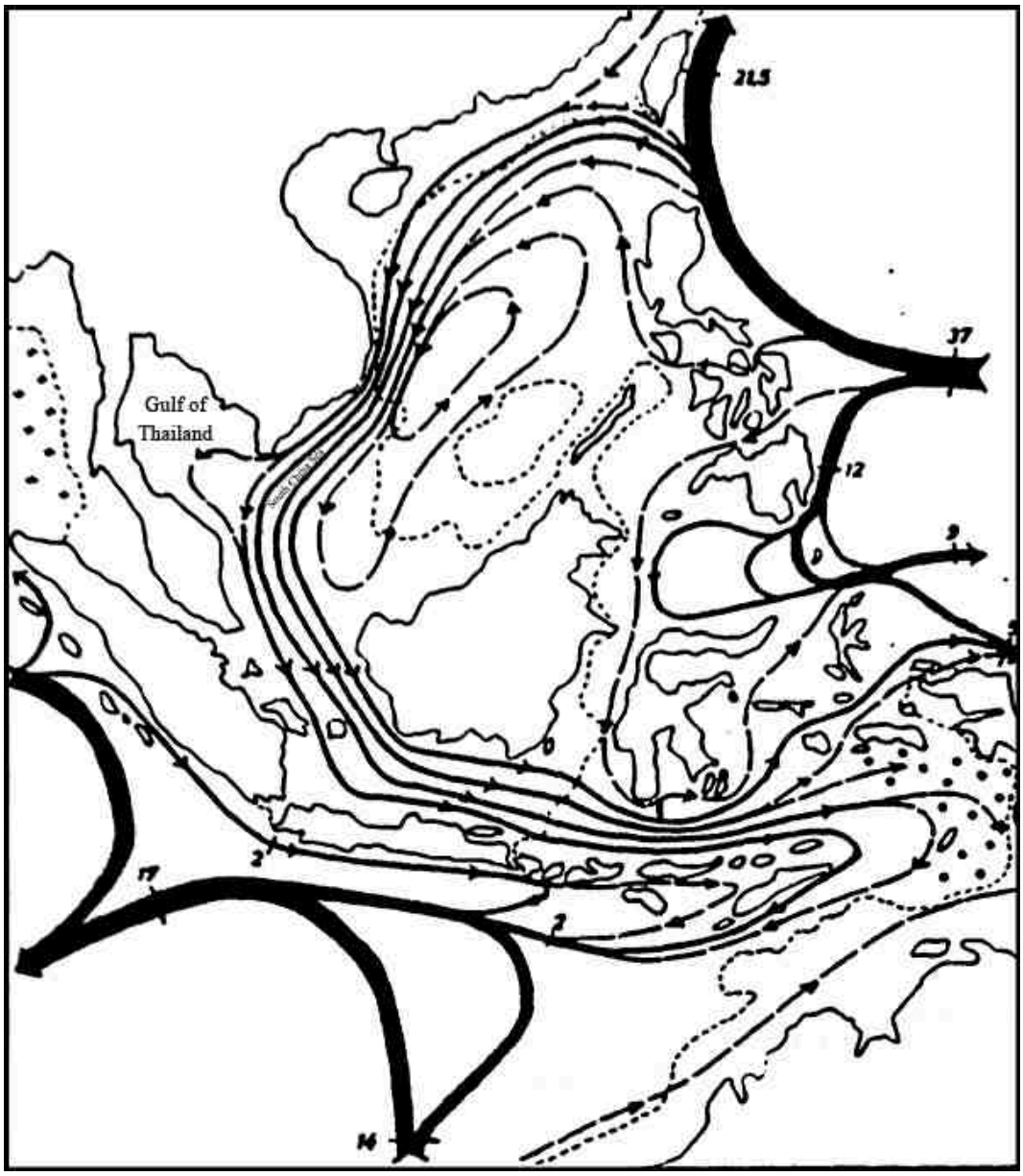

Figure 4.211 The directions of water mass transports of the Southeast Asian Waters in December from Wyrtki (1961).

It can be seen that the directions of water mass transports in June and December from Wyrtki (1961) have moving into and out of the Gulf of Thailand, respectively. These results are corresponding with our results. For comparing the values of the water mass transports from our results and Wyrtki's results, they have similar tendencies. Although the locations of comparison are not the same points, at this time, it is the best method to look for corresponding tendencies.

CHAPTER 5 CONCLUSION AND DISCUSSION

In this research, we investigated the heat content of volume in the Gulf of Thailand and heat, freshwater, and water mass transports in the Gulf of Thailand. The model grid is the orthogonal curvilinear grid and the vertical coordinate is the sigma coordinate. Initial data have been prepared for solving the primitive equations. The initial data consist of bottom topography, wind, potential temperature, and salinity. The Princeton Ocean Model is applied in this research. It is used to solve the primitive equations in order to determine the current velocities, temperature, salinity, and density. These data are used to calculate the heat content of volume and transports of heat, freshwater, and water mass for each month. The results show that the heat content of volume in the third and fourth layers are the highest values because in these layers there are large volumes and high temperatures. The lowest heat content of volume is in the last layer. Actually, the highest and lowest heat content of volume are at the sea surface and bottom, respectively, but in this research the first and second layers have low heat content of volume as a result of small volumes. Thus, the heat content of volume is mainly dependent on the volume and temperature. The total heat contents of volume in the Gulf of Thailand are high during May to October and low during November to April. For transportation in the Gulf of Thailand, the results show that the highest and lowest values of heat, freshwater, and water mass transports in each month occur at the same region, and the direction of heat and water mass transports are all same in the Gulf of Thailand, but the freshwater transport is the opposite direction of heat and water mass transports. The highest values of heat, freshwater, and water mass transports occur between latitudes 8°N to 9°N in the rainy season and at the connection section between the Gulf of Thailand and the South China Sea in the winter, summer, and the end of the rainy season. Their lowest values occur at latitude 9°N in the winter and summer, and between latitudes 10°N to 11°N in the rainy season and the end of the rainy season. For the direction of heat and water mass transports, the heat and water mass at the upper Gulf of Thailand which is upper than 9°N in the end of the winter and summer move northward, and they move southward in the end of the rainy season, and northward and southward alternately in the onset of the winter. At the lower Gulf of Thailand which is lower than 9°N, they move out of the Gulf of Thailand in the winter, and they move in and out of the Gulf of Thailand alternately in the summer and the end of the rainy season. For the rainy season, they move northward at the upper Gulf of Thailand which is upper than 10°N, and they move in and out of the Gulf of Thailand alternately at lower Gulf of Thailand which is lower than 10°N. These results are very useful to manage fisheries and resources in the sea. Each species of life needs a different livelihood. Some kinds live in warm water, and some kinds live in cool water. The research also points out that various species of life move into or out of the Gulf of Thailand, depending on its need.

REFERENCES

[1] Alves, J., Carton, X. and Ambar, I., 2011, "Hydrological Structure, Circulation and Water Mass Transport in the Gulf of Cadiz", **International Journal of Geosciences**, Vol. 2, No. 4, pp. 432-456.

[2] Aschariyaphotha, N., Wongwises, P., Wongwises, S. and Humphries, U.W., 2007, "Simulation of Current Circulations in the Gulf of Thailand", **The IASTED Asian Conference on Modelling and Simulation (AsiaMS 2007)**, October 8-10, Beijing, China.

[3] Aschariyaphotha, N., Wongwises, P., Wongwises, S., Humphries, U.W. and You, X.B., 2008, "Simulation of Seasonal Circulations and Thermohaline Variabilities in the Gulf of Thailand", **Advances in Atmospheric Sciences**, Vol. 25, No. 3, pp. 489-506.

[4] Aschariyaphotha, N. and Wongwises, S., 2012, "Simulations of Seasonal Current Circulations and its Variabilities Forced by Runoff from Freshwater in the Gulf of Thailand", **Arabian Journal for Science and Engineering (AJSE)**, Vol. 37, No. 5, pp. 1389-1404.

[5] Blumberg, A., 1988, "**General Circulation Model Orthogonal Curvilinear Coordinate Grid Generator**", Mahwah, United States of America.

[6] Chu, P.C., 2011, "Upper Ocean Heat Content and Climate Variability", **Ocean Dynamics**, Vol. 61, No. 8, pp. 1189-1204.

[7] Chu, P.C., Lu, S.H., and Chen, Y.C., 2001, "Evaluation of the Princeton Ocean Model using the South China Sea Monsoon Experiment (SCSMEX) Data", **Journal of Atmospheric and Oceanic Technology**, Vol. 18, No. 9, pp. 1521-1539.

[8] Hernández-Guerra, A., López-Laatzen, F., Machín, F., Armas, D.D. and Pelegrí, J.L., 2001, "Water Masses, Circulation and Transport in the Eastern Boundary Current of the North Atlantic Subtropical Gyre", **Scientia Marina**, Vol. 65, No. 1, pp. 177-186.

[9] Heywood, K.J. and Stevens, D.P., 2007, "Meridional Heat Transport Across the Antarctic Circumpolar Current by the Antarctic Bottom Water Overturning

Cell", **Geophysical Research Letters**, Vol. 34, pp. 1-5.

[10] Hui-Er, M. and Yong-Qiang, Y., 2012, "Simulation of Volume and Heat Transport along 26.5°N in the Atlantic", **Atmospheric and Oceanic Science Letters**, Vol. 5, No. 5, pp. 373-378.

[11] Jónsson, S. and Valdimarsson, H., 2012, "Water Mass Transport Variability to the North Icelandic Shelf, 1994-2010", **ICES Journal of Marine Science**, Vol. 69, No. 5, pp. 809-815.

[12] Liu, P.L., 1977, "Mass Transport in Water Waves Propagated over a Permeable Bed", **Coastal Engineering**, Vol. 1, pp. 79-96.

[13] Longuet-Higgins, M.S., 1953, "Mass Transport in Water Waves", **Philosophical Transactions of the Royal Society A**, Vol. 245, No. 903, pp. 535-581.

[14] Madala, R.V. and Piacsek, S.A., 1977, "A Semi-Implicit Numerical Model for Baroclinic Oceans", **Journal of Computational Physics**, Vol. 23, pp. 167-178.

[15] Mellor, G.L. and Blumberg, A.F., 1985, "Modeling Vertical and Horizontal Diffusivities with the Sigma Coordinate System", **Monthly Weather Review**, Vol. 113, pp. 1380-1383.

[16] Mellor, G.L., 2004, **Users Guide for a Three-Dimensional Primitive Equations, Numerical Ocean Model**, Princeton, Princeton University, pp. 5-36.

[17] Mock, C.A., 2011, "**Water Masses, Mass Transport and Variability of the Canary Current in Autumn**", Universidad de Las Palmas de Gran Canaria, Spain.

[18] Murray, J.W., 2004, **Chpt. 3: Properties of Water and Seawater** [online], Available : http://www.ocean.washington.edu/courses/oc400/LectureNotes/CHPT3.pdf [2013, May 7].

[19] Oey, L.Y., Mellor, G.L., and Hires, R.I., 1985a, "A Three-Dimensional Simulation of the Hudson Raritan Estuary, Part I: Description of the Model and Model Simulations", **Journal of Physical Oceanography**, Vol. 15, pp. 1676-1692.

[20] Oey, L.Y., Mellor, G.L., and Hires, R.I., 1985b, "A Three-Dimensional Simulation of the Hudson Raritan Estuary, Part II: Comparison with Observation", **Journal of Physical Oceanography**, Vol. 15, pp. 1693-1709.

[21] Phaksopa, J. and Sojisuporn, P., 2006, "Storm Surge in the Gulf of Thailand Generated by Typhoon Linda in 1997 using Princeton Ocean Model (POM)", **Kasetsart Journal (Natural Science)**, Vol. 40, No. 5, pp. 260-268.

[22] Simons, T.J., 1974, "Verification of Numerical Models of Lake Ontario. Part I, Circulation in Spring and Early Summer", **Journal of Physical Oceanography**, Vol. 4, pp. 507-523.

[23] Stammer, D., Wunsch, C., Giering, R., Eckert, C., Heimbach, P., Marotzke, J., Adcroft, A., Hill, C.N. and Marshall, J., 2003, "Volume, Heat and Freshwater Transports of the Global Ocean Circulation 1992-1997, Estimated from a General Circulation Model Constrained by WOCE Data", **Journal of Geophysical Research**, Vol. 107, No. C9, pp. 1-27.

[24] Talley, L.D., 1984, "Meridional Heat Transport in the Pacific Ocean", **Journal of Physical Oceanography**, Vol. 14, pp. 231-241.

[25] Talley, L.D., 2008, "Freshwater Transport Estimates and the Global Overturning Circulation: Shallow, Deep and Throughflow Components", **Progress in Oceanography**, Vol. 78, pp. 257-303.

[26] Vallis, G.K. and Farneti, R., 2009, "Meridional Energy Transport in the Coupled Atmosphere-Ocean System: Scaling and Numerical Experiments", **Quarterly Journal of the Royal Meteorological Society**, Vol. 135, pp. 1643-1660.

[27] Weatherly, G. and Martin, P.J., 1978, "On the Structure and Dynamics of the Ocean bottom Boundary Layer", **Journal of Physical Oceanography**, Vol. 8, pp. 557-570.

[28] Wijffels, S.E., Schmitt, R.W., Bryden, H.L., and Stigebrandt, A., 1992, "Transport of Freshwater by the Oceans", **Journal of Physical Oceanography**, Vol. 22, pp. 155-162.

[29] Wyrtki, K., 1961, "Scientific Results of Marine Investigations of the South China Sea and the Gulf of Thailand 1959-1961", **Naga Report**, Vol. 2, pp. 1-30.

[30] Yaiprasert, C., Jaroensutasinee, K., and Veruttipong, T., 2005, "Floating Circle of Objects Simulation with the Princeton Ocean Model for the Gulf of Thailand", **Walailak Journal of Science and Technology (WJST)**, Vol. 2, No. 1, pp. 99-113.

APPENDIX

The derivation of the primitive equations in the sigma coordinate

Let

$$\phi(x, y, z, t) = \phi(x^*, y^*, \sigma, t^*), \tag{1}$$

$$x^* = x, \tag{2}$$

$$y^* = y, \tag{3}$$

$$\sigma = \frac{z - \eta(x, y, t)}{D(x, y, t)}, \tag{4}$$

and

$$t^* = t \tag{5}$$

where $D(x, y, t) = H(x, y) + \eta(x, y, t)$.
The chain rule for ϕ is

$$\frac{\partial \phi}{\partial x} = \frac{\partial \phi^*}{\partial x^*} + \frac{\partial \phi^*}{\partial \sigma}\frac{\partial \sigma}{\partial x} = \frac{\partial \phi^*}{\partial x^*} - \frac{\partial \phi^*}{\partial \sigma}\frac{1}{D}\left(\frac{\partial \eta}{\partial x} + \sigma\frac{\partial D}{\partial x}\right), \tag{6}$$

$$\frac{\partial \phi}{\partial y} = \frac{\partial \phi^*}{\partial y^*} + \frac{\partial \phi^*}{\partial \sigma}\frac{\partial \sigma}{\partial y} = \frac{\partial \phi^*}{\partial y^*} - \frac{\partial \phi^*}{\partial \sigma}\frac{1}{D}\left(\frac{\partial \eta}{\partial y} + \sigma\frac{\partial D}{\partial y}\right), \tag{7}$$

$$\frac{\partial \phi}{\partial t} = \frac{\partial \phi^*}{\partial t^*} + \frac{\partial \phi^*}{\partial \sigma}\frac{\partial \sigma}{\partial t} = \frac{\partial \phi^*}{\partial t^*} - \frac{\partial \phi^*}{\partial \sigma}\frac{1}{D}\left(\frac{\partial \eta}{\partial t} + \sigma\frac{\partial D}{\partial t}\right), \tag{8}$$

and

$$\frac{\partial \phi}{\partial z} = \frac{\partial \phi^*}{\partial \sigma}\frac{1}{D}. \tag{9}$$

The transformation from the Cartesian vertical velocity to the sigma vertical velocity is

$$W = \omega + U\left(\sigma\frac{\partial D}{\partial x} + \frac{\partial \eta}{\partial x}\right) + V\left(\sigma\frac{\partial D}{\partial y} + \frac{\partial \eta}{\partial y}\right) + \sigma\frac{\partial D}{\partial t} + \frac{\partial \eta}{\partial t}. \tag{10}$$

The continuity equation

The continuity equation in the Cartesian coordinate is

$$\frac{\partial U}{\partial x} + \frac{\partial V}{\partial y} + \frac{\partial W}{\partial z} = 0. \tag{11}$$

Apply the chain rule similarly with Eqs. (6) to (9), we obtain

$$\frac{\partial U^*}{\partial x^*} - \frac{\partial U^*}{\partial \sigma}\frac{1}{D}\left(\frac{\partial \eta}{\partial x} + \sigma\frac{\partial D}{\partial x}\right) + \frac{\partial V^*}{\partial y^*} - \frac{\partial V^*}{\partial \sigma}\frac{1}{D}\left(\frac{\partial \eta}{\partial y} + \sigma\frac{\partial D}{\partial y}\right) + \frac{\partial W^*}{\partial \sigma}\frac{1}{D} = 0. \tag{12}$$

All asterisks in Eq. (12) are dropped and substituting Eq. (10) into Eq. (12), it yields

$$\frac{\partial U}{\partial x}-\frac{\partial U}{\partial \sigma}\frac{1}{D}\left(\frac{\partial \eta}{\partial x}+\sigma\frac{\partial D}{\partial x}\right)+\frac{\partial V}{\partial y}-\frac{\partial V}{\partial \sigma}\frac{1}{D}\left(\frac{\partial \eta}{\partial y}+\sigma\frac{\partial D}{\partial y}\right)+\frac{\partial \omega}{\partial \sigma}\frac{1}{D}+U\frac{\partial D}{\partial x}\frac{1}{D}$$
$$+\frac{\partial U}{\partial \sigma}\left(\sigma\frac{\partial D}{\partial x}+\frac{\partial \eta}{\partial x}\right)\frac{1}{D}+V\frac{\partial D}{\partial y}\frac{1}{D}+\frac{\partial V}{\partial \sigma}\left(\sigma\frac{\partial D}{\partial y}+\frac{\partial \eta}{\partial y}\right)\frac{1}{D}+\frac{\partial D}{\partial t}\frac{1}{D}=0. \quad (13)$$

After some algebra, we obtain

$$\frac{\partial U}{\partial x}+\frac{\partial V}{\partial y}+\frac{\partial \omega}{\partial \sigma}\frac{1}{D}+U\frac{\partial D}{\partial x}\frac{1}{D}+V\frac{\partial D}{\partial y}\frac{1}{D}+\frac{\partial D}{\partial t}\frac{1}{D}=0. \quad (14)$$

Multiply all terms by D, that is

$$D\frac{\partial U}{\partial x}+D\frac{\partial V}{\partial y}+\frac{\partial \omega}{\partial \sigma}+U\frac{\partial D}{\partial x}+V\frac{\partial D}{\partial y}+\frac{\partial D}{\partial t}=0. \quad (15)$$

We can rewrite Eq. (15) in the form of

$$\frac{\partial DU}{\partial x}+\frac{\partial DV}{\partial y}+\frac{\partial \omega}{\partial \sigma}+\frac{\partial D}{\partial t}=0 \quad (16)$$

Since $\frac{\partial D}{\partial t}=\frac{\partial \eta}{\partial t}$, that is

$$\frac{\partial DU}{\partial x}+\frac{\partial DV}{\partial y}+\frac{\partial \omega}{\partial \sigma}+\frac{\partial \eta}{\partial t}=0 \quad (17)$$

Eq. (17) is the continuity equation in the sigma coordinate.

The momentum equations

The momentum equation in the x-direction in the Cartesian coordinate is

$$\frac{\partial U}{\partial t}+U\frac{\partial U}{\partial x}+V\frac{\partial U}{\partial y}+W\frac{\partial U}{\partial z}-fV=-\frac{1}{\rho_0}\frac{\partial p}{\partial x}+\frac{\partial}{\partial z}\left(K_M\frac{\partial U}{\partial z}\right)+F'_x. \quad (18)$$

Apply the chain rule similarly with Eqs. (6) to (9), we obtain

$$\frac{\partial U^*}{\partial t^*}-\frac{\partial U^*}{\partial \sigma}\frac{1}{D}\left(\frac{\partial \eta}{\partial t}+\sigma\frac{\partial D}{\partial t}\right)+U\left[\frac{\partial U^*}{\partial x^*}-\frac{\partial U^*}{\partial \sigma}\frac{1}{D}\left(\frac{\partial \eta}{\partial x}+\sigma\frac{\partial D}{\partial x}\right)\right]$$
$$+V\left[\frac{\partial U^*}{\partial y^*}-\frac{\partial U^*}{\partial \sigma}\frac{1}{D}\left(\frac{\partial \eta}{\partial y}+\sigma\frac{\partial D}{\partial y}\right)\right]+W\frac{\partial U^*}{\partial \sigma}\frac{1}{D}-fV$$
$$=-\frac{1}{\rho_0}\frac{\partial p}{\partial x}+\frac{1}{D}\frac{\partial}{\partial \sigma}\left(K_M\frac{\partial U^*}{\partial \sigma}\frac{1}{D}\right)^*+F'_x. \quad (19)$$

All asterisks in Eq. (19) are dropped and substituting Eq. (10) into Eq. (19), it yields

$$\frac{\partial U}{\partial t}-\frac{\partial U}{\partial \sigma}\frac{1}{D}\left(\frac{\partial \eta}{\partial t}+\sigma\frac{\partial D}{\partial t}\right)+U\frac{\partial U}{\partial x}-U\frac{\partial U}{\partial \sigma}\frac{1}{D}\left(\frac{\partial \eta}{\partial x}+\sigma\frac{\partial D}{\partial x}\right)+V\frac{\partial U}{\partial y}$$

$$-V\frac{\partial U}{\partial \sigma}\frac{1}{D}\left(\frac{\partial \eta}{\partial y}+\sigma\frac{\partial D}{\partial y}\right)+\omega\frac{\partial U}{\partial \sigma}\frac{1}{D}+U\left(\sigma\frac{\partial D}{\partial x}+\frac{\partial \eta}{\partial x}\right)\frac{\partial U}{\partial \sigma}\frac{1}{D}+V\left(\sigma\frac{\partial D}{\partial y}+\frac{\partial \eta}{\partial y}\right)\frac{\partial U}{\partial \sigma}\frac{1}{D}$$
$$+\left(\sigma\frac{\partial D}{\partial t}+\frac{\partial \eta}{\partial t}\right)\frac{\partial U}{\partial \sigma}\frac{1}{D}-fV=-\frac{1}{\rho_0}\frac{\partial p}{\partial x}+\frac{1}{D}\frac{\partial}{\partial \sigma}\left(K_M\frac{\partial U}{\partial \sigma}\frac{1}{D}\right)+F'_x. \quad (20)$$

After some algebra, we obtain

$$\frac{\partial U}{\partial t}+U\frac{\partial U}{\partial x}+V\frac{\partial U}{\partial y}+\omega\frac{\partial U}{\partial \sigma}\frac{1}{D}-fV=-\frac{1}{\rho_0}\frac{\partial p}{\partial x}+\frac{1}{D}\frac{\partial}{\partial \sigma}\left(K_M\frac{\partial U}{\partial \sigma}\frac{1}{D}\right)+F'_x. \quad (21)$$

Multiply all terms by D, that is

$$D\frac{\partial U}{\partial t}+UD\frac{\partial U}{\partial x}+VD\frac{\partial U}{\partial y}+\omega\frac{\partial U}{\partial \sigma}-fVD=-\frac{D}{\rho_0}\frac{\partial p}{\partial x}+\frac{\partial}{\partial \sigma}\left(\frac{K_M}{D}\frac{\partial U}{\partial \sigma}\right)+DF'_x. \quad (22)$$

Since the momentum equation in the x-direction is the prognostic equation for U, the continuity equation, Eq. (16), is multiplied through by U and add to the above equation. That is

$$D\frac{\partial U}{\partial t}+UD\frac{\partial U}{\partial x}+VD\frac{\partial U}{\partial y}+\omega\frac{\partial U}{\partial \sigma}-fVD+U\frac{\partial DU}{\partial x}+U\frac{\partial DV}{\partial y}$$
$$+U\frac{\partial \omega}{\partial \sigma}+U\frac{\partial D}{\partial t}=-\frac{D}{\rho_0}\frac{\partial p}{\partial x}+\frac{\partial}{\partial \sigma}\left(\frac{K_M}{D}\frac{\partial U}{\partial \sigma}\right)+DF'_x. \quad (23)$$

We can rewrite Eq. (23) in the form of

$$\frac{\partial UD}{\partial t}+\frac{\partial U^2D}{\partial x}+\frac{\partial UVD}{\partial y}+\frac{\partial U\omega}{\partial \sigma}-fVD=-\frac{D}{\rho_0}\frac{\partial p}{\partial x}+\frac{\partial}{\partial \sigma}\left(\frac{K_M}{D}\frac{\partial U}{\partial \sigma}\right)+DF'_x. \quad (24)$$

Mellor and Blumberg (1985) have shown that the conventional model for horizontal viscosity and diffusion are incorrect when bottom topographical slopes are large. A new formulation has been suggested which is simpler than DF'_x, DF'_y, DF'_T, and DF'_S, and make it possible to model realistically bottom boundary layers over sharply sloping bottoms. The variable F_x, F_y, F_T, and F_S are used to be a new formulation instead of DF'_x, DF'_y, DF'_T, and DF'_S, respectively. The horizontal viscosity and diffusion terms are defined according to

$$F_x=\frac{\partial}{\partial x}\left(2DA_M\frac{\partial U}{\partial x}\right)+\frac{\partial}{\partial y}\left[DA_M\left(\frac{\partial U}{\partial y}+\frac{\partial V}{\partial x}\right)\right], \quad (25)$$

$$F_y=\frac{\partial}{\partial y}\left(2DA_M\frac{\partial V}{\partial y}\right)+\frac{\partial}{\partial x}\left[DA_M\left(\frac{\partial U}{\partial y}+\frac{\partial V}{\partial x}\right)\right], \quad (26)$$

$$F_T=\frac{\partial}{\partial x}\left(HA_H\frac{\partial T}{\partial x}\right)+\frac{\partial}{\partial y}\left(HA_H\frac{\partial T}{\partial y}\right), \quad (27)$$

and

$$F_S=\frac{\partial}{\partial x}\left(HA_H\frac{\partial S}{\partial x}\right)+\frac{\partial}{\partial y}\left(HA_H\frac{\partial S}{\partial y}\right) \quad (28)$$

where H is the bottom topography; A_M is the horizontal kinematic viscosity, and A_H is the horizontal heat diffusivity.
Thus, Eq. (24) is rewritten as

$$\frac{\partial UD}{\partial t}+\frac{\partial U^2D}{\partial x}+\frac{\partial UVD}{\partial y}+\frac{\partial U\omega}{\partial \sigma}-fVD=-\frac{D}{\rho_0}\frac{\partial p}{\partial x}+\frac{\partial}{\partial \sigma}\left(\frac{K_M}{D}\frac{\partial U}{\partial \sigma}\right)+F_x. \quad (29)$$

For the pressure gradient term, $\frac{\partial p}{\partial x}$, it is calculated from the hydrostatic equation, which is

$$-\frac{\partial p}{\partial z} = \rho g. \tag{30}$$

Eq. (30) can be rearranged to give

$$-dp = \rho g dz. \tag{31}$$

Integrate the vertical component of the above equation from z to the sea surface elevation, η, which is

$$-\int_z^\eta dp = \int_z^\eta \rho' g dz'. \tag{32}$$

After integration, we obtain

$$p(x, y, z, t) = \rho(\eta) g\eta + \int_z^\eta \rho' g dz' + p_{atm} \tag{33}$$

where p_{atm} is the atmospheric pressure which is assumed constant. The derivative of p with respect to x is

$$\frac{\partial p}{\partial x} = \rho(\eta) g \frac{\partial \eta}{\partial x} + \frac{\partial}{\partial x} \int_z^\eta \rho' g dz'. \tag{34}$$

Since the second term of the right hand side of the above equation can be written as $\int_z^\eta \frac{\partial \rho'}{\partial x} g dz'$, thus Eq. (34) be rewritten as

$$\frac{\partial p}{\partial x} = \rho(\eta) g \frac{\partial \eta}{\partial x} + \int_z^\eta \frac{\partial \rho'}{\partial x} g dz'. \tag{35}$$

Transform the above equation into the sigma coordinate, we obtain

$$\frac{\partial p}{\partial x} = \rho(0) g \frac{\partial \eta}{\partial x} + g \int_\sigma^0 \left[\frac{\partial \rho'^*}{\partial x^*} - \frac{\partial \rho'^*}{\partial \sigma'} \frac{1}{D} \left(\frac{\partial \eta}{\partial x} + \sigma' \frac{\partial D}{\partial x} \right) \right] D d\sigma'. \tag{36}$$

All asterisks in Eq. (36) are dropped and the secon term in the square brackets can be integrated, that is

$$\frac{\partial p}{\partial x} = \rho(0) g \frac{\partial \eta}{\partial x} + g \int_\sigma^0 \left(\frac{\partial \rho'}{\partial x} - \frac{\sigma'}{D} \frac{\partial D}{\partial x} \frac{\partial \rho'}{\partial \sigma'} \right) D d\sigma' - \rho(0) g \frac{\partial \eta}{\partial x} + \rho(\sigma) g \frac{\partial \eta}{\partial x}. \tag{37}$$

After some algebra, we obtain

$$\frac{\partial p}{\partial x} = \rho(\sigma) g \frac{\partial \eta}{\partial x} + gD \int_\sigma^0 \left(\frac{\partial \rho'}{\partial x} - \frac{\sigma'}{D} \frac{\partial D}{\partial x} \frac{\partial \rho'}{\partial \sigma'} \right) d\sigma'. \tag{38}$$

In the past, $\rho(\sigma)$ has been approximated with the constant, ρ_0, which is a valid approximation in most applications. Thus, Eq. (38) can be rewritten as

$$\frac{\partial p}{\partial x} = \rho_0 g \frac{\partial \eta}{\partial x} + gD \int_\sigma^0 \left(\frac{\partial \rho'}{\partial x} - \frac{\sigma'}{D} \frac{\partial D}{\partial x} \frac{\partial \rho'}{\partial \sigma'} \right) d\sigma'. \tag{39}$$

substituting Eq. (39) into Eq. (29), it yields

$$\frac{\partial UD}{\partial t} + \frac{\partial U^2 D}{\partial x} + \frac{\partial UVD}{\partial y} + \frac{\partial U\omega}{\partial \sigma} - fVD + gD \frac{\partial \eta}{\partial x}$$

$$+\frac{gD^2}{\rho_0}\int_\sigma^0\left[\frac{\partial\rho'}{\partial x}-\frac{\sigma'}{D}\frac{\partial D}{\partial x}\frac{\partial\rho'}{\partial\sigma'}\right]d\sigma'=\frac{\partial}{\partial\sigma}\left[\frac{K_M}{D}\frac{\partial U}{\partial\sigma}\right]+F_x. \tag{40}$$

Eq.(40) is the momentum equation in the x-direction in the sigma coordinate. For the momentum equation in the y-direction in the sigma coordinate, it is obtained in the same manner. That is

$$\frac{\partial VD}{\partial t}+\frac{\partial UVD}{\partial x}+\frac{\partial V^2D}{\partial y}+\frac{\partial V\omega}{\partial\sigma}+fUD+gD\frac{\partial\eta}{\partial y}$$

$$+\frac{gD^2}{\rho_0}\int_\sigma^0\left[\frac{\partial\rho'}{\partial y}-\frac{\sigma'}{D}\frac{\partial D}{\partial y}\frac{\partial\rho'}{\partial\sigma'}\right]d\sigma'=\frac{\partial}{\partial\sigma}\left[\frac{K_M}{D}\frac{\partial V}{\partial\sigma}\right]+F_y. \tag{41}$$

The conservation equations for temperature and salinity

The prognostic equations for T and S are obtained in the manner as same as the momentum equations. A difference is that these equations do not contain the pressure gradient term. The conservation equations for temperature and salinity in the sigma coordinate are expressed as

$$\frac{\partial TD}{\partial t}+\frac{\partial TUD}{\partial x}+\frac{\partial TVD}{\partial y}+\frac{\partial T\omega}{\partial\sigma}=\frac{\partial}{\partial\sigma}\left[\frac{K_H}{D}\frac{\partial T}{\partial\sigma}\right]+F_T \tag{42}$$

and

$$\frac{\partial SD}{\partial t}+\frac{\partial SUD}{\partial x}+\frac{\partial SVD}{\partial y}+\frac{\partial S\omega}{\partial\sigma}=\frac{\partial}{\partial\sigma}\left[\frac{K_H}{D}\frac{\partial S}{\partial\sigma}\right]+F_S, \tag{43}$$

respectively.

BIOGRAPHY

Name	Mr. Kriangsak Piampholphan
Date of Birth	25 September 1986
Educational Record	
High school	High School Graduation Trimit Witthayalai School, 2004
Bachelor's Degree	Bachelor of Science (Mathematics) King Mongkut's University of Technology Thonburi, 2008
Master's Degree	Master of Science (Applied Mathematics) King Mongkut's University of Technology Thonburi, 2010
Doctoral Degree	Doctor of Philosophy (Applied Mathematics) King Mongkut's University of Technology Thonburi, 2014
Scholarship	-
Publication	Piampholphan, K, Luadsong, A., and Aschariyaphotha, N., 2014, "A Study of Heat Content of Volume in the Gulf of Thailand", **The 5th National and International Hatyai Conference**, May 16, 2014, Hatyai University. Piampholphan, K, Luadsong, A., and Aschariyaphotha, N., 2014, "Heat and Freshwater Transports between the Gulf of Thailand and the South Chaina Sea", **The 1st International Conference on Applied Science, Technology and Management**, April 23-25, 2014, Graduate School of Applied Statistics, National Institute of Development Administration. Piampholphan, K, Luadsong, A., and Aschariyaphotha, N., 2014, "A Study of Water Mass Transports between the Gulf of Thailand and the South China Sea", **Advances and Applications in Fluid Mechanics (AAFM)**, 2014, Pushpa Publishing House, Allahabad, India.